Examining Cancer Metabolism *in vivo*

by

Shawn Michael Davidson

B.S. Biology, Providence College (2010)

Submitted to the Department of Biology
in partial fulfillment of the requirements for the degree of

Doctor of Philosophy in Biology

at the

MASSACHUSETTS INSTITUTE OF TECHNOLOGY

February 2017

Author ..... Signature redacted

Department of Biology
February 1, 2016

Certified by ..... Signature redacted

Matthew G. Vander Heiden
Associate Professor of Biology
Thesis Supervisor

Accepted by ..... Signature redacted

Amy Keating
Chair, Department Committee on Graduate Theses

Examining Cancer Metabolism *in vivo*

by

Shawn Davidson

Submitted to the Department Biology
on January 31, 2017 in Partial Fulfillment of the
Requirements for the Degree
of Doctor of Philosophy in Biology

ABSTRACT

Nutrient requirements for cancer cells are different from those of most normal cells. Understanding these differences, and the factors that are responsible for creating different metabolic dependencies, is critical to understanding the basic requirements of rapid proliferation and identifying potential therapeutic vulnerabilities. In particular, oncogene status, tissue-of-origin, cell-of-origin, and microenvironmental factors all can contribute to defining these requirements, but how to characterize which dependencies exist in various physiological setting are unknown.

In this thesis, we address key challenges to study cancer metabolism in the living organism. We present novel experimental and analytical methods to study tumor metabolism in mouse models. This includes: (1) an approach to determine the metabolic fate of any radioactive or stable-isotope tracer in tumors and tissues (2) strategies to create stable-isotope macromolecular (protein) tracers (3) a plasmapheresis strategy to deliver labeled protein in vivo (4) qualitative and quantitative methods to define kinetics of extracellular protein catabolism in live tumors in real-time (5) the characterization of a conditional allele to test the requirements for isoform-specific pyruvate kinase expression.

We applied these methods to three mouse models of cancer (models of human lung, pancreas, and prostate cancer) to better characterize metabolism and identify potential metabolic vulnerabilities in these tumors. Our results show that tumors *in vivo* utilize a metabolic program that is distinct from cells in tissue culture derived from those same tumors. Additionally, we identified that the uptake and subsequent catabolism of extracellular protein provides a substantial proportion of free intracellular amino acids for pancreatic cancer cells in tumors. Finally, we have identified prostate cancer as a tumor type that may benefit from pharmacological activation of pyruvate kinase.

Overall, our results demonstrate the importance of studying cancer metabolism in the correct physiological setting. Data generated from patients corroborates our findings in these mouse models and suggests that these approaches can be used to define more effective cancer therapeutic strategies. The methods presented here are adaptable to study the metabolic phenotypes in any tumor or tissue of interest. Further use of these methods enable the examination of cell autonomous and non-cell autonomous metabolic consequences of oncogene status, microenvironment, and in organismal metabolism as a function of cancer initiation and progression.

Thesis Supervisor: Professor Matthew G. Vander Heiden
Title: Associate Professor of Biology

Overview

ALL LIVING THINGS share the common ability to extract energy and generate precursors needed for self-replication. Although there is astonishing diversity in nutrient utilization, all of life is composed of DNA, RNA, proteins, lipids, and an assortment of other small molecules. Metabolism is totality of the reactions that take place inside cells to use nutrients to create and combine these fundamental building blocks.

The importance of metabolism to human health and disease has been a focus of scientific investigation since the birth of biochemistry in the nineteenth century. In cancer, changes in cellular metabolism were among the earliest observed features that distinguished tumor cells from normal cells. While early observations of cancer metabolism were made using tissue slices from primary tumors, many contemporary cancer metabolism investigations have relied on studies of cancer cells in tissue culture.

Studies focused on understanding the nutrient requirements of cancer cells *in vitro* to support proliferation have provided significant insight. The limitations of these systems, however, are numerous. They include the lack of relevant normal tissue controls; non-physiological oxygen, carbon dioxide, and bicarbonate levels; altered macro- and micro-environmental hormonal influences; altered spatial relationships to blood vessels and neighboring cells; lack of nervous innervation; and exhibit nutrient concentrations more than those found *in vivo*. As a result, many drugs that demonstrate efficacy in this setting often fail in clinical trials. More fundamentally, how to answer questions about multi-step nature of tumorigenesis from initiation, progression, and metastasis in these systems is not clear.

Techniques developed to assess tumor metabolism *in vivo* can provide diagnostic and prognostic information in the clinic. However, some limitations of current approaches to studying cancer metabolism *in vivo* are: (a) PET typically only informs about uptake of a nutrient of interest (b) other imaging modalities (e.g. DNP-MRSI) available only provide information about several metabolites (c) NMR-based imaging modalities are limited in sensitivity and require highly technical expertise and instrumentation (d) metabolomics approaches are not always predictive of the activity of individual enzymes.

Traditional metabolite labeling experiments conducted in both tissue culture and animals have been used to trace the fate of a radiolabeled nutrient (the tracer) that is chemically and functionally identical. These labeling experiments are used to ascertain information in three ways: 1) pharmacokinetics and pharmacodynamics to determine the distribution of the tracer 2) rate of incorporation to calculate the rate of synthesis of macromolecules (e.g. DNA, RNA, protein) 3) rates of oxidation, degradation, clearance of the tracer. The typical procedure for these experiments is to add or infuse radiolabeled tracer into cells in culture or animal models. The tracer or fate of the tracer in cells or tissues of interest are analyzed by scintillation counting, but methods to purify any downstream resulting labeled metabolites of interest requires significant investment.

In contrast to radiolabeled isotope studies, stable-isotope tracing studies are facilitated by the development of nuclear magnetic resonance (NMR) spectroscopy and modern chromatography coupled mass-spectrometry, and the fate of any given tracer can be assessed in a high-throughput and untargeted manner. In the absence of a tracer, these methods provide relative or quantitative concentration measurements of thousands of metabolites (metabolomics). However, concentrations of metabolites are not necessarily correlated with enzyme activity and information about pool sizes do not inform about the origin of the metabolite of interest. Employing tracing experiments using stable-isotopes enable the determination of metabolic flux as a result of knowing atom transition in metabolites as they progress through pathways. Therefore, we developed methods to deliver stable-isotope labeled tracers though direct intravenous infusion, which allowed us to conduct a series of investigations concerning metabolism of tumors in genetically engineered mouse models of cancer. In these systems, we observed significant differences in metabolism as compared to the cell culture setting. We were further able to make and validate predictions of specific enzymes that were responsible for these differences.

Contributions of this thesis

THE GOAL OF THIS THESIS is to develop systematic approaches to determine metabolic phenotypes in tumors and tissues in a robust manner. First, we developed methods to perform infusion of stable-isotope labeled nutrients and determined how to analyze the fate of each of these tracers. We further highlight advantages of using multiple modern mass-spectrometric analyses for these studies. We employ orthogonal methods, such as local delivery approaches and intravital microscopy, that enable qualitative and quantitative assessments of protein catabolism in tissues. Finally, we use and generate mouse models of cancer that have been shown to recapitulate features of the human disease. Together, these approaches allowed us to understand metabolic phenotypes and vulnerabilities of cancer arising from the lung, pancreas, and prostate.

CHAPTER 1 We provide background for our studies in cancer metabolism along with an extended experimental strategy section to discuss practical implementation of these methods with emphasis on studies in mouse models of cancer.

CHAPTER 2 AND APPENDIX A We present methods for the delivery of stable-isotope labeled tracers in tissues in mouse models of cancer. We observed that lung tumors *in vivo* exhibit different metabolism concerning cells derived from those same tumors *in vitro*. We further validate hypotheses generated from the inferences of our tracing studies about enzymes accounting for these differences with functional pharmacological and genetic experiments. These studies suggest that the environment is a major determinant of metabolism, independent of oncogene status.

CHAPTER 3 AND APPENDIX B We produce a stable-isotope tracer of the protein mouse serum albumin to test our hypothesis that tumor cells consume protein based on previous observations *in vitro*. Next, we implement a miniaturized plasmapheresis strategy to exchange endogenous albumin with our labeled albumin in a mouse model of pancreatic cancer. To better understand the kinetics of protein catabolism, we further implement a microdevice that allows local delivery of fluorescent proteins directly to pancreatic tumors. We observe preferential uptake and catabolism of labeled protein substrates by tumors. Overall, these results show that extracellular protein is a nutrient source for pancreatic cancer.

CHAPTER 4 We examine the role of the glycolytic enzyme pyruvate kinase (PK) and whether differential isoform expression of this enzyme (isoform M1 or M2), contribute to tumor initiation and progression in a mouse model of prostate cancer. We generate a conditional allele for the PKM1 and use an existing PKM2 conditional allele. In this mouse model, PKM1 expression is tumor suppressive and PKM2 expression promotes tumor proliferation. We further observe the preliminary efficacy of a pharmacological activator targeting PKM2. Finally, we observe many cases of human prostate cancer that express PKM2, and we suggest that pharmacological activators may be useful in this setting.

CHAPTER 5 Given the importance of extracellular protein catabolism from our observations in Chapter 3 and the challenges of studying compartmentalized metabolism, we focus on a discussion about lysosomal involvement in maintaining cellular homeostasis of nutrients and emerging roles that the lysosome plays in cancer (Chapter 5).

CHAPTER 6 We conclude with a discussion regarding therapeutic strategies based on these approaches and potential future directions to continue understanding cancer metabolism *in vivo*.

In summary, this thesis aims to describe methods to study cancer metabolism in the physiologically relevant setting and provides the possibility of using these methods to identify metabolic vulnerabilities in tumors. It moves past traditional single-output modalities such as PET studies and instead allows us to infer information about specific enzymes *in vivo*. Determining a metabolic phenotype for individual tumors in animal models and applying similar strategies in the clinic may enable the discovery of new therapies for cancer.

Acknowledgements

I am indebted to a number of enthusiastic and remarkably inspirational teachers, professors, colleagues, and friends that I have found myself fortunate to be surrounded by throughout life. My scientific journey began with my biology teacher in high school, Mr. Ted Duluk. He convinced me to pursue an undergraduate degree in biology from his *alma mater*, Providence College. I thank Father Nicanor Austriaco for always believing in me, making time for me, and for allowing me to have an independent project while working as an undergraduate in his lab. Michael Sehorn of Clemson University gave me an opportunity to work in his biochemistry lab to study DNA repair, despite not yet having taken a biochemistry course. Michael Bonkowski's generosity in lab and life shaped me as a scientist and person. I am still able to laugh at nearly every failed experiment because of the quote, "If it worked the first time, it would just be called 'search!' " These early training experiences, and the lessons learned while there, were invaluable.

I am fortunate to have worked in Matthew Vander Heiden's Lab for my doctoral studies. Matt, you have helped me grow tremendously and I am forever grateful. You believed in me and I am appreciative of the latitude you gave me while teaching me to be a rigorous and careful scientist. Your enthusiasm for my work pushed me to do things that seemed impossible. I will always be proud to have been one of your first students.

I am grateful for the input, guidance, and advice from my thesis committee members, Professors Lenny Guarente and Tyler Jacks. Lenny also allowed me to work in his lab as an undergraduate and I was captivated in thinking about a topic as vast as aging. Rotating in Tyler's lab and numerous collaborations with his group were also formative to thesis work and my development as a scientist.

I thank David Housman for his support, friendship, and teaching me a great deal about life and science.

Much of the work in this thesis would not exist if not for the help of excellent people. I remember gratefully:

For their persistence, enthusiasm, friendship, and dedication to science and to me, Alice Chen, Amy Liu, Julia Heyman, James O'Brien, Matthew Bauer, Nathaniel Swanson, Ben Olenchock, Natalia Drosu, Thales Papagiannakopolous, Mark Keibler, Chris Chin, and Oliver Jonas. I have learned so much from all of you.

For the valuable input and a collegial atmosphere in the MVH lab, Brian Fiske, Will Israelsen, Katie Mattaini, Talya Dayton, Jared Mayers, Sophia Lunt, Amelia Yu, Anna Nyugen, Zach Johnson, Caroline Lewis, Lucas Sullivan, Dan Gui, Dan Schmidt, and Alba Luengo. For the fun rotations, Jeff Meng, Laurens Lambert, and Kendall Condon.

For their generosity and fun in the Koch Institute, members of the Housman (Chris Ng, Alina Li, Theresa Wasylenko), Jacks, Hemann (especially Mike), Amon, and Manalis labs.

For their collaborations in the Greater Boston Area and across the country, Scott Manalis, Christian Metallo, Sarah Fendt, Massimo Loda, Lorelai Mucci, Thomas Wasylenko, Abhishek Jha, Rachel Kelly, Bashar Hamza, and Clary Clish. I also thank Dick Kibbey, Michael Jurczack, and David Wasserman for always having an open door and helping me begin to study *in vivo* metabolism.

For the support from many talented individuals in the animal and core facilities, Scott Malstrom, Kathy Cormier, Mike Brown, Lisa Freinkman, Tsering Sherpa, and Sonam Palzom.

For their financial support, The National Science Foundation GRFP and the Broad Institute SPARC Program

Finally, I thank my family for their love and support.

Contents

List of Figures

1
Cancer Metabolism

Author statement

Some passages and figures have been adapted or quoted verbatim from the following published articles:
1. Davidson, SM, & Vander Heiden, MG (2012). *MET*abolic adaptations in the tumor *MYC*roenvironment. *Cell Metabolism*, 15(2), 131–133.
2. Davidson, SM, & Vander Heiden, MG (2017). Critical functions of the lysosome in cancer biology. *Annual Review of Pharmacology and Toxicology*, 57(1), 481-507.

WHAT ARE THE ENERGETICS OF LIFE? Is there a quantitative difference between the metabolism of cancer cells and normal cells? Around the year 1920, a newly appointed professor at the Kaiser Wilhelm Institute named Otto Warburg became fascinated with these two questions. Having just received financial support from his famous one-line application (it read: "I need ten thousand marks."), he surrounded himself with highly capable and intelligent technical staff. By 1924, he was equipped with the latest technologies of his day and set out to find the answers to his questions (Otto, 2016). Using a manometer to measure CO_2 evolution and recently developed pH indicators to measure changes in media conditions, he initially observed that tumors exhibited a significantly higher rate of CO_2 evolution and higher lactate production as compared to normal tissues. This altered metabolism was one of the first differences observed between cancer cells and normal cells, but why cancer cells performed metabolism differently remained unclear (Warburg et al., 1926). Warburg's seminal observation of this phenomenon was contextualized by the contemporary understanding of biochemistry, and subsequently by discoveries from each scientific era.

Findings from the late eighteenth century framed Warburg's initial interpretation of cancer metabolism. At the time, understanding how alcohol was produced through the process fermentation was a problem that had captivated several chemists in France. A.L. Lavoisier, who had previously discovered the role of oxygen in the process of combustion, described the phenomenon of fermentation as 'one of the most extraordinary in chemistry' (Barnett, 1998). While trying to solve this new puzzle, he performed one of the first metabolic accounting experiments. No sophisticated methods were required: Add grapes, ferment, and measure the products. Through these experiments, Lavoisier invented the concept of the chemical equation and wrote the first one to explain the reaction based on his results:

$$\text{grape must} = \text{carbonic acid} + \text{alcohol}$$

In the course of understanding this reaction, scientists provided the basis for the systematic determination of the individual enzymes and metabolic pathways responsible for these complicated biochemical processes. In the end, Warburg's work and most of modern biochemistry were framed by several critical discoveries made during this time.

In 1815, the equation for fermentation was further refined at the chemical level. The process was still not understood, but there appeared to be a new product observed in the fermented solution: yeast. On one side, many chemists logically reasoned that the final product in any process would likely be some reshuffled combination of the original ingredients and argued that yeast were formed in the act of fermentation. The other, more heretical hypothesis, was that the yeast were a living reactant and critical contributor to this process. This contentious debate between the greatest chemists of the time was ultimately settled by visualizing dividing yeast with an early microscope invented by Cagniard-Latour, Kutzing, and Schwann in 1837 (Barnett, 1998).

Twenty years later, Louis Pasteur observed that something more than yeast was alive in some

of these wines, specifically in batches that had gone bad. He noted that a black, rod-shaped bacteria had taken over the culture. In the course of dissecting the microbial contents of these contaminated wines, Pasteur established cultivation techniques that enabled the experimental study of microorganisms, findings that would contribute the development of his idea for the germ-theory of disease. He made the first defined medium to better understand the phenomenon of fermentation. He also demonstrated that fermentation could yield two products: ethanol in the case of yeast or lactate in the case of the bacteria.

Critical to Warburg's interpretation of cancer metabolism was Pasteur's demonstration, through his newly established culture methods, that cellular respiration is in opposition to fermentation (the "Pasteur effect"). Through this lens, cancer cells performed metabolism in an analogous way to how yeast performed fermentation, with lactate rather than ethanol as the final end-product. From these observations, Warburg surmised that respiration was somehow defective, and although this interpretation was not universally endorsed, contemporary data being generated were consistent with this idea (Otto, 2016). Unlike fermenting yeast, however, these cancer cells had plenty of oxygen.

Warburg's work was further interpreted by discoveries made in the years after his observation by him and his contemporary colleagues in what would be the beginning of "golden age of biochemistry." Work done in this period was facilitated by the methodology developed to understand fermentation. Procedures developed during this time enabled the systematic purification of enzymes of glycolysis and enzymes in intermediary metabolism. Franz Lipmann discovered that the phosphate bond of ATP could be used for energy requiring reactions in 1941 (Lipmann, 1941) and these discoveries culminated in Peter Mitchell's chemiosmotic theory which explained how ATP could be used to power cellular processes (Mitchell, 1966).

By the time Warburg published his seminal paper in 1956, "On the Origin of Cancer," things

seemed clear. Defective mitochondria in cancer cells resulted in an energy deficiency, and therefore, which necessitates higher levels of glycolysis. Aerobic glycolysis is relatively inefficient with respect to ATP production as compared to mitochondrial glucose oxidation (2 net ATP generated per molecule of glucose under anaerobic glycolytic conditions and roughly 30-36 ATP are generated through complete mitochondrial oxidation) so cancer cells must perform this at higher rates to compensate.

Warburg's explanation of cancer cell metabolism did not fit all contemporary data and was less clear to some. Sidney Weinhouse responded to Warburg's paper immediately following its publication, citing his work using isotope tracers from a year earlier: "The results of [my previous] studies leave no doubt of the ability of miscellaneous tumors to convert glucose (and fatty acids) to carbon dioxide at rates similar in magnitude to that of nonneoplastic tissues" (Weinhouse, 1956). Despite this commentary and strong supporting data in hand, there also remained plenty of supporting evidence for aerobic glycolysis. But, as molecular biology and genetics took center-stage, along with the fact that all of the glycolytic and intermediary metabolism enzymes had been mostly discovered by the late 1950s metabolism was viewed as a solved problem, the findings from this era were relegated to biochemistry textbooks. Moreover, cancer metabolism would be deemed a largely uninteresting epiphenomenal consequence of tumorigenesis.

Renaissance Why cancer cells perform aerobic glycolysis remains incompletely understood (Lunt and Vander Heiden, 2011), and as logic might follow, textbook biochemistry does not apply to proliferating cells (Ward and Thompson, 2012). In the time since Warburg's 1956 publication, we have learned what Weinhouse may have already known: that mitochondria in cancer cells are active and respiring. In most instances, mitochondria are either more active or even required for transformation (Weinberg et al., 2010). Further, it is also clear ATP is not limiting is most settings

in cancer (Zu and Guppy, 2004) and that the ATP requirement in cancer cells is not that much different from normal cells (Vander Heiden et al., 2009). Still, surprisingly little is known about the limiting substrates of cancer cells. As a result of the revolution in molecular biology and genetics that once diverted attention from metabolism, four major themes have placed cancer metabolism back in the spotlight.

1. the delineation of common signaling pathways and their targets in normal and cancer cells

> *We know too little to analyze cells in the way engineers analyze their systems. But, the question is whether we would be able to understand what we need to learn if we do not use a formal description. The biochemists would measure rates and concentrations to understand how biochemical processes work. A discrepancy between the measured and calculated values would indicate a missing link and lead to the discovery of a new enzyme, and a better understanding of the subject of investigation. Do we know what to measure to understand a signal transduction pathway? Are we even convinced that we need to measure something?*
>
> – **Y. Lazebnik**, *2004, "Can a Biologist Fix a Radio?"*

ALL metazoan cells require extracellular signals for cell survival, and these signals govern the fundamental processes of apoptosis, nutrient uptake, and proliferation (Raff, 1992; Rathmell et al., 2003). Apoptosis, or programmed cell death, is a highly evolutionarily conserved process (Hengartner and Horvitz, 1994). When the apoptotic program is activated, mitochondrial membrane permeabilization occurs along with caspase activation, and this results in the initiation of the canonical programmed cell death pathway (PCD Type I, reviewed in (Elmore, 2007)). Accordingly, a fine balance is maintained for the expression of the anti-apoptotic *Bcl-2* family members (Vaux et al., 1988) which function to inhibit the critical apoptosis initiators, *Bax* and *Bak* (Kuwana et al., 2005). In the absence of cell-extrinsic signals such as growth factors, cells undergo apoptosis, and this is often the default program (Raff, 1992).

Two fascinating observations connecting signaling and metabolism in cells were made when the

default apoptotic pathway is inhibited. First, growth-factor dependent cells that overexpressed the anti-apoptotic *Bcl-2* gene *in vitro* and *in vivo* were viable and continued to proliferate, even in the absence of growth factors, conditions that would normally promote cell death (McDonnell et al., 1989; Vaux et al., 1988). In a complementary experiment, single cell suspensions were made from tissues of mice that were null for the pro-apoptotic genes Bax and Bak ($bax^{-/-}$ $bak^{-/-}$) or from normal control animals. Cells from mice that were $bax^{-/-}$ $bak^{-/-}$ survived in culture for longer than cells from tissues of their wild-type counterparts, similar to *Bcl-2* overexpressing cells (Lindsten and Thompson, 2006). The kinetics observed in these experiments revealed variable latency until cell death in cells from different tissues, and it was also observed that $bax^{-/-}$ $bak^{-/-}$ mice are also critically dependent on genes in the autophagy pathway. Along with upregulating genes for self-digestion, the cells lost the ability to take up nutrients. This finding was explained mechanistically by data that demonstrated the failure of a glucose transporter, GLUT1, to localize to the cell membrane. Therefore, in the absence of these signals, cells either undergo apoptosis or a second kind of cell death, "death by neglect" (Rathmell et al., 2003; Lindsten and Thompson, 2006). Taken together, these findings demonstrated the essentiality of extrinsic signaling for the maintenance of cellular energetics in normal cells.

NORMAL CELLS ARE TRANSFORMED through a multi-step process that gives rise to the disease called cancer (Vogelstein and Kinzler, 1993; Evans, 1976). Cellular transformation occurs by mutational events that cause the activation of proto-oncogenes or loss of tumor suppressor genes (Stehelin et al., 1976; Hanahan and Weinberg, 2011). Like normal cells, cancer cells are also frequently addicted to the signaling programs promoted by these oncogenic events (Weinstein, 2002) and these signaling pathways promote many hallmarks of cancer (Hanahan and Weinberg, 2011). Oncogenic signaling also rewires cellular metabolism to sustain the energy requirements of cancer cells. This can occur in a cell autonomous manner and act directly to modify metabolic enzyme

activity or indirectly to activate effector pathways that alter levels of metabolic enzymes. Alternatively, other oncogenic signaling programs proceed through coordinated non-cell autonomous mechanisms. Neovascularization and oxygen sensing have so far uniquely tied signaling and physiology to metabolism and explain important features about nutrient requirements for tumor growth *in vivo*.

Cell autonomous control of metabolism

Oncogenic signaling targets metabolism directly In 2008, Lewis Cantley and colleagues observed the first direct link between oncogenic signaling and the modification of a metabolic enzyme to explain the Warburg effect with molecular resolution. These experiments demonstrated that tyrosine phosphorylated peptides could bind to the human M2 isoform of the glycolytic enzyme pyruvate kinase (PKM2) to promote the release of the endogenous allosteric activator, fructose-1,6-bisphosphate, resulting in PKM2 that had lower specific activity (Christofk et al., 2008b). They further demonstrated that PKM2 was the isoform expressed by most cancer cells in culture (Christofk et al., 2008a) and that PKM2 expression in these settings promoted the anabolic use of glucose metabolism and supported proliferation (Christofk et al., 2008b). The low activity form was determined to be functionally relevant in the original (Christofk et al., 2008b) and the importance of low PKM2 activity for proliferation has since been extensively characterized (Lunt and Vander Heiden, 2011). An independent study further corroborated this data with observations that PKM2 was a biomarker that reflects metabolic activity and proliferation capacity of tumors (Mazurek, 2011). Beyond providing a molecular mechanism for the Warburg effect, the discovery of PK isoform selectivity by cancer cells that conferred low activity gave rise to the possibility of an entirely new way to think about cancer therapy: the activation of a metabolic enzyme.

Oncogenic signaling targets metabolism indirectly *LDH-A* was the first metabolic enzyme reported to play a role in its altered expression in response to oncogenic activation. Chi Dang and colleagues demonstrated that *c-Myc*-transformed human lymphoblastoid cells and Burkitt lymphoma cells exhibited high levels of lactic acid production. Using representational difference analysis, Dang and colleagues determined that Myc binds to the E-box consensus sequence CACGTG of the *LDH-A* promoter activate transcription (Shim et al., 1997). This provided a link between the Warburg effect and *LDH-A* expression, but the consequences of *LDH-A* inhibition in this study through shRNA did not reduce tumor cell growth (Shim et al., 1997). Two follow-up experiments, using either a small-molecule *LDH-A* inhibitor or RNA interference targeting *LDH-A*, prevented tumor progression (Fantin et al., 2006; Le et al., 2010). Data from mouse models suggested that LDH-A was also likely involved in tumor initiation and maintenance, providing the first evidence modulating LDH-A activity may be a viable strategy in cancer (Le et al., 2010). In parallel, it was determined by DNA footprinting that c-Myc regulates to several other glycolytic genes and promotes the Warburg effect (Kim et al., 2004).

Non-cell autonomous control of metabolism

Angiogenesis The discovery of angiogenesis and realization that tumors needed access to vasculature provided a foundation for understanding the metabolic requirements of cancer in the physiological setting. It had been proposed since 1939 that there was a factor specific to tumors that stimulated the growth of blood vessels and evidence was acquired for the existence of neovascularization by 1945 (Algire et al., 1945). By 1968, it had been discovered that a diffusible and filterable agent released by tumors could stimulate growth. While building an argument for the

existence of such factors, Folkman and colleagues systematically gathered evidence for the existence of this potential Tumor Angiogenesis Factor (TAF) and compiled it into a list that culminated in his seminal hypothesis that tumors growth is dependent on the formation of new blood vessels (Sherwood et al., 1971). Chief among these reasons was related to the acquisition of nutrients and his observation that "[tumors] enter a dormant phase because they are forced to live by simple diffusion of nutrients and wastes and that tumors required access of vasculature provide evidence that tumors need access to the blood supply to gain access to the nutrient supply" (Folkman, 1976). Folkman also noticed that small tumors formed frequently, but could not form in isolated perfused organs and that proper vascularization was essential to form tumors at distinct sites that were larger than 1–2 mm^3 (Folkman et al., 1963; Ribatti, 2008). However, what are these small lesions and what happens to tumors that lack access to nutrients oxygen?

Hypoxia inducible factor 1 (HIF-1α) In 1991 Gregg Semenza and colleagues discovered the transcription factor HIF-1α, the cellular oxygen sensor (Semenza et al., 1991). Subsequently, Semenza along with William Kaelin and Peter Ratcliffe would describe the molecular partners and regulation of this sensor (Thompson, 2016). HIF-1α-mediated oxygen sensing is fundamental at the organismal level for adaptations to altitudes with different oxygen tensions, and the role of HIF-1α has also played a critical role in our understanding of cancer biology and metabolism.

As an oxygen sensor, HIF-1α can exist in two states depending on oxygen levels. Under well-oxygenated conditions, HIF-1α is hydroxylated by prolyl hydroxylases (PHDs), which utilize molecular O_2 and α-ketoglutarate as substrates (Kaelin and Ratcliffe, 2008). This modification causes HIF-1α to bind to the von-Hippel-Lindau (VHL) tumor suppressor protein for degradation (Maxwell et al., 1999). Under hypoxia, HIF-1α is stabilized (Semenza, 2010) and exerts its function as a transcription factor to promote expression of several genes in glycolysis that results in elevated

glycolytic flux.

Upon stabilization, HIF-1α exerts some cell autonomous affects by regulating transcription of genes containing HIF-responsive elements (HREs). These include the glucose transporters, GLUT1 and GLUT3, and glycolytic enzymes including hexokinase I and II, aldolase, phosphoglycerate kinase, enolase, pyruvate kinase, and lactate dehydrogenase (reviewed in (Semenza et al., 1994)). Additionally, HIF-1α is a transcriptional transactivator of pyruvate dehydrogenase kinase (PDK1-4) govern mitochondrial glucose flux by directly phosphorylating and inactivating pyruvate dehydrogenase (PDH) (Semenza, 2010). Therefore, HIF-1α is partly responsible for the rewiring of cellular metabolism in conditions where oxygen is limiting.

HIF-1α is also capable of promoting expression of genes that result in non-cell autonomous responses upon cellular sensing of low molecular oxygen. HIF-1α was determined to regulate an angiogenic response through activating VEGFR (Brugarolas et al., 2003). Therefore, HIF-1α oxygen sensing function acts to to stimulate angiogensis, and to provided a molecular basis for Folkman's observations of tumor growth. Lactate generated as a consequence of hypoxia can reduce NDRG3 activity and prevent c-Raf activation, which is required for angiogenesis (Lee et al., 2015). Taken together, these data connect lactate levels, HIF-1α, and angiogenesis. How the function of different cell types is altered in low oxygen conditions or microenvironments with altered pH is not well studied owing to limitations in methodology.

2. identification of mutations in metabolic enzymes that are tumor suppressors and oncogenes

Metabolic enzymes as tumor suppressors

FOUR genes coding for enzymes of the tricarboxylic acid (TCA) cycle were initially implicated and

identified through genetic mapping. Mutations in three different subunits of enzymes in the succinate dehydrogenase (SDH) complex were first identified in pheochromocytoma and familial paraganglioma (Baysal et al., 2004; Niemann and Müller, 2000; Astuti et al., 2001). Mutations in fumarate hydratase (FH) were identified shortly after that in hereditary leiomyomatosis and renal cell cancer (Wei et al., 2006; Tomlinson et al., 2002). Both SDH and FH followed a genetic inheritance pattern in that was consistent with the distribution predicted by Knudson's two-hit hypothesis (Knudson, 1971).

Metabolic enzymes as oncogenes

Fatty acid synthase (FASN) *FASN* overexpression was originally implicated in prostate cancer (Baron et al., 2004) and experiments performed by Massimo Loda and colleagues demonstrated that overexpression of FASN was sufficient to drive the transformation of immortalized human prostate epithelial cells (Migita et al., 2009). FASN is the enzyme responsible for catalyzing the reaction to generate palmitate, a saturated fatty acid, from acetyl-CoA and is a critical enzyme in *de novo* lipogenesis (Liu et al., 2010). Inhibition of FASN through genetic and pharmacological approaches have been effective in pre-clinical models of prostate and ovarian cancers (Yoshii et al., 2013; Bauerschlag et al., 2015). A first-in-class FASN inhibitor (TVB-2640) is being used in an ongoing clinical trial in patients with non-small cell lung, breast, and ovarian cancers (Martinez-Outschoorn et al., 2016). While some cancer cells scavenge lipids (Currie et al., 2013), many cancer cells are highly dependent on de novo lipogenesis (Daniëls et al., 2014; Menendez and Lupu, 2007) and these cells may be especially sensitive to FASN inhibition.

Isocitrate dehydrogenase 1/2 (IDH1/2) Two new oncogenes emerged from a series of genomics efforts, beginning with an observation in glioblastoma multiforme. Isocitrate dehydrogenase 1 (*IDH1*), a cytosolic enzyme catalyzing the conversion of isocitrate and citrate, was first identified as a candidate oncogene after examining glioblastoma multiforme (Parsons et al., 2008). Subsequently, *IDH2* (the mitochondrial homolog of *IDH1*), mutations were found in gliomas (Yan et al., 2009). Mutations in *IDH1/2* genes were next determined to have neomorphic enzymatic activity and produce the oncometabolite, 2-hydroxyglutarate (2-HG) (Ward et al., 2010). Both *IDH1/2* mutations were discovered to be present in acute myelogenous leukemias (Mardis et al., 2009) and *IDH1* and *IDH2* have since been demonstrated to be mutated, albeit in low frequency, in cholangiocarcinomas, chondrosarcomas, and lymphomas (Kaelin and McKnight, 2013).

Phosphoglycerate dehydrogenase (PHGDH) Other efforts in genomics revealed copy number variants (amplifications) in an enzyme in the serine biosynthesis pathway phosphoglycerate dehydrogenase (*PHGDH*) that occur in breast cancer and melanoma (Possemato et al., 2011; Locasale et al., 2011). PHGDH catalyzes the first committed step of the serine biosynthesis pathway using the glycolytic precursor 3-phosphoglycerate (3PG) (Mullarky et al., 2011) Metabolites of serine, such as glycine and cysteine, can also contribute to the generation of the antioxidant glutathione and to one-carbon metabolism (Mattaini et al., 2016) through the transsulfuration pathway. It has further been suggested that *PHGDH* expression may be a driver of epigenetic status by generating one-carbon subunits for the maintenance of methylation (Locasale, 2013). Whether the expression of *PHGDH* is sufficient for transformation remains unknown.

3. causal roles for metabolite products in oncogenesis (oncometabolites)

2-hydroxyglutarate (2-HG), fumarate, and succinate The mechanisms by which metabolites are produced by the loss-of-function mutations of *FH* and *SDH*, or the gain-of-function mutations in IDH1/2 demonstrated a causal role for metabolites in tumorigenesis, and these have been coined "oncometabolites" (Dang et al., 2009). Mutations in *FH*, *SDH*, and *IDH* cause accumulation of the oncometabolites fumarate (Yang et al., 2012a), succinate (Xiao et al., 2012; Yang et al., 2012a), and 2-hydroxyglutarate, respectively, at millimolar levels (>10mM in some cases). The accumulation of these metabolites acts to affect the epigenetic state of the cell.

The discovery of point mutations in *IDH1/2* and the utilization of untargeted metabolomic analyses resulted in the discovery of the oncometabolite 2-HG. *IDH* normally catalyzes the reaction from isocitrate to α-ketoglutarate. Mutations in *IDH* result in enzymes with neomorphic activity, the activity of which converts α-ketoglutarate to 2-hydroxyglutarate (enantiomeric R-2-hydroxyglutarate has been determined to be the oncometabolite) (Frezza et al., 2010). *IDH1* and *-2* mutations have been shown to alter epigenetic status of cells through *TET2* 5-methylcytosine hydroxylase (Lu, 2013) and the jumonji (*JmjC*) histone demethylases (Cairns and Mak, 2013; Lu, 2013). Clinical trials are underway to inhibit the specific IDH1/2 mutant enzymes caused by mutations and have been met with initially promising success, particularly in leukemia. While accumulation of succinate and fumarate have similar epigenetic consequences (for review, see (Sullivan et al., 2016)), loss-of-function mutations in *FH* and *SDH* present the challenge of restoring enzymatic activity to reduce levels of these metabolites.

Acetate Further investigations of epigenetic modifications caused by metabolites produced in cancer cells have also been fueled by re-emerging interest in acetate metabolism. Many tumors exhibit increased acetate uptake, and ^{11}C and ^{18}F-labeled acetate PET probes have been useful clinical compounds for diagnostic purposes (Grassi et al., 2012). As a nutrient, acetate is converted

to acetyl-CoA and can be used as a nutrient to contribute to citrate and lipid biosynthesis (Hosios and Vander Heiden, 2014), particularly in response to hypoxia (Gao et al., 2016).

ACETATE LEVELS are further important for maintaining the epigenetic modification of acetylation of histones or proteins (Wellen and Thompson, 2012). Sirtuins are one important group of proteins at the center of energy balance, acetate, and cancer metabolism (Pietrocola et al., 2015). The expression of sirtuins were originally described to alter replicative lifespan in *Saccharomyces cerevisiae* in the lab of Leonard Guarente in 1991 (Kennedy et al., 1995). Seven mammalian orthologues (SIRT1-7) were subsequently identified and are NAD^+-dependent histone deacetylases and mono-[ADP-ribosyl] transferases. Sirtuins can regulate acetyl-CoA levels through their conserved function in regulating the expression of acetyl-CoA synthetase (AceCS), an enzyme that converts acetate to acetyl-CoA (North and Sinclair, 2007). How acetate, NAD^+/NADH ratios, and sirtuin expression are linked and affect different cancers remains incompletely understood. As the expression of sirtuins has been shown to play a role in a host of human diseases, and nearly every sirtuin has been shown to play a role in different hallmarks of cancer (for review, see (Chalkiadaki and Guarente, 2015)), this is an exciting area of investigation.

4. technological advances that enabled discoveries in cancer metabolism

Technological advances across many disciplines have enabled a systematic investigation of cancer metabolism. Our ability to measure metabolites with high-sensitivity, throughput, and mass-accuracy have enabled studies in cancer metabolism, and in particular, aided in the detection and discovery of 2-HG. Technological advances that have aided metabolic studies further include: (a) analytical platforms beginning with nuclear magnetic resonance spectroscopy (NMR) and evolving into modern day mass-spectrometric methods became available to interrogate metabolic

pathways in a high-throughput and quantitative manner. Systems biological approaches further facilitated the interpretation of data generated by these modalities. (b) advances in biochemistry and molecular biology have facilitated the ability to identify and characterize enzymes and place them in the context of signaling pathways (c) mouse models of cancer that faithfully recapitulate elements of the human disease (d) modern genome editing methodologies enable rapid determination of the consequences of genetically modifying metabolic enzymes in cell culture and animal models. Many of these tools have been utilized and will be discussed in greater detail in the sections and chapters to follow.

Oncogenic coordination of metabolism

ONCOPHENOTYPES OF GLUCOSE AND GLUTAMINE METABOLISM Cancer cells exhibit metabolic alterations to support rapid proliferation. Different metabolic phenotypes in cell lines have been attributed to specific genetic events associated with cancer. *KRAS* and *p53* are among the most mutated genes in cancer and clear links between oncogene expression, and metabolism has been observed in studies *in vitro*. As glucose and glutamine are consumed in far excess to any other nutrient by many cancer cell lines, many studies have emphasized understanding the differences in the metabolism of these nutrients, and we examine these nutrients in the context of KRAS activation or p53 mutation.

CONTEXT-DEPENDENCY OF METABOLIC ENZYMES We place extended emphasis on two examples of metabolic that play a role in glucose and glutamine metabolism which are the focus of subsequent chapters. In Chapter 2, we examine pyruvate carboxylase (Pcx) in mouse models of lung cancer and Chapter 4 we examine alternative isoform expression of pyruvate kinase (PK) in a mouse model of prostate cancer.

ALTERNATIVE SUBSTRATES Many amino acids besides glutamine are also important for cancer cell metabolism. These can come from exogenous sources (e.g. diet), are synthesized by the cell, or are acquired from intracellular and extracellular protein catabolism. We discuss endocytic pathway called macropinocytosis as a novel nutrient supply route for amino acids and other nutrients in *Kras*-driven pancreatic cancer in cell lines *in vitro* and discuss the potential relevance of macropinocytosis *in vivo* from the physiological and epidemiological perspective.

Oncophenotypes of glucose and glutamine metabolism

The "phenotype-first" approach While normal cells perform metabolism to maintain cellular homeostasis, cancer cells have increased demands to sustain proliferation. Research in cancer metabolism has frequently employed the "phenotype-first" approach to understanding how mutations in oncogenes or tumor suppressors alter metabolism to support chronic proliferation. The goals of many of these studies are to identify different metabolic phenotypes in cell lines as they are related to specific genetic events associated with cancer. Further, it is of interest to understand the general requirements of proliferative metabolism and to determine metabolic pathways or enzymes that may be amenable to therapeutic strategies.

Glucose metabolism

The current understanding of the "Warburg effect" The diversion of glucose metabolism toward lactate production, regardless of oxygen availability, is the best-described example of altered cancer cell metabolism ("the Warburg effect"). While the notion that these high levels of glycolysis are required to sustain ATP production has been dispelled (Zu and Guppy, 2004) and that mitochondria are not dysfunctional even required in some cases (Weinberg et al., 2010), why cancer performs this metabolic program remains incompletely understood. The currently favored hypothesis is that high levels of glycolysis result in shunting glucose-derived carbon into anabolic pathways, such as those required for the production of NADPH, nucleotides, and amino acids (Brand, 1985; Hsu and Sabatini, 2008; DeBerardinis et al., 2007; Lunt and Vander Heiden, 2011). Several glycolytic intermediates are diverted to fulfill these anabolic roles and the enzymes that catalyze reactions that have been shown to be overexpressed or exhibit preferential isoform

expression in many types of cancer. Carbon derived from glucose can be fully oxidized through mitochondrial oxidative phosphorylation or used for anaplerosis of the tricarboxylic acid (TCA) cycle. Despite our understanding of these pathways, glucose consumption seems to be in excess of calculated requirements in proliferating normal cells (Bauer et al., 2004) and cancer cells (DeBerardinis et al., 2008).

Elevated glucose uptake: glucose transporters and hexokinase Glycolysis is a highly allosterically regulated metabolic pathway consisting of ten reactions that convert glucose into pyruvate. Glucose is transported into cells by members of a class of thirteen facilitative glucose transporters (GLUTs) and subsequently phosphorylated by hexokinase (isoforms I-IV) to produce glucose-6-phosphate. Increased glucose uptake associated with the Warburg effect forms the basis for the use of FDG-PET scanning to stage some cancers (Fletcher et al., 2008). Three classes of GLUTs exist Class I (GLUT1-4), Class II (a fructose transporter GLUT5; and GLUT7,9,11), and Class III (GLUT6,8,10,12) (Macheda et al., 2005). Each class exhibits different affinities for hexoses such as glucose or fructose. Cancer cells commonly exhibit increases in expression in GLUT1, and GLUT1 is also a transcriptional target of HIF-1α (Okino et al., 1998). HKI and II are frequently overexpressed in many cancers, and this is the first committed step of glycolysis. In contrast to other HK isozymes, HKII is bound to the outer mitochondrial membrane and is not subject to allosteric regulation. The proximity to the mitochondria is thought to enable access to ATP to phosphorylate glucose and is the isoform that is preferentially expressed in many cancers (Bustamante and Pedersen, 1977).

Precursors for anabolic metabolism Glucose-6-phosphate, the product of the hexokinase, can be shunted into the *pentose phosphate pathway (PPP)* and diverted into either the oxidative or

non-oxidative branch to generate either NADPH or ribose-5-phosphate. NADPH is produced through the oxidative branch of the PPP and is used for fatty acid synthesis and also to scavenge reactive oxygen species. Ribose-5-phosphate is generated through the non-oxidative branch of the PPP and contributes to *de novo* nucleotide biosynthesis. Many cancers modulate flux through this pathway, including those driven by *RAS* and *p53* (Patra and Hay, 2014; Ngoh et al., 2011; Denzel et al., 2014).

FRUCTOSE-6-PHOSPHATE can be diverted into the PPP or the *hexosamine biosynthesis pathway (HBP)*. Flux through the hexosamine synthase pathway results in the production of N-acetylglucosamine (GlcNAc), and also requires acetyl-CoA and glutamine. GlcNAc is used for the post-translational modification of proteins and is also frequently altered in cancer (Ying et al., 2012; Cairns et al., 2011; Perera and Bardeesy, 2015). Beyond maintaining proper glycosylation of newly synthesized protein, non-metabolic roles for HBP are emerging. In some cases, this pathway seems required for maintaining signaling pathways under certain conditions or promoting malignant processes, such as epithelial to mesenchymal transition (EMT) through the production of UDP–GlcNAc (Jones et al., 2014; Taparra et al., 2016).

GLYCERALDEHYDE-3-PHOSPHATE can be converted to dihydroxyacetone phosphate and subsequently converted to glycerol, essential components of triacylglycerol and phospholipids. This node has been considered as a potential target in cancer metabolism, but how to best target GAPDH in cancer cells remains unclear (Krasnov et al., 2013). 3-phosphoglycerate can enter the *serine biosynthesis pathway* and either metabolized to glycine or cysteine, or to ceramide, a precursor for sphingomyelin, cerebroside, and gangliosides. The serine biosynthesis pathway also contributes significantly to one-carbon and folate metabolism which is required for DNA synthesis and maintenance of DNA methylation.

Reduction, oxidation, and anaplerosis Oxidation of glucose-derived carbon occurs through mitochondrial *oxidative phosphorylation* and generates pyruvate which can enter the mitochondria through the mitochondrial pyruvate carrier (MPC). After pyruvate enters the mitochondria, it is subsequently decarboxylated by the pyruvate dehydrogenase complex (PDH) to generate acetyl-CoA. Acetyl-CoA can be further metabolized for ATP or used for lipid production. Cancer cells in culture typically exhibit less oxidative flux than untransformed cells, and the fate of pyruvate in most cancer cells is lactate. The production of lactate through pyruvate is essential for NAD^+ regeneration to maintain glycolysis. Glucose carbon can also enter the mitochondria through pyruvate carboxylase (PC) in an *anaplerotic* reaction to generate the four-carbon TCA cycle intermediate oxaloacetate. Pyruvate carboxylase is discussed more in the section to follow.

Glutamine metabolism

Glutamine is consumed at high rates by cancer cells Most cancer cells in culture require glutamine to grow (Jain et al., 2012). Glutamine enters cells through glutamine transporters that are also frequently upregulated in cancer cells as a result of oncogenic signaling (Hensley et al., 2013). Glutamine contributes to many metabolic pathways by providing carbon and nitrogen for biosynthesis of nucleotides, lipids, and other amino acids. However, while glutamine plays many important roles, it has been determined that glutamine is consumed in far greater excess than what is required for nucleotide and lipid biosynthesis.

Precursor for energy and anabolic metabolism Glutamate enters the TCA cycle and proceeds both oxidatively and reductively, to support ATP synthesis and generation of citrate, respectively. Glutamine can support NADPH production in some cancers (DeBerardinis et al., 2007). NAPDH

production is important for nucleotide and lipid biosynthesis, and citrate made from the reduction of glutamine is also used to generate acetyl-CoA for lipid biosynthesis. Under hypoxic conditions, glutamine is the main contributing nutrient for the maintenance of anaplerosis and contributes a significant fraction of carbon to the TCA cycle.

Nitrogen metabolism In addition to providing carbon, glutamine acts as a nitrogen donor for the synthesis of amino acids, nucleotides, and hexosamines. Free glutamine is required for the synthesis of protein and can be directly incorporated into growing macromolecules and can also be converted to glutamate by the mitochondrial enzyme glutaminase (*Gls*). Glutamine also plays a major role in nitrogen metabolism by acting as a nitrogen donor. As a nitrogen donor, glutamine is essential for nitrogen in purine (PRPP and FGAM) and pyrimidine synthesis (CTP synthetase, CPSII). Glutamine can donate nitrogen to pyruvate or oxaloacetate to generate the non-essential amino acids alanine or aspartate, respectively. Aspartate is also a precursor for asparagine biosynthesis and glutamine also donates a nitrogen to this reaction (Hensley et al., 2013). Both glutamate and α-ketoglutarate generated by the process of glutamine catabolism (glutaminolysis) and can be used as nitrogen acceptors.

Conditionally essential It has also been demonstrated that the oxidation of glutamine is critical when the mitochondrial pyruvate transporter is blocked (Quek et al., 2016) or under conditions of low glucose. Interestingly, glutamine is uniquely essential for reasons that are unclear, and even other five-carbon backbone metabolites (proline, α-ketoglutarate) that can enter the TCA cycle cannot fully rescue glutamine deficiency. Therefore, these data seem to suggest a plausible role for glutamine in other fundamental cellular processes that may be independent of its role as a nutrient.

Analogs for therapy Glutamine analogs such as Acivin, 6-diazo-6-oxo-L-norleucine, Azaserine, and γ-glutamyl hydroxamate have been used clinically in combination with chemotherapy, but have been met with limited success and in most cases exhibit neuro- and gastrointestinal toxicity (Bhutia et al., 2015). As many normal cells and organs require glutamine as a substrate, the utility in glutamine analogs derives most utility for potential tumor detection properties using imaging modalities such as PET (Venneti et al., 2015).

Oncogenic *KRAS* in cancer and metabolism

Overview *RAS* is the second most commonly mutated gene in cancer and is found in approximately 20% of all human cancers, with highest mutational frequency observed in the pancreas, colon, and lung (Bos, 1989). As a monomeric GTPase, *RAS* is principally regulated by the activity of is regulated by guanine nucleotide exchange factors (GEFs) *SOS1* and *SOS2* which catalyze the GTP-bound "ON" state (Downward, 2003). When *RAS* is in the GTP-bound state, it is active and signals to the downstream effector pathways. In contrast, *RAS* can be turned to the GDP-bound "OFF" state by GTPase activating proteins (GAPs) (Konstantinopoulos et al., 2007). Guanine disassociation factors (GDIs) can also play a role in regulating the activity of *RAS* (Vigil et al., 2010). *RAS* proteins are post-translationally modified by farnesylation or geranylgeranylation allowing for incorporation to the inner face of the cell membrane (Konstantinopoulos et al., 2007).

Oncogenic activation Gain-of-function mutations in *RAS* due to single point mutations in positions 12, 13, or 61 are observed with mutations coding for single amino acid substitutions (Stolze et al., 2015), such as those commonly found at position 12 which result in glycine to valine, aspartic acid, or cysteine (G12V, G12D, and G12C, respectively). These mutations result in *RAS*

that is in a constitutively GTP-bound "ON" state and results in constitutive signaling to downstream effector pathways. *RAS* has many effector pathways, and activation of these pathways have been implicated in having metabolic consequences, such as PI(3)-kinase pathway and downstream MAPK pathways (for reviews see (Mendoza et al., 2011; Vigil et al., 2010)).

RAS and glucose metabolism Several studies have characterized glucose metabolism in NIH-3T3 mouse fibroblasts expressing oncogenic $Kras^{G12V}$ (Baracca et al., 2010; Chiaradonna et al., 2006). *Kras*-transformed cells in this setting exhibit classical features of the Warburg effect. These include: increased sensitivity to low glucose; upregulation of GLUT1 expression and glucose uptake (Yun et al., 2009; Flier et al., 1987); increased aerobic glycolysis (Baracca et al., 2010); elevated glucose uptake and aerobic glycolysis (Baracca et al., 2010); increased lactate production (Gaglio et al., 2011); decreased oxidative phosphorylation; decreased mitochondrial Complex I function (Baracca et al., 2010); and decreased oxidation of pyruvate to Acetyl-CoA (Gaglio et al., 2011).

The consequences of *Kras* activation on metabolism has been studied in the setting of pancreatic cancer *in vivo*. Using an inducible allele of $Kras^{G12D}$ (iKras), Ying et al. (2012) examined gene expression and metabolomic data from arising tumor and normal pancreas. These studies revealed that expression of $Kras^{G12D}$ resulted in an elevated flux through the hexosamine biosynthesis pathway (Ying et al., 2012). This mouse model exhibited many changes in gene expression and metabolomic profiles that are consistent with those changes observed in culture and with the Warburg effect (Ying et al., 2012).

Ras and glutamine metabolism $Kras^{G12V}$ transformed mouse fibroblasts rely on glutamine to fuel the TCA cycle. Careful tracing studies demonstrate that the cells are more sensitive to glutamine deprivation than untransformed cells and use carbon and nitrogen from glutamine for the synthesis

of amino acids and nucleotides (Gaglio et al., 2011). Glutamine metabolism has also been demonstrated to be important in a *Kras*-driven pancreatic cancer model *in vitro* and *in vivo*. One recent study demonstrated that (*GOT1*) increased while glutamate dehydrogenase (*GLUD1*) decreases as a function of *Kras* expression. GLUD1 converts glutamate into α-ketoglutarate, while GOT1 is required for the transamination of glutamate to aspartate. (Son et al., 2013). Genetic knockdown of either GOT1 or GLUD1 resulted in increased levels of reactive oxygen species and depleted levels of reduced gluathione. These findings suggest that *Kras* transformed cells rely on and reprogram glutamine metabolism and that this reprogrammed metabolism helps contribute aspartate and glutathione biosynthesis.

Ras, ROS, and mitochondrial function Kras-transformed cells exhibit dysfunctional mitochondrial metabolism. Through gene expression analysis, it was determined that genes encoding mitochondrial Complex I was repressed upon *Kras* activation (Baracca et al., 2010). As a result of Complex I repression, ROS levels increase, and this feature in cancer cells is a critical event for cellular transformation in some contexts (Weinberg et al., 2010). *Kras* transformed cell lines are also dependent on glutamine for a source of anaplerotic TCA cycle metabolism and the production of glutathione. Upon activation of an inducible allele for $KRAS^{G12V}$, human pancreatic duct epithelial cell (HPDE) cells exhibit high levels of ROS (Hu et al., 2012), and in contrast to the untransformed line, can form tumors *in vivo*. In addition to increased ROS levels, mitochondrial dysfunction can cause Akt activation and subsequently increase levels of HKII (Hu et al., 2012). The increase in ROS levels can stimulate *HIF-1α* ("pseudohypoxia") response through redox-regulated factors *p53, AP1, NRF2, and NF- KB* (Sabharwal and Schumacker, 2014). Also *HIF-1α* is a transcriptional transactivator of pyruvate dehydrogenase kinase 1 (PDK1) which phosphorylates and inactivates pyruvate dehydrogenase E1α, (*PDH-E1α*), an essential member of

the come PDH complex. Along with the transcriptional activities of *HIF-1α*, inactivation of PDH is thought to be partially responsible for the diversion of glucose to lactate observed in cancer cells.

The tumor suppressor, *TP53*, in cancer and metabolism

Overview The tumor suppressor *TP53* (hereafter, *p53*) is the most commonly mutated gene in all cancer, with somatic missense mutations seen in approximately 50% of all cases (Soussi and Wiman, 2007). P53 is a pleiotropic transcription factor involved in numerous cellular stress responses (Vousden and Ryan, 2009). Under normal conditions is an unstable protein with a short half-life as a result of constitutive degradation by *MDM2*, a *p53*-specific E3 ubiquitin ligase (Soussi and Wiman, 2007). p53 exists in the tetrameric, dimeric, or monomeric state and performs its transcriptional activity in the tetrameric state. Numerous stress signals can trigger the activation and stabilization of p53 including DNA damage (Serrano et al., 1997), oncogene activation (Serrano et al., 1997), hypoxia, metabolic stress (Kruiswijk et al., 2015). Any of these signals can act to stabilize *p53* and cause cell-cycle arrest, apoptosis, or senescence programs (Brosh and Rotter, 2009).

Consequences of p53 mutation The most common *p53* mutations are point mutations which cause dominant-negative activity and result in loss of *p53* function. Indeed, *p53* was originally characterized as an oncogene for this gain-of-function activity (Soussi, 2010). *p53* has three functional domains: A transactivation and proline-rich domain at the N-terminal region, a DNA-binding domain in the middle of the protein, and tetramerization and regulatory regions located at the C-terminus. Point mutations frequently occur in the DNA-binding domain, and this domain is primarily responsible for the tumor suppressive activity of *p53* (Pavletich et al., 1993). In mouse models, point mutations in one allele of *p53* frequently result in genomic instability (Shao

et al., 2000), and these point mutations can further lead to the loss of heterozygosity through gene conversion (C. and Monica, 1993). Indirect mechanisms, such as amplification or overexpression of *MDM2* also result in the loss of *p53* function. For example, increased MDM2 expression has been observed in human papillomavirus (HPV)-related cancers, such as cervical cancer (Olivier et al., 2010). More directly, the E6 protein of HPV can bind to p53, causing rapid ubiquitination and subsequent degradation of the E6-AP p53 complex (Mantovani and Banks, 2001).

p53 and glucose metabolism The positive and negative transcriptional activities of p53 have been shown to play a major role in glucose metabolism in cancer. The normal role and expression of p53 results in the repression glucose metabolism through its activity as a transcription factor. The expression of the glucose transporter *GLUT1* (Zhang et al., 2014) and another glycolytic enzyme, phosphoglycerate mutase (*PGM*) (Puzio-Kuter, 2011), are repressed by p53. Flux through glycolysis can also be modulated by the p53 target *TIGAR* (Tp53-Inducible Glycolysis and Apoptosis Regulator). *TIGAR* was originally identified through the time-course microarray analysis of p53 induction and exhibited changes in expression that were similar to the kinetics of other p53 transcriptional targets (Nakano et al., 2000). This gene was subsequently determined (and named *TIGAR*) to play a role in metabolism by acting as a fructose-2,6-bisphosphatase by Karen Vousden and colleagues in 2006 (Bensaad et al., 2006). Thus, when *TIGAR* is expressed, levels of fructose-2,6-bisphosphate (Fru-2,6-P2) decrease inside of the cell. Fru-2,6-P2 levels act to allosterically activate the enzyme phosphofructokinase, the second enzyme of glycolysis. Under conditions of stress, *TIGAR* is activated by p53 fructose-2,6-bisphosphate (Fru-2,6-P2), resulting in repression of phosphofructokinase. Loss-of-function mutations in *p53* lead to reduced *TIGAR* expression and can cause high levels of (Fru-2,6-P2), thereby resulting in the allosteric activation of phosphofructokinase. Taken together, p53 loss-of-function mutations results in derepression of

glucose transporters and glycolytic enzymes, and this results in elevated glycolytic flux.

p53 and glutamine metabolism Glutaminase 2 (*GLS2*) has been demonstrated to be a direct transcriptional target of p53 (Hu et al., 2010; Locasale and Cantley, 2010). Interestingly *GLS2* has been shown to be correlated with senescence. While glutaminase (*GLS1*) has been correlated with upregulation in many cancers (Pérez-Gómez et al., 2005), the expression of both glutaminase isozymes has not been extensively characterized in tumors as a function of p53 status. It has been demonstrated that p53 is also essential for growth and adaptation to low glutamine conditions, but the metabolic program p53 promotes under these conditions has not been well characterized (Reid et al., 2013).

p53, ROS, and mitochondrial function In addition to activating glycolysis, p53 loss-of-function also results in direct mitochondrial consequences. Under normal conditions, p53 regulates mitochondrial respiration through the upregulation of the cytochrome c oxidase 2 (*SCO2*) gene required for cytochrome c oxidase complex. This complex is an essential component of the electron transport chain between Complex III and Complex IV. p53 is also thought to regulate Complex I activity of the mitochondria through its activity as a transcription factor (Seth et al., 2005).

Oncogenic *MYC* in cancer and metabolism

Glutamine addicts Numerous other efforts have been made to ascribe metabolic phenotypes to certain oncogenic events, especially examining the proto-oncogene *MYC*. Although *PKM2* was the first directly targeted enzyme by an oncogenic process, *LHDA* was the first observed metabolic enzyme determined to be regulated by *MYC* expression (Shim et al., 1997). For cells with *MYC*

amplification, metabolic hallmarks of this cancer include upregulation of the glutamine transporter *SLC1A5*, upregulation of enzymes required for glutaminolysis, and microRNA expression which normally act to suppress glutaminase activity. Numerous studies have demonstrated that *MYC* can promote glutamine metabolism in cells (Wise and Thompson, 2010). The neutral amino acid transporter *SLC1A5*, a major transporter for glutamine uptake, is upregulated following oncogenic *MYC* expression, and *c-Myc* suppresses the microRNA *mIR23a/b* to promote glutaminase (*Gls*) expression and glutamine consumption (Gao et al., 2009). Both glutamine and glutamate are important nitrogen sources for anabolic metabolism, but in many cells, glutamine is consumed in far greater excess than predicted for the nitrogen requirement. This hypermetabolism explained at least in part by the metabolism of glutamine-derived carbon to fuel the TCA cycle and support mitochondrial ATP production as well as to supply important precursors for biosynthesis (Metallo et al., 2011; Wise and Thompson, 2010). The exact role glutamine metabolism plays in cancer cells is still debated and is likely context-dependent; however, it is clear that many cancer cells require glutamine for growth.

Summary of oncogenic influence on metabolism

Most cancer cells use aerobic glycolysis in vitro The summary of this work, primarily examining cancer metabolism *in vitro*, is that these oncogenes do elicit tumor-autonomous metabolic functions and the highly controlled genetic systems have facilitated our understanding of these events. In general, the most common glycolytic enzymes altered by oncogenic mutations that are promising for therapy include *PKM2*, *GLU1*, *HKII*, *PHGDH*, and *LDH-A* (Hamanaka and Chandel, 2012). Glutaminolysis has also been a major focus as many cells are dependent on glutamine in culture and several drugs to inhibit glutaminase and the analogs mentioned above are currently in clinical trials.

Studies in culture demonstrate that *RAS* and *P53* act through different mechanisms to promote the Warburg effect. *KRAS* seems to exert many of its metabolic activities through the stabilization of *HIF-1α*. Ectopic expression oncogenic-*RAS* promotes a state that causes a switch from oxidative phosphorylation to aerobic glycolysis. These findings collectively demonstrate *RAS* to perform a metabolic program that is quintessentially Warburg-like.

Two additional conclusions arose from investigations of cells in culture with mutant *Kras*. First, *HIF-1α* expression and activity in the presence of oxygen was surprising at the time given the presence of oxygen. The pseudohypoxic response is not fully understood, nor is the nature of the ROS species that promotes this state. Current data suggest that ROS in this setting is generated through Complex I suppression and therefore likely to be H_2O_2. Second, a careful observation of data from one study revealed that glucose and glutamine failed to account for all of the carbon that contributes to the TCA cycle (Gaglio et al., 2011). This was unexpected, as consumption of these two nutrients far exceeds consumption of any other nutrient in most cancer cell lines in culture. We will discuss alternative substrates for these cells in the section to follow.

p53 loss-of-function and gain-of-function mutations result in a metabolic program that is consistent with the Warburg effect through the loss-of-function of its normal transcriptional activities. Normal transcription of canonical and recently discovered p53 targets results in the repression of glycolysis and increases oxidative phosphorylation. Therefore, loss-of-function p53 mutations have been shown to down-regulate oxidative phosphorylation and promote high levels of glucose uptake and glycolytic activity (Kruiswijk et al., 2015). As p53 is a pleiotropic transcription factor, it is probable that some metabolic consequences are either epiphenomenal or the result of other cellular processes that have been altered in response to p53 mutations. The connection between how antioxidants act to promote tumorigenesis or prevent tumorigenesis remains even less clear.

Targeting essential tumor-specific metabolic processes represent a powerful approach to treating cancer. *RAS* and *p53* mutations are among the most common mutations in cancer, and mutations in these genes present unique therapeutic challenges. *RAS* has earned the reputation of being "undruggable" (Cox et al., 2014). A recent discovery of the small-molecule, rigosertib is in Phase III clinical trials for myelodysplastic syndromes (for phase I results, see (Komrokji et al., 2013)), should inform this notion (Athuluri-Divakar et al., 2016). Whether *RAS* can be targeted directly remains to be determined. Targeting *p53* from the angle of inducing or maintaining cellular senescence has been viewed as an attractive approach (Pérez-Mancera et al., 2014; Kuilman et al., 2010), but how to best do this pharmacologically from the metabolic perspective is not yet clear. While each oncogene or tumor suppressor gene stimulate different effector pathways or activate transcriptional targets, limiting metabolic components of proliferation may be shared by some cancers.

Context-dependency of enzymes in glucose and glutamine metabolism

The pyruvate node Pyruvate is the final metabolite of glycolysis and is a significant crossroad metabolite. Cytosolic pyruvate can be reduced to lactate through lactate dehydrogenase (LDH). Pyruvate can also be shuttled from the cytosol into the mitochondria by the mitochondrial pyruvate carrier (MPC) and subsequently transaminated to alanine by alanine aminotransferases (ALT), carboxylated to oxaloacetate through pyruvate carboxylase (PC), or converted to acetyl-CoA through the pyruvate dehydrogenase complex. The products of pyruvate metabolism contribute to carbohydrate metabolism, lipogenesis, gluconeogenesis, and amino acid metabolism and the activity of the pyruvate node is dynamic and dependent on the rate of glycolysis. Pyruvate and lactate levels in the surrounding culture medium or microenvironment also influence pyruvate metabolism and directionality of the monocarboxylate transporters (MCTs) which can serve as either importers

or exporters of both pyruvate and lactate. In most cases, the largest pool of pyruvate is generated through glycolytic flux.

Mitochondrial pyruvate carrier Once pyruvate is made through PK, lactate dehydrogenase catalyzes the reduction of pyruvate into lactate in the cytosol. The existence of a mitochondrial pyruvate transporter (MPC) had been posited from observations with studies demonstrating that mitochondrial import of pyruvate. This was assessed through the observations that pyruvate oxidation and pyruvate-dependent CO_2 fixation was inhibited at micromolar concentrations by the compound α-cyano-4-hydroxycinnamate (Halestrap and Denton, 1974). Building on this knowledge, the highly conserved mitochondrial pyruvate carrier was recently discovered (Herzig et al., 2012; Hsin et al., 2012). A remarkable amount of work has already been done characterizing this transporter and it has so far been shown to play a role in promoting the Warburg effect (Schell et al., 2014). Interestingly, when the MPC is blocked, cancer cells also become dependent on glutamine consumption (Yang et al., 2014a).

Pyruvate carboxylase

Pyruvate carboxylase (PC, human; Pcx, mouse; EC 6.4.1.1) was discovered while defining other enzymes of gluconeogenesis in 1960 by Merton Utter and Bruce Keech based on an activity found in extracts of chicken and beef livers that they observed to catalyze the formation of oxaloacetate from pyruvate and CO_2 (Utter and Keech, 1960). The overall reaction catalyzed by PC is:

$$\text{Pyruvate} + HCO_3^- + \text{ATP} \xrightarrow[\text{acetyl}-\text{CoA}]{Mg^{2+},} \text{Oxaloacetate} + \text{ADP} + P_i$$

Allosteric interactions In mammals, pyruvate carboxylase is active in the homotetrameric configuration, is composed of four identical subunits of approximately 120kDa, and is located in the mitochondrial matrix (Wallace, 2010). PC is allosterically activated by acetyl-CoA, and this facilitates biotin prosthetic group interactions, which is required as a critical co-factor for the first part of two partial reactions.

Role in normal cells in vivo While PC was originally described by examining gluconeogenesis, it has since been observed to play fundamental roles in anaplerosis of the citric acid cycle, lipogenesis, and glyceroneogenesis (Wallace, 2010). PC is highly expressed throughout the body with highest expression levels observed in the brain and pancreatic islets, kidney, liver, and muscle. PC is essential for gluconeogenesis particularly under fasting conditions where gluconeogenesis accounts for nearly all glucose production (Rothman et al., 1991). In the brain, it is thought that PC is essential for the synthesis of glutamine by astrocytes to maintain the activity of the glutamate/glutamine cycle and for generating precursors for nutrients required for myelination (Chrast et al., 2011). In the pancreatic islets, PC governs insulin secretion in pancreatic β-cells (Schuit et al., 2001). Outside of the specialized role of lipid production for myelination in the brain and its role in the liver and kidney in sustaining gluconeogenesis, most other tissue types rely on PC for anaplerosis of the TCA cycle.

Role in cancer in vitro In cancer, as PC can play an important role in maintaining anaplerotic

flux into the TCA cycle in the normal setting, it would be reasonable to hypothesize that this enzyme may play a role in promoting anabolic growth. However, the importance of pyruvate carboxylase activity *in vitro* has not been well established. Multiple studies using ^{13}C based NMR methodology showed that PC activity is low in most cancer cell lines in culture (Cheng et al., 2011). PC plays a compensatory role in anaplerosis upon *Gls1* knockdown and was further shown to predict resistance to glutamine depletion (Cheng et al., 2011). Conclusions from these studies reasonably suggest that cancer cells in culture can use PC as an alternative mechanism fuel anaplerosis under low-glutamine conditions. However, typically flux through PC is thought to be a minor contributor to anaplerosis when compared to glutamine *in vitro*.

Role in cancer in vivo The role for PC in cancer has been more interesting *in vivo*. At the time of beginning this work, emerging evidence from multiple studies using stable isotope tracers observed labeling patterns that were indicative that PC was in different cancer settings, including lung and glioma (Yuneva et al., 2012; Maher et al., 2012). However, while these studies observed expression and metabolite labeling that was consistent with PC activity, one limitation of these studies was a lack of functional experiments to determine whether PC activity contributed to oncogenic processes. Furthermore, if the mechanism for preferential use of PC by cancer cells is glutamine independence as concluded from *in vitro* studies, it is not clear why tumors would prefer this method as glutamine is the most abundant amino acid in the body.

Therapy Multiple drugs have been developed to inhibit pyruvate carboxylase function and act by exploiting allosteric properties (reviewed in (Zeczycki et al., 2010)) or by directly modulating expression levels with anti-sense oligonucleotides (Kumashiro et al., 2013). However, many of the small molecules developed suffer from non-optimal pharmacokinetic and pharmacodynamic

properties to achieve efficacious therapeutic concentrations. We extend the discussion on PC in Chapter 2, where functional data demonstrate that PC is essential for lung tumor formation in a mouse model of lung cancer and speculate further on the available small-molecules in the context of therapeutic strategy.

Pyruvate kinase

Pyruvate kinase (PK, EC 2.7.1.40) was one of the first glycolytic enzymes discovered (Parnas JK, Ostern P, 1934). The amino acid sequence for PK is highly conserved in mammals and has orthologues in most known organisms (Jurica et al., 1998). PK catalyzes the reaction from phosphoenolpyruvate (PEP) to pyruvate while generating 2 ATP per molecule of glucose.

$$\text{ADP} + \text{phosphenolpyruvate} \longrightarrow \text{ATP} + \text{pyruvate}$$

Alternative splicing and isoform expression In mammals, PK is encoded for by two different genes, *PKLR* and *PKM* and these genes give rise to four gene products through mutually exclusive exon splicing. *PKLR* encodes *PKL* and *PKR*. *PKL* is predominantly expressed in the liver, with some expression observed in cells of the kidney and intestine while *PKR* is expressed in erythrocytes (Noguchi et al., 1987). *PKLR* has not been extensively studied in cancer and is not further discussed here. *PKM* encodes *PKM1* and *PKM2*, and the expression of these isoforms has been extensively studied in normal and malignant tissues in mouse and human. PKM splicing is governed by the concentration of the splicing repressors *hnRNPA1/2* that are activated by *c-Myc*. hnRNPA1/2 and another protein, polypyrimidine-tract binding protein (PTB), bind and recognize

a splice site that is downstream of exon nine (Chen et al., 2012). As *PKM1* retains exon nine, binding by high concentrations of splicing factors promote *PKM2* expression. (Takenaka et al., 1996). A rigorous examination of *PKM* isoform expression was performed in the mouse. *PKM1* has highest and almost exclusive expression in the heart, skeletal muscle, smooth muscle, and brain. *PKM2* has highest and nearly exclusive expression in the kidney, white adipose tissue, lung, lymphocytes, thymus, spleen, ovaries, testis. All other tissues exhibit a mixture of both *PKM1* and *PKM2* (Dayton et al., 2016). The function of preferential isoform expression at the organ level is unknown, although speculatively, it appears that *PKM2* is also expressed at high levels in cells that are responsible for biosynthetic processes, such as the choroid plexus in the brain, which contains cells that produce cerebrospinal fluid (Dayton, communication).

Allosteric interactions PK exists as a monomer, homodimer, or homotetramer, with each monomer of about 56kDa and exhibits the highest activity in the tetrameric form. *PKM1* is found in cells almost exclusively as a homotetramer. *PKM2* exists in cells as a monomer, dimer, or tetramer and is subject to numerous allosteric regulators that can promote tetramerization or act through other mechanisms to elicit high activity. The most well characterized are fructose-1,6,-bisphosphate which acts by binding the dimer-dimer interface to stablize the tetrameric state (Murcott et al., 1992). Other endogenous activators include the nucleotide intermediate SAICAR (Keller et al., 2012) and serine (Chaneton et al., 2012) but the mechanism of how these activate Pkm2 remain less well understood. Pkm2 can also be inhibited post-translationally in several ways, including inhibition of tyrosine phosphorylation of y^{105} (Hitosugi et al., 2010) and autophagic degradation by acetylation (Lv et al., 2011).

Role in cancer in vitro The M2 splice isoform of pyruvate kinase is preferentially expressed in

most cancer cell lines examined. These studies also highlight the importance of low PK-total activity for tumor growth (Christofk et al., 2008a). This data has further been corroborated in mouse embryonic fibroblasts (MEFs) made from genetically engineered mice harboring a $Pkm2^{fl/fl}$ conditional allele. In this system, *Pkm2* deletion in mouse embryonic fibroblasts (MEFs) results in *Pkm1* expression and cells exhibit proliferative arrest (quiescence) (Lunt et al., 2015). To better understand the mechanism of proliferative arrest, metabolomics was conducted. These experiments revealed reduced nucleotides and nucleotide bases upon *Pkm2* deletion. Low nucleotide base levels were determined to be the limiting nutrient for proliferation, and upon addition of exogenous nucleotides, this proliferative defect was strongly rescued. These studies support the model that low *Pk* activity promote anabolic metabolism, particularly with respect to nucleotide biosynthesis, and enable cellular proliferation.

Role in cancer in vivo Studies in mouse models have yielded less clear results for the involvement of *Pkm2* in cancer. Mice harboring the same conditional alleles for Pkm2 ($Pkm^{fl/fl}$) were crossed to a *Brca1;p53*-driven mouse model of breast cancer. Tumors in this mouse were examined to have the deletion of *Pkm2* as predicted, but unexpectedly, did not express any *Pkm1*. The lack of *Pkm1* is inconsistent with predictions based on previously observed expression levels, where compensatory isoform expression is observed. These tumors were, therefore, *Pkm*-total null tumors (Israelsen, 2014). While inconsistent with our hypothesis that *Pkm2* expression is required for tumor growth, this finding is consistent with the model that low (and in the case, no) pyruvate kinase activity promotes tumorigenesis. We have also created *Pkm*-null cell lines which are viable and proliferate in culture, yet express no gene products of either *Pkm* or *Pklr* (Davidson, unpublished). In another surprising study, it was determined that germline deletion of *Pkm2* gives rise to liver tumors with high penetrance. As the liver does not normally express *Pkm2*, these data suggest the possibility

that non-cell autonomous mechanisms create whole animal metabolic stress. Indeed, many features of this mouse model are similar to the human disease, including the formation of steatotic lesions that progress to hepatocellular carcinoma (Dayton et al., 2016). These findings taken together highlight the importance and diverse consequences of pyruvate kinase expression and activity in cancer cells and normal cells.

Alternative functions Many alternative activities of pyruvate kinase have been described. In addition to its role as a metabolic enzyme, a number of papers have appeared examining the possibility that *Pkm2* can act as a moonlighting transcription factor that acts to stimulate β-catenin expression (Liang et al., 2016; Yang et al., 2012b; Luo et al., 2011). These findings are of great interest and further disentangling any metabolic role from these alternative roles will be an important area of research. Several other papers have also emerged to show that in addition to kinase for PEP, PK can also directly act as a protein kinase and phosphorylate other proteins (Yang et al., 2012b). Work from our lab suggests the previous observations may be due to contaminating ATP that was regenerated by pyruvate kinase (Hosios et al., 2015).

PKM2 regulation enables anabolic metabolism Our lab has suggested that Pkm2 is the preferential isoform expressed in cancer because it can be subjected to numerous allosteric regulations, depending on endogenous metabolite levels in the cell, that reflect nutrient availability (Gui et al., 2013; Wong et al., 2013). The overall theme from studies to date is that low PK activity promotes tumorigenesis by promoting anabolic metabolism through complete deletion of total pyruvate kinase or selective expression of Pkm2. The final and most interesting element about pyruvate kinase biology is the observation that there may be an alternative activity, but this enzyme has yet to be purified (Vander Heiden et al., 2010).

Pharmacological activation of PKM2 for cancer therapy Several small-molecules have been developed to activate or inhibit PK activity (Yacovan et al., 2012; Anastasiou et al., 2012; Walsh et al., 2011). Some Pkm2 activators have been shown to create non-canonical activation by binding the dimer-dimer interface that is not occupied by fructose-1,6-bisphophate to promote tetramerization (Anastasiou et al., 2012; Walsh et al., 2011). Using of one of these activators, TEPP-46, xenograft tumors exhibited regression and a metabolite profile that was consistent with high PK activity, including low serine levels and decreased lactate production (Anastasiou et al., 2012). Interest in Pkm2 as a therapeutic target waned as further studies *in vivo* demonstrated that Pkm2 is dispensable for tumor growth in both Hct116 cells (Cortés-Cros et al., 2013) and a *Brca1* breast cancer model (Israelsen et al., 2013). Although these activators seem promising from the chemical perspective, it remains of great interest to determine tumor contexts that promote high expression levels of Pkm2.

Alternative substrates

Cancer cells use amino acids for energy and biosynthesis Glucose and glutamine are a major source of both carbon and nitrogen that supports tumor growth, but how cancer cells proliferate with the limited delivery of glucose and other nutrients via the vasculature is a critical question. The commonly studied nutrients consisting of glucose, glutamine, and lipids cannot account for total *de novo* lipid, protein, and nucleotide biosynthesis, further suggesting that tumor cells rely on unidentified alternative substrate(s) (Gaglio et al., 2011). Additionally, it is now clear that most of the biomass in cancers comes from amino acids (Hosios et al., 2016). Quantitative analyses demonstrate that amino acids are primarily used for the synthesis of proteins, but they also serve as a source of energy upon deamination and oxidation. Eleven amino acids can be synthesized by the

cell itself, while nine amino acids remain essential and are derived from the diet. These essential amino acids include the branched-chain amino acids, isoleucine, leucine, and valine, in addition to methionine, phenylalanine, tyrosine, histidine, lysine, and threonine. Amino acids are consumed at high levels by cells. In particular, glycine has been shown to be highly utilized by cells in culture (Jain et al., 2012). The source of free amino acids in cancer cells *in vivo* is incompletely described.

Autophagy Bulk degradation of intracellular proteins is one possible source of amino acids and nutrients. In the developing embryo of mammals, it has been shown that genes that promote the intracellular recycling process of autophagy are required. *ATG5* and *-7* null mice do not develop past the embryo stage and it has been suggested that this is due to amino acid deficiencies observed in neonates which allow for energy maintenance (Kuma et al., 2004). These genes involved in autophagy have been intimately linked to many cancers, highlighting the importance of autophagy and the possibility that autophagy may also serve to provide nutrients to these cells. These opposing roles of autophagy in cancer are discussed further in Chapter 5.

Macropinocytosis

Discovery and early observations of pinocytosis In 1929, Warren H. Lewis entered the world of cell culture as it was being developed. He was most fascinated by cell morphology and mechanics. To better observe these processes, he began to observe macrophages in culture by filming them and speeding up the videos. In one of these first attempts at time-lapse microscopy, Lewis noted that cells were taking up fluid droplets from the surrounding medium at a remarkable rate: almost one-third of their volume per hour (Lewis, 1937). However, the function of this bulk fluid uptake by cells in culture remained unclear.

In 1937, Lewis examined malignant sarcomas from rat and mouse cells and defined the process of pinocytosis in greater detail. From these recordings of tumor cells, Lewis initially described the order of events by which pinocytosis occurs:

1. Pinocytosis never takes place unless there are ruffle pseudopodia, and not always then.
2. When globules are first taken in they are entirely enclosed by surface membrane...globules when first taken in vary greatly with size. Often several fuse quickly to form larger ones.
3. ...where ruffle pseudopodia are active, one can see that globules taken in general, move centrally, often fuse, and finally shrink and disappear.
4. Almost immediately after globules enter the cell they begin to move more or less centrally; they may shift about somewhat...They finally reach the central part of the cell in the neighborhood of or close to the nucleus, but rarely touch it (Lewis, 1937).

Growth factor and oncogenic stimulation In the course of discovering epidermal growth factor (EGF), Stanley Cohen and colleagues were looking for a cell-free system to develop an assay to test the binding properties of his radiolabeled EGF. Cohen and colleagues began using membranes purified from human squamous carcinoma cell (A431), as they had been shown to have orders of magnitude more receptors than normal cells (Cohen, 2004). Using these cells, Cohen first demonstrated that the addition of EGF induced a rapid change in membrane structure (Chinkers et al., 1979). In a subsequent observation, he discovered pinocytosis could be stimulated and occurred at high levels with EGF addition (Haigler et al., 1979). Further studies confirmed Cohen's findings in these cell lines, and it was hypothesized that macropinocytosis was a distinct endocytic pathway (West et al., 1989). In addition to growth factors, phorbol esters and diacylglycerols have also been demonstrated to stimulate macropinocytosis in normal or quiescent cells (Swanson and Watts, 1995).

In 1986, Dafna Bar-Sagi demonstrated that ectopic expression of oncogenic H-ras^{G12V} was

sufficient to activate high levels of constitutive pinocytosis upon expression in rat embryonic fibroblasts (Bar-Sagi and Feramisco, 1986). Ras was confirmed to be sufficient for macropinocytosis induction in these experiments by microinjection of an anti-Ras antibody, which inhibited pinocytosis (Bar-Sagi et al., 1987). In the years to follow, it was determined that other oncogenes could activate constitutive macropinocytosis, including *v-Src* (Veithen et al., 1996). Signaling pathways that activate *PI3K*, such as in *RAS* or *Pten*-mutated tumors may perform this activity due to the initial membrane ruffling associated with macropinocytosis.

> "It is scarcely conceivable that this does not play an important role in modifying and keeping the tissue juices in proper condition, and perhaps supplying certain split products to other cells."
>
> - W.H. Lewis, 1937

A nutrient supply route Lewis originally proposed that macropinocytosis may be a relevant nutrient uptake mechanism in the cells that he was examining. The recognition and importance of the function that macropinocytosis plays in cancer began again with Dafna Bar-Sagi and Cosimmo Commisso at New York University in 2011. In an unsurprising observation, they noted that *KRAS* driven cancer cells grown in low-glutamine in cell culture exhibit defects in proliferation. Surprisingly, however, simply adding albumin to the cell culture media restored proliferation of these cells to nearly normal levels. These data suggested that these cancer cells could extract glutamine from albumin presumably through catabolism of the macromolecule and subsequent release of constituent amino acids, including glutamine. These findings were supported by the fact that albumin supplementation did not rescue cell proliferation when cells were grown in these same conditions in the presence of a macropinocytosis inhibitor, ethylisopropylamiloride (EIPA). In orthogonal data using fluorescently labeled heavy-dextran (molecular weight, 70kDa), a size of dextran that is too large to be taken up by traditional endocytic pathways and is mostly specific to

macropinocytosis, it was demonstrated that *Kras* expression was sufficient to stimulate this process. These data were consistent with previous findings in rat embryonic fibroblasts upon ectopic *Hras* expression (Bar-Sagi and Feramisco, 1986).

These data suggested that protein was going into the cell, but to test the hypothesis that extracellular protein contributed directly to the amino acid supply of cells, we created fluorescent and stable-isotope versions of size-selected (>70kDa) labeled protein from whole yeast extracts of *Saccharomyces cerevisiae.* We first demonstrated that our fluorescently tagged yeast protein co-localized with heavy-dextran to ensure it was entering through macropinocytosis, as opposed to other endocytic pathways (Figure 1.1A). Using our stable-isotope labeled version, we further showed that under standard culture conditions that this exogenous protein source could account for a significant fraction of intracellular free amino acids inside of the cell (Figure 1.1b) and these amino acids can contribute to TCA metabolism (Figure 1.1C,D). These data, taken together, demonstrate that *Kras*-transformed cells derive nutrients from the macropinocytic pathway.

More than amino acids? It seemed unlikely that these tumor cells would only use glutamine-derived from extracellular protein, and it is now clear that macropinocytosis and the role this process plays in scavenging nutrients are not limited to the acquisition of amino acids. Indeed, it has been shown that cancer cells can also acquire lipids and other micronutrients from the process of macropinocytosis. Intriguingly, it appears that some of the macropinocytic processes are governed through the hypoxia response and act to scavenge lipids in addition to protein (Kamphorst et al., 2013). It has been further posited by Harold Varmus and colleagues demonstrate that macropinocytosis may be a critical factor underlying synthetic lethality observed between *EGFR* and mutant *KRAS.* Interestingly, Varmus and colleagues high levels of macropinocytosis when both mutant genes were expressed together (Unni et al., 2015). These data suggest that there

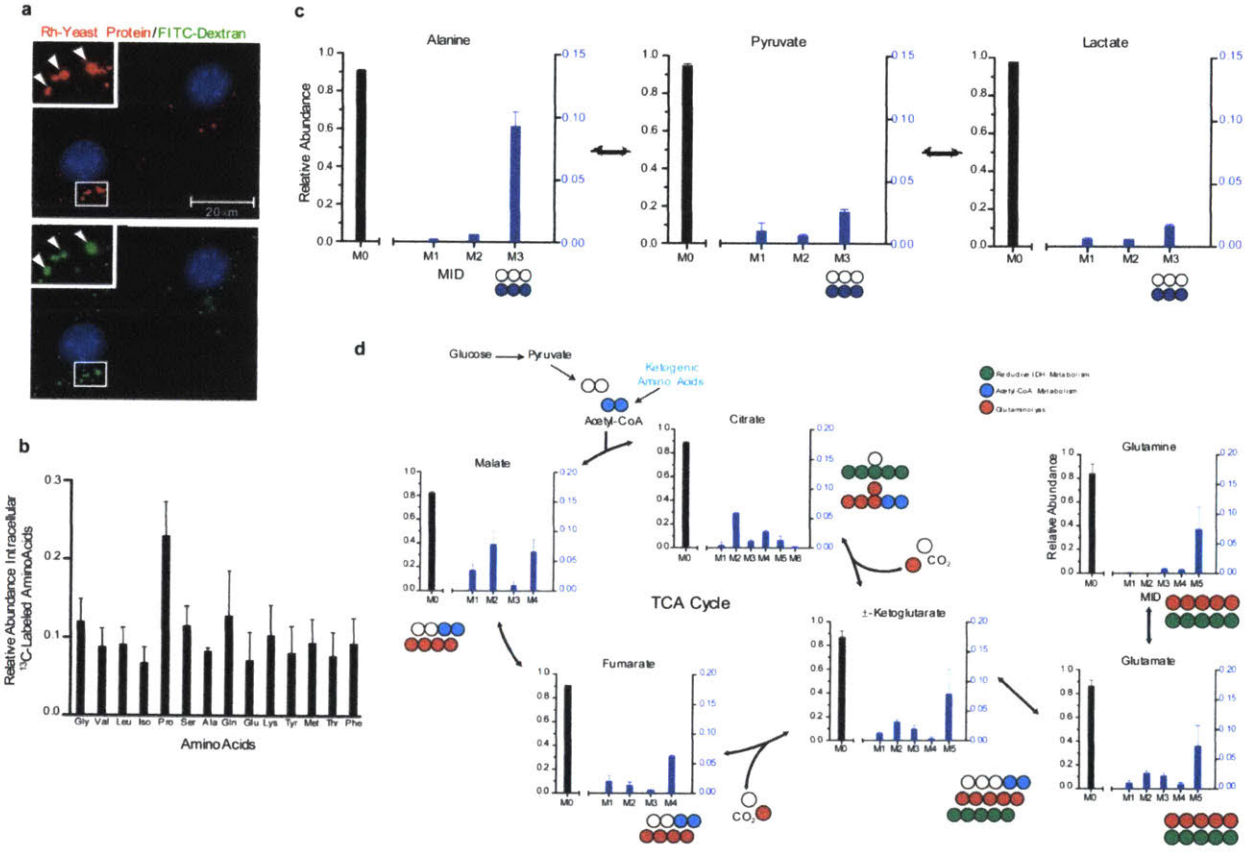

Figure 1.1. Macropinocytic uptake of extracellular protein drives the accumulation of catabolic intermediates and entry of protein-derived amino acids into central carbon metabolism. A. Rhodamine (Rh)-labelled yeast protein (red) is internalized into puncta (arrowheads) that co-localize with FITC-dextran (green). Insets represent a higher magnification of the boxed areas. B. Uniformly ^{13}C-labelled intracellular amino acid pools were detected in NIH3T3^{KrasV12} cells after culture in low-glutamine-containing medium (0.2mM) supplemented with 2% ^{13}C-labelled yeast protein. C. Protein-derived alanine enters central carbon metabolism upon transamination to pyruvate, and pyruvate can be directly converted to lactate. M3 reflects fully labeled alanine, pyruvate, and lactate, whereas M0 abundances reflect metabolites with no ^{13}C label. M1 and M2 represent partially labeled species that are not present in substantial amounts. D. Atom-transition map depicting a model for the entry of amino-acid-derived carbons into the TCA cycle and isotopic labeling of various metabolites. Open circles represent unlabelled carbon, and different-coloured circles highlight labeling patterns that correspond to specific pathways as indicated in the key. For all graphs, error bars indicate mean ±s.d. for three independent experiments. IDH, isocitrate dehydrogenase; MID, mass isotopomer distribution.

Figure 1.1

must be an upper limit of macropinocytosis levels for cell viability and provide the possibility of activating macropinocytosis for cancer therapy.

The cellular machinery The machinery of pinocytosis was poorly described for decades following the initial observation by Lewis. Pinocytosis and endocytosis were later elucidated, and macropinocytosis became defined as a cell-biological process in the late 1990s (Swanson and Watts, 1995). Much of what we know about macropinocytosis comes from studies examining cells of the immune system, including dendritic cells and macrophages. These cells perform constitutive macropinocytosis, and this facilitates constant monitoring of their environment for their role in antigen sensing. Large viruses, such as Ebola, Filamentous Influenza, and HIV exploit macropinocytosis to gain entry into cells of the immune system (Kaplan et al., 2005; Nakase et al., 2004; Maréchal et al., 2001). The macropinocytic machinery is further discussed in Chapter 5 (Figure 1.2).

In vivo relevance Epidemiological studies have demonstrated conflicting prognostic indications on albumin levels in cancer. Further, little is known about albumin catabolism in general. As albumin is the most abundant extracellular protein, it could serve as a potential source of amino acids for cells that use macropinocytosis *in vivo* (Merlot et al., 2014). In addition to potentially providing amino acids, albumin also serves as a serum transporter for lipids and small metabolites. It is known that cancer cells can import albumin into lysosomal vesicles (Schilling et al., 1992; Ichioka et al., 2004), but the fate of imported albumin has not been studied. This is owing in part to the lack of tools and tracers to interrogate albumin catabolism. These efforts are further hindered by physiological considerations, including slow turnover and a large volume of distribution of endogenous albumin (Schilling et al., 1992). Tumors preferentially take up albumin, and this has

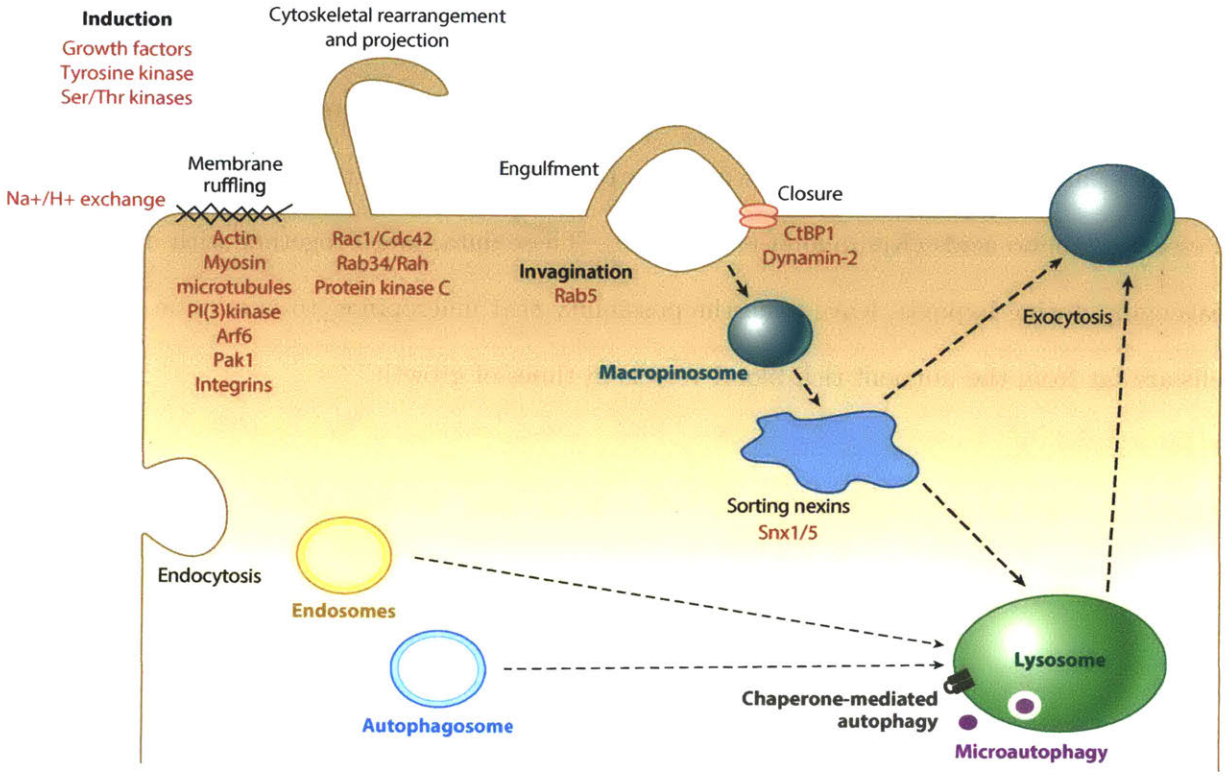

Figure 1.2. Like endocytosis and autophagy, macropinocytosis can deliver material to the lysosome Macropinocytosis is a clathrin-independent endocytic process that allows non-specific and non-receptor based uptake of extracellular material. Growth factor signaling and other stimuli lead to actin-dependent membrane ruffling followed by membrane protrusion and closure of the projection and concomitant invagination to form a macropinocytotic vehicle, or "macropinosome." Macropinosomes can either be recycled to the membrane or like endosomes derived from clathrin-mediated endocytosis and autophagosomes, can be trafficked to deliver their contents to the lysosome. The molecular machinery for macropinocytosis is incompletely elucidated. The proteins known to be involved in macropinocytosis are shown in red.

Figure 1.2

been exploited by using 5-aminofluorescein albumin during surgery to create a fluorescent dissection boundary and by conjugating drugs to albumin for delivery (such as paclitaxel) (Ding et al., 2011). Hypoalbuminemia is frequently observed in patients with advanced cancer, and when examined, this state has been associated with increased albumin degradation or decreased albumin synthesis by the liver (West et al., 1989; Gupta and Lis, 2010; Nazha et al., 2015). Two studies provide provacative evidence that protein catabolism is an early and important event in pancreatic cancer. First, branched-chain amino acid elevation seems to be an early feature of pancreatic cancer (Mayers et al., 2014). Next, patients with pancreatic ductal adenocarcinoma exhibit elevated levels of essential amino acids (Kamphorst et al., 2015). These data, taken together with data on lipid scavenging during hypoxia, leave open the possibility that macropinocytosis may be utilized when cells are far from the nutrient rich blood vessels in times of growth.

Studying cancer metabolism in mouse models

ONE ONCOGENE-ONE METABOLIC PHENOTYPE? We begin by examining data emerging in a *MYC* and *MET*-driven mouse model of lung and liver cancer. Tendencies to ascribe metabolic function to oncogenes are prevalent, and this study looked at this idea in the context of two different tissues.

QUESTIONS ABOUT CANCER METABOLISM in vivo. We examine the technologies that gave rise to mouse models of human disease, the relevance of each model used to study cancer examined in the sections to follow, and the methods that are currently used to study metabolism *in vivo*. As there is growing evidence that metabolism in tumors *in vivo* is significantly different from cancer cells in culture, developing a methodology to study these differences in a physiologically relevant setting is necessary. We seek to identify any distinguishing factors in tumors that may allow for therapeutic intervention. Methods developed to examine cancer metabolism *in vivo* will enable us answer some of the following questions:

(1) Is there an oncogene influence on tumor metabolism *in vivo*?

(2) Do the same mutations exhibit the same metabolic phenotypes?

(3) Is there any preference for metastasis at distant sites with an underlying metabolic mechanism (e.g. local nutrient availability and oxygen concentration)?

(4) Do tumors arising from the same tissue exhibit similar metabolism?

(5) What are the consequences of having a tumor on systemic metabolism?

One oncogene-one metabolic phenotype?

Different metabolic phenotypes in cell lines have been attributed to specific genetic events associated with cancer. However, there is a paucity of evidence exploring whether the same relationships between genotype and phenotype persist *in vivo*. In one study, Yuneva et al. (2012) evaluated metabolic changes in tumors arising in genetically engineered mouse models to show that the tissue of origin, even in the presence of the same activating oncogenic mutation, can differentially influence the metabolic rewiring of glucose and glutamine metabolism *in vivo*. This study examines whether tumors initiated by either *MYC* or *MET* expression exhibit elevated glucose consumption with lactate production. By following labeled glucose fate, the authors observed increased glucose catabolism across all tumors profiled. Increased lactate production relative to control tissues was observed in *MYC*-induced liver and lung tumors, but not in *MET*-induced liver tumors despite increased lactate dehydrogenase (*Ldha*) expression in all three tissues. These findings demonstrate that increased glucose to lactate conversion is not a feature of all cancers. They also illustrate that changes in enzyme expression are not necessarily predictive of a metabolic phenotype. Nevertheless, the *MYC*-induced liver tumors had elevated glucose uptake relative to the *MET*-induced liver tumors as measured by FDG-PET, suggesting that increased lactate correlates with glucose uptake *in vivo* (Figure 1.3). Together, these results suggest that cancer cells utilize different metabolic programs to support tumor growth.

The glutamine-tracing experiments performed in this study underscore the importance of glutamine catabolism by tumors, but also show that glutamine can be synthesized by cancers. Some cell lines can grow in the absence of glutamine, and the endogenous production of glutamine implies that this may also be the case for some cancer cells *in vivo*. Low tumor glutamine levels with increased labeling of TCA cycle intermediates from ^{13}C-labeled glutamine were observed in

MYC-induced liver tumors. This finding matches the increased expression of *Slc1A5* and *Gls* together with repression of glutamine synthetase (*Glul*) in these tumors. It is also consistent with tissue culture studies arguing that *MYC* expression control expression of *Slc1A5* and *Gls* to promote dependence on exogenous glutamine, while *MYC*-overexpressing cells undergo apoptosis when glutamine is absent (Wise and Thompson, 2010).

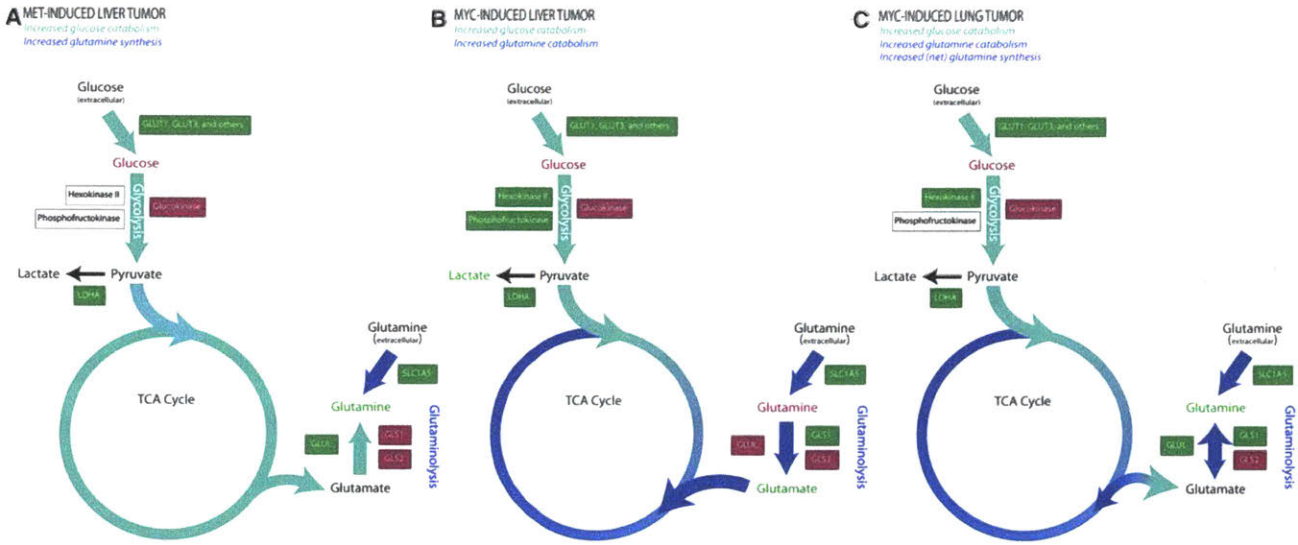

Figure 1.3. Functional analysis of metabolism is necessary to reveal the metabolic heterogeneity of tumors (A) Liver tumors induced by MET have increased glucose uptake but despite increased Ldha expression show no increase in lactate levels. Net glutamine synthesis is observed along with downregulation of Gls2 and upregulation of Glul. (B) Like MET-induced liver tumors, MYC-induced liver tumors also exhibit increased glucose uptake. However, in these tumors increased Ldha expression is associated with increased lactate production. In addition, these tumors use glutamine to fuel the citric acid cycle. (C) *MYC*-induced lung tumor metabolism resembles MET-induced liver tumor metabolism, with apparent net glutamine synthesis resulting from increased Glul expression. While it is likely these tumors still consume glutamine, glutamine levels are high, suggesting that glutamine synthesis outpaces consumption. Green, upregulated compared to control tissue at the level of transcription, translation, or metabolite levels. Red, downregulated compared to control tissue at the level of transcription, translation, or metabolite levels. Black, no change in enzyme/metabolite levels compared to control tissue, or the enzyme/metabolite was not explicitly examined.

Figure 1.3

In contrast, the *MET*-induced liver tumors expressed *Glu1* and had low *Gls* levels. This is consistent endogenous glutamine production, and these tumors had increased labeled glutamine from ^{13}C-labeled glucose. Strikingly, Glul expression was also increased in the *MYC*-induced lung tumors, and these tumors had elevated levels of glutamine compared to normal tissue. *Glul* is regulated by β-catenin, and therefore possibly by MET, but is not a known *MYC* target.

Therefore, the authors hypothesize that *Glul* expression may be secondary to an inflammatory microenvironment in the tumor. If true, this effect must be dominant over the *MYC* effect on glutamine metabolism. Taken together, this evaluation in different tumor types suggest that the metabolic program of cancer cells *in vivo* is determined by multiple factors. Neither the tissue of origin and associated microenvironment nor the presence of a single genetic driver event is sufficient to define the metabolic phenotype. The data also argue that *MYC*-driven tumor cells may have a variable dependence on glutamine metabolism for growth and survival *in vivo*. The authors show high expression of *Gls1* protein in *MYC*-induced lung tumor cells, and it is possible that these cells remain dependent on glutamine catabolism even though the cells are producing glutamine more than consumption. Furthermore, *MYC*-induced lung cancers do not fully regress following *MYC* inactivation, implying a decreased role for *MYC* in tumor maintenance (Tran et al., 2008). Incomplete regression following *MYC* inactivation is also observed in an *MYC*-driven breast cancer model (Boxer et al., 2004). Studies of these tumors could inform whether differences in glutamine metabolism are a marker of *MYC* dependence *in vivo*.

Use and generation of mouse models in cancer research

Mouse models are a fundamental part of cancer research and are rapidly evolving. These models have served great utility to model different elements of the multistep nature of oncogenes and tumor suppressor genes (Wu and Pandolfi, 2001). Further, models have been created that faithfully recapitulate features of the human disease have greatly facilitated our understanding of the many aspects of tumor biology (for review see (Frese and Tuveson, 2007)). The development of these models has been chaperoned by our identification of oncogenes, tumor suppressors, and disease modifiers from classical techniques in genetics and modern efforts arising from the sequencing of the

human genome (Lander et al., 2001; Venter et al., 2001).

Transplant models of cancer

Allograft and xenograft models Two mutations discovered in mouse models facilitated the routine transplantation and propagation of human cancer cells. First, genetic linkage studies enabled the discovery of the 'Nude' (*nu*) gene (so named for giving rise to mice with an apparent lack of fur) (Flanagan, 1966), a pleiotropic gene later characterized as forkhead box N1, *FoxN1*.
Loss-of-function in this gene results in mice congenital athymia and lack functional T-cells causing immunodeficiency. The subsequent discovery of the severe combined immunodeficiency (SCID) mutation in mice allowed impairment in antigen receptor genes causing B-cell and T-cell deficiencies (Bosma and Carroll, 1991). The utility of these models has been called into question with respect to translational findings (Voskoglou-nomikos et al., 2003; Johnson et al., 2001a), although this is controversial and the implementation of patient-derived transplants seem useful in predicting clonal characteristics of breast cancer (Whittle et al., 2015).

Genetically engineered mouse models of cancer

Transgenics Rudolf Jaenisch and colleagues first demonstrated the ability to introduce foreign DNA into mouse models using retroviruses and *SV40* (Jaenisch and Mintz, 1974). Transgenic technologies allow us to test hypotheses about the transformative nature of oncogenes and tumor suppressor genes. Transgenic mice have served great utility for introducing oncogenes and introducing transgenes, particularly those that enable tissue-specific promotion of *Cre*-recombinase drivers. However, by the nature of random integration, this approach does not allow for specificity

in targeting the genomic region of integration. As a result, are frequently expressed at non-physiological levels.

Knockin/Knockout In 1978, Gerald Fink discovered how to perform transformation by homologous recombination in yeast, the process by which "naked DNA is introduced into a cell, resulting in a heritable change." This discovery was critical to the development of gene targeting strategies in molecular biology (Hinnen et al., 1978) and subsequently enabled the transformation of mammalian cells to introduce oncogenes. These studies were adapted to embryonic cells and allowed the transfer of foreign DNA that could be introduced it into specific regions in the genome *in vitro* (Evans and Kaufman, 1981). It was further demonstrated in 1988 that this technology could target the β-globin locus to create the first knockout mouse (Nandi et al., 1988). By engineering constructs to have a positive-negative selection with thymidine kinase (TK) and neomycin-resistance (Neo-R) selection in ES cells, more specific integration could be accomplished and became routine (Mansour et al., 1988). These technologies further allow fine dissection of oncogenesis and determination of events that are required for tumor initiation, progression, maintenance, and metastasis.

More modifications The generation of a latent allele of oncogenic *Kras* in was implemented by Johnson et al. (2001b). In this mouse model, spontaneous intrachromosomal causes recombination of an endogenous exon is replaced by an engineered mutant exon. Further manipulations, such as the introduction of conditional alleles, allowed for even more precise control of gene deletion or expression. Conditional alleles typically refer to an allele with either two flanking loxP sites around a tumor suppressor gene to cause deletion and inactivation or the addition of a lox-STOP-lox cassette in front of a proto-oncogene with the designated mutation. A required component for this system is the introduction of an additional transgene or viral delivery system to introduce

Cre-recombinase or FlpO-recombinase. The implementation and utilization of Cre/loxP and FlpO/frt have allowed for spatiotemporal interrogation of gene activity in mouse models (Green and Ried, 2012). Cre can be introduced in combination with tissue specific promoters, as in the case of the mouse model of pancreatic cancer below, or through intranasal or intratracheal viral infection as in the mouse model of lung cancer below.

Genome editing The clustered regularly interspaced short palindromic repeat (CRISPR) and CRISPR-associated proteins (Cas) are part of the innate immune system of bacteria and archaea that act to destroy invading pathogens (Wiedenheft et al., 2012; Horvath and Barrangou, 2010). The first key realization was that the protospacer adjacent motif (PAM) sequence could be recognized by Cas9, and subsequently, small guide RNAs (sgRNAs) targeting genomic DNA could be created. This technology has been used to create knockouts at the germline level to knock out up to three genes at once (Wang et al., 2013). The CRISPR genome editing machinery can be delivered to tissues *in vivo* including hydrodynamic injection (Xue et al., 2014) and viral transduction (Sánchez-Rivera et al., 2014). More utility has been found through the delivery of vectors containing sgRNAs and Cre-recombinase in mice harboring conditional alleles of lox-STOP-lox-Cas9 (Yang et al., 2014b). CRISPR/Cas9 has also been used to create oncogenic fusions, such as *EML4-ALK* (Maddalo et al., 2014). The ability to use an all-in-one genome editing system allows the researcher to simultaneously express Cre to trigger the recombination between pre-existing loxP sites (in this case, those that flank oncogenic *Kras*), Cas9 to promote genome editing, and small-guide RNAs targeting gene(s) of interest (such as pSECC (Sánchez-Rivera et al., 2014)).

ONGOING EFFORTS indicate that CRISPR is reliable and robust, with few off-target effects in the genome (Kleinstiver et al., 2016). However, the extent to which this is true must be further studied. Somatic genome editing reduces the experimental procedure time. The use of lentiviruses

with tissue-specific promoters will also allow for more rapid questions regarding cell-of-origin without conducting rigorous lineage-tracing studies. For now, the possibilities seem endless. These studies are of great utility for metabolism in particular, as the previous technology with incomplete knockdown or siRNA-based methods suffered from having residual enzymatic activity.

Mouse models of human cancer

LUNG CANCER is the leading cause of cancer-related deaths worldwide (Siegel et al., 2015). Lung cancer is classified into non-small cell lung cancer (NSCLC) and small cell lung cancer (SCLC). NSCLC accounts for 85% of all cases. There are four common histological subtypes: adenocarcinoma, squamous-cell carcinoma, large-cell cancer, and NSCLC not otherwise specified (NOS). Adenocarcinoma is the most common histological subtype and also the most common in patients that are non-smokers. *KRAS* was first identified in a patient with lung cancer and mutations in *KRAS* are the second most common mutation for non-small cell lung adenocarcinoma (30%) (Thomas et al., 2015). The most common mutation in patients is a single point mutation in position 12 that changes a codon which normally encodes glycine to valine, aspartic acid, or cysteine. p53 mutations are found in approximately 45% of human lung adenocarcinomas (Hammerman et al., 2012; Brosh and Rotter, 2009) and is the highest co-mutated gene associated with NSCLC, and it is estimated that as many as 50% of patients with Kras mutations also have mutations in p53.

$Kras^{LA2}$ allele (K) This mouse was created by homologous recombination to introduce a tandem duplication of an exon containing the $Kras^{G12D}$ allele. This model results in mice that develop lung tumors with 100% penetrance (Johnson et al., 2001b). Tumors observed here are typically

low-grade, and this arrest is thought to be due to suppression by functional *p53* (Overmyer et al., 2015).

$Kras^{LSL\text{-}G12D/+}$; $p53^{flox/flox}$ (KP) This mouse model employs the knockin targeting to introduce an oncogenic version of the *Kras* allele, *$Kras^{G12D}$* with a Lox-STOP-Lox cassette (LSL) (Jackson et al., 2001). Upon addition of Cre-recombinase, either through the use of tissue specific promoters or in the case of these lung cancer models by intranasal/intratracheal injection of adeno-Cre-recombinase, the LSL cassette is excised and oncogenic $Kras_{G12D}$ is expressed. These mice also harbor a *p53* allele which was also introduced at the endogenous locus *p53* with flanking loxP sites around exons 2-10 (Jonkers et al., 2001). This model progresses through all stages of the disease and progress in a similar way as the human disease at the histological level, from hyperplasias to adenomas to lung adenocarcinomas (Jackson et al., 2005). Importantly, these animals also exhibit local invasion and develop distant metastases (Winslow et al., 2011).

PANCREATIC CANCER is the 9th and 10th most common cancer for women and men in the US. Alarmingly, it has an approximate 4-6% 5-year survival rate, owing to the lack of knowledge of reliable biomarkers or other detection methods. Pancreatic ductal adenocarcinoma (PDAC) accounts for 95% of all pancreatic cancer cases. The human disease progresses through the following histopathological stages: intraepithelial neoplasias or PanINs, high-grade PanINs, and eventually local invasion and distant metastasis (Ryan et al., 2015; Hruban et al., 2008). Desmoplasia and dense stroma are prominent features of this disease, further making detection and drug delivery challenging (Schober et al., 2014; Mahadevan and Von Hoff, 2007; Whatcott et al., 2014). *KRAS* is mutated in 95% of human pancreatic cancers, and 50% of pancreatic cancer also has p53 mutations. Therefore, to create mouse models that faithfully recapitulate features of the disease, mouse models

with similar mutations are utilized to study PDAC.

KP Model The KP mouse model of PDAC uses the same alleles as the mouse model of lung cancer and also progresses through the histopathological stages from PanIN to frank metastatic cancer. This mouse uses the pancreas-specific *Pdx1* promoter to drive expression of *Cre*-recombinase (*Pdx1-Cre*) in place of the viral delivery used for the mouse model of lung adenocarcinoma. LSL-tdTomato alleles are utilized to enable detection of *Cre* activity and presumably the activity of Cre-mediated recombination events.

PROSTATE CANCER is the most common cancer and second leading cause of cancer-related deaths among men in the United States (Siegel et al., 2015). Approximately 81 men die of prostate cancer each day, yet because of disease heterogeneity, there also is a high rate of over-treatment due to the inability to distinguish lethal from an indolent disease in many patients. The stages of human prostate cancer progress from hyperplasia, to prostatic intraepithelial neoplasia (PIN), to high-grade PIN, and subsequently to castration-resistant prostate cancer.

PTEN is one of the most recently discovered tumor suppressor genes, and it is found that at least one copy of *PTEN* is lost in 70% in prostate cancer. *PTEN* undergoes loss-of-heterozygosity (LOH) in approximately 90% of human glioblastomas (Rasheed et al., 1992). The lab of Ramon Parsons discovered that *PTEN* was frequently deleted through their representational difference analysis (RDA) on breast tumors. This enabled the identification of the genomic region where the *PTEN* gene resides (Li et al., 1997). In a parallel effort, Sean Tavtigian's lab used bacteria artificial chromosome libraries to perform a high-density scan on the region of chromosome 10q that had been reported to have undergone LOH in human glioblastoma multiforme (Steck et al., 1997). Recent efforts from The Cancer Genome Atlas has classified primary prostate cancer into seven

molecular subtypes, and additional efforts have identified mutations in metastatic prostate cancer and castration-resistant metastatic prostate cancer (Abeshouse et al., 2015; Cancer Research UK, 2016). Further characterization of these mutations will generate hypotheses about oncogenic driver and passenger mutations that can be tested by generating mouse models.

$Pten^{pc-/-}$ Mouse Model of Prostate Cancer The $Pten^{pc-/-}$ mouse model of prostate cancer harbors flanking loxP sites around the catalytic active site of the lipid phosphatase domain of Pten (exon 5) (Song et al., 2012; Lesche et al., 2002; Wang et al., 2003; Trotman et al., 2003). This model is typically driven by the probasin (PB)-Cre4 line, which is expressed in the prostate epithelium (Birbach, 2013; Zhang et al., 2000). When loxP sites undergo recombination in the presence of a prostate-specific Cre-recombinase, the result is the progressive mouse model of prostate cancer that models multiple features of the human disease, including progression from PIN through local invasion (Valkenburg and Williams, 2011; Trotman et al., 2003; Chen et al., 2005; Wu and Pandolfi, 2001). In Chapter 3, we cross these established lines to PKM1 and PKM2 conditional mice to test whether PKM isoform expression is required for prostate cancer.

Examining cancer metabolism in vivo

Positron emission tomography (PET) PET is one of the most widely used imaging modalities in the clinic and has been extensively used for diagnostic, prognostic, and therapeutic applications in cancer (Condeelis and Weissleder, 2010). The most prevalent tracer is [^{18}F]- fluoro-2-deoxy-D-glucose (^{18}FDG). As a glucose analog, ^{18}FDG enters cells through glucose transporters (GLUTs) where it is phosphorylated to generate phospho-2DG (P-2DG) by the first enzyme in glycolysis, hexokinase (Gambhir, 2002). Due to the negative charge of the phosphorylated product (P-2DG), P-2DG is retained in the cell and is not recognized by other enzymes in the cell, resulting

in accumulation. The spatial resolution of PET is estimated at approximately 6-8 mm^3 and is highly sensitive with an order of 10^{-11} moles/liter detection limit (Gambhir, 2002). However, the half-life of this of the [^{18}F] isotope is approximately 109 minutes, and as 2DG is not metabolized by the cell, it is not possible to acquire information beyond levels of glucose uptake.

Although limited in spatial resolution and tracer availability, PET imaging remains an important clinical tool in diagnosing pre-malignant, malignant, and metastatic lesions. Of relevance to this thesis, ^{18}FDG-PET is particularly useful for staging primary tumors, particularly non-small cell lung adenocarcinomas (Pennant et al., 2010). In general, PET can also be used determine post-operative success or response to therapy. Prostate cancer is a challenging disease to use PET tracers, especially ^{18}FDG-PET, given its proximity to the bladder. Further, to date, there is no metabolomic or other biomarker of prostate than is more predictive than prostate serum antigen (PSA) (Kelly et al., 2016).

Many other probes have been developed and implemented with clinical success. ^{11}C and ^{18}F choline PET probes have also been developed as those nutrients are taken up preferentially by many breast and primary prostate tumors (Schwarzenböck et al., 2012; Aboagye and Bhujwalla, 1999; Vali et al., 2015) and metastases. Some studies using ^{11}C and ^{18}F choline have had preliminary success for detecting and staging of distant metastases, such as those found in the lymph node (Skanjeti and Pelosi, 2011). For detection purposes, glutamine PET probes have also been developed, as this nutrient is highly utilized in culture and has demonstrated efficacy at detecting gliomas (Venneti et al., 2015). A better understanding of how cancer metabolism is performed by cancer cells will enable the development of additional PET tracers. This is best exemplified in cancer by the resurgent interest in acetate metabolism and its contribution to mitochondrial metabolism (Grassi et al., 2012; Hosios and Vander Heiden, 2014). Beyond using PET for cancer detection, efforts to use tracers to provide more functional information are underway. Proliferation can be measured

using fluorothymidine (FLT), and these and similar tracers are currently being tested understand the correlation of tracer signal with proliferation index (Tran and Jensen, 2013).

Dynamic nuclear hyperpolarization magnetic resonance spectroscopy imaging (DNP-MRSI) Dynamic nuclear polarization coupled to magnetic resonance spectroscopy imaging (DNP-MRSI) have been utilized in pre-clinical mouse models and the clinical setting in cancer for diagnosis, detection, and response to therapy. With this approach, a tracer of interest can he hyperpolarized and downstream metabolites can be detected. This approach is limiting as only several metabolites have a nuclear composition that permits hyperpolarization. It is further limited by the ability to detect labeled metabolites past one or two reactions downstream of the original tracer.

The most commonly employed tracer is [1-^{13}C]pyruvate and has been used in mouse models of prostate cancer (Kurhanewicz et al., 2011). Recently, in a first-in-man imaging study, this methodology was used successfully to monitor treatment in prostate cancer (Nelson et al., 2013). DNP-MRSI has also been used to characterize metabolic changes associated with *de novo* tumor formation in *c-Myc*-induced liver tumors (Hu et al., 2011). Similar to Yuneva et al. (2012), this study found increased lactate production in *MYC*-driven liver tumors. Also, Hu et al. (2011) found increased conversion of pyruvate to alanine as a hallmark of *MYC*-dependent tumor initiation. These studies are powerful due to their ability to obtain longitudinal data on metabolic parameters and observe metabolism with some spatial resolution within a tumor.

Infusions and stable isotope tracing in mice Metabolomic profiling studies are one common approach for studying metabolic pathways *in vivo*. While these studies provide a useful "snapshot" of metabolism, they are limited in that flux through various metabolic pathways cannot be determined. Metabolic flux analysis (MFA) is a computational approach that has been developed to

infer flux information from the distribution of nutrient-derived isotope-labeled carbons within a metabolic network (Buescher et al., 2015). MFA is greatly simplified when the system of interest is at isotopic steady-state, and no delivery methods have been adequate to demonstrate whether this is possible in mouse tissue using stable isotope tracers. Previous efforts in animal studies have employed bolus injections of stable isotopes and used NMR to examine metabolites from *ex vivo* tumors. These studies provide important information, but due to limitations in instrument sensitivity and delivery time of the tracer, these studies obtained low metabolic pathway coverage.

THE HYPERINSULINEMIC-EUGLYCEMIC CLAMP is one of the most far-reaching methods in diabetes research since its discovery in the years leading up to the 1979 publication of this technique (DeFronzo et al., 1979). In this procedure, patients are injected with a high dose of insulin and a tracer amount of glucose to determine insulin action on certain tissues. These studies are typically performed with harmless doses of radioactivity. Following the biopsy of individual insulin-responsive tissues, glucose uptake rates can be ascertained. This technique was miniaturized with the discovery that the internal jugular vein of the mouse could be cannulated to achieve vascular access and enable infusion of insulin and glucose (Bardelmeijer et al., 2003). We adapted surgical and technical procedures, such as jugular vein cannulation and infusion, from Yale University and Vanderbilt University and we replaced techniques where radioactivity was used with stable-isotope tracers. The methods adopted from these studies allow the evaluation of metabolism which preserves physiology and does not require the use of other methods that perturb metabolism (Figure 1.4).

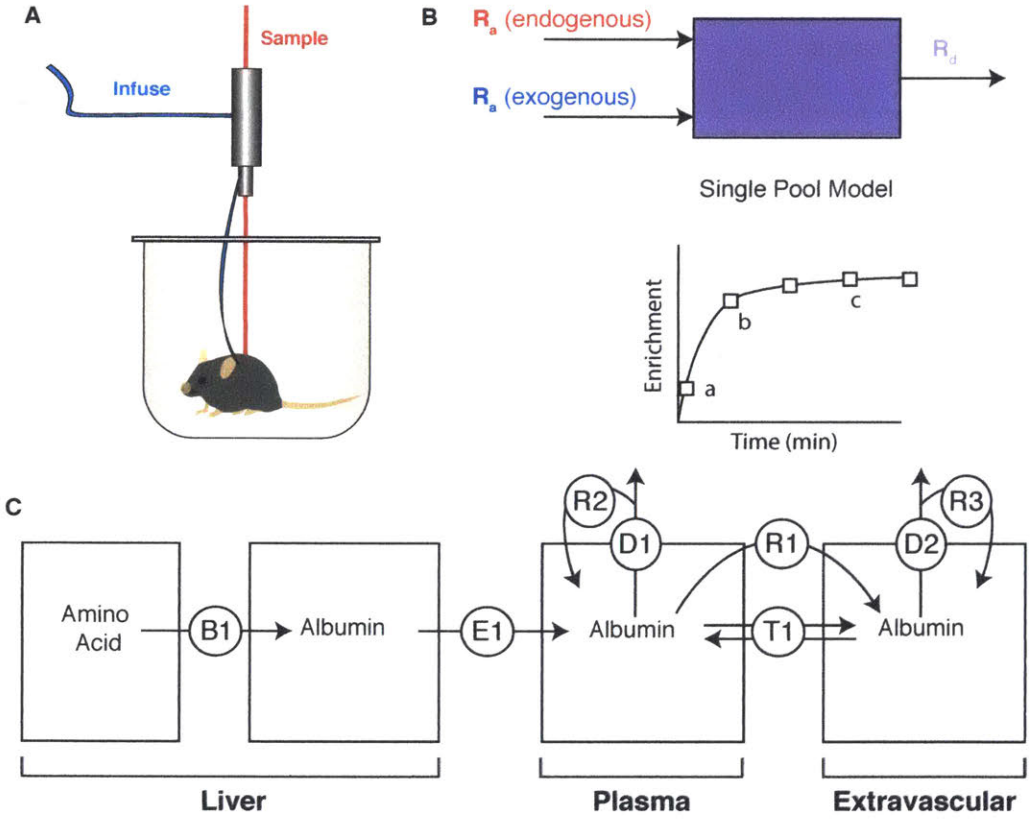

Figure 1.4. Infusion to an isotopic steady-state in the conscious mouse (A) Infusions are adaptable to any mouse model of disease and occur under highly physiological conditions that account for stress hormones, circadian rhythm, diet, strain and sex, and other parameters. (B) A simple single pool model for a tracer like glucose. Glucose is infused at some rate (blue, Exogenous R_a) and there is a source of glucose from gluconeogenesis (red, Endogenous R_a). At the beginning of the infusion (a), isotopic enrichment increases. As steady state is approached (b), levels of tracer reach an isotopic equilibrium (c) (Adapted from Wolfe and Chinkes (2005)). (C) A more complicated tracer is albumin, which takes amino acid inputs from the body (B1) and is synthesized in the liver. Albumin is then transported in the plasma and can be either recycled by the liver and other tissues (R1,2,3) or degraded (D1,2) or transferred between sites (T1). (Adapted from Kim et al. (2006)).

Figure 1.4

Conclusion

The availability of mouse models that faithfully model the pathophysiological progression of cancer coupled with modern day analytical methods has enabled the studies found in the Chapters to follow. Our aims throughout these studies were to characterize the metabolic phenotypes of resulting malignant lesions. The overall efforts of our investigations are to identify metabolic processes that are preferentially or exclusively used by cancer cells to identify potential therapies targeting these metabolic vulnerabilities.

References

Abeshouse A, Ahn J, Akbani R, Ally A, Amin S, et al. The molecular taxonomy of primary prostate cancer. *Cell* **163**, 1011 (2015).

Aboagye E, Bhujwalla Z. Malignant transformation alters membrane choline phospholipid metabolism of human mammary epithelial cells. *Cancer Research* **59**, 80 (1999).

Algire G, HW C, HW C. Vascular reactions of normal and malignant tissues in vivo. i. vascular reactions of mice to wounds and to normal and neoplastic transplants. *Journal of the National Cancer Institute* **6**, 73 (1945).

Anastasiou D, Yu Y, Israelsen WJ, Jiang JK, Boxer MB, et al. Pyruvate kinase M2 activators promote tetramer formation and suppress tumorigenesis. *Nature Chemical Biology* **8**, 839 (2012).

Astuti D, Latif F, Dallol A, Dahia PL, Douglas F, et al. Gene mutations in the succinate dehydrogenase subunit SDHB cause susceptibility to familial pheochromocytoma and to familial paraganglioma. *American Journal of Human Genetics* **69**, 49 (2001).

Athuluri-Divakar SK, Vasquez-Del Carpio R, Dutta K, Baker SJ, Cosenza SC, et al. A small molecule RAS-Mimetic disrupts RAS association with effector proteins to block signaling. *Cell* **165**, 643 (2016).

Bar-Sagi D, Feramisco JR. Induction of membrane ruffling and fluid-phase pinocytosis in quiescent fibroblasts by Ras proteins. *Science* **233**, 1061 (1986).

Bar-Sagi D, McCormick F, Milley RJ, Feramisco JR. Inhibition of cell surface ruffling and fluid-phase pinocytosis by microinjection of anti-Ras antibodies into living cells. *Journal of Cellular Physiology Supplement* **5**, 69 (1987).

Baracca A, Chiaradonna F, Sgarbi G, Solaini G, Alberghina L, et al. Mitochondrial Complex I decrease is responsible for bioenergetic dysfunction in K-ras transformed cells. *Biochimica et Biophysica Acta* **1797**, 314 (2010).

Bardelmeijer HA, Buckle T, Ouwehand M, Beijnen JH, Schellens JHM, et al. Cannulation of the jugular vein in mice: a method for serial withdrawal of blood samples. *Laboratory animals* **37**, 181 (2003).

Barnett JA. A history of research on yeasts 1: work by chemists and biologists 1789-1850. *Yeast* **14**, 1439 (1998).

Baron A, Migita T, Tang D, Loda M. Fatty acid synthase: a metabolic oncogene in prostate cancer? *Journal of Cellular Biochemistry* **91**, 47 (2004).

Bauer DE, Harris MH, Plas DR, Lum JJ, Hammerman PS, et al. Cytokine stimulation of aerobic glycolysis in hematopoietic cells exceeds proliferative demand. *FASEB Journal* **18**, 1303 (2004).

Bauerschlag DO, Maass N, Leonhardt P, Verburg FA, Pecks U, et al. Fatty acid synthase overexpression: target for therapy and reversal of chemoresistance in ovarian cancer. *Journal of Translational Medicine* **13**, 1 (2015).

Baysal BE, Willett-Brozick JE, Filho Paa, Lawrence EC, Myers EN, et al. An Alu-mediated partial SDHC deletion causes familial and sporadic paraganglioma. *Journal of Medical Genetics* **41**, 703 (2004).

Bensaad K, Tsuruta A, Selak MA, Vidal MNC, Nakano K, et al. TIGAR, a p53-inducible regulator of glycolysis and apoptosis. *Cell* **126**, 107 (2006).

Bhutia YD, Babu E, Ramachandran S, Ganapathy V. Amino acid transporters in cancer and their relevance to "glutamine addiction": novel targets for the design of a new class of anticancer drugs. *Cancer Research* **75**, 1782 (2015).

Birbach A. Use of PB-Cre4 mice for mosaic gene deletion. *PLoS ONE* **8**, e53501 (2013).

Bos JL. RAS oncogenes in human cancer : a review. *Cancer Research* **49**, 4682 (1989).

Bosma MJ, Carroll AM. The SCID mouse mutant: definition, characterization, and potential uses. *Annual Review of Immunology* **9**, 323 (1991).

Boxer RB, Jang JW, Sintasath L, Chodosh LA. Lack of sustained regression of c-MYC-induced mammary adenocarcinomas following brief or prolonged MYC inactivation. *Cancer Cell* **6**, 577 (2004).

Brand K. Glutamine and glucose metabolism during thymocyte proliferation. Pathways of glutamine and glutamate metabolism. *The Biochemical Journal* **228**, 353 (1985).

Brosh R, Rotter V. When mutants gain new powers: news from the mutant p53 field. *Nature Reviews Cancer* **9**, 701 (2009).

Brugarolas JB, Vazquez F, Reddy A, Sellers WR, Kaelin WG. TSC2 regulates VEGF through mTOR-dependent and -independent pathways. *Cancer Cell* **4**, 147 (2003).

Buescher JM, Antoniewicz MR, Boros LG, Burgess SC, Brunengraber H, et al. A roadmap for interpreting 13C metabolite labeling patterns from cells. *Current Opinion in Biotechnology* **34**, 189 (2015).

Bustamante E, Pedersen PL. High aerobic glycolysis of rat hepatoma cells in culture: role of mitochondrial hexokinase. *Proceedings of the National Academy of Sciences* **74**, 3735 (1977).

C HC, Monica H. Clinical Implications of the p53 Tumor-Suppressor Gene. *The New England Journal of Medicine* **329**, 1318 (1993).

Cairns R, Harris I, Mak T. Regulation of cancer cell metabolism. *Nature Reviews Cancer* **11**, 85 (2011).

Cairns RA, Mak TW. Oncogenic isocitrate dehydrogenase mutations: mechanisms, models, and clinical opportunities. *Cancer Discovery* **3**, 730 (2013).

Cancer Research UK. *Types of prostate cancer* (2016).

Chalkiadaki A, Guarente L. The multifaceted functions of sirtuins in cancer. *Nature Reviews Cancer* **2**, 608 (2015).

Chaneton B, Hillmann P, Zheng L, Martin ACL, Maddocks ODK, et al. Serine is a natural ligand and allosteric activator of pyruvate kinase M2. *Nature* **491**, 458 (2012).

Chen M, David CJ, Manley JL. Concentration-dependent control of pyruvate kinase M mutually exclusive splicing by hnRNP proteins. *Nature Structural & Molecular Biology* **19**, 346 (2012).

Chen Z, Trotman LC, Shaffer D, Lin HK, Dotan ZA, et al. Crucial role of p53-dependent cellular senescence in suppression of Pten-deficient tumorigenesis. *Nature* **436**, 725 (2005).

Cheng T, Sudderth J, Yang C, Mullen AR, Jin ES, et al. Pyruvate carboxylase is required for glutamine-independent growth of tumor cells. *Proceedings of the National Academy of Sciences* **108**, 8674 (2011).

Chiaradonna F, Gaglio D, Vanoni M, Alberghina L. Expression of transforming K-Ras oncogene affects mitochondrial function and morphology in mouse fibroblasts. *Biochimica et Biophysica Acta* **1757**, 1338 (2006).

Chinkers M, McKanna Ja, Cohen S. Rapid induction of morphological changes in human carcinoma cells A-431 by epidermal growth factor. *The Journal of Cell Biology* **83**, 260 (1979).

Chrast R, Saher G, Nave KA, Verheijen MHG. Lipid metabolism in myelinating glial cells: lessons from human inherited disorders and mouse models. *Journal of Lipid Research* **52**, 419 (2011).

Christofk HR, Vander Heiden MG, Harris MH, Ramanathan A, Gerszten RE, et al. The M2 splice isoform of pyruvate kinase is important for cancer metabolism and tumour growth. *Nature* **452**, 230 (2008a).

Christofk HR, Vander Heiden MG, Wu N, Asara JM, Cantley LC. Pyruvate kinase M2 is a phosphotyrosine-binding protein. *Nature* **452**, 181 (2008b).

Cohen S. Origins of growth factors: NGF and EGF. *Annals of the New York Academy of Sciences* **1038**, 98 (2004).

Condeelis J, Weissleder R. In vivo imaging in cancer. *Cold Spring Harbor Perspectives in Biology* **2** (2010).

Cortés-Cros M, Hemmerlin C, Ferretti S, Zhang J, Gounarides JS, et al. M2 isoform of pyruvate kinase is dispensable for tumor maintenance and growth. *Proceedings of the National Academy of Sciences* **110**, 489 (2013).

Cox AD, Fesik SW, Kimmelman AC, Luo J, Der CJ. Drugging the undruggable RAS: mission possible? *Nature Reviews Drug Discovery* **13**, 828 (2014).

Currie E, Schulze A, Zechner R, Walther TC, Farese RV. Cellular fatty acid metabolism and cancer. *Cell Metabolism* **18**, 153 (2013).

Dang L, White DW, Gross S, Bennett BD, Bittinger MA, et al. Cancer-associated IDH1 mutations produce 2-hydroxyglutarate. *Nature* **462**, 739 (2009).

Daniëls VW, Smans K, Royaux I, Chypre M, Swinnen JV, et al. Cancer cells differentially activate and thrive on de novo lipid synthesis pathways in a low-lipid environment. *PLoS ONE* **9**, 13 (2014).

Dayton TL, Gocheva V, Miller KM, Israelsen WJ, Bhutkar A, et al. Germline loss of PKM2 promotes metabolic distress and hepatocellular carcinoma. *Genes & Development* **30**, 1 (2016).

DeBerardinis RJ, Lum JJ, Hatzivassiliou G, Thompson CB. The biology of cancer: metabolic reprogramming fuels cell growth and proliferation. *Cell Metabolism* **7**, 11 (2008).

DeBerardinis RJ, Mancuso A, Daikhin E, Nissim I, Yudkoff M, et al. Beyond aerobic glycolysis: transformed cells can engage in glutamine metabolism that exceeds the requirement for protein and nucleotide synthesis. *Proceedings of the National Academy of Sciences* **104**, 19345 (2007).

DeFronzo Ra, Tobin JD, Andres R. Glucose clamp technique: a method for quantifying insulin secretion and resistance. *The American Journal of Physiology* **237**, E214 (1979).

Denzel MS, Storm NJ, Gutschmidt A, Baddi R, Hinze Y, et al. Hexosamine pathway metabolites enhance protein quality control and prolong life. *Cell* **156**, 1167 (2014).

Ding R, Frei E, Fardanesh M, Schrenk HH, Kremer P, et al. Pharmacokinetics of 5-aminofluorescein-albumin, a novel fluorescence marker of brain tumors during surgery. *Journal of Clinical Pharmacology* **51**, 672 (2011).

Downward J. Targeting RAS signalling pathways in cancer therapy. *Nature Reviews Cancer* **3**, 11 (2003).

Elmore S. Apoptosis: a review of programmed cell death. *Toxicologic Pathology* **35**, 495 (2007).

Evans AS. Causation and disease: the Henle-Koch postulates revisited. *Yale Journal of Biology and Medicine* **49**, 175 (1976).

Evans MJ, Kaufman MH. Establishment in culture of pluripotential cells from mouse embryos. *Nature* **292**, 154 (1981).

Fantin VR, St-Pierre J, Leder P. Attenuation of LDH-A expression uncovers a link between glycolysis, mitochondrial physiology, and tumor maintenance. *Cancer Cell* **9**, 425 (2006).

Flanagan SP. 'Nude', a new hairless gene with pleiotropic effects in the mouse. *Genetical research* **8**, 295 (1966).

Fletcher JW, Djulbegovic B, Soares HP, Siegel BA, Lowe VJ, et al. Recommendations on the use of 18F-FDG PET in oncology. *J Nucl Med* **49**, 480 (2008).

Flier JS, Mueckler MM, Usher P, Lodish HF. Elevated levels of glucose transport and transporter messenger RNA are induced by ras or src oncogenes. *Science* **235**, 1492 (1987).

Folkman J. Angiogenesis in psoriasis: therapeutic implications. *Nature* **263**, 797 (1976).

Folkman J, Long DM, Becker FF. Growth and metastasis of tumor in organ culture. *Cancer* **16**, 453 (1963).

Frese KK, Tuveson Da. Maximizing mouse cancer models. *Nature Reviews Cancer* **7**, 654 (2007).

Frezza C, Tennant DA, Gottlieb E. IDH1 mutations in gliomas: when an enzyme loses its grip. *Cancer Cell* **17**, 7 (2010).

Gaglio D, Metallo CM, Gameiro PA, Hiller K, Danna LS, et al. Oncogenic K-Ras decouples glucose and glutamine metabolism to support cancer cell growth. *Molecular Systems Biology* **7**, 523 (2011).

Gambhir SS. Molecular imaging of cancer with positron emission tomography. *Nature Reviews Cancer* **2**, 683 (2002).

Gao P, Tchernyshyov I, Chang TC, Lee YS, Kita K, et al. c-Myc suppression of miR-23a/b enhances mitochondrial glutaminase expression and glutamine metabolism. *Nature* **458**, 762 (2009).

Gao X, Lin SH, Ren F, Li JT, Chen JJ, et al. Acetate functions as an epigenetic metabolite to promote lipid synthesis under hypoxia. *Nature Communications* **7**, 11960 (2016).

Grassi I, Nanni C, Allegri V, Morigi JJ, Montini GC, et al. The clinical use of PET with (11)C-acetate. *American Journal of Nuclear Medicine and Molecular Imaging* **2**, 33 (2012).

Green JE, Ried T. *Genetically engineered mice for cancer research: Design, analysis, pathways, validation and pre-clinical testing.* Springer Science and Business Media, Medford, MA (2012).

Gui DY, Lewis Ca, Vander Heiden MG. Allosteric regulation of PKM2 allows cellular adaptation to different physiological states. *Science Signaling* **6**, 1 (2013).

Gupta D, Lis CG. Pretreatment serum albumin as a predictor of cancer survival: a systematic review of the epidemiological literature. *Nutrition Journal* **9**, 69 (2010).

Haigler HT, McKanna JA, Cohen S. Rapid stimulation of pinocytosis in human carcinoma cells A-431 by epidermal growth factor. *Journal of Cell Biology* **83**, 82 (1979).

Halestrap AP, Denton RM. Specific inhibition of pyruvate transport in rat liver mitochondria and human erythrocytes by alpha-cyano-4-hydroxycinnamate. *The Biochemical Journal* **138**, 313 (1974).

Hamanaka RB, Chandel NS. Targeting glucose metabolism for cancer therapy. *The Journal of Experimental Medicine* **209**, 211 (2012).

Hammerman PS, Lawrence MS, Voet D, Jing R, Cibulskis K, et al. Comprehensive genomic characterization of squamous cell lung cancers. *Nature* **489**, 519 (2012).

Hanahan D, Weinberg RA. Hallmarks of cancer: the next generation. *Cell* **144**, 646 (2011).

Hengartner MO, Horvitz HR. C. elegans cell survival gene ced-9 encodes a functional homolog of the mammalian proto-oncogene bcl-2. *Cell* **76**, 665 (1994).

Hensley CT, Wasti AT, Deberardinis RJ. Glutamine and cancer: cell biology, physiology, and clinical opportunities. *Journal of Clinical Investigation* **123**, 3678 (2013).

Herzig S, Raemy E, Montessuit S, Veuthey JLL, Zamboni N, et al. Identification and functional expression of the mitochondrial pyruvate carrier. *Science* **337**, 93 (2012).

Hinnen A, Hicks JB, Fink GR. Transformation of yeast. *Proceedings of the National Academy of Sciences* **75**, 1929 (1978).

Hitosugi T, Kang S, Vander Heiden MG, Chung Tw, Elf S, et al. Tyrosine phosphorylation inhibits PKM2 to promote the Warburg effect and tumor growth. *Growth (Lakeland)* **2**, 1 (2010).

Horvath P, Barrangou R. CRISPR/Cas, the immune system of bacteria and archaea. *Science* **327**, 167 (2010).

Hosios AM, Fiske BP, Gui DY, Vander Heiden MG. Lack of evidence for PKM2 protein kinase activity. *Molecular Cell* **59**, 850 (2015).

Hosios AM, Hecht VC, Danai LV, Johnson MO, Rathmell JC, et al. Amino acids rather than glucose account for the majority of cell mass in proliferating mammalian cells. *Developmental Cell* **36**, 540 (2016).

Hosios AM, Vander Heiden MG. Acetate metabolism in cancer cells. *Cancer & Metabolism* **2**, 27 (2014).

Hruban RH, Maitra A, Schulick R, Laheru D, Herman J, et al. Emerging molecular biology of pancreatic cancer. *Gastrointestinal Cancer Research* **2**, S10 (2008).

Hsin JP, Sheth A, Manley JL, Bricker DK, Taylor EB, et al. A Mitochondrial Pyruvate Carrier Required for Pyruvate Uptake in Yeast, Drosophila, and Humans. *Science* **337**, 96 (2012).

Hsu PP, Sabatini DM. Cancer cell metabolism: Warburg and beyond. *Cell* **134**, 703 (2008).

Hu S, Balakrishnan A, Bok RA, Anderton B, Larson PEZ, et al. 13C-pyruvate imaging reveals alterations in glycolysis that precede c-Myc-induced tumor formation and regression. *Cell Metabolism* **14**, 131 (2011).

Hu W, Zhang C, Wu R, Sun Y, Levine A, et al. Glutaminase 2, a novel p53 target gene regulating energy metabolism and antioxidant function. *Proceedings of the National Academy of Sciences* **107**, 7455 (2010).

Hu Y, Lu W, Chen G, Wang P, Chen Z, et al. K-ras(G12V) transformation leads to mitochondrial dysfunction and a metabolic switch from oxidative phosphorylation to glycolysis. *Cell Research* **22**, 399 (2012).

Ichioka T, Miyatake SI, Asai N, Kajimoto Y, Nakagawa T, et al. Enhanced detection of malignant glioma xenograft by fluorescein-human serum albumin conjugate. *Journal of Neuro-Oncology* **67**, 47 (2004).

Israelsen WJ. *The Role of Pyruvate Kinase Regulation in Tumor Growth and Metabolism.* Ph.D. thesis, Massachusetts Institute of Technology (2014).

Israelsen WJ, Dayton TL, Davidson SM, Fiske BP, Hosios AM, et al. PKM2 isoform-specific deletion reveals a differential requirement for pyruvate kinase in tumor cells. *Cell* **155**, 397 (2013).

Jackson EL, Olive KP, Tuveson DA, Bronson R, Crowley D, et al. The differential effects of mutant p53 alleles on advanced murine lung cancer. *Cancer Research* **65**, 10280 (2005).

Jackson EL, Willis N, Mercer K, Bronson RT, Crowley D, et al. Analysis of lung tumor initiation and progression using conditional expression of oncogenic K-ras. *Genes & Development* **15**, 3243 (2001).

Jaenisch R, Mintz B. Simian virus 40 DNA sequences in DNA of healthy adult mice derived from preimplantation blastocysts injected with viral DNA. *Proceedings of the National Academy of Sciences* **71**, 1250 (1974).

Jain M, Nilsson R, Sharma S, Madhusudhan N, Kitami T, et al. Metabolite profiling identifies a key role for glycine in rapid cancer cell proliferation. *Science* **336**, 1040 (2012).

Johnson JI, Decker S, Zaharevitz D, Rubinstein LV, Venditti JM, et al. Relationships between drug activity in NCI preclinical in vitro and in vivo models and early clinical trials. *British Journal of Cancer* **84**, 1424 (2001a).

Johnson L, Mercer K, Greenbaum D, Bronson RT, Crowley D, et al. Somatic activation of the K-ras oncogene causes early onset lung cancer in mice. *Nature* **410**, 1111 (2001b).

Jones DR, Keune WJ, Anderson KE, Stephens LR, Hawkins PT, et al. The hexosamine biosynthesis pathway and O-GlcNAcylation maintain insulin-stimulated PI3K-PKB phosphorylation and tumour cell growth after short-term glucose deprivation. *FEBS Journal* **281**, 3591 (2014).

Jonkers J, Meuwissen R, van der Gulden H, Peterse H, van der Valk M, et al. Synergistic tumor suppressor activity of BRCA2 and p53 in a conditional mouse model for breast cancer. *Nature Genetics* **29**, 418 (2001).

Jurica MS, Mesecar A, Heath PJ, Shi W, Nowak T, et al. The allosteric regulation of pyruvate kinase by fructose-1,6-bisphosphate. *Structure* **6**, 195 (1998).

Kaelin WG, McKnight SL. Influence of metabolism on epigenetics and disease. *Cell* **153**, 56 (2013).

Kaelin WG, Ratcliffe PJ. Oxygen sensing by metazoans: the central role of the HIF hydroxylase pathway. *Molecular Cell* **30**, 393 (2008).

Kamphorst JJ, Cross JR, Fan J, de Stanchina E, Mathew R, et al. Hypoxic and Ras-transformed cells support growth by scavenging unsaturated fatty acids from lysophospholipids. *Proceedings of the National Academy of Sciences* **110**, 8882 (2013).

Kamphorst JJ, Nofal M, Commisso C, Hackett SR, Lu W, et al. Human pancreatic cancer tumors are nutrient poor and tumor cells actively scavenge extracellular protein. *Cancer Research* **75**, 544 (2015).

Kaplan IM, Wadia JS, Dowdy SF. Cationic TAT peptide transduction domain enters cells by macropinocytosis. *Journal of Controlled Release* **102**, 247 (2005).

Keller KE, Tan IS, Lee YS. SAICAR stimulates pyruvate kinase isoform M2 and promotes cancer cell survival in glucose-limited conditions. *Science* **1069**, 1 (2012).

Kelly RS, Heiden MGV, Giovannucci E, Mucci LA. Metabolomic biomarkers of prostate cancer: prediction, diagnosis, progression, prognosis, and recurrence. *Cancer Epidemiology Biomarkers and Prevention* **25**, 887 (2016).

Kennedy BK, Austriaco NR, Zhang J, Guarente L. Mutation in the silencing gene S/R4 can delay aging in S. cerevisiae. *Cell* **80**, 485 (1995).

Kim J, Bronson CL, Hayton WL, Radmacher MD, Roopenian DC, et al. Albumin turnover: FcRn-mediated recycling saves as much albumin from degradation as the liver produces. *American Journal of Physiology Gastrointestinal and Liver Physiology* **290**, G352 (2006).

Kim JW, Zeller KI, Wang Y, Jegga AG, Aronow BJ, et al. Evaluation of Myc E-Box phylogenetic footprints in glycolytic genes by chromatin immunoprecipitation assays. *Molecular and Cellular Biology* **24**, 5923 (2004).

Kleinstiver BP, Pattanayak V, Prew MS, Tsai SQ, Nguyen NT, et al. High-fidelity CRISPR–Cas9 nucleases with no detectable genome-wide off-target effects. *Nature* **529**, 490 (2016).

Knudson AG. Mutation and cancer: statistical study of retinoblastoma. *Proceedings of the National Academy of Sciences* **68**, 820 (1971).

Komrokji RS, Raza A, Lancet JE, Ren C, Taft D, et al. Phase I clinical trial of oral rigosertib in patients with myelodysplastic syndromes. *British Journal of Haematology* **162**, 517 (2013).

Konstantinopoulos PA, Karamouzis MV, Papavassiliou AG. Post-translational modifications and regulation of the RAS superfamily of GTPases as anticancer targets. *Nature Reviews Drug Discovery* **6**, 541 (2007).

Krasnov GS, Dmitriev Aa, Snezhkina AV, Kudryavtseva AV. Deregulation of glycolysis in cancer: glyceraldehyde-3-phosphate dehydrogenase as a therapeutic target. *Expert Opinion on Therapeutic Targets* **17**, 681 (2013).

Kruiswijk F, Labuschagne CF, Vousden KH. P53 in survival, death and metabolic health: a lifeguard with a licence to kill. *Nature Reviews Molecular Cell Biology* **16**, 393 (2015).

Kuilman T, Michaloglou C, Mooi WJ, Peeper DS. The essence of senescence. *Genes & Development* **24**, 2463 (2010).

Kuma A, Hatano M, Matsui M, Yamamoto A, Nakaya H, et al. The role of autophagy during the early neonatal starvation period. *Nature* **432**, 1032 (2004).

Kumashiro N, Beddow SA, Vatner DF, Majumdar SK, Cantley JL, et al. Targeting pyruvate carboxylase reduces gluconeogenesis and adiposity and improves insulin resistance. *Diabetes* **62**, 2183 (2013).

Kurhanewicz J, Vigneron DB, Brindle K, Chekmenev EY, Comment A, et al. Analysis of cancer metabolism by imaging hyperpolarized nuclei: prospects for translation to clinical research. *Neoplasia* **13**, 81 (2011).

Kuwana T, Bouchier-Hayes L, Chipuk JE, Bonzon C, Sullivan BA, et al. BH3 domains of BH3-only proteins differentially regulate Bax-mediated mitochondrial membrane permeabilization both directly and indirectly. *Molecular Cell* **17**, 525 (2005).

Lander ES, Linton LM, Birren B, Nusbaum C, Zody MC, et al. Initial sequencing and analysis of the human genome. *Nature* **409**, 860 (2001).

Le A, Cooper CR, Gouw AM, Dinavahi R, Maitra A, et al. Inhibition of lactate dehydrogenase A induces oxidative stress and inhibits tumor progression. *Proceedings of the National Academy of Sciences* **107**, 2037 (2010).

Lee DC, Sohn HA, Park ZY, Oh S, Kang YK, et al. A lactate-induced response to hypoxia. *Cell* **161**, 595 (2015).

Lesche R, Groszer M, Gao J, Wang Y, Messing A, et al. Cre/loxP-mediated inactivation of the murine Pten tumor suppressor gene. *Genesis* **32**, 148 (2002).

Lewis WH. Pinocytosis by malignant cells. *Cancer Research* **29**, 666 (1937).

Li J, Yen C, Liaw D, Podsypanina K, Bose S, et al. PTEN, a putative protein tyrosine phosphatase gene mutated in human brain, breast, and prostate cancer. *Science* **275**, 1943 (1997).

Liang J, Cao R, Zhang Y, Xia Y, Zheng Y, et al. PKM2 dephosphorylation by Cdc25A promotes the Warburg effect and tumorigenesis. *Nature Communications* **7**, 12431 (2016).

Lindsten T, Thompson CB. Cell death in the absence of Bax and Bak. *Cell Death and Differentiation* **13**, 1272 (2006).

Lipmann F. Metabolic generation and utilization of phosphate bond energy. *Advances in Enzymology and Related Areas of Molecular Biology* **1**, 99 (1941).

Liu H, Liu JY, Wu X, Zhang JT. Biochemistry, molecular biology, and pharmacology of fatty acid synthase, an emerging therapeutic target and diagnosis/prognosis marker. *International Journal of Biochemistry and Molecular Biology* **1**, 69 (2010).

Locasale JW. Serine, glycine and one-carbon units: cancer metabolism in full circle. *Nature Reviews Cancer* **13**, 572 (2013).

Locasale JW, Cantley LC. Altered metabolism in cancer. *BMC Biology* **8**, 88 (2010).

Locasale JW, Grassian AR, Melman T, Lyssiotis CA, Mattaini KR, et al. Phosphoglycerate dehydrogenase diverts glycolytic flux and contributes to oncogenesis. *Nature Genetics* **43**, 869 (2011).

Lu C. *Epigenetic basis for the oncogenic potential of Idh mutations.* Ph.D. thesis, University of Pennsylvania (2013).

Lunt SY, Muralidhar V, Hosios AM, Israelsen WJ, Gui DY, et al. Pyruvate kinase isoform expression alters nucleotide synthesis to impact cell proliferation. *Molecular Cell* **57**, 95 (2015).

Lunt SY, Vander Heiden MG. Aerobic glycolysis: meeting the metabolic requirements of cell proliferation. *Annual Review of Cell and Developmental Biology* **27**, 441 (2011).

Luo W, Hu H, Chang R, Zhong J, Knabel M, et al. Pyruvate kinase M2 is a PHD3-stimulated coactivator for hypoxia-inducible factor 1. *Cell* **145**, 732 (2011).

Lv L, Li D, Zhao D, Lin R, Chu Y, et al. Acetylation targets the M2 isoform of pyruvate kinase for degradation through chaperone-mediated autophagy and promotes tumor growth. *Molecular Cell* **42**, 719 (2011).

Macheda ML, Rogers S, Best JD. Molecular and cellular regulation of glucose transporter (GLUT) proteins in cancer. *Journal of Cellular Physiology* **202**, 654 (2005).

Maddalo D, Manchado E, Concepcion CP, Bonetti C, Vidigal JA, et al. In vivo engineering of oncogenic chromosomal rearrangements with the CRISPR/Cas9 system. *Nature* **516**, 423 (2014).

Mahadevan D, Von Hoff DD. Tumor-stroma interactions in pancreatic ductal adenocarcinoma. *Molecular cancer therapeutics* **6**, 1186 (2007).

Maher EA, Marin-Valencia I, Bachoo RM, Mashimo T, Raisanen J, et al. Metabolism of [U-13C]glucose in human brain tumors in vivo. *NMR in Biomedicine* **25**, 1234 (2012).

Mansour SL, Thomas KR, Capecchi MR. Disruption of the proto-oncogene int-2 in mouse embryo-derived stem cells: a general strategy for targeting mutations to non-selectable genes. *Nature* **336**, 348 (1988).

Mantovani F, Banks L. The human papillomavirus E6 protein and its contribution to malignant progression. *Oncogene* **20**, 7874 (2001).

Mardis ER, Ding L, Dooling DJ, Larson DE, McLellan MD, et al. Recurring mutations found by sequencing an acute myeloid leukemia genome. *The New England Journal of Medicine* **361**, 1058 (2009).

Maréchal V, Prevost Mc, Petit C, Perret E, Heard Jm, et al. Human immunodeficiency virus type 1 entry into macrophages mediated by macropinocytosis. *Journal of Virology* **75**, 11166 (2001).

Martinez-Outschoorn UE, Peiris-Pagés M, Pestell RG, Sotgia F, Lisanti MP. Cancer metabolism: a therapeutic perspective. *Nature Reviews Clinical Oncology* 1–21 (2016).

Mattaini KR, Sullivan MR, Vander Heiden MG. The importance of serine metabolism in cancer. *Journal of Cell Biology* **214**, 249 (2016).

Maxwell PH, Wiesener MS, Chang GW, Clifford SC, Vaux EC, et al. The tumour suppressor protein VHL targets hypoxia-inducible factors for oxygen-dependent proteolysis. *Nature* **399**, 271 (1999).

Mayers JR, Wu C, Clish CB, Kraft P, Torrence ME, et al. Elevation of circulating branched-chain amino acids is an early event in human pancreatic adenocarcinoma development. *Nature Medicine* **20**, 1193 (2014).

Mazurek S. Pyruvate kinase type M2: a key regulator of the metabolic budget system in tumor cells. *International Journal of Biochemistry and Cell Biology* **43**, 969 (2011).

McDonnell TJ, Deane N, Platt FM, Nunez G, Jaeger U, et al. bcl-2-Immunoglobulin transgenic mice demonstrate extended B cell survival and follicular lymphoproliferation. *Cell* **57**, 79 (1989).

Mendoza MC, Er EE, Blenis J. The Ras-ERK and PI3K-mTOR pathways: cross-talk and compensation. *Trends in Biochemical Sciences* **36**, 320 (2011).

Menendez JA, Lupu R. Fatty acid synthase and the lipogenic phenotype in cancer pathogenesis. *Nature Reviews Cancer* **7**, 763 (2007).

Merlot AM, Kalinowski DS, Richardson DR. Unraveling the mysteries of serum albumin-more than just a serum protein. *Frontiers in Physiology* **5**, 1 (2014).

Metallo CM, Gameiro PA, Bell EL, Mattaini KR, Yang J, et al. Reductive glutamine metabolism by IDH1 mediates lipogenesis under hypoxia. *Nature* **481**, 380 (2011).

Migita T, Ruiz S, Fornari A, Fiorentino M, Priolo C, et al. Fatty acid synthase: a metabolic enzyme and candidate oncogene in prostate cancer. *Journal of the National Cancer Institute* **101**, 519 (2009).

Mitchell P. Chemiosmotic coupling in oxidative and photosynthetic phosphorylation. *Biological Reviews* **41**, 1507 (1966).

Mullarky E, Mattaini KR, Vander Heiden MG, Cantley LC, Locasale JW. PHGDH amplification and altered glucose metabolism in human melanoma. *Pigment Cell and Melanoma Research* **24**, 1112 (2011).

Murcott TH, Gutfreund H, Muirhead H. The cooperative binding of fructose-1,6-bisphosphate to yeast pyruvate kinase. *The EMBO Journal* **11**, 3811 (1992).

Nakano K, Bálint E, Ashcroft M, Vousden KH. A ribonucleotide reductase gene is a transcriptional target of p53 and p73. *Oncogene* **19**, 4283 (2000).

Nakase I, Niwa M, Takeuchi T, Sonomura K, Kawabata N, et al. Cellular uptake of arginine-rich peptides: roles for macropinocytosis and actin rearrangement. *Molecular Therapy* **10**, 1011 (2004).

Nandi AK, Roginski RS, Gregmt RG, Smithiest O, Skoultchi AI. Regulated expression of genes inserted at the human chromosomal beta-globin locus by homologus recombination. *Proceedings of the National Academy of Sciences* **85**, 3845 (1988).

Nazha B, Moussaly E, Zaarour M, Weerasinghe C, Azab B. Hypoalbuminemia in colorectal cancer prognosis: nutritional marker or inflammatory surrogate? *World Journal of Gastrointestinal Surgery* **7**, 370 (2015).

Nelson SJ, Kurhanewicz J, Vigneron DB, Larson PEZ, Harzstark AL, et al. Metabolic imaging of patients with prostate cancer using hyperpolarized [1-^{13}C]pyruvate. *Science Translational Medicine* **5**, 1 (2013).

Ngoh GA, Watson LJ, Facundo HT, Jones SP. Augmented O-GlcNAc signaling attenuates oxidative stress and calcium overload in cardiomyocytes. *Amino Acids* **40**, 895 (2011).

Niemann S, Müller U. Mutations in SDHC cause autosomal dominant paraganglioma, type 3. *Nature Genetics* **26**, 268 (2000).

Noguchi T, Yamada K, Inoue H, Matsuda T, Tanaka T. The L- and R-type isozymes of rat pyruvate kinase are produced from a single gene by use of different promoters. *Journal of Biological Chemistry* **262**, 14366 (1987).

North BJ, Sinclair DA. Sirtuins: a conserved key unlocking AceCS activity. *Trends in Biochemical Sciences* **32**, 1 (2007).

Okino ST, Chichester CH, Withlock JP. Hypoxia-indicible mammalian gene expression analysed in vivo at a TATA-driven promoter and at an-initiator-driven promoter. *Journal of Biological Chemistry* **273**, 23837 (1998).

Olivier M, Hollstein M, Hainaut P. TP53 mutations in human cancers: origins, consequences, and clinical use. *Cold Spring Harbor Perspectives in Biology* **2**, a001008 (2010).

Otto AM. Warburg effect(s)-a biographical sketch of Otto Warburg and his impacts on tumor metabolism. *Cancer & Metabolism* **4**, 5 (2016).

Overmyer KA, Thonusin C, Qi NR, Burant CF, Evans CR. Impact of anesthesia and euthanasia on metabolomics of mammalian tissues: Studies in a C57BL/6J mouse model. *PLoS ONE* **10**, 1 (2015).

Parnas JK, Ostern P MT. Ober die Verkettung der chemischen vorgange im muskel. *Biochemische Zeitschrift* **272**, 64 (1934).

Parsons DW, Jones S, Zhang X, Lin JCH, Leary RJ, et al. An integrated genomic analysis of human glioblastoma multiforme. *Science* **321**, 1807 (2008).

Patra KC, Hay N. The pentose phosphate pathway and cancer. *Trends in Biochemical Sciences* **39**, 347 (2014).

Pavletich NP, Chambers KA, Pabo CO. The DNA-binding domain of 53 contains the four conserved regions the major mutation hot spots. *Genes & Development* **7**, 2556 (1993).

Pennant M, Takwoingi Y, Pennant L, Davenport C, Fry-Smith A, et al. A systematic review of positron emission tomography (PET) and positron emission tomography/computed tomography (PET/CT) for the diagnosis of breast cancer recurrence. *Health Technology Assessment* **14**, 1 (2010).

Perera RM, Bardeesy N. Pancreatic cancer metabolism: breaking it down to build it back up. *Cancer Discovery* **5**, 1247 (2015).

Pérez-Gómez C, Campos-Sandoval Ja, Alonso FJ, Segura Ja, Manzanares E, et al. Co-expression of glutaminase K and L isoenzymes in human tumour cells. *The Biochemical Journal* **386**, 535 (2005).

Pérez-Mancera PA, Young ARJ, Narita M. Inside and out: the activities of senescence in cancer. *Nature Reviews Cancer* **14**, 547 (2014).

Pietrocola F, Galluzzi L, Bravo-San Pedro JM, Madeo F, Kroemer G. Acetyl coenzyme A: a central metabolite and second messenger. *Cell Metabolism* **21**, 805 (2015).

Possemato R, Marks KM, Shaul YD, Pacold ME, Kim D, et al. Functional genomics reveal that the serine synthesis pathway is essential in breast cancer. *Nature* **476**, 346 (2011).

Puzio-Kuter AM. The role of p53 in metabolic regulation. *Genes & Cancer* **2**, 385 (2011).

Quek LE, Liu M, Joshi S, Turner N. Fast exchange fluxes around the pyruvate node: a leaky cell model to explain the gain and loss of unlabelled and labelled metabolites in a tracer experiment. *Cancer & Metabolism* **4**, 13 (2016).

Raff MC. Social controls on cell survival and cell death. *Nature* **356**, 397 (1992).

Rasheed BK, Fuller GN, Friedman aH, Bigner DD, Bigner SH. Loss of heterozygosity for 10q loci in human gliomas. *Genes, Chromosomes & Cancer* **5**, 75 (1992).

Rathmell JC, Fox CJ, Plas DR, Hammerman PS, Cinalli RM, et al. Akt-directed glucose metabolism can prevent Bax conformation change and promote growth factor-independent survival. *Molecular and cellular biology* **23**, 7315 (2003).

Reid MA, Wang WI, Rosales KR, Welliver MX, Pan M, et al. The B55α Subunit of PP2A Drives a p53-Dependent Metabolic Adaptation to Glutamine Deprivation. *Molecular Cell* **50**, 200 (2013).

Ribatti D. Judah Folkman, a pioneer in the study of angiogenesis. *Angiogenesis* **11**, 3 (2008).

Rothman DL, Magnusson I, Katz LD, Shulman RG, Shulman GI. Quantitation of hepatic glycogenolysis and gluconeogenesis in fasting humans with 13C NMR. *Science* **254**, 573 (1991).

Ryan DP, Hong TS, Bardeesy N. Pancreatic adenocarcinoma. *The New England Journal of Medicine* **371**, 1039 (2015).

Sabharwal SS, Schumacker PT. Mitochondrial ROS in cancer: initiators, amplifiers or an Achilles' heel? *Nature Reviews Cancer* **14**, 709 (2014).

Sánchez-Rivera FJ, Papagiannakopoulos T, Romero R, Tammela T, Bauer MR, et al. Rapid modelling of cooperating genetic events in cancer through somatic genome editing. *Nature* **516**, 428 (2014).

Schell JC, Olson KA, Jiang L, Hawkins AJ, VanVranken JG, et al. A role for the mitochondrial pyruvate carrier as a repressor of the Warburg effect and colon cancer cell growth. *Molecular Cell* **56**, 400 (2014).

Schilling U, Friedrich EA, Sinn H, Schrenk HH, Clorius JH, et al. Design of compounds having enhanced tumour uptake, using serum albumin as a carrier. Part I. *Nuclear Medicine and Biology* **19**, 685 (1992).

Schober M, Jesenofsky R, Faissner R, Weidenauer C, Hagmann W, et al. Desmoplasia and chemoresistance in pancreatic cancer. *Cancers* **6**, 2137 (2014).

Schuit FC, Huypens P, Heimberg H, Pipeleers DG. Glucose sensing in pancreatic B-cells: a model for the study of other glucose-regulated cells in gut, pancreas, and hypothalamus. *Diabetes* **50**, 1 (2001).

Schwarzenböck S, Souvatzoglou M, Krause BJ. Choline PET and PET/CT in primary diagnosis and staging of prostate cancer. *Theranostics* **2**, 318 (2012).

Semenza G. HIF-1:upstream and downstream of cancer metabolism. *Current Opinion in Genetics & Development* **20**, 51 (2010).

Semenza GL, Nejfelt MK, Chi SM, Antonarakis SE. Hypoxia-inducible nuclear factors bind to an enhancer element located 3' to the human erythropoietin gene. *Proceedings of the National Academy of Sciences* **88**, 5680 (1991).

Semenza GL, Roth PH, Fang HM, Wang GL. Transcriptional regulation of genes encoding glycolytic enzymes by hypoxia-inducible factor 1. *The Journal of Biological Chemistry* **269**, 23757 (1994).

Serrano M, Lin AW, McCurrach ME, Beach D, Lowe SW. Oncogenic ras provokes premature cell senescence associated with accumulation of p53 and p16(INK4a). *Cell* **88**, 593 (1997).

Seth R, Yang C, Kaushal V, Shah SV, Kaushal GP. P53-dependent Caspase-2 activation in mitochondrial release of apoptosis-inducing factor and its role in renal tubular epithelial cell injury. *The Journal of Biological Chemistry* **280**, 31230 (2005).

Shao C, Deng L, Henegariu O, Liang L, Stambrook PJ, et al. Chromosome instability contributes to loss of heterozygosity in mice lacking p53. *Proceedings of the National Academy of Sciences* **97**, 7405 (2000).

Sherwood LM, Parris EE, Folkman J. Tumor angiogenesis: therapeutic implications. *The New England Journal of Medicine* **285**, 1182 (1971).

Shim H, Dolde C, Lewis BC, Wu CS, Dang G, et al. c-Myc transactivation of LDH-A: implications for tumor metabolism and growth. *Proceedings of the National Academy of Sciences* **94**, 6658 (1997).

Siegel R, Miller K, Jemal A. Cancer statistics, 2015. *CA Cancer Journal for Clinicians* **65**, 5 (2015).

Skanjeti A, Pelosi E. Lymph node staging with choline PET/CT in patients with prostate cancer: a review. *International Scholarly Research Network Oncology* **2011**, 1 (2011).

Son J, Lyssiotis Ca, Ying H, Wang X, Hua S, et al. Glutamine supports pancreatic cancer growth through a KRAS-regulated metabolic pathway. *Nature* **496**, 101 (2013).

Song MS, Salmena L, Pandolfi PP. The functions and regulation of the PTEN tumour suppressor. *Nature Reviews Molecular Cell Biology* **13**, 283 (2012).

Soussi T. The history of p53. *EMBO reports* **11**, 822 (2010).

Soussi T, Wiman KG. Shaping Genetic Alterations in Human Cancer: The p53 Mutation Paradigm. *Cancer Cell* **12**, 303 (2007).

Steck Pa, Pershouse Ma, Jasser Sa, Yung WK, Lin H, et al. Identification of a candidate tumour suppressor gene, MMAC1, at chromosome 10q23.3 that is mutated in multiple advanced cancers. *Nature Genetics* **15**, 356 (1997).

Stehelin D, Varmus HE, Bishop JM, Vogt PK. DNA related to the transforming gene(s) of avian sarcoma viruses is present in normal avian DNA. *Nature* **260**, 170 (1976).

Stolze B, Reinhart S, Bulllinger L, Fröhling S, Scholl C. Comparative analysis of KRAS codon 12, 13, 18, 61, and 117 mutations using human MCF10A isogenic cell lines. *Scientific Reports* **5**, 8535 (2015).

Sullivan LB, Gui DY, Heiden MGV. Altered metabolite levels in cancer: implications for tumour biology and cancer therapy. *Nature Reviews Cancer* **16**, 680 (2016).

Swanson JA, Watts C. Macropinocytosis. *Trends in Cell Biology* **5**, 424 (1995).

Takenaka M, Yamada K, Lu T, Kang R, Tanaka T, et al. Alternative splicing of the pyruvate kinase M gene in a minigene system. *European Journal of Biochemistry* **235**, 366 (1996).

Taparra K, Tran PT, Zachara NE. Hijacking the hexosamine biosynthetic pathway to promote EMT-mediated neoplastic phenotypes. *Frontiers in Oncology* **6**, 85 (2016).

Thomas A, Liu SV, Subramaniam DS, Giaccone G. Refining the treatment of NSCLC according to histological and molecular subtypes. *Nature Reviews Clinical Oncology* **12**, 1 (2015).

Thompson CB. Into thin air: how we sense and respond to hypoxia. *Cell* **167**, 9 (2016).

Tomlinson IPM, Alam NA, Rowan AJ, Barclay E, Jaeger EEM, et al. Germline mutations in FH predispose to dominantly inherited uterine fibroids, skin leiomyomata, and papillary renal cell cancer. *Nature Genetics* **30**, 406 (2002).

Tran DKT, Jensen RL. Treatment-related brain tumor imaging changes: so-called "pseudoprogression" vs. tumor progression: review and future research opportunities. *Surgical Neurology International* **4**, S129 (2013).

Tran PT, Fan AC, Bendapudi PK, Koh S, Komatsubara K, et al. Combined inactivation of MYC and K-ras oncogenes reverses tumorigenesis in lung adenocarcinomas and lymphomas. *PLoS ONE* **3** (2008).

Trotman LC, Niki M, Dotan ZA, Koutcher JA, Di Cristofano A, et al. Pten dose dictates cancer progression in the prostate. *PLoS Biology* **1**, e9 (2003).

Unni AM, Lockwood WW, Zejnullahu K, Lee-Lin SQ, Varmus H. Evidence that synthetic lethality underlies the mutual exclusivity of oncogenic KRAS and EGFR mutations in lung adenocarcinoma. *eLife* **4**, 1 (2015).

Utter MF, Keech DB. Formation of oxaloacetate from pyruvate and carbon dioxide. *The Journal of Biological Chemistry* **235**, 17 (1960).

Vali R, Loidl W, Pirich C, Langesteger W, Beheshti M. Imaging of prostate cancer with PET/CT using (18)F-Fluorocholine. *American Journal of Nuclear Medicine and Molecular Imaging* **5**, 96 (2015).

Valkenburg KC, Williams BO. Mouse models of prostate cancer. *Prostate Cancer* **2011**, 895238 (2011).

Vander Heiden MG, Cantley LC, Thompson CB. Understanding the Warburg effect: the metabolic requirements of cell proliferation. *Science* **324**, 1029 (2009).

Vander Heiden MG, Locasale JW, Swanson KD, Sharfi H, Heffron GJ, et al. Evidence for an alternative glycolytic pathway in rapidly proliferating cells. *Science* **329**, 1492 (2010).

Vaux DL, Cory S, Adams JM. Bcl-2 gene promotes haemopoietic cell survival and cooperates with c-myc to immortalize pre-B cells. (1988).

Veithen a, Cupers P, Baudhuin P, Courtoy PJ. v-Src induces constitutive macropinocytosis in rat fibroblasts. *Journal of Cell Science* **109**, 2005 (1996).

Venneti S, Dunphy MP, Zhang H, Pitter KL, Zanzonico P, et al. Glutamine-based PET imaging facilitates enhanced metabolic evaluation of gliomas in vivo. *Science Translational Medicine* **7**, 1 (2015).

Venter JC, Adams MD, Myers EW, Li PW, Mural RJ, et al. The sequence of the human genome. *Science* **291**, 1304 (2001).

Vigil D, Cherfils J, Rossman KL, Der CJ. Ras superfamily GEFs and GAPs: validated and tractable targets for cancer therapy? *Nature Reviews Cancer* **10**, 842 (2010).

Vogelstein B, Kinzler KW. The multistep nature of cancer. *Trends in Genetics* **9**, 138 (1993).

Voskoglou-nomikos T, Pater JL, Seymour L. Clinical predictive value of the in vitro cell line, human xenograft, and mouse allograft preclinical cancer models. *Clinical Cancer Research* **9**, 4227 (2003).

Vousden KH, Ryan KM. P53 and metabolism. *Nature Reviews Cancer* **9**, 691 (2009).

Wallace JC. My favorite pyruvate carboxylase. *IUBMB Life* **62**, 535 (2010).

Walsh MJ, Brimacombe KR, Veith H, Bougie JM, Daniel T, et al. 2-Oxo-N-aryl-1,2,3,4-tetrahydroquinoline-6-sulfonamides as activators of the tumor cell specific M2 isoform of pyruvate kinase. *Bioorganic & Medicinal Chemistry Letters* **21**, 6322 (2011).

Wang H, Yang H, Shivalila CS, Dawlaty MM, Cheng AW, et al. One-step generation of mice carrying mutations in multiple genes by CRISPR/cas-mediated genome engineering. *Cell* **153**, 910 (2013).

Wang S, Gao J, Lei Q, Rozengurt N, Pritchard C, et al. Prostate-specific deletion of the murine Pten tumor suppressor gene leads to metastatic prostate cancer. *Cancer Cell* **4**, 209 (2003).

Warburg O, Wind F, Negelein E. Über den Stoffwechsel von Tumoren im Körper. *Klinische Wochenschrift* **5**, 829 (1926).

Ward PS, Patel J, Wise DR, Abdel-Wahab O, Bennett BD, et al. The common feature of leukemia-associated IDH1 and IDH2 mutations is a neomorphic enzyme activity converting Alpha-Ketoglutarate to 2-Hydroxyglutarate. *Cancer Cell* **17**, 225 (2010).

Ward PS, Thompson CB. Metabolic reprogramming: a cancer hallmark even Warburg did not anticipate. *Cancer Cell* **21**, 297 (2012).

Wei MH, Toure O, Glenn GM, Pithukpakorn M, Neckers L, et al. Novel mutations in FH and expansion of the spectrum of phenotypes expressed in families with hereditary leiomyomatosis and renal cell cancer. *Journal of Medical Genetics* **43**, 18 (2006).

Weinberg F, Hamanaka R, Wheaton WW, Weinberg S, Joseph J, et al. Mitochondrial metabolism and ROS generation are essential for Kras-mediated tumorigenicity. *Proceedings of the National Academy of Sciences* **107**, 8788 (2010).

Weinhouse S. On Respiratory Impairment in Cancer Cells. *Science* **124**, 267 (1956).

Weinstein IB. Cancer. Addiction to oncogenes–the Achilles heal of cancer. *Science* **297**, 63 (2002).

Wellen KE, Thompson CB. A two-way street: reciprocal regulation of metabolism and signalling. *Nature Reviews Molecular Cell Biology* **13**, 270 (2012).

West MA, Bretscher MS, Watts C. Distinct endocytotic pathways in epidermal growth factor-stimulated human carcinoma A431 cells. *Journal of Cell Biology* **109**, 2731 (1989).

Whatcott C, Watanabe A, LoBello J. Desmoplasia in primary tumors and metastatic lesions of pancreatic cancer. *Clinical Cancer Research* **21**, 3561 (2014).

Whittle JR, Lewis MT, Lindeman GJ, Visvader JE. Patient-derived xenograft models of breast cancer and their predictive power. *Breast Cancer Research* **17**, 17 (2015).

Wiedenheft B, Sternberg SH, Doudna Ja. RNA-guided genetic silencing systems in bacteria and archaea. *Nature* **482**, 331 (2012).

Winslow MM, Dayton TL, Verhaak RGW, Kim-Kiselak C, Snyder EL, et al. Suppression of lung adenocarcinoma progression by Nkx2-1. *Nature* **473**, 101 (2011).

Wise DR, Thompson CB. Glutamine addiction : a new therapeutic target in cancer. *Trends in Biochemical Sciences* **35**, 427 (2010).

Wolfe RR, Chinkes DL. *Isotope Tracers in Metabolic Research: Principles and Practice of Kinetic Analysis.* Wiley (2005).

Wong N, De Melo J, Tang D. PKM2, a central point of regulation in cancer metabolism. *International Journal of Cell Biology* **2013**, 242513 (2013).

Wu X, Pandolfi PP. Mouse models for multistep tumorigenesis. *Trends in Cell Biology* **11**, 2 (2001).

Xiao M, Yang H, Xu W, Ma S, Lin H, et al. Inhibition of a-KG-dependent histone and DNA demethylases by fumarate and succinate that are accumulated in mutations of FH and SDH tumor suppressors. *Genes & Development* **26**, 1326 (2012).

Xue W, Chen S, Yin H, Tammela T, Papagiannakopoulos T, et al. CRISPR-mediated direct mutation of cancer genes in the mouse liver. *Nature* **514**, 380 (2014).

Yacovan A, Ozeri R, Kehat T, Mirilashvili S, Sherman D, et al. 1-(sulfonyl)-5-(arylsulfonyl)indoline as activators of the tumor cell specific M2 isoform of pyruvate kinase. *Bioorganic and Medicinal Chemistry Letters* **22**, 6460 (2012).

Yan H, Parsons DW, Jin G, McLendon R, Rasheed BA, et al. Mutations in gliomas. *The New England Journal of Medicine* **360**, 765 (2009).

Yang C, Ko B, Hensley CT, Jiang L, Wasti AT, et al. Glutamine oxidation maintains the TCA cycle and cell survival during impaired mitochondrial pyruvate transport. *Molecular Cell* **56**, 414 (2014a).

Yang H, Wang H, Jaenisch R. Generating genetically modified mice using CRISPR/Cas-mediated genome engineering. *Nature Protocols* **9**, 1956 (2014b).

Yang M, Soga T, Pollard PJ, Adam J. The emerging role of fumarate as an oncometabolite. *Frontiers in Oncology* **2**, 1 (2012a).

Yang W, Xia Y, Hawke D, Li X, Liang J, et al. PKM2 phosphorylates histone H3 and promotes gene transcription and tumorigenesis. *Cell* **150**, 685 (2012b).

Ying H, Kimmelman AC, Lyssiotis CA, Hua S, Chu GC, et al. Oncogenic kras maintains pancreatic tumors through regulation of anabolic glucose metabolism. *Cell* **149**, 656 (2012).

Yoshii Y, Furukawa T, Oyama N, Hasegawa Y, Kiyono Y, et al. Fatty acid synthase is a key target in multiple essential tumor functions of prostate cancer: uptake of radiolabeled acetate as a predictor of the targeted therapy outcome. *PLoS ONE* **8** (2013).

Yun J, Rago C, Cheong I, Pagliarini R, Angenendt P, et al. Pathway mutations in tumor cells. *Science* **325**, 1555 (2009).

Yuneva MO, Fan TWM, Allen TD, Higashi RM, Ferraris DV, et al. The metabolic profile of tumors depends on both the responsible genetic lesion and tissue type. *Cell Metabolism* **15**, 157 (2012).

Zeczycki TN, Maurice MS, Attwood PV. Inhibitors of pyruvate carboxylase. *Open Enzyme Inhibition Journal* **3**, 8 (2010).

Zhang C, Liu J, Wu R, Liang Y, Lin M, et al. Tumor suppressor p53 negatively regulates stimulated by hypoxia through its target RRAD glycolysis. *Oncotarget* **5**, 5535 (2014).

Zhang J, Thomas TZ, Kasper S, Matusik RJ. A small composite probasin promoter confers high levels of prostate-specific gene expression through regulation by androgens and glucocorticoids in vitro and in vivo. *Endocrinology* **141**, 4698 (2000).

Zu XL, Guppy M. Cancer metabolism: facts, fantasy, and fiction. *Biochemical and Biophysical Research Communications* **313**, 459 (2004).

2

Environment impacts the metabolic dependencies of Ras-driven non-small cell lung cancer

Author statement

Some passages and figures have been adapted or quoted verbatim from the following published article:
Davidson, SM, Papagiannakopoulos, T, Olenchock, BA, Heyman, JE, Keibler, MA, Luengo, A, Vander Heiden, MG (2016). Environment impacts the metabolic dependencies of ras-driven non-small cell lung cancer. Cell Metabolism, 23(3), 517–528.

Authors

Shawn M. Davidson[1,2,3], Thales Papagiannakopoulos[1], Benjamin A. Olenchock[1,3,4], Julia E. Heyman[1], Mark A. Keibler[5], Alba Luengo[1,2], Matthew R. Bauer[1], Abhishek K. Jha[6], James P. O'Brien[1], Kerry A. Pierce[3], Dan Y. Gui[1], Lucas B. Sullivan[1], Thomas M. Wasylenko[5], Lakshmipriya Subbaraj[1], Christopher R. Chin[1], Gregory Stephanopolous[5], Bryan T. Mott[7], Tyler Jacks[1,2], Clary B. Clish[3], and Matthew G. Vander Heiden[1,2,3,8]

Author affilations

1. Koch Institute for Integrative Cancer Research, Massachusetts Institute of Technology, Cambridge, Massachusetts, USA
2. Department of Biology, Massachusetts Institute of Technology, Cambridge, Massachusetts, USA.
3. Broad Institute of MIT and Harvard University, Cambridge, Massachusetts, USA.
4. Division of Cardiovascular Medicine, Department of Medicine, The Brigham and Women's Hospital, Boston, MA 02115, USA
5. Department of Chemical Engineering, Massachusetts Institute of Technology, Cambridge, Massachusetts, USA.
6. Elucidata Corporation, Cambridge MA 02139.
7. National Center for Advancing Translational Sciences, NIH, Bethesda, Maryland, USA.
8. Dana-Farber Cancer Institute, Boston, Massachusetts, USA.

Author contributions

Conceptualization: S.M.D, T.P., B.A.O., M.G.V.H. Methodology: S.M.D, T.P., B.A.O., M.A.K., A.L., Formal Analysis: S.M.D., T.P., A.L. Investigation: J.E.H., A.L., J.P.O, M.R.B., A.K.J., J.P.O., K.A.P., D.Y.G., L.B.S., T.M.W., L.S., C.R.C. Writing: S.M.D., M.G.V.H. Visualization: S.M.D. Supervision: T.J., C.B.C., M.G.V.H. Funding Acquisition: S.M.D., B.A.O., M.G.V.H.

Abstract

Cultured cells convert glucose to lactate and glutamine is the major source of tricarboxylic acid (TCA) cycle carbon, but whether the same metabolic phenotype is found in tumors is less studied. We infused mice with lung cancers with isotope-labeled glucose or glutamine and compared the fate of these nutrients in tumor and normal tissue. As expected, lung tumors exhibit increased lactate production from glucose. However, glutamine utilization by both lung tumors and normal lung was minimal, with lung tumors showing increased glucose contribution to the TCA cycle relative to normal lung tissue. Deletion of enzymes involved in glucose oxidation demonstrates that glucose carbon contribution to the TCA cycle is required for tumor formation. These data suggest that understanding nutrient utilization by tumors can predict metabolic dependencies of cancers *in vivo*. Furthermore, these data argue that the *in vivo* environment is an important determinant of the metabolic phenotype of cancer cells.

Introduction

Metabolism is altered in cancer to sustain the energetic and biosynthetic demands of uncontrolled proliferation, and increased glucose uptake is a common feature of cancer cells in culture and tumors (Cairns et al., 2011; Vander Heiden et al., 2009) Positron emission tomography detection of ^{18}F-2-deoxyglucose uptake together with magnetic resonance spectroscopy studies have confirmed increased glucose-to-lactate conversion in tumors (Warburg effect) (Keshari et al., 2013; Rodrigues et al., 2014), but understanding the metabolic phenotype of cancer is based mostly on cell culture studies, including the idea that glucose oxidation in the TCA cycle is limited (Bonnet et al., 2007; Cairns et al., 2011). Indeed, other data suggests mitochondrial function is required for tumor growth (Weinberg et al., 2010) and oxidative glucose metabolism has been observed in tumors

(Yuneva et al., 2012; Marin-Valencia et al., 2012; Sellers et al., 2015). Whether tumors require glucose to support the TCA cycle remains unknown.

Non-small cell lung cancer (NSCLC) is a leading cause of cancer mortality (Herbst et al., 2008). Mutations in *Kras* are frequent in NSCLC and *Ras* activation has specific metabolic consequences (White, 2013). *Ras*-driven cancer cells display increased glucose uptake and aerobic glycolysis that supports both nucleotide biosynthesis and protein glycosylation for growth signaling (Son et al., 2013; Jones and Thompson, 2009; Onetti et al., 1997). However, recent work suggests that there is selective pressure to maintain functional mitochondria in tumors (Tan et al., 2015). Limited studies of tumor metabolism have suggested the driver mutation, tissue of origin, and microenvironment all can impact metabolic phenotypes (Davidson and Vander Heiden, 2012; Yuneva et al., 2012), highlighting the need to understand metabolism in spontaneously arising tumors.

Glutamine is an important nutrient for most cancer cells in culture (Hensley et al., 2013; Mayers and Vander Heiden, 2015), and can provide carbon for TCA cycle anaplerosis in Ras-driven cancer cells (White, 2013). Indeed, the GAC splice isoform of glutaminase (*Gls1*) is essential in NSCLC-derived cell lines (Van Den Heuvel et al., 2012). Glutamine also acts as a direct nitrogen donor for nucleotide biosynthesis and can supply alpha-ketoglutarate (α-KG) to support amino acid catabolism (White, 2013; Commisso et al., 2013). Glutamine catabolism in Kras-driven pancreatic cancer cells also has been implicated in NADPH production and redox balance (Lyssiotis et al., 2013; Son et al., 2013). However, the extent of glutamine metabolism *in vivo* is controversial, with evidence for net glutamine synthesis in some tumors (Yuneva et al., 2012). Analysis of NSCLC tumor metabolism in patients argues both glucose and glutamine can be important for TCA anaplerosis (Cheng et al., 2011; Sellers et al., 2015). Drugs targeting Gls1 are being explored as therapies for human cancers, highlighting the importance of understanding glutamine use by tumors (Gross et al., 2014).

To understand how lung tumors utilize nutrients relative to normal lung, we examined tissue metabolism in mouse lung cancer models. This analysis suggested glucose oxidation is important for lung tumors, a finding that was not evident from examination of lung cancer cell lines *in vitro*. We utilized CRISPR/Cas9-based genome editing to understand whether tumors were dependent on glucose contribution to the TCA cycle. While glucose oxidation is dispensable for lung cancer cell proliferation in culture, enzymes involved in glucose oxidation are required for tumor growth *in vivo*. Conversely, preferential glutamine metabolism is not observed in lung tumors, and neither genetic deletion nor pharmacological inhibition of Gls1 affected the growth of $Kras^{G12D}$-induced lung tumors. Together, these data better define the metabolic landscape of NSCLC and inform pathways that are required for cancer growth in a pathophysiological tissue context.

Results

Analysis of glucose metabolism in normal tissues

To study tissue glucose metabolism, we performed euglycemic [U-^{13}C]glucose infusion in conscious unrestrained C57Bl/6J mice (Ayala et al., 2010). Blood glucose and plasma insulin levels remained within the normal range throughout (Figure 2.1A, B), and isotopic enrichment of plasma glucose reached steady-state within 120 minutes (Figure 2.1C). To compare the labeling of tissues with different glucose uptake rates, we established the time required for glucose labeling of metabolites in tissues to reach isotopic steady-state. Because tissues with lower uptake will take longer to reach steady-state, this timing was established in normal tissues since most tumors, including Kras-driven lung tumors, exhibit elevated glucose uptake (Engelman et al., 2008). Tissue metabolites from wild-type [U-^{13}C]glucose infused mice were analyzed by liquid-chromatography mass spectrometry (LC-MS) (Figure 2.1D-L, Figure A1). The percentage of fully labeled lactate (M3 isotopomer) in

lung tissue reached steady-state by 1-hour and was similar to the percentage of hexose-6-phosphate enrichment (Figure 2.1D, F). This suggests glucose is the primary source of lactate in normal lung tissue. Labeling of other glycolytic intermediates, TCA cycle metabolites, and TCA cycle-derived amino acids from glucose reached isotopic steady-state in the lung with similar kinetics (Figure 2.1D-L). The finding that TCA cycle intermediate labeling occurred with similar kinetics as glycolytic intermediates is consistent with glucose oxidation being a major fate of glucose in lung tissue. Labeling of glutamate and glutamine from glucose is also observed (Figure 2.1K, L).

Glucose metabolism in lung tumor tissue

To examine metabolic differences between lung tumor and normal tissue we analyzed three mouse models of $Kras^{G12D}$-driven NSCLC. The mouse models initiate lung tumors through different mechanisms and result in lesions of different grades and invasiveness. We utilized two autochthonous mouse models of NSCLC: 1) The $Kras^{LA2/+}$ (LA2) model involves spontaneous recombination of an oncogenic $Kras^{G12D}$ allele in somatic cells and initiates primarily low grade lung adenomas that progress to invasive adenocarcinomas over the period of 6-8 months (Johnson et al., 2001), 2) Intratracheal delivery of adenoviral Cre (Ad5-CMV-Cre) to the lungs of animals harboring conditional $Kras^{LSL\text{-}G12D/+}$; $p53^{loxP/loxP}$ (KP) alleles results in higher grade, metastatic tumors that progress rapidly and cause death within 12-16 weeks (DuPage et al., 2009; Jackson et al., 2001; Jonkers et al., 2001; Tuveson et al., 2004). Cell lines derived from lung tumors arising in C57Bl/6J KP mice were introduced into the lungs of syngeneic animals via intratracheal injections (KPS), with lung tumor formation observed with even faster kinetics (Curtis et al., 2010). We also sought to determine how metabolism in these $Kras^{G12D}$-driven tumors compared to xenograft tumors derived from two human lung cancer cell lines: 1) A549 cells with a *KRAS* mutation and 2) H1975 cells with an *EGFR* mutation.

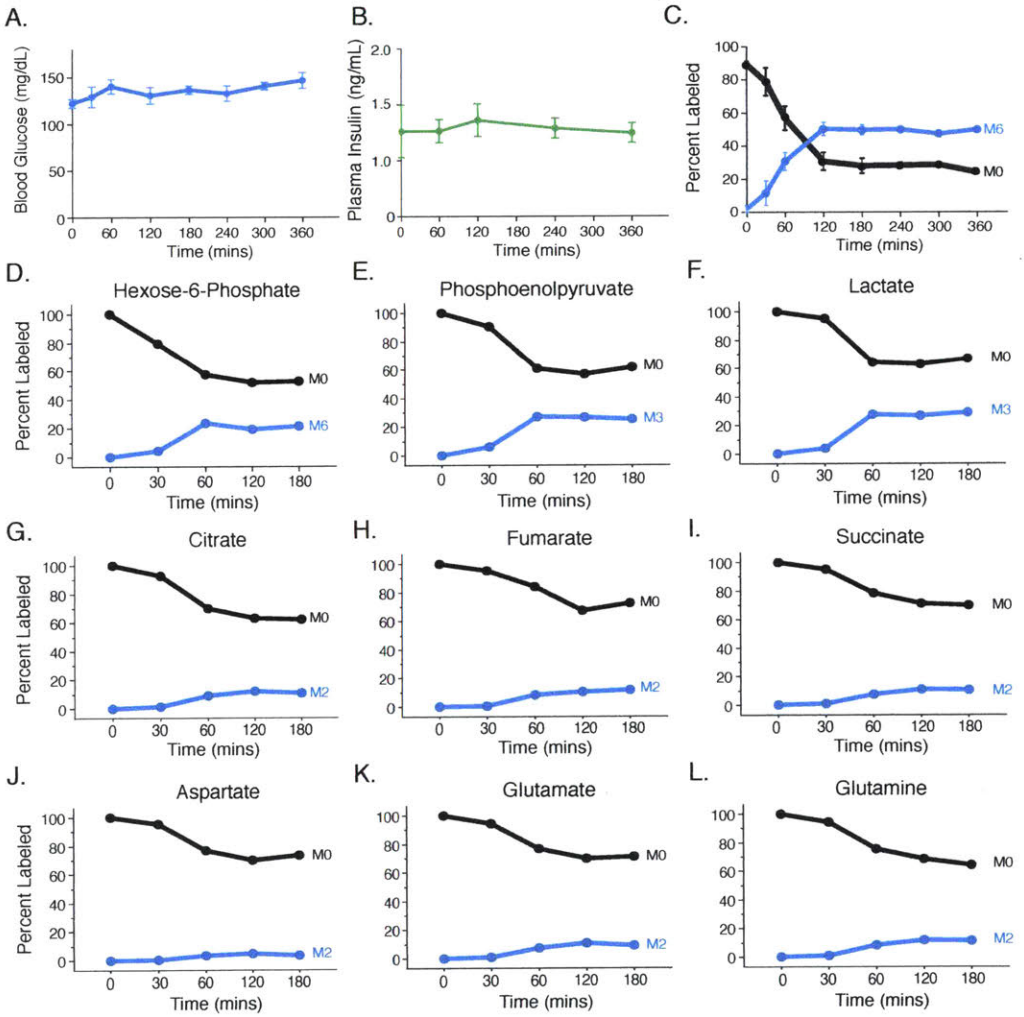

Figure 2.1. Steady state labeling of metabolites in tissues. (A) Steady state labeling of metabolites in tissues. Blood glucose levels over time in mice infused with [U-^{13}C]glucose. Values shown are mean ±SEM, n = 4. (B) Plasma insulin levels over time in mice infused with [U-^{13}C]glucose. Values shown are mean ±SEM, n = 4. (C) Plasma enrichment of fully labeled glucose (M6) in animals infused with [U-^{13}C]glucose over time. Values shown are mean ±SEM, n = 4. (D-F) Representative serial sacrifice (n=1) of WT animals after infusion of [U-^{13}C]glucose. Labeling of glycolytic intermediates in lung tissue from wild type mice infused with [U-^{13}C]glucose for the indicated time at 20mg/kg/min. The unlabeled (M0) and fully-labeled (M3 or M6) isotopomer is shown for each species. (G-H) Representative serial sacrifice (n=1) of WT animals after infusion of [U-^{13}C]glucose. Labeling of TCA intermediates in lung tissue from wild type mice infused with [U-^{13}C]glucose for the indicated time at 20mg/kg/min. The unlabeled (M0) and prominent M2 labeled isotopomer are shown for each species. (J-L) Representative serial sacrifice (n=1) of WT animals after infusion of [U-^{13}C]glucose. Labeling of aspartate, glutamate, and glutamine in in lung tissue from wild type mice infused with [U-^{13}C]glucose for the indicated time at 20mg/kg/min. The unlabeled (M0) and prominent M2 labeled isotopomer are shown for each species.

Figure 2.1

LA2, KP, and KPS mice underwent micro-computed tomography (μCT) scanning to select mice with tumors for analysis, and [U-^{13}C]glucose was infused to reach a plasma enrichment of >65.78% (Figure 2.2A). To ensure isotopic steady-state was reached in both tumor and normal lung tissue, tissues were harvested after a 6-hour infusion and metabolites from tumor and normal lung tissue were analyzed using gas-chromatography mass-spectrometry (GC-MS). Labeling of lactate and pyruvate from glucose carbon was similar in tumors and adjacent lung tissue in all three models (Figure 2.2B, C, D), consistent with glucose acting as a source of lactate in these tissues. Lactate pool sizes were higher in KP and KPS tumors while levels of many other metabolites were similar to normal lung, suggesting that these tumors may be more glycolytic than LA2 tumors (Figure 2.2A, B). Despite no differences in percent lactate labeling, the increased uptake of glucose in tumors and the increased amount of lactate present in KP and KPS tumors argues relative glucose metabolism to lactate is increased in these NSCLC models compared to normal lung.

Glucose carbon can enter the TCA cycle as acetyl-CoA, with acetyl-CoA derived from oxidation of glucose-derived pyruvate via the pyruvate dehydrogenase complex (PDH) (Figure 2.2B). Thus, entry of PDH-derived glucose carbon into the TCA cycle results in isotopomer species with two labeled carbons (M2), and species with more labeled carbons are generated by addition of labeled acetyl-CoA to labeled oxaloacetate produced by TCA cycling (M3 and M4). When compared to the adjacent lung, the percent M2 and M4 citrate was increased in LA2 and KPS tumors, but not in KP tumors (Figure 2.2E). A similar pattern was observed in both glutamate and aspartate, amino acids that reflect TCA cycle labeling of αKG and oxaloacetate (OAA) (Figure 2.2F, 2G). Glucose label was observed in glutamine in both lung tumors and normal lung, suggesting both tissues synthesize glutamine from glucose (Figure 2.2H). Additionally, LA2 tumors exhibited an increase in M2 glutamine labeling, suggesting that glucose use to synthesize glutamine can be increased in some tumors (Figure 2.2H). To determine whether similar

metabolism is observed in xenograft tumors derived from established human lung cancer cell lines, [U-^{13}C]glucose was infused to an average final plasma enrichment of 78% (±9.78 %) in mice harboring tumors derived from A549 or H1975 cells. Analysis of the labeling patterns and metabolite pool sizes in these tumors relative to normal lung was similar to what was observed in LA2 and KPS tumors (Figure 2.2I, J, Figure A2C, D, E). Together, these data suggest that lung tumors oxidize glucose through PDH.

TCA cycle anaplerosis involving glucose-derived carbon and pyruvate carboxylase (*Pcx*) has been described as a feature of some human lung tumors (Cheng et al., 2011; Hensley and DeBerardinis, 2015; Sellers et al., 2015), and Pcx could contribute to the increased three carbon labeling (M3) of TCA cycle intermediates from glucose in all lung tumors examined (Figure 2.2B, E, F, G, I, J, Figure A2C and D). To specifically examine Pcx activity in tumor tissue, we infused tumor-bearing KP animals with [1-^{13}C]pyruvate to a final enrichment of 10.3 (±2.178%) and assessed metabolite labeling in normal lung and lung tumor tissue (Figure A3A and B). The ratio of M1 labeled aspartate, citrate and malate to M1 labeled pyruvate was higher in tumors compared to normal lung (Figure A3B). Because the labeled carbon on [1-^{13}C]pyruvate is lost during the PDH reaction, these data argue that pyruvate carboxylation is active in these tumors. Consistent with these studies, M3-labeled TCA cycle intermediates are observed in all models, with increased M3 species observed relative to M4 species (Figure 2.2E, F, G, I, J, Figure A2C, and D). Furthermore, the presence of M1 labeled species in amounts that are similar to M2 labeled species, and in excess of M3 and M4 species, raises the possibility that addition of a labeled CO2, derived from glucose oxidation and pyruvate carboxylase activity contributes to the labeling patterns observed (Figure A3A, C). Taken together, analysis of glucose fate in lung tumors suggests that in addition to lactate production, glucose is metabolized by the PDH complex and Pcx in lung tumors, and glucose is a major source of TCA cycle carbon in these tumor models.

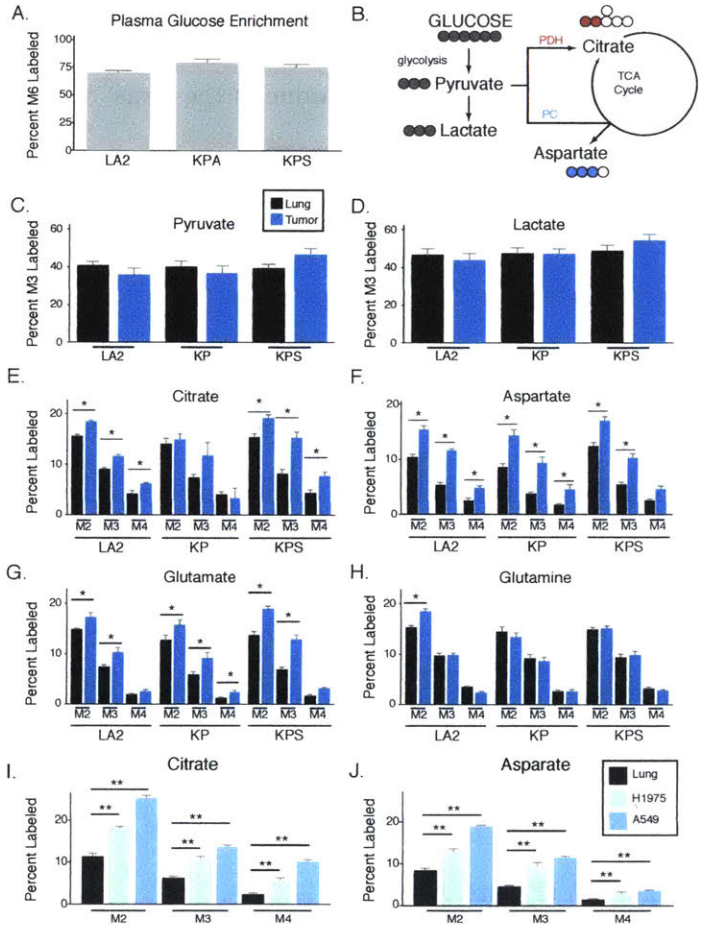

Figure 2.2. Increased glucose carbon contribution to the TCA in autochthonous Kras-driven lung tumors and xenografted lung cancer cells compared to adjacent lung. (A) Enrichment of fully labeled glucose (M6) in plasma from mice after a 6-hour [U-^{13}C]glucose infusion. (LA2, n = 4; KP, n = 6; KPS, n = 5). (B) Schematic showing major isotopomer transitions from glucose to label glycolytic and TCA cycle intermediates. The dominant TCA cycle isotopomers derived from the oxidation of glucose-derived pyruvate by the PDH complex has two labels (as shown in red for citrate), while the dominant isotopomer derived from pyruvate carboxylase (PC) retains three labeled carbon (as shown in blue for aspartate). (C, D) The percent M3 labeled pyruvate and lactate in lung (black) and lung tumors (blue) from mice following a 6-hour [U-^{13}C]glucose infusion. (LA2, n = 4; KP, n = 6; KPS, n = 5). (E-H) The percent labeling of citrate, aspartate, glutamate, and glutamine in lung (black) and lung tumors (blue) from mice following a 6-hour [U-^{13}C]glucose infusion. The M2, M3 and M4 isotopomers are shown for each metabolite. (LA2, n = 4; KP, n = 6; KPS, n = 5 for tumor and adjacent lung). For all panels, values represent the mean ±SEM. * Difference is statistically significant by two-tailed paired T-test, * $p < 0.05$. (I, J) The percent labeling of citrate and aspartate in normal lung (black) and xenografts derived from H1975 cells (EGFR-driven human lung cancer cells, green) or A549 cells (KRAS-driven human lung cancer cells, blue) from mice following a 6-hour [U-^{13}C]glucose infusion. The M2, M3 and M4 isotopomers are shown for each metabolite. (Lung, n = 8; H1975 tumor, n = 8; A549 tumor n = 8). For all panels, values represent the mean ±SEM. * Difference is statistically significant by two-tailed paired T-test, * $p < 0.05$ or ** $p < 0.01$.

Figure 2.2

Glutamine metabolism in lung tumor and normal lung tissue

Studies of Kras-transformed cells in culture suggest glutamine can also be an important source of TCA cycle carbon. To determine the fate of glutamine in the $Kras^{G12D}$-driven mouse tumor models, the human lung cancer cell line xenograft models, and normal lung tissue, [U-^{13}C]glutamine was infused into tumor-bearing animals to a final plasma enrichment between 30-60 % (Figure 2.3A). Surprisingly, we observed minimal labeling of glutamate and TCA intermediates in normal lung, autochthonous, syngeneic, or xenografted lung tumors despite the presence of labeled glutamine in these tissues (Figure 2.3B, C, D, Figure A4A-C). Furthermore, no significant differences in labeling of TCA cycle intermediates from glutamine was observed in tumors relative to normal lung tissue, with the exception of a small increase in M5 citrate in lung tumors relative to normal lung (Figure 2.3D, Figure A4D). Cultured cells that were transplanted into the lung demonstrated decreased intracellular glutamine labeling as compared to normal lung despite comparable glutamate labeling, suggesting that these tumors may exhibit increased glutamine conversion to glutamate relative to normal lung tissue, although even in these tumors the labeling of TCA cycle intermediates was less than 5% (Figure A4A-C).

To understand whether enzyme expression levels reflected the metabolic phenotypes we observe, expression of *Gls1*, *Pcx* and *Pdha1* in KP tumors were determined by Western blot and/or immunohistochemistry (Figure 2.3E, Figure A4E, Figure A4F). Of those enzymes, only Pcx expression was increased in KP tumors relative to normal lung. Phosphorylation of the E1α subunit of PDH (encoded by the *Pdha1* gene) can limit flux through the PDH complex to decrease glucose oxidation. In line with increased glucose labeling of TCA cycle intermediates, levels of phosphorylated PDHE1α were similar in both tumor and normal lung (Figure 2.3E). Furthermore, in all three $Kras^{G12D}$-driven mouse cancer models labeling of TCA intermediates from glucose is

observed while labeling from glutamine is minimal, suggesting that glucose rather than glutamine is a major source of carbon for the TCA cycle in these lung tumors (Figure 2.3F).

Environment influences the metabolic phenotype of $Kras^{G12D}$ lung cancer derived cells

To understand whether cells derived from autochthonous tumors retained the same metabolic phenotypes in cell culture, we traced [U-^{13}C]glucose and glutamine in cell lines derived from lung tumors arising in KP mice. Consistent with previous studies examining glucose metabolism in *Ras*-transformed cell lines, KP tumor-derived cell lines convert glucose to lactate at nearly a 1:2 molar ratio, suggesting the primary fate of glucose is lactate in these cells in culture (Figure 2.4A). To quantify the relative fate of glucose carbon under these conditions, we performed metabolic flux analysis (MFA) using stable isotope tracing of [1,2-^{13}C]glucose and [U-^{13}C]glutamine (Figure 2.4B and Appendix A Methods). These data support that the dominant fate of glucose in these lung cancer cells in culture is lactate, while relatively little glucose-derived carbon contributes to the TCA cycle. In addition, as observed in most cultured cells, glutamine labels TCA intermediates to high levels when the lung cancer cells are cultured in either 2D or 3D culture conditions (Figure 2.4C, D, Figure A5A). Consistent with glutamine metabolism by these cells, their ability to proliferate in culture is dependent on the concentration of glutamine in the media (Figure 2.4E), and they are sensitive to the glutaminase inhibitor CB-839 (Figure 2.4F) (Gross et al., 2014). Dose dependent reduction in M5-glutamate was observed with addition of CB-839 while M5-glutamine levels remained constant (Figure A5B, C), confirming that CB-839 inhibits glutaminase in these cells. These data suggest that despite a lack of preferential glutamine use by tumors *in vivo*, cell lines derived from KP lung tumors rely on glutamine metabolism for proliferation *in vitro*. Furthermore, because transplantation of the same KP cells back into the lung (KPS model) results in tumors with a metabolic phenotype similar to spontaneously arising lung cancers, the lung tissue

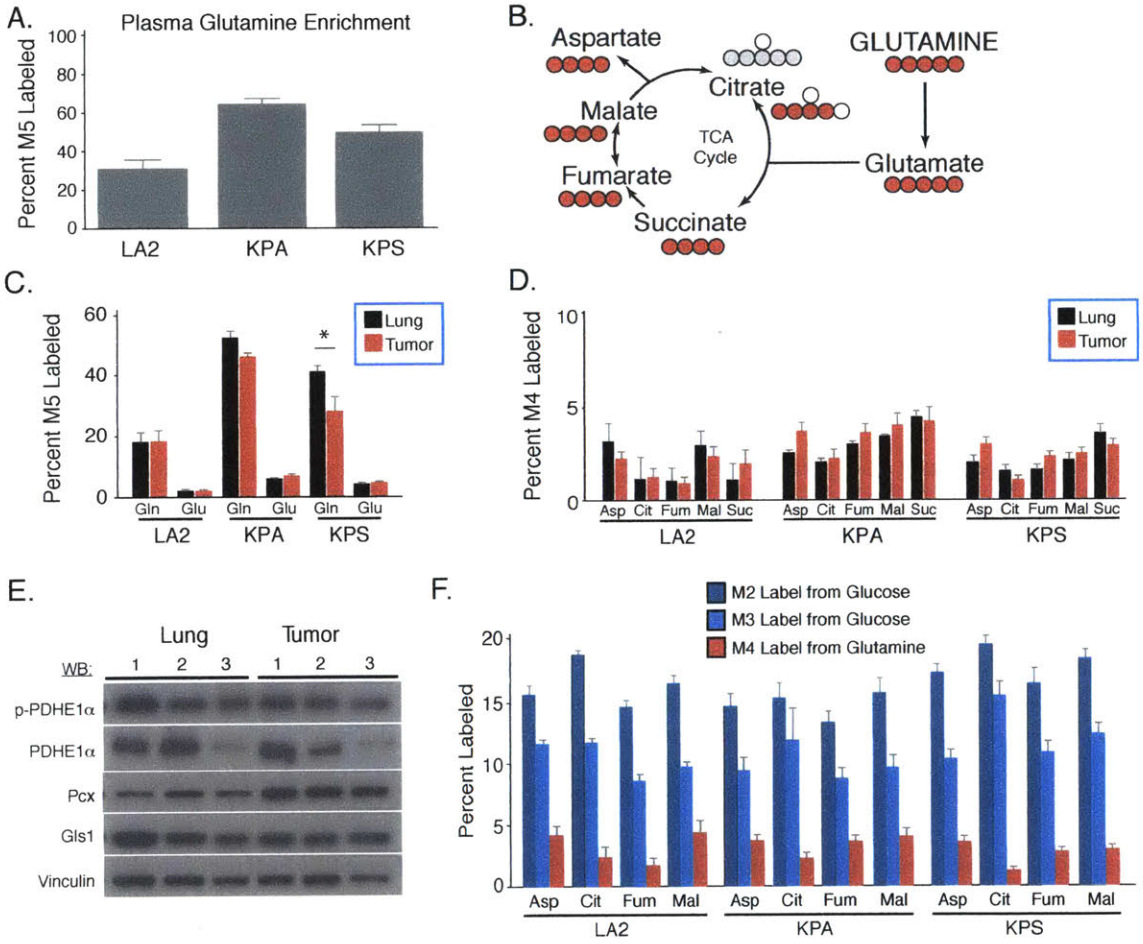

Figure 2.3. Glutamine carbon contributes minimally to the TCA cycle in *Kras* driven lung tumors and adjacent lung. (A) Enrichment of fully labeled glutamine (M5) in plasma from mice following 6-hour [U-^{13}C]glutamine infusion. (LA2, n = 4; KP, n = 4; KPS, n = 4). (B) Schematic showing major isotopomer transitions from glutamine to label TCA cycle intermediates. The dominant TCA cycle isotopomers produced by oxidative of glutamine metabolism have 4 labeled carbons for all species shown (red circles), while the dominant isotopomer of citrate from reductive glutamine metabolism is M5 (grey circles). (C) The percent M5 labeled glutamate and glutamine in lung (black) and lung tumors (red) from mice following 6-hour [U-^{13}C]glutamine infusion. (LA2, n = 4; KP, n = 4; KPS, n = 4). (D) The percent M4 labeling of aspartate (Asp), citrate (Cit), fumarate (Fum), malate (Mal) and succinate (Suc) in the lung (black) and lung tumors (red) from mice following 6-hour [U-^{13}C]glutamine infusion. (LA2, n = 4; KP, n = 4; KPS, n = 4). (E) Western blot analysis of phospho-pyruvate dehydrogenase subunit E1α (p-PDHE1α), total PDHE1α, pyruvate carboxylase (Pcx), and glutaminase (Gls1) expression in three representative KP lung tumors (Tumor) and normal lung tissue from three mice (Lung). Vinculin expression was also assessed in all samples as a loading control. (F) The percent labeling of aspartate (Asp), citrate (Cit), fumarate (Fum), and malate (Mal) in tumor tissue from the indicated models after a 6 hour infusion of [U-^{13}C]glucose and [U-^{13}C]glutamine. Values were normalized to plasma enrichment of glucose or glutamine to allow comparison of the indicated isotopomers. (For [U-^{13}C]glucose infusions, LA2, n = 4; KP, n = 6; KPS, n = 5. For [U-^{13}C]glutamine infusions, LA2, n = 4; KP, n = 4; KPS, n = 4). For all panels, values represent the mean ±SEM. *Difference is statistically significant by two-tailed paired T-test, $p < 0.05$.

Figure 2.3

environment must be an important determinant of lung cancer nutrient metabolism.

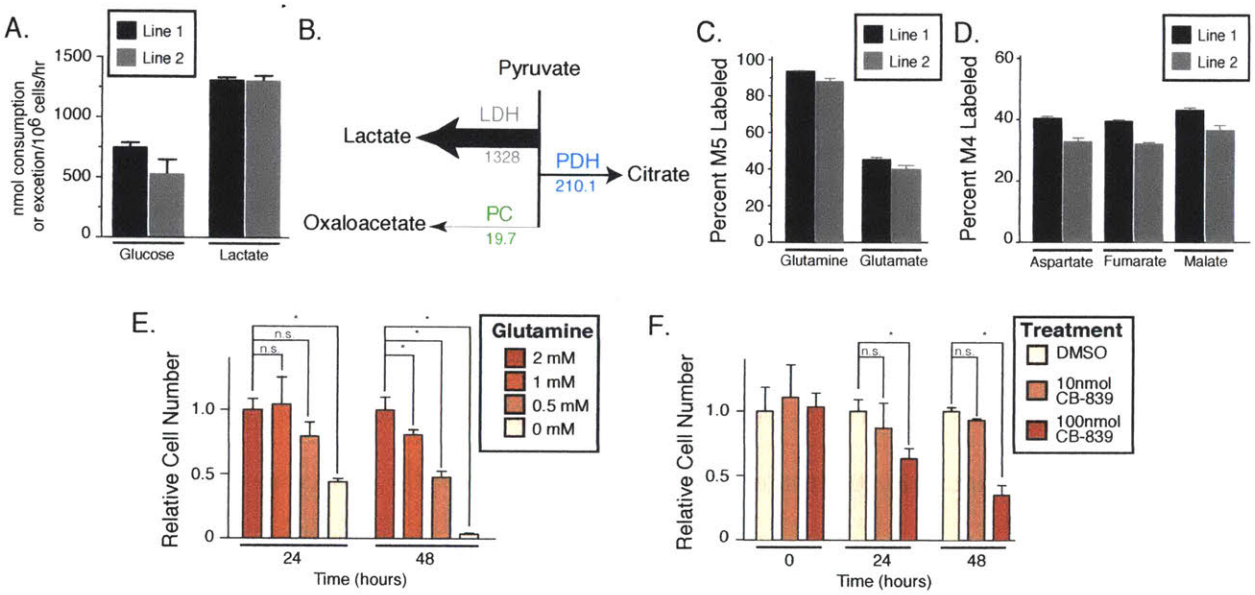

Figure 2.4. Metabolism of glucose and glutamine by cell lines derived from KP lung tumors. Rate of glucose consumption and lactate excretion by two independently derived lung cancer cell lines from KP lung tumors (Line 1 and Line 2), n = 3. Absolute fluxes downstream of pyruvate calculated from glucose and glutamine ^{13}C labeling data in the lung cancer cell lines derived from KP lung tumors. The values shown for each flux are fmol/cell/hr, and the arrows indicating each flux are to scale. (C) The percent M5 labeled glutamate and glutamine from [U-^{13}C]glutamine in the lung cancer cell lines derived from KP lung tumors, n = 3. (D) The percent M4 labeled aspartate, fumarate, and malate from [U-^{13}C]glutamine in the lung cancer cell lines derived from KP lung tumors, n = 3. (E) Equal numbers of the lung cancer cell lines derived from KP mice were placed in media containing the indicated concentration of glutamine. Relative cell numbers present after 24 and 48 hours are shown, n=3. (F) Equal numbers of the lung cancer cell lines derived from KP mice were plated, and then cultured in the presence of vehicle alone (DMSO) or the indicated concentration of CB-839, a glutaminase inhibitor. Relative cell numbers present at the time of vehicle or CB-839 addition or after 24 or 48 hours of exposure are shown, n=3. For all panels, values represent mean ±SD, * denotes difference is statistically significant by two-tailed T-test, $p < 0.05$.

Figure 2.4

$Kras^{G12D}$ tumors do not preferentially rely on glutamine for tumor growth

To determine whether the metabolic phenotype observed in lung tumors reflects metabolic dependencies of these tumors, we examined whether glutaminase is required for KP tumor growth *in vivo*. Tumor-bearing KP mice with lung tumors identified using micro-computed tomography imaging (μCT) were treated with vehicle or 200mg/kg oral CB-839 (Figure 2.5A). Examination of tumor size by μCT scans showed no differences after 4 weeks of continuous treatment with once

daily dosing of vehicle or CB-839. The level of CB-839 in the tumor was approximately 1.5 nmol/g of tissue, an amount similar to that reported previously (Figure 2.5B) (Gross et al., 2014). Furthermore, when lung tumors were examined by μCT scan after 4 weeks of treatment with vehicle or CB-839, gross tumor burden was similar in both groups (Figure 2.5A). When tumors were harvested the histological appearance of the tumors was unchanged and no change in proliferation assessed by Ki-67 staining was observed with CB-839 treatment (Figure 2.5C, D). Additionally, unlike sensitive tumor models (Gross et al., 2014), no increase in apoptosis was observed by cleaved-caspase-3 staining (Figure 2.5E). To confirm CB-839 exposure in this model was adequate to inhibit glutaminase, lung tumor-bearing animals treated with vehicle or CB-839 were infused with [U-^{13}C]glutamine prior to tumor collection. Consistent with glutaminase inhibition in CB-839 treated tumors, relative intratumoral glutamate-to-glutamine concentration ratios decreased (Figure 2.5F). In addition, although the percent labeled glutamine (M5) in the tumors was similar in vehicle and CB-839 treated mice, significantly less labeled glutamate was noted in tumors exposed to CB-839 (Figure 2.5G). These data are consistent with CB-839 inhibiting glutaminase in the tumors and suggest that this degree of glutaminase inhibition is not sufficient to slow tumor growth in this model.

To test glutaminase dependency genetically, we attempted to delete *Gls1* in KP tumor-derived cell lines using CRISPR/Cas9-based gene disruption (Figure A6A). However, in line with dependence on glutamine metabolism for proliferation in culture, we were unable to generate any *Gls1* knockout cell lines (0/71 screened clones). This suggests that *Gls1* is essential for KP tumor cell proliferation in culture. To assess whether *Gls1* is required for the growth of autochthonous KP tumors, we utilized CRISPR/Cas9-based somatic editing to disrupt *Gls1* in lung tumor tissue. A lentiviral vector containing sgRNA to *Gls1*, *Cas9*, and *Cre*-recombinase (pSECC) was delivered to the lungs of KP mice (Sánchez-Rivera et al., 2014), and a spectrum of tumors formed with both

high and low Gls1 expression (Figure 2.5H, Figure A6K). These findings argue that high Gls1 activity or expression is not required for lung tumor initiation or progression in this model and is consistent with pharmacological inhibition of glutaminase having no effect on growth of these tumors. These findings are also consistent with the metabolite tracing data showing minimal contribution of glutamine carbon to the TCA cycle in these *Kras*-driven lung tumors.

Mitochondrial metabolism of pyruvate is essential for tumor formation in vivo

To determine whether enzymes involved in mitochondrial glucose metabolism are required for cancer cell proliferation in culture and *in vivo*, we deleted enzymes required for entry of glucose carbon into the TCA cycle. The PDH complex and Pcx are required for oxidative glucose metabolism, with PDH generating acetyl-CoA for the TCA cycle and Pcx required for the generation of oxaloacetate from pyruvate as a source of anaplerotic TCA cycle carbon. Using CRISPR/Cas9, both *Pcx* and the E1α subunit of PDH (*Pdha1*) were disrupted in cancer cells derived from KP lung tumors (Figure A6B, C). Stable cell lines lacking *Pdha1* and *Pcx* were confirmed to harbor disruptions in these genes, and their protein products are not expressed (Figure 2.6A, Figure 2.7A, Figure A6B, C). The ability to oxidize glucose and to utilize glucose for anaplerosis was also decreased following deletion of Pdha1 or Pcx (Figure 2.6B, Figure 2.7B, Figure A7). Consistent with previous studies arguing glucose oxidation is not required for proliferation of most cells in culture, we observed minimal difference in the proliferation of *Pdha1*- and *Pcx*-deleted cells relative to wild-type cells in 2D or in 3D culture conditions (Figure 2.6A, Figure A7A, Figure A6D, F, H). However, when transplanted into the flanks of syngeneic recipient mice, cells harboring mutations in either *Pcx* or *Pdha1* fail to form tumors that grow larger than the initial mass of cells injected (Figure 2.6C, Figure 2.7C, Figure A6E, and G). We confirmed that unlike tumors that form from control cells, the *Pcx*- and *Pdha1*-deleted cells still present at the injection site as cytostatic masses did not express

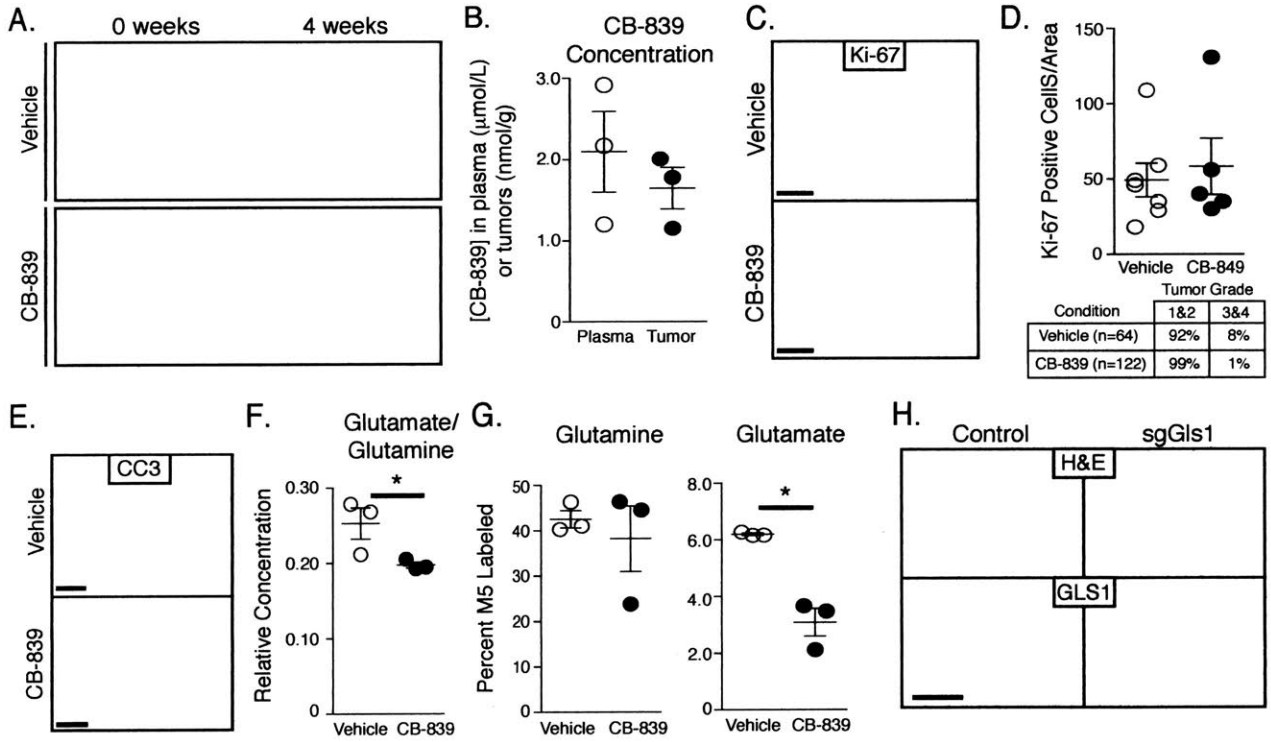

Figure 2.5. KP-lung tumors are not dependent on high glutaminase activity. (A) Coronal µCT scan sections showing the lungs of mice prior to treatment, and after treatment for 4 weeks with vehicle or the glutaminase inhibitor CB-839 treated mice. The images are representative of those obtained from 5 vehicle- and 6 CB-839-treated mice after 4 weeks of CB-839 treatment. (B) Concentration of glutaminase inhibitor CB-839 in plasma and tumor, with each circle representing a value in a single animal. The mean value and SD are also shown. (C) Ki-67 staining of lung tumor sections obtained from KP mice treated with vehicle or CB-839 for 4 weeks. The staining shown is representative of that observed in tissue from 5 vehicle- and 6 CB-839-treated mice. Scale bar: 200µM. (D) Quantification of Ki-67 staining in KP lung tumor sections obtained from mice treated with vehicle or CB-839 for 4 weeks. Each point represents data from an independently derived tumor, and the mean ±SEM is indicated as are the percent tumors graded histologically as grade 1 and 2 or 3 and 4. (E) Representative immunohistochemical staining of Cleaved-Caspase 3 (CC3) in vehicle versus CB-839 treated mice. Scale bars indicate 200µM. (F) Relative concentration of glutamate to glutamine in tumors from KP mice treated with vehicle or glutaminase inhibitor for 4 weeks. (G) The percent M5 labeled glutamine and glutamate in lung tumors from KP mice infused for 6-hours with [U-^{13}C]glutamine. Animals were treated for 4 weeks with vehicle or CB-839 as indicated. Each point represents data from an independently derived tumor, and the mean ±SEM is indicated. (H) Short guide RNA sequences to disrupt Gls1 or a non-targeted control were delivered along with Cas9 and Cre recombinase to induce KP lung tumors. Representative IHC images examining Gls1 expression in tumors arising in mice exposed to control sgRNAs, or sgRNAs that target Gls1 is shown. Scale bar: 200µM. *Difference is statistically significant by two-tailed T-test, $p < 0.05$.

Figure 2.5

Pcx and *Pdha1*, respectively (Figure 2.6E, Figure 2.7E), and showed changes in metabolite labeling that are consistent with enzyme deletion (Figure 2.6D, Figure A7D). In addition, when transplanted orthotopically into the lungs of syngeneic mice, tumor formation from *Pcx*- and *Pdha1*-deleted cells was severely compromised (Figure 2.6F, Figure A7F, Figure A6I). Finally, disruption of *Pdha1* or *Pcx* using pSECC-derived Lentivirus to deliver sgRNAs and Cas9 together with Cre-recombinase to the lungs of KP mice (Sánchez-Rivera et al., 2014) resulted in tumors that retained *Phda1* expression (animals injected with *sgPhda1*, Figure A6G and Figure A6J) or no detectable tumors (animals injected with sgPcx, Figure 2.7G and Figure A6J). These data suggest that both *Pcx* and *Pdha1* are required for tumor initiation and proliferation *in vivo*, and are consistent with TCA cycle metabolism being an important fate of glucose in *Kras*-driven lung tumors. These findings also argue that assessment of nutrient fates in tumors reflects metabolic dependencies of cancer cells in a physiological tissue environment.

Discussion

These findings suggest increased glucose uptake in *Kras*-driven NSCLC is used to support both increased lactate production and increased TCA cycle metabolism, challenging the notion that tumors switch from oxidative glucose metabolism to aerobic glycolysis (Vander Heiden et al., 2009). The exclusive metabolism of glucose to lactate by tumors has also been questioned by analysis of glucose fate in glioblastoma, lung cancers and liver cancers (Maher et al., 2012; Marin-Valencia et al., 2012; Yuneva et al., 2012). The finding that oxidative metabolism of glucose is increased *in vivo* raises the possibility that the use of glucose to support the TCA cycle is important to support cell proliferation under the conditions present in tissues.

It has been hypothesized that high flux through glycolysis benefits tumors by allowing ATP production in the absence of oxygen and by promoting anabolic metabolism (Gatenby and Gillies,

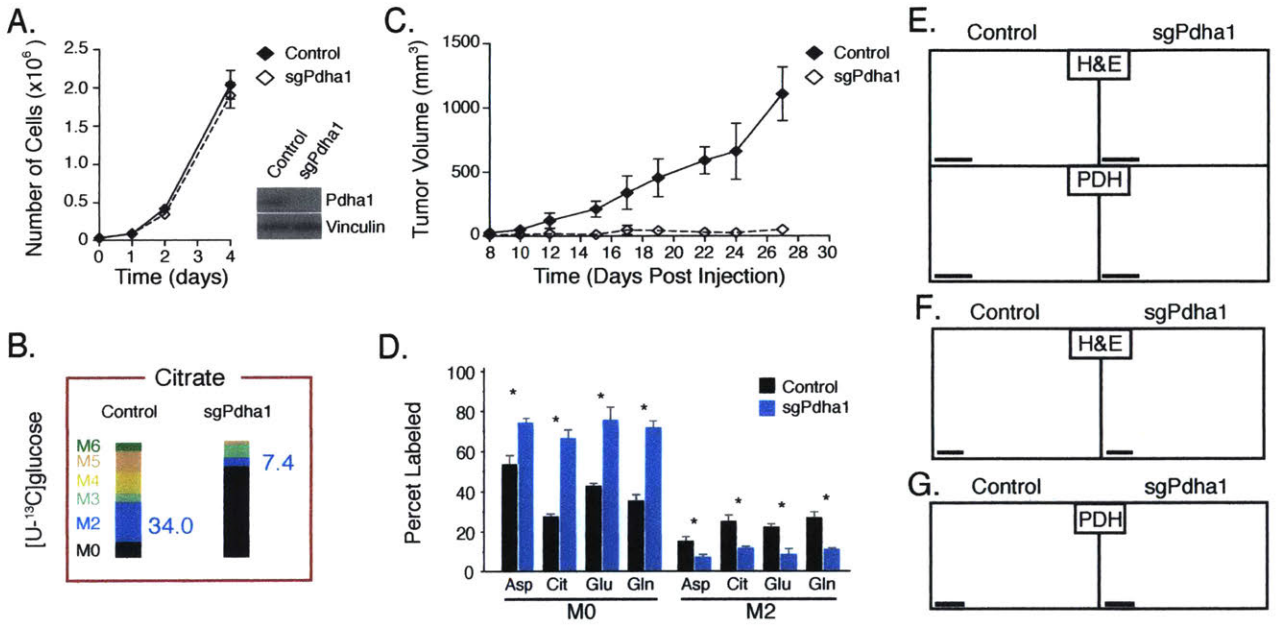

Figure 2.6. Lung cancer cells require *Pdha1* for tumor formation *in vivo*. (A) sgRNAs targeting *Pdha1* or control were introduced into lung cancer cells derived from KP lung tumor. Proliferation of control and Pdha1 disrupted cells in culture is shown (n=3), as is a Western blot analysis showing *Pdha1* expression from isogenic clones. (B) The same cells described in (A) were cultured in the presence of [U-^{13}C]glucose. Percent labeling of citrate isotopomers is shown for Control and *Pdha1*-disrupted cell lines. The percent M2 isotopomer of citrate that can be generated from glucose via flux through *Pdha1* is also presented in blue, and percent labeling of other isotopomers of citrate displayed, n = 3. (C) The same cells described in (A) were introduced as allografts into the flanks nu/nu mice. Tumor growth over time is shown. n = 4/cell line. (D) The same cells described in (A) were introduced as allografts into the flanks of mice. The percent labeling of aspartate (Asp), citrate (Cit), glutamate (Glu), and glutamine (Glu) in lung tumors derived from control cells (black) or material present at the injection site from *Pdha1*-disrupted cells (blue) was determined following a 6-hour [U-^{13}C]glucose infusion. The M0 and M2 isotopomers are shown for each metabolite. All values in mean ±SEM. *Difference is statistically significant by two-tailed T-test, $p < 0.05$. (E) The same cells described in (A) were introduced as allografts into the flanks of nu/nu mice. Immunohistochemistry assessing *Pdha1* expression in lung tumors derived from control cells or material present at the injection site from *Pdha1*-disrupted cells is shown. Scale bar: 200µM. (F) Representative H&E staining of the same cells described in (A) 4 weeks after orthotopic transplantation into the lungs of *nu/nu* mice. Scale bar: 200µM. (G) Representative immunohistochemical staining for *Pdha1* in tumors arising in KP mice infected with pSECC containing a control sgRNA (Control) or sgPdha1 (n = 25 tumors from ctrl and 18 tumors from sgPdha1 from 3 mice analyzed, all tumors retained *Pdha1* expression). Scale bar indicates 200µm.

Figure 2.6

2004). Increased lactate production supports NAD^+ regeneration in the absence of oxygen consumption and may provide other benefits to tumor cells related to altered pH or supplying lactate to other tumor cells (Sonveaux et al., 2008). Near quantitative conversion of glucose to lactate is a phenotype observed in proliferating cells in culture, raising the possibility that a similar phenotype is present in proliferating cells of lung tumors. Because a substantial fraction of the tumor is not actively proliferating, the increase in oxidative glucose metabolism might reflect the metabolic phenotype of non-proliferating cells. In mouse breast cancer, proliferating and non-proliferating cells regulate glucose metabolism differently such that the non-proliferating cells select for increased pyruvate kinase activity, a regulatory state associated with increased oxidative glucose metabolism (Israelsen et al., 2013). Differences in lactate production are present across the NSCLC models considered for this study. Whereas the KP, KPS, and xenograft models form tumors with a higher proliferative index, the LA2 model forms lower grade tumors. Consistent with a model where increased lactate production tracks with increased proliferation, lactate levels are increased in KP, KPS, and xenograft tumors relative to normal tissue but not in LA2 tumors. However, KPS tumors proliferate faster than KP tumor, and if anything lactate levels are lower in the KPS tumors arguing that lactate levels do not always scale with proliferation. While all of the tumor models examined contain a high proportion of cancer cells relative to other cell types, differences in glucose metabolism are observed in different regions of human cancers (Hensley et al., 2016). Thus, unknown factors driving tumor heterogeneity might also contribute to the metabolic phenotype differences observed in tumor tissue.

Decreased PDH flux has been described as a property of tumors, with PDH reactivation proposed as a cancer therapy (Michelakis et al., 2008). Surprisingly, glucose metabolism through PDH is increased in tumors relative to normal lung tissues and the cancer cells are dependent on this enzyme for tumor formation. Increased inhibitory phosphorylation of PDHE1α was also not

observed in these tumors. One possibility is the lack of increased PDHE1α phosphorylation reflects increased oxygenation. Indeed, the lung is a relatively well-perfused organ providing access to circulating nutrients and oxygen, although as lung cancers grow vascularization can become limiting and even large human lung tumors have elevated PDH flux ((Hensley et al., 2016)). This suggests that oxidative glucose metabolism may provide benefits to tumor cells such as the production of aspartate (Sullivan et al., 2015) regardless of tumor size.

Despite exposure to among the highest oxygen tensions in the body, normal lung uses 30-50 % of consumed glucose to make lactate and 20% to make CO2 while contributing relatively minor amounts to protein and lipid biosynthesis (Fisher, 1984). Outside of cytosolic ATP production and NAD^+ regeneration, the benefit for normal lung physiology of relatively high flux to lactate remains unclear. Although the flux from glucose to lactate in the lung is high relative to other tissues, glucose also supports production of TCA cycle intermediates in the lung. Notably, glucose fuels glutamate and glutamine production in lung tissue in rats and humans, and lung tissue is among the highest producers of glutamine (Hensley et al., 2013).

Glutamine is the most abundant amino acid in tissue culture media and in the blood, yet in contrast to observations in cell culture, blood glutamine contributes minimally to both normal lung and lung tumor metabolism. Labeled glutamine was abundant in both tissues suggesting ineffective glutamine delivery cannot explain why this amino acid is not used as a fuel. Instead, both normal lung and lung tumors synthesize α-ketoglutarate, glutamate and glutamine from glucose-derived carbon. This is consistent with findings in MYC-driven lung tumors and glioblastoma (Maher et al., 2012; Marin-Valencia et al., 2012; Yuneva et al., 2012) and may reflect the glutamine use to excrete excess nitrogen from amino acid catabolism. Urea production for nitrogen excretion is restricted primarily to the liver and kidney in mammals, and glutamine carries excess nitrogen from peripheral tissues to these organs. Because the use of glutamine as a carbon source produces

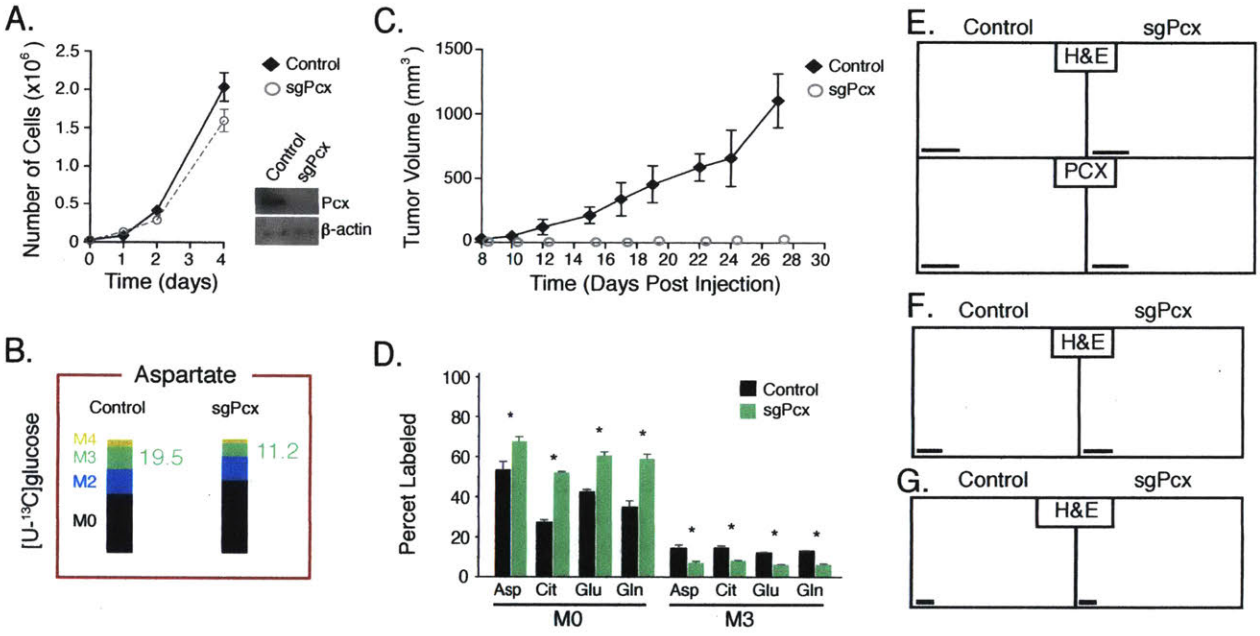

Figure 2.7. Lung cancer cells require Pcx for tumor formation *in vivo*. (A) sgRNAs targeting *Pcx* or control were introduced into lung cancer cells derived from KP lung tumor. Proliferation of control and *Pcx* disrupted cells in culture is shown (n=3), as is a Western blot analysis showing *Pcx* expression from isogenic clones. (B) The same cells described in (A) were cultured in the presence of [U-^{13}C]glucose. Percent labeling of aspartate isotopomers is shown for Control and *Pcx*-disrupted cell lines. The percent M3 isotopomer of aspartate that can be generated from glucose via flux through *Pcx* is also presented in green, and percent labeling of other isotopomers of aspartate displayed, n = 3. (C) The same cells described in (A) were introduced as allografts into the flanks of nu/nu mice. Immunohistochemistry assessing Pcx expression in lung tumors derived from control cells or material present at the injection site from *Pcx*-disrupted cells is shown. (D) The same cells described in (A) were introduced as allografts into the flanks of mice. The percent labeling of aspartate (Asp), citrate (Cit), glutamate (Glu), and glutamine (Glu) in lung tumors derived from control cells (black) or material present at the injection site from *Pcx*-disrupted cells (green) was determined following a 6-hour [U-^{13}C]glucose infusion. The M0 and M3 isotopomers are shown for each metabolite. All values in mean ±SEM. *Difference is statistically significant by two-tailed T-test, $p < 0.05$. (E) The same cells described in (A) were introduced as allografts into the flanks of nu/nu mice. Immunohistochemistry assessing Pcx expression in lung tumors derived from control cells or material present at the injection site from *Pcx*-disrupted cells is shown. Scale bar: 200μM. (F) Representative H&E staining of the same cells described in (A) 4 weeks after orthotopic transplantation into the lungs of mice. Scale bar: 200μM. (G) Representative hematoxylin and eosin staining of KP mice infected with pSECC containing a control sgRNA (Control) and sgPcx (n = 4 mice analyzed, no tumors were observed in the sgPcx mice). Scale bar indicates 2mm.

Figure 2.7

ammonia, glutaminase activity may be better tolerated in tissue culture where large media volumes prevent ammonia accumulation to toxic levels. However, because of an increased need for glutathione (Sellers et al., 2015), nucleotides, and amino acids; tumor nitrogen requirement is higher than that of normal tissues (Mayers and Vander Heiden, 2015). Nevertheless, the net production of glutamine by lung tumors despite the availability of this amino acid from the circulation suggests alternative sources of nitrogen are used, possibly reflecting the propensity of *RAS*-cancers to catabolize extracellular protein (Commisso et al., 2013; Kamphorst et al., 2015).

The use of pyruvate carboxylase appears to be an important for anaplerosis in tumors *in vivo* (Fan et al., 2009; Sellers et al., 2015). Consistent with these findings, genetic deletion of Pcx prevents tumor growth while genetic deletion or inhibition of glutaminase has no observable effect. The fact that opposite dependencies were suggested by cell culture experiments highlights the importance of selecting targets for cancer therapy based on nutrient use in a relevant tissue context. The possibility that tissue context is an important determinant of how tumors utilize nutrients might also explain why chemotherapies targeting nucleotide metabolism show efficacy based on cancer tissue of origin. More directly, it suggests that targeting PDH or *Pcx* might inhibit lung tumor growth. In fact, lipoate derivatives act in part through PDH activity suppression and can be potent anticancer drugs *in vivo* (Zachar et al., 2011).

This study highlights the importance of model selection to identify metabolic cancer targets. Cell culture conditions are non-physiological with respect to nutrients, oxygen, and tolerance for excretion of toxic metabolites such as ammonia. Cell culture also selects for the most rapidly proliferating cells, and many tumor cells cannot be cultured *in vitro.* The fact that transplanted tumors exhibit a phenotype more similar to tumors arising in the lung that are never exposed to cell culture suggests that environment has a greater impact on how nutrients are utilized than genetic or epigenetic selection associated with cell line formation. The similarities between *Kras*-driven

NSCLC, an *EGFR*-driven lung tumor, and published studies of genetically distinct tumors further argues that tissue environment can dictate metabolic phenotypes across tumor types. This highlights the importance of considering environmental context in addition to genetics in metabolism studies, particularly in considering how best to target cancer metabolism.

Experimental Procedures

Mouse Cancer Models

All animal studies were approved by the MIT Committee on Animal Care. For autochthonous models, mice from a mixed 129/Sv and C57Bl/6J genetic background were used. C57Bl/6J or nu/nu mice were used for allografts and xenografts respectivley. Flank tumor growth was measured with calipers. Lung tumor volumes were assessed using an eXplore CT120-whole mouse μCT (GE Healthcare) with MicroView 3D Image Viewing (Parallax-Innovations) and OsiriX (OsiriX-Viewer) used for image analysis.

Glucose and Glutamine Infusion

Arterial and venous catheters were surgically implanted into the jugular veins and/or carotid artery of animals 3-4 days prior to infusions. Infusions were performed in free-moving conscious animals after a 6 hour fast. Mice were infused for a 6-hours at the specified rate prior to terminally anesthesia with sodium pentobarbital and rapid tissue harvest. Tissue was rapidly frozen using a BioSqueezer (BioSpec Products) to quench metabolism and stored at -80°C prior to metabolite extraction. Plasma insulin levels were determined using an ultrasensitive mouse insulin ELISA kit (Crystal Chem,#90080). Blood glucose levels from the same mice were measured using a handheld glucometer (One Touch).

Cell Culture

Cell lines from KP lung tumors were established by standard protocols. Isogenic clones were selected for comparison of CRISPR cell lines. For labeling studies and MFA, cells were cultured for 24 hours in DMEM containing 17.5mmol/L [U-^{13}C]glucose, [1,2-^{13}C]glucose, or 4mmol/L

[U-^{13}C]glutamine (Cambridge Isotopes Laboratories) prior to metabolite extraction. For labeling in 3D culture, Adherence plates (Corning) were used. Proliferation in 3D was assessed using CellTiter-Glo (Promega).

Metabolite Measurement

For metabolite extraction, 10-40mg tissue was weighed and homogenized cryogenically (Retsch Cryomill) prior to extraction in chloroforom:methanol:water (400:600:300). Samples were centrifuged to separate aqueous and organic layers, and polar metabolites dried under nitrogen gas for subsequent analysis by mass-spectrometry. For liquid chromatography mass spectrometry (LC-MS), dried metabolites were resuspended in water based on tissue weight with valine-D8 included as an injection control. Polar metabolites were analyzed using a Nexera X2 U-HPLC (Shimadzu, Marlborough, MA) and a Q-Exactive hybrid quadrupole orbitrap mass spectrometer (Thermo Fisher Scientific; Waltham, MA). Hydrophobic interaction liquid chromatography (HILIC) was used for positive ion mode (Townsend et al., 2013) and negative ion mode (Avanesov et al., 2014) as previously descrbied. MS data were processed using Tracefinder (version 3.2, Thermo Fisher Scientific; Waltham, MA). For gas chromatography mass spectrometry (GC-MS) dried metabolites were dissolved in 10µL/10mg wet tissue weight of 2 % methoxyamine hydrochloride in pyridine (Sigma) and held at 37°C for 1.5h, norvaline was added as an injection control. Tert-butyldimethylsilyl derivatization was initiated by adding 15µL/10mg wet weight of N-methyl-N-(tert-butyldimethylsilyl)trifluoroacetamide + 1% tert-butyldimethylchlorosilane (Sigma) and incubated at 37°C for 1hr. GC-MS analysis was performed using an Agilent 7890 GC equipped with 30m DB-35MS capillary column connected to an Agilent 5975B MS operating under electron impact ionization at 70eV with helium as a carrier gas and the detector in scanning mode. MIDs were corrected for natural isotope abundance as previously reported (Commisso et al., 2013).

Glucose, lactate, glutamine, and glutamate were measured using YSI biochemistry analyzer (Yellow Springs Instruments, Yellow Springs, OH). Exponential growth over the culture period was assumed for flux calculations.

CRISPR/Cas9 Gene Editing

sgRNAs were designed using E-CRISP (e-crisp.org) to *Pdha1*, *Pcx*, and *Gls1* with restriction enzyme compatible sites and a G was added to the +1 position where not already present for U6 transcription. sgRNAs cloned in U6-sgRNA-EFS-Cas9-2A-Puro or U6-sgRNA-EFS-Cas9-2A-Cre (pSECC) were used for cell lines and *in vivo* experiments respectively as previously described (Sánchez-Rivera et al., 2014).

Western Blot and Immunohistochemistry

Western blotting was conducted using manufacturer's recommended concentrations of antibodies against Vinculin (Sigma/V9131), Pcx (Thermo-Fisher/PA5-23055), Gls1 (Abcam/AB93434), p-Pdha1α (Calbiochem/AP1062), and Pdha1 (Proteintech/18068). For IHC, whole lungs and tumors were perfused with 4 % PFA and fixed overnight at room temperature. Tissues were paraffin embedded and cut into 5µM sections. Following antigen retrieval, sections were stained with Ki-67 (BD Pharmingen/556003), Cleaved Caspase 3 (Cell Signaling Technology/#9661), or the above antibodies using ABC Vectastain kit (Vector Laboratories) and developed with DAB and counterstained with hematoxylin and eosin. Quantification of Ki-67 and Cleaved Caspase 3 were performed using ImageJ (http://imagej.nih.gov).

Glutaminase Inhibitor

Animals were treated with 200mg/kg CB-839 or vehicle for 4 weeks after observing initial masses by μCT in the lung. The vehicle contained 25 % (w/v) hydroxypropyl-β-cyclodextrin in 10mmol/L citrate, pH 2.0 and CB-839 was formulated at 20mg/mL for a final dosing volume of 10mL/kg as previously described (Gross et al., 2014). CB-839 was quantified in tissues and plasma using LC-MS.

Statistical Analysis

Two-tailed paired and unpaired Student's T-test were performed for all experiments unless otherwise specified. Results for independent experiments are presented as mean ±SEM; results for technical replicates are presented as mean ±SD; results for MFA are presented with 95 % confidence intervals.

Acknowledgements

We thank Natalia Drosu for reagents and advice, the Swanson Biotechnology Center for mouse tissue processing, and the Vander Heiden Laboratory for thoughtful discussions. S.M.D. and A.L. were supported by an NSF Graduate Research Fellowship and T32GM007287. T.P. received support from Hope Funds for Cancer Research Fellowship. B.A.O. received support from K08HL119355 and Gilead Sciences Research Scholars Program. D.Y.G. received support from T32GM007753. M.G.V.H acknowledges support from the Broad Institute SPARC program, the Ludwig Center at MIT, the Burroughs Wellcome Fund and the NIH (P30CA1405141, R01CA168653).

References

Avanesov AS, Ma S, Pierce KA, ee Yim SH, heon Lee BC, et al. Age- and diet-associated metabolome remodeling characterizes the aging process driven by damage accumulation. *eLife* **3**, e02077 (2014).

Ayala JE, Samuel VT, Morton GJ, Obici S, Croniger CM, et al. Standard operating procedures for describing and performing metabolic tests of glucose homeostasis in mice. *Disease Models & Mechanisms* **3**, 525 (2010).

Bonnet S, Archer SL, Allalunis-turner J, Haromy A, Beaulieu C, et al. A mitochondria-K+ channel axis is suppressed in cancer and its normalization promotes apoptosis and inhibits cancer growth. *Cancer Cell* **11**, 1 (2007).

Cairns R, Harris I, Mak T. Regulation of cancer cell metabolism. *Nature Reviews Cancer* **11**, 85 (2011).

Cheng T, Sudderth J, Yang C, Mullen AR, Jin ES, et al. Pyruvate carboxylase is required for glutamine-independent growth of tumor cells. *Proceedings of the National Academy of Sciences* **108**, 8674 (2011).

Commisso C, Davidson SM, Soydaner-Azeloglu RG, Parker SJ, Kamphorst JJ, et al. Macropinocytosis of protein is an amino acid supply route in Ras-transformed cells. *Nature* **497**, 633 (2013).

Curtis SJ, Sinkevicius KW, Li D, Lau AN, Roach RR, et al. Primary tumor genotype is an important determinant in identification of lung cancer propagating cells. *Cell Stem Cell* **7**, 127 (2010).

Davidson SM, Vander Heiden MG. METabolic adaptations in the tumor MYCroenvironment. *Cell Metabolism* **15**, 131 (2012).

DuPage M, Dooley AL, Jacks T. Conditional mouse lung cancer models using adenoviral or lentiviral delivery of Cre recombinase. *Nature Protocols* **4**, 1064 (2009).

Engelman Ja, Chen L, Tan X, Crosby K, Guimaraes AR, et al. Effective use of PI3K and MEK inhibitors to treat mutant Kras G12D and PIK3CA H1047R murine lung cancers. *Nature Medicine* **14**, 1351 (2008).

Fan TWM, Lane AN, Higashi RM, Farag MA, Gao H, et al. Altered regulation of metabolic pathways in human lung cancer discerned by (13)C stable isotope-resolved metabolomics (SIRM). *Molecular Cancer* **8**, 41 (2009).

Fisher AB. Intermediary metabolism of the lung. *Environmental Health Perspectives* **VOL. 55**, 149 (1984).

Gatenby RA, Gillies RJ. Why do cancers have high aerobic glycolysis? *Nature Reviews Cancer* **4**, 891 (2004).

Gross MI, Demo SD, Dennison JB, Chen L, Chernov-Rogan T, et al. Antitumor activity of the glutaminase inhibitor CB-839 in triple-negative breast cancer. *Molecular Cancer Therapeutics* **13**, 890 (2014).

Hensley CT, DeBerardinis RJ. In vivo analysis of lung cancer metabolism: nothing like the real thing. *Journal of Clinical Investigation* **125**, 495 (2015).

Hensley CT, Faubert B, Yuan Q, Lev-Cohain N, Jin E, et al. Metabolic heterogeneity in human lung tumors. *Cell* **164**, 681 (2016).

Hensley CT, Wasti AT, Deberardinis RJ. Glutamine and cancer: cell biology, physiology, and clinical opportunities. *Journal of Clinical Investigation* **123**, 3678 (2013).

Herbst RS, Heymach JV, Lippman SM. Lung cancer. *The New England Journal of Medicine* **359**, 1367 (2008).

Israelsen WJ, Dayton TL, Davidson SM, Fiske BP, Hosios AM, et al. PKM2 isoform-specific deletion reveals a differential requirement for pyruvate kinase in tumor cells. *Cell* **155**, 397 (2013).

Jackson EL, Willis N, Mercer K, Bronson RT, Crowley D, et al. Analysis of lung tumor initiation and progression using conditional expression of oncogenic K-ras. *Genes & Development* **15**, 3243 (2001).

Johnson L, Mercer K, Greenbaum D, Bronson RT, Crowley D, et al. Somatic activation of the K-ras oncogene causes early onset lung cancer in mice. *Nature* **410**, 1111 (2001).

Jones RG, Thompson CB. Tumor suppressors and cell metabolism: A recipe for cancer growth. *Genes & Development* **23**, 537 (2009).

Jonkers J, Meuwissen R, van der Gulden H, Peterse H, van der Valk M, et al. Synergistic tumor suppressor activity of BRCA2 and p53 in a conditional mouse model for breast cancer. *Nature Genetics* **29**, 418 (2001).

Kamphorst JJ, Nofal M, Commisso C, Hackett SR, Lu W, et al. Human pancreatic cancer tumors are nutrient poor and tumor cells actively scavenge extracellular protein. *Cancer Research* **75**, 544 (2015).

Keshari KR, Sriram R, Van Criekinge M, Wilson DM, Wang ZJ, et al. Metabolic reprogramming and validation of hyperpolarized 13C lactate as a prostate cancer biomarker using a human prostate tissue slice culture bioreactor. *Prostate* **73**, 1171 (2013).

Lyssiotis CA, Son J, Cantley LC, Kimmelman AC. Pancreatic cancers rely on a novel glutamine metabolism pathway to maintain redox balance. *Cell Cycle* **12**, 1987 (2013).

Maher EA, Marin-Valencia I, Bachoo RM, Mashimo T, Raisanen J, et al. Metabolism of [U-13C]glucose in human brain tumors in vivo. *NMR in Biomedicine* **25**, 1234 (2012).

Marin-Valencia I, Yang C, Mashimo T, Cho S, Baek H, et al. Analysis of tumor metabolism reveals mitochondrial glucose oxidation in genetically diverse human glioblastomas in the mouse brain in vivo. *Cell Metabolism* **15**, 827 (2012).

Mayers JR, Vander Heiden MG. Famine versus feast: understanding the metabolism of tumors in vivo. *Trends in Biochemical Sciences* **40**, 130 (2015).

Michelakis ED, Webster L, Mackey JR. Dichloroacetate (DCA) as a potential metabolic-targeting therapy for cancer. *British Journal of Cancer* **99**, 989 (2008).

Onetti R, Baulida J, Bassols A. Increased glucose transport in ras-transformed fibroblasts: A possible role for N-glycosylation of GLUT1. *FEBS Letters* **407**, 267 (1997).

Rodrigues TB, Serrao EM, Kennedy BWC, Hu DE, Kettunen MI, et al. Magnetic resonance imaging of tumor glycolysis using hyperpolarized 13C-labeled glucose. *Nature Medicine* **20**, 93 (2014).

Sánchez-Rivera FJ, Papagiannakopoulos T, Romero R, Tammela T, Bauer MR, et al. Rapid modelling of cooperating genetic events in cancer through somatic genome editing. *Nature* **516**, 428 (2014).

Sellers K, Fox MP, Ii MB, Slone SP, Higashi RM, et al. Pyruvate carboxylase is critical for non-small-cell lung cancer proliferation. *The Journal of Clinical Investigation* **125**, 687 (2015).

Son J, Lyssiotis Ca, Ying H, Wang X, Hua S, et al. Glutamine supports pancreatic cancer growth through a KRAS-regulated metabolic pathway. *Nature* **496**, 101 (2013).

Sonveaux P, Vegran F, Schroeder T, Wergin MC, Verrax J, et al. Targeting lactate-fueled respiration selectively kills hypoxic tumor cells in mice. *Journal of Clinical Investigation* **118**, 3930 (2008).

Tan AS, Baty JW, Dong LF, Bezawork-Geleta A, Endaya B, et al. Mitochondrial genome acquisition restores respiratory function and tumorigenic potential of cancer cells without mitochondrial DNA. *Cell Metabolism* **21**, 81 (2015).

Townsend MK, Clish CB, Kraft P, Wu C, Souza AL, et al. Reproducibility of metabolomic profiles among men and women in 2 large cohort studies. *Clinical Chemistry* **59**, 1657 (2013).

Tuveson DA, Shaw AT, Willis NA, Silver DP, Jackson EL, et al. Endogenous oncogenic K-rasG12D stimulates proliferation and widespread neoplastic and developmental defects. *Cancer Cell* **5**, 375 (2004).

Van Den Heuvel APJ, Jing J, Wooster RF, Bachman KE. Analysis of glutamine dependency in non-small cell lung cancer: GLS1 splice variant GAC is essential for cancer cell growth. *Cancer Biology and Therapy* **13**, 1185 (2012).

Vander Heiden MG, Cantley LC, Thompson CB. Understanding the Warburg effect: the metabolic requirements of cell proliferation. *Science* **324**, 1029 (2009).

White E. Exploiting the bad eating habits of Ras-driven cancers. *Genes & Development* **27**, 2065 (2013).

Yuneva MO, Fan TWM, Allen TD, Higashi RM, Ferraris DV, et al. The metabolic profile of tumors depends on both the responsible genetic lesion and tissue type. *Cell Metabolism* **15**, 157 (2012).

Zachar Z, Marecek J, Maturo C, Gupta S, Stuart SD, et al. Non-redox-active lipoate derivates disrupt cancer cell mitochondrial metabolism and are potent anticancer agents in vivo. *Journal of Molecular Medicine* **89**, 1137 (2011).

3

Direct evidence for cancer cell-autonomous extracellular protein catabolism in pancreatic tumors

Author statement

Some passages and figures have been adapted or quoted verbatim from the following published articles:
Davidson, SM, Jonas, O, Keibler, MA, Hou, HW, Luengo, A, Vander Heiden, MG (2016). Direct evidence for cancer-cell-autonomous extracellular protein catabolism in pancreatic tumors. Nature Medicine, (December). *in press*

Authors

Shawn M. Davidson[1,2,3+], Oliver Jonas[1+], Mark A. Keibler[4], Han Wei Hou[5], Alba Luengo[1,2], Jared R. Mayers[1,2], Jeffrey Wyckoff[1], Amanda Del Rosario[1], Matthew Whitman[1], Christopher R. Chin[1], Kendall J. Condon[1,2], Alex Lammers[1], Katherine A. Kellersberger[6], Brian J. Stall[6], Gregory Stephanopoulos[4], Dafna Bar-Sagi[7], Jongyoon Han[4], Joshua D. Rabinowitz[8], Michael Cima[1], Robert Langer[1,4], and Matthew G. Vander Heiden[1,2,3,9*]

Author affilations

1. Koch Institute for Integrative Cancer Research, Massachusetts Institute of Technology, Cambridge, Massachusetts, USA
2. Department of Biology, Massachusetts Institute of Technology, Cambridge, Massachusetts, USA.
3. Broad Institute of MIT and Harvard University, Cambridge, Massachusetts, USA.
4. Department of Chemical Engineering, Massachusetts Institute of Technology, Cambridge, Massachusetts, USA.
5. Department of Electrical Engineering and Computer Science, Massachusetts Institute of Technology, Cambridge, Massachusetts, USA.
6. Bruker Daltronics, Inc. 40 Manning Rd, Billerica, MA 01821.
7. Department of Biochemistry and Molecular Pharmacology, New York University, New York, New York, USA.
8. Department of Chemistry and Integrative Genomics, Princeton University, Princeton, New Jersey, USA.
9. Department of Medical Oncology, Dana-Farber Cancer Institute and Harvard Medical School, Boston, Massachusetts, USA.
+ These authors contributed equally to this work.

Author contributions

Conceptualization: S.M.D, O.J., and M.G.V.H. Methodology: S.M.D., O.J., M.A.K., H.W.H., A.L., J.R.M., J.W., A.M.D., M.W., C.R.C., K.J.C., A.L., K.A.K., B.K.S., G.S., J.H. and D.B.-S.., Formal Analysis S.M.D., O.J., A.M.D. Investigation S.M.D. and O.J. Writing Original Draft: S.M.D., O.J., and M.G.V.H. Visualization S.M.D., O.J., and M.G.V.H. Supervision M.J.C., R.L., and M.G.V.H. Funding Acquisition O.J., J.D.R., R.L. and M.G.V.H.

Abstract

Protein scavenging by macropinocytosis can serve as a source of nutrients for pancreatic cancer cells. We provide direct evidence that extracellular protein is a fuel source for pancreatic cancer cells *in vivo*. We demonstrate that albumin-derived peptides and amino acids accumulate in tumors in a Kras-driven mouse model of pancreatic ductal adenocarcinoma. In addition, we implement a device to deliver large molecules directly into the tumor and observe protein catabolism and macropinocytosis by cancer cells within pancreatic tumors. Local release of a macropinocytosis inhibitor leads to a drastic reduction in amino acids levels in tumor tissue arguing that the direct uptake and catabolism of extracellular protein is necessary to provide amino acids to pancreatic cancer cells in tumors. These data provide evidence for albumin catabolism by tumors and also suggest a method for testing therapies that take advantage of the propensity of pancreatic cancer cells to scavenge extracellular protein.

Introduction

Mammalian tissues rely on a variety of nutrients to support physiological function(Metallo and Vander Heiden, 2013). Altered metabolic processes are involved in the pathogenesis of cancer, but which nutrients support inappropriate cancer cell growth within intact tumors is incompletely understood (Mayers and Vander Heiden, 2015; White, 2013; Vander Heiden et al., 2009). Amino acids, particularly glutamine and serine, have been shown to be essential nutrients for many cancer cell lines (Locasale, 2013; Wise and Thompson, 2010). Some cancer cells can also obtain key amino acids through catabolism of extracellular protein via macropinocytosis to fuel anabolic pathways required for growth (White, 2013; Kamphorst et al., 2015; Commisso et al., 2013). However, the source of amino acids contributing to cancer cell proliferation within intact tumors is less well

studied.

Albumin is the most abundant extracellular protein in blood and in tissues, and has been previously shown to be internalized into lysosomes of cells in tumors (Steinfeld, 1960; Schilling et al., 1992). Hypoalbuminemia is observed in many patients with cancer and epidemiological studies suggest that levels of serum albumin prior to therapy can be a predictor of survival (Rothschild et al., 1975; Gupta and Lis, 2010). Decreased albumin levels observed in cancer patients and tumor-bearing animals has been posited to be a result of decreased hepatic synthesis or increased degradation by the liver or other organs such as skeletal muscle (Jewell et al., 1975; Andersson et al., 1991; Fearon et al., 1998). Direct catabolism of albumin by the tumor itself might also contribute to hypoalbuminemia, but the extent to which this occurs *in vivo* remains controversial due to the lack of reliable methods to trace albumin fate.

Macropinocytosis is a conserved, actin-dependent, endocytic process that results in non-specific bulk internalization of extracellular material, including protein and other macromolecules, into the cell (Commisso et al., 2013; Kamphorst et al., 2015; Swanson and Watts, 1995). Pharmacological and genetic inhibition of macropinocytosis can inhibit cell line proliferation and xenograft tumor growth, presenting a potential therapeutic target for a subset of tumors (Commisso et al., 2013; Kamphorst et al., 2015). Protein scavenging has been posited based on levels of amino acids observed in human pancreatic tumors (Kamphorst et al., 2015), but direct evidence that protein is catabolized in a tumor-autonomous manner *in vivo* is lacking.

We utilize miniaturized plasma exchange to deliver labeled albumin to tissues in live mice and demonstrate albumin breakdown contributes to free amino acids in pancreatic tumors *in vivo*. In addition, we deliver albumin directly into the tumor using an implantable microdevice, adapted and modified from (Jonas et al., 2015), and directly observe protein catabolism and macropinocytosis in situ by cancer cells in pancreatic tumors but not in adjacent non-cancerous pancreatic tissue.

Intratumoral inhibition of macropinocytosis results in a decrease in amino acid levels. Taken together, these data suggest pancreatic cancer cells consume extracellular protein, including albumin, as a source of amino acids in spontaneously arising pancreatic tumors *in vivo.*

Results

Isotope-labeled mouse serum albumin ([^{15}N]MSA) was produced using the yeast Pichia pastoris (Swanson and Watts, 1995; Daly and Hearn, 2005; Tolner et al., 2006) (Figure B2A-C) in order to determine whether albumin could be used as a nutrient source by tumors *in vivo.* Exchanging endogenous albumin in the plasma for labeled albumin is necessary to obtain sufficient enrichment of labeled protein over reasonable infusion times to trace the fate of labeled albumin in tissues. Because albumin has a large volume of distribution in the body and slow turnover (approximately 1-2% total per day)(Rothschild et al., 1975; Merlot et al., 2014), we designed a plasmapheresis approach to exchange endogenous albumin with [^{15}N]MSA using a modified perfusion based microfluidic strategy (Hou et al., 2010, 2012) in mice with and without spontaneously arising pancreatic ductal adenocarcinoma (PDAC) (Figure B1D, E). PDAC was initiated by pancreas restricted Cre-recombinase (Pdx1-Cre) expression in $Kras^{LSL\text{-}G12D/+}$; $p53^{loxP/loxP}$ (KP) mice to induce mutant $Kras^{G12D}$ expression and loss of p53.

Following plasmapheresis in control (WT) and KP mice, we achieved an initial plasma enrichment of approximately 45% +/- 9.2% labeled albumin (Figure 3.1A) with minimal total protein loss from the plasma (Figure B2A). Despite slightly lower basal levels of protein in KP plasma as compared to WT mice, albumin levels were unchanged even in end-stage disease in mice with high tumor burden (Figure B2B). We reasoned that if albumin is being catabolized, [^{15}N]-labeled amino acids derived from albumin may be present in the plasma of these animals after plasma exchange (Figure 3.1B). Increased levels of labeled alanine, leucine, and phenylalanine were

observed in the plasma of tumor-bearing KP mice as compared to WT control mice approximately 12 hours after plasma exchange indicating the presence of albumin-derived amino acids in the blood and supporting previous work suggesting that whole body protein turnover is increased in KP animals with pancreatic tumors (Mayers et al., 2014) (Figure 3.1B). To determine the site(s) of albumin catabolism, we first examined labeled albumin peptides and free amino acids in normal pancreas from WT mice and PDAC tissue from KP mice. Labeled albumin peptides were increased in tumor relative to normal pancreas tissue, suggesting that labeled albumin uptake is increased in tumors (Figure 3.1C). Next, we examined free amino acids in tumor and normal pancreas following plasma-exchange. We observed a significant increase in many labeled free amino acids in the tumor relative to the normal pancreas demonstrating that amino acids from the breakdown of labeled albumin are enriched in the tumor relative to normal pancreas (Figure 3.1D).

To determine whether albumin-derived amino acids might be generated outside the pancreas through catabolism at distant sites, we examined labeled peptides and free amino acids in the liver, lung, and muscle of normal (WT) and tumor-bearing (KP) animals (Figure 3.1E, F and Figure B2C-F). In contrast to the findings in pancreatic tumors compared to normal pancreas, we observed no significant increase in albumin peptides in the livers of mice with pancreatic cancer relative to mice without pancreatic cancer (Figure 3.1E). Some ^{15}N-labeled free amino acids were increased in the livers of animals with pancreatic cancer (Figure 3.1F) and we also observed elevation in some labeled free amino acids in the lungs of tumor-bearing animals (Figure B2D). However labeled amino acids were not increased in skeletal muscle of mice with PDAC, and neither the lungs nor the skeletal muscle showed an increase in albumin peptides (Figure B2C, E). Together, the findings suggest that pancreatic tumors uptake more albumin than normal pancreatic tissues, and amino acids from the breakdown of albumin contribute more to the tumor than normal pancreas. The presence of labeled amino acids in the liver and other organs (Figure B2C-F) leaves

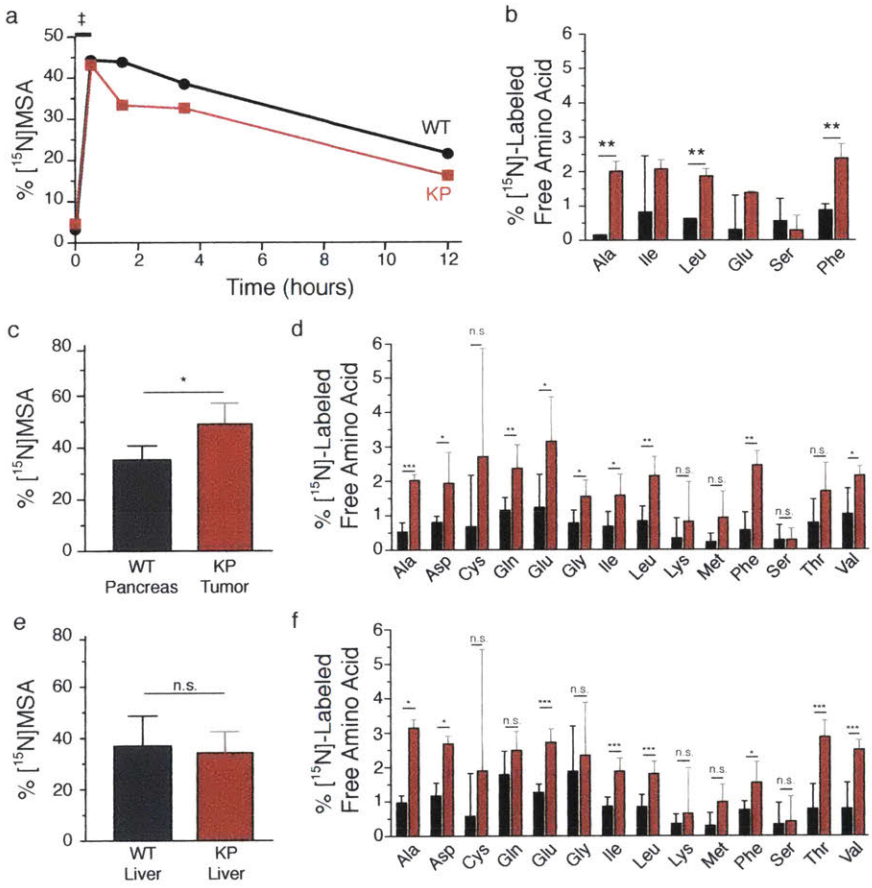

Figure 3.1. Albumin-derived amino acids are found in pancreatic tumors. (A) Representative albumin enrichment in the plasma of WT and KP mice following plasma exchange of [^{15}N]-labeled mouse serum albumin ([^{15}N]MSA) for endogenous albumin as assessed by analysis of labeled albumin peptides. The %[^{15}N]MSA shown was obtained by analysis of the albumin peptide LVQEVTDFAK in plasma by LC-MS/MS over time during and after plasma exchange (n = 5 per genotype). The time indicated by the double dagger corresponds to the 30-minute period of plasma exchange. (B) Labeled amino acids in the plasma of WT and KP mice following plasma exchange of [^{15}N]-labeled MSA for endogenous MSA. Plasma was sampled at the time of tissue collection (12 hours post-exchange). The presence of [^{15}N]-labeled amino acids was determined by GC-MS, (n = 5 per genotype). (C) Following plasma exchange of [^{15}N]-labeled MSA for endogenous MSA in WT and KP mice, the presence of [^{15}N]MSA in tissue was determined by analysis of multiple labeled peptides from normal pancreas (WT) or pancreatic tumors (KP) by LC-MS/MS, (n = 5 per genotype). (D) The presence of labeled amino acids in the pancreas (WT) or tumor (KP) from WT and KP mice respectively following plasma exchange of [^{15}N]-labeled MSA for endogenous MSA. Tissues were collected 12 hours post-exchange and labeled amino acids determined by GC-MS (n = 5 per genotype). (E) Following plasma exchange of [^{15}N]-labeled MSA for endogenous MSA in WT and KP mice, the presence of [^{15}N]MSA in tissue was determined by analysis of multiple labeled peptides from livers of animals with pancreatic tumors (KP) or without pancreatic tumors (WT) by LC-MS/MS, (n = 5 per genotype). (F) The presence of labeled amino acids in the livers of WT or KP mice 12 hours following plasma exchange of [^{15}N]-labeled albumin for endogenous albumin. Labeled amino acids were determined by GC-MS. For all panels, (Ala = alanine; Asp = aspartate; Cys = cysteine; Gln = glutamine; Glu = glutamate; Gly = glycine; Ile = isoleucine; Leu = leucine; Lys = lysine; Met = methionine; Phe = phenylalanine; Ser = serine; Thr = threonine; Val = valine), significance differences are noted as P * < 0.05; ** < 0.01; ***<0.001 (Student's t-test), n.s. difference not significant.

Figure 3.1

open the possibility that the labeling of amino acids in pancreatic tumor tissue results from a combination of local albumin catabolism and/or the uptake free labeled amino acids derived from albumin breakdown in non-tumor tissues.

To determine whether tumor-autonomous albumin catabolism is a feature of pancreatic tumors, we used an implantable device for delivery of small and large molecules into solid tissues (Figure 3.2A). The device was adapted from (Jonas et al., 2015) by modifying its diameter and reservoir sizes to allow for more effective release of large molecules into the pancreas. This device allows direct, controlled delivery of materials into the tumor microenvironment in a defined location that can be tracked via microscopy. Macropinocytosis can be visualized by tracking the fate of fluorescently labeled high molecular weight dextran (70kDa) a previously demonstrated marker of macropinocytosis (Racoosin and Swanson, 1993). Protein degradation can be assessed by employing self-quenched, BODIPY-labeled albumin (DQ-BSA), which becomes fluorescent upon enzymatic cleavage in the lysosomes of cells (Klionsky, 2009).

Devices loaded with 1µg of Rh-Dextran and DQ-BSA were implanted into subcutaneous xenografts derived from the MIA PaCa-2 (mutant RAS^{V12}) and BxPC-3 (WT *RAS*) human PDAC cell lines. These two cells lines have been reported previously to differ in their use of macropinocytosis for proliferation *in vivo* (Commisso et al., 2013). The implanted devices allowed local release of Rh-Dextran and DQ-BSA adjacent to (Figure 3.2B). We tracked the fate of DQ-BSA and 70kDa Rh-dextran delivered by the micro-devices to investigate whether internalization of proteins by macropinocytosis in cells can be observed in these xenograft tumors (Figure 3.2B, C, D). 24h after device implantation, high levels of dextran uptake and DQ-BSA fluorescence are observed to 650µm from the device in MIA PaCa-2 tumor tissue (Figure 3.2B). Dextran was also released into BxPC-3 tumors, exhibiting a similar gradient of intratumoral release as in MIA PaCa-2 tumors (Figure 3.2C). Combined local release with EIPA, an agent known to

inhibit the formation of macropinosomes, eliminated dextran uptake in MIA PaCa-2 tumors (Figure 3.2C). We monitored DQ-BSA fluorescence over two days to determine whether the observed Dextran diffusion is accompanied by cellular uptake by tumor cells and to further examine the kinetics of this degradation. Bright narrow regions of fluorescence observed in MIA PaCa-2 tumors indicate local protein degradation that appeared approximately 150μm from the device by 24h after device implantation (Figure 3.2D). At 48h, fluorescent regions appeared at approximately 400μm from the device (Figure 3.2D). The observed diffusion distances are congruent with previously observed intratumoral release studies of several large and small molecules (Jonas et al., 2015). In contrast, intratumoral fluorescence from DQ-BSA was not observed when identical devices were placed into BxPC-3 xenograft tumors (Figure 3.1D). These findings argue that local delivery of DQ-BSA allows determination of intratumoral albumin catabolism by macropinocytosis.

To determine if we can observe uptake and catabolism of protein in real time, we utilized live multiphoton imaging of fluorescence from both DQ-BSA and 70kDa Rh-Dextran released from micro-devices in MIA PaCa-2 and BxPC-3 tumors. We observed uptake of dextran and an increase in fluorescent signal from DQ-BSA in cells within xenografted MIA PaCa-2 tumors in mice (Figure 3.2E). Dextran uptake is observed in the majority of tumor cells present within the exposed region at one-hour post-device implantation. Uptake of albumin by tumor cells occurs at steady rates, with approximately 2/3 of the cells in an exposed region showing internalized Rh-Dextran and DQ-BSA fluorescence within 3 hours of device implantation (Figure 3.2E), a time consistent with the presence of albumin-derived amino acids observed in tumors in mice (Figure 3.1). In contrast, the BxPC-3 cell line exhibited Rh-Dextran labeling only of cell outlines, and few punctate spots from DQ-BSA were observed indicating minimal albumin degradation in these tumors (Figure 3.2E). Images from the DQ-BSA studies were also used to determine "macropinocytic index", a metric previously described to quantitate macropinocytosis in fixed samples (Bardeesy

et al., 2006). By this metric, MIA PaCa-2 cells exhibit 4-fold higher levels of macropinocytosis relative to BxPC3 cells (Figure 3.2F).

To assess macropinocytosis and local protein degradation in KP tumors, microdevices containing DQ-BSA were surgically implanted directly into the pancreas of 8-week old KP mice harboring autochthonous pancreatic tumors using a biopsy needle. In 8-week old KP mice the pancreas appears as a heterogeneous array of tumor and normal tissue (Mayers and Vander Heiden, 2015; Bardeesy et al., 2006) (Figure 3.3a and Figure B3A). 24h after device delivery, tissue adjacent to device reservoirs containing DQ-BSA exhibits fluorescence only when reservoirs were adjacent to tumor tissue (Figure 3.3A). No fluorescence of DQ-BSA was detected in non-tumor pancreas regions, suggesting an absence of albumin degradation at these sites. We next sought to determine the kinetics of dextran uptake and DQ-BSA degradation and whether these processes occurred in cells with K-ras^{G12D} activation within the pancreas. To distinguish Cre-expressing cells, multi-photon live microscopy was utilized in a KP mouse that also harbored a tdTomato $^{LSL/+}$ allele as a fluorescent marker of Cre-recombinase activity and, therefore, K-ras^{G12D} activation. Using multi-photon intravital microscopy, we observed a high degree of co-localization of fluorescent tdTomato signal and fluorescent DQ-BSA signal (Figure 3.3b) and an increase in fluorescence due to DQ-BSA degradation was observed over a 90-minute time period in tumor cells with tomato fluorescence (Figure 3.3C, D). When a microdevice is introduced into a KP mouse lacking the tdTomato allele comparable fluorescence from DQ-BSA is observed in tumor tissue, arguing that the observed DQ-BSA is not the result of overlap in the tdTomato and DQ-BSA emission/excitation spectra (Figure B3B). Based on DQ-BSA fluorescence, we further observed that the spontaneous KP tumors exhibit a level of macropinocytosis comparable to that observed in MIA PaCa-2 xenografts (Figure B3C).

One hallmark of pancreatic tumors, including tumors found in KP mice, is a dense stroma that

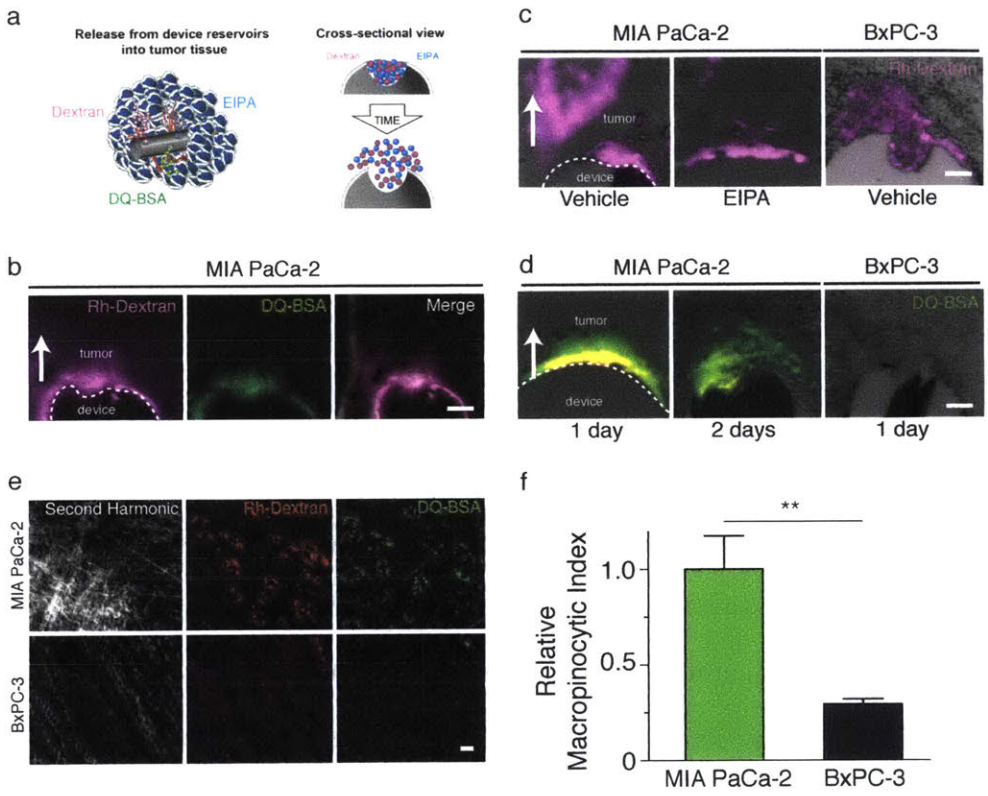

Figure 3.2. Direct assessment of macropinocytosis and albumin catabolism in tumors. (A) Schematic depicting device implanted directly into the tumor to release specified contents from reservoirs into distinct tissue regions. Radially outward diffusion of compounds from reservoirs is shown in 3-dimensional (left) and cross-sectional views (right). The orientation of the schematic on the right matches the orientation of device placement relative to tissue in panels b, c, and d. (B) Combined delivery of 70 kDa rhodamine-dextran (Rh-Dextran) and self-quenched, BODIPY-labeled bovine serine albumin (DQ-BSA). Both compounds are released from a single reservoir in MIA PaCa-2 tumors. Radial transport of compound is 150 µm from the device into tissue after a 24h incubation period. Scale bar, 200 µm. (images are representative of n = 6 from mice per cell line per condition with triplicate reservoirs). (C) Delivery of 70 kDa Rh-Dextran from the device into MIA PaCa-2 and BxPC-3 tumor tissue at 48h. Unlike MIA PaCa-2 tumors, BxPC-3 tumors have been shown previously not to engage in macropinocytosis8. Tissue penetration up to 550 µm is observed in each tumor. Co-delivery of 70kDa Rh-Dextran with the macropinocytosis inhibitor EIPA leads to reduced Rh-Dextran uptake in MIA PaCa-2 tumor tissue as shown. Scale bar, 150 µm. (images are representative of n = 6 from two mice per cell line per condition with triplicate reservoirs). (D) Comparison of albumin breakdown in MIA PaCa-2 and BxPC-3 tumor sections. Devices containing DQ-BSA were implanted into MIA PaCa-2 and BxPC-3 tumors as indicated. Degradation of BSA, indicated by fluorescence signal from DQ-BSA, increases over time in MIA PaCa-2 tumors a depth of 200 µm from the device after 1 day, and up to 350µm from the device after 2 days. Scale bar, 200 µm. (images are representative of n = 6 from two mice per cell line per condition with triplicate reservoirs). (E) Examination of albumin and dextran uptake in MIA PaCa-2 and BxPC-3 tumors. Multiphoton images of live tumors implanted with devices containing 70kDa Rh-Dextran and DQ-BSA. Fluorescence from DQ-BSA is observed in individual cells in MIA PaCa-2 tumors by 4h after device implantation, and high concordance is observed between cells that display Rh-Dextran uptake and DQ-BSA fluorescence. Scale bar, 50 µm. (images are representative of n = 2 mice per cell line per condition with duplicate reservoirs). (F) Quantification of relative macropinocytic index in MIA PaCa-2 and BxPC-3 xenograft tumors based on DQ-BSA fluorescence. Macropinocytic index is a ratio of the total area of all macropinosomes in a field of designated area (n=5 distinct fields per cell line). For all panels, white arrows indicate direction of delivery of DQ-BSA, Rh-Dextran, or EIPA. (data from n = 2 mice per cell line per condition with duplicate reservoirs used to calculate macropinocytic index).

Figure 3.2

is rich in extracellular matrix (ECM)(Whatcott et al., 2015; Mahadevan and Von Hoff, 2007). To determine whether tumor cells can internalize ECM-derived proteins, we utilized the microdevice to deliver TRITC-labeled fibronectin (440kDa), one of the largest protein components of the extracellular matrix. Using intravital microscopy in live mice, we observed clear uptake of fibronectin in tumor tissue in KP mice and not in the WT pancreas (Figure 3.3E). Taken together, these observations suggest that cells in spontaneously arising pancreatic tumors can consume protein in their environment.

Hydroxychloroquine is a lysosomal inhibitor being studied as a potential therapy for PDAC (Manic et al., 2014). To determine whether we could inhibit catabolism of DQ-BSA, we delivered devices with reservoirs containing DQ-BSA and vehicle or hydroxychloroquine. We observed decreased DQ-BSA signal around reservoirs with hydroxychloroquine as compared to vehicle reservoirs (Figure 3.3F, G), suggesting that the lysosome is involved in the catabolism of DQ-BSA in PDAC cancer cells in tumors.

We next sought to determine whether inhibiting macropinocytosis with EIPA had an effect on amino acid levels in pancreatic tumors. Devices containing EIPA were implanted into tumors in KP mice for 24 hours, and tumor tissue adjacent to the device was analyzed using matrix-assisted laser desorption ionization coupled to imaging mass spectrometry (MALDI-IMS). This allowed us to simultaneously measure the distribution of EIPA released from the microdevice in tumor tissue, as well as relative levels of choline and some amino acids in adjacent tissue sections (Figure 3.4 and Figure B4A, B). We observed decreases in relative amino acid levels in tumor regions where EIPA was also detected, but in not in tumor regions adjacent to vehicle control reservoirs (Figure 3.4), consistent with the hypothesis that tumors derive a meaningful fraction of their amino acids from catabolism of extracellular protein obtained by macropinocytosis.

EIPA inhibits macropinocytosis at the concentrations used for these studies (Commisso et al.,

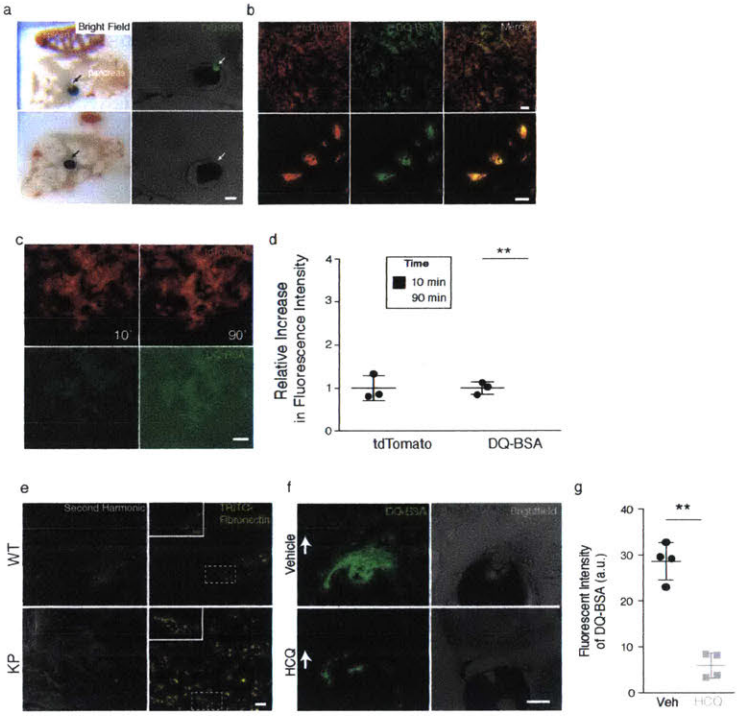

Figure 3.3. Albumin catabolism and fibronectin internalization in autochthonous $Kras^{G12D}$-driven pancreatic tumors catabolize albumin and internalize fibronectin. (A) Differential albumin breakdown in tumor compared to normal pancreatic tissue. Devices containing self-quenched, BODIPY-labeled bovine serine albumin (DQ-BSA) were implanted directly into the pancreas of KP mice with pancreatic tumors. Tissue sections visualized by bright-field (left) and fluorescence (right) microscopy are shown. Arrows indicate reservoir position that corresponds to the site of DQ-BSA delivery. DQ-BSA fluorescence is observed only in areas where the device contacts tumor tissue (top), and not when the device is adjacent to non-malignant pancreatic tissue (bottom). (images are representative of n = 2 mice per cell line per condition with triplicate reservoirs). (B) Cellular fate of albumin catabolism. Multiphoton microscopy images of pancreatic tumors in live KP mice that also harbor a tdTomatoLSL allele (KPT) to mark cancer cells with red fluorescence. Images were obtained 4h post device implantation to deliver DQ-BSA. Green fluorescence corresponding to catabolism of DQ-BSA localizes with tumor cells marked by red fluorescence. Low (top) and high power (bottom) images are shown. Scale bar, 20 µm for both low and high power images. (images are representative of n = 4 mice per cell line per condition with duplicate reservoirs). (C) Multiphoton images of pancreatic tumors in live KPT mice showing increasing fluorescence from DQ-BSA over time. Red fluorescence marking tumor cells (top) and green fluorescence from DQ-BSA (bottom) are shown at 10- and 90-minutes post device implantation. Scale bar, 50 µm. (images are representative of n = 2 mice per genotype per condition with duplicate reservoirs). (D) Quantification of DQ-BSA fluorescence from the experiment in (C) reveals greater than 3-fold increase in fluorescence from 10- to 90-minutes. tdTomato fluorescence is also shown and changes minimally over the same 90-minute period. (n = 2 mice per genotype per condition with duplicate reservoirs). (E) Multiphoton images of normal pancreas (WT) and pancreatic tumors (KP) in live mice. Second harmonic generation is used to detect fibrillar collagen and displayed to demonstrate background auto-fluorescence in the TRITC channel. Images were obtained 30min post device implantation to deliver TRITC-Fibronectin (yellow). Cellularity of internalized TRITC-fibronectin was visualized and observed only in KP mice. White arrow indicates direction of diffusion from the device at the bottom left of the images. Scale bar, 20µM. (Images are representative of n = 2 mice per genotype per condition with duplicate reservoirs). (F) Devices containing self-quenched, BODIPY-labeled bovine serine albumin (DQ-BSA) with vehicle or the lysosomal inhibitor hydroxychloroquine (HCQ) were implanted directly into the pancreas of KP mice with pancreatic tumors. Tissue sections visualized by bright-field (left) and fluorescence (right) microscopy are shown. White arrows indicate reservoir position that corresponds to the site of DQ-BSA delivery. A strong decrease in DQ-BSA is observed in the presence of HCQ (images are representative of n = 5 distinct regions of tumor per condition). (G) Quantification of fluorescent intensity of DQ-BSA in the presence and absence of HCQ (n = 5 distinct regions of tumor per condition). Significance values indicated as P * < 0.05 (Student's t-test).

Figure 3.3

2013; Kamphorst et al., 2015; Palm et al., 2015); however, EIPA is also an inhibitor of Na+/H+ exchange and may affect amino acid levels by other mechanisms. To test this possibility, we determined whether EIPA affected branched-chain amino acid (BCAAs) levels under conditions where past work had shown acquisition of BCAAs is or is not dependent on macropinocytosis33,34. We found that BCAA levels were decreased when pancreatic cancer cells were cultured in media lacking BCAAs, that BCAA levels could be rescued by providing cells with excess albumin, and the ability to rescue BCAA levels with albumin was inhibited by EIPA while EIPA had no effect on BCAA levels otherwise (Figure B4C). We also assessed whether EIPA affected intracellular amino acid levels in pancreatic cancer cells in culture where amino acids are freely available, and whether EIPA affected uptake of labeled amino acids from the media. EIPA had no effect on levels most amino acid under these conditions (Figure B4D, E), including glutamine, glutamate and aspartate, three of the amino acids found to be depleted by EIPA in tumors. These data argue that at the doses use, EIPA has minimal effect on the uptake or exchange of free amino acids and strengthens the conclusion that macropinocytosis is important to maintain amino acid levels within tumors.

Conclusion

In contrast to previous studies examining albumin synthesis and degradation by different organs in tumor bearing animals (Andersson et al., 1991; Fearon et al., 1998; Andersson et al., 1990), we provide direct evidence that pancreatic tumors catabolize albumin and derive a fraction of amino acids from the breakdown of extracellular protein. While these findings remain consistent with breakdown of host tissue proteins as a nutrient contributor to pancreatic tumors (Mayers et al., 2014), they further suggest that cancer cells in these tumors catabolize host-derived proteins in their environment. Hypoalbuminemia is not observed in KP mice, suggesting that the quantity of albumin catabolized by tumors is not sufficient to directly result in hypoalbuminemia over the time

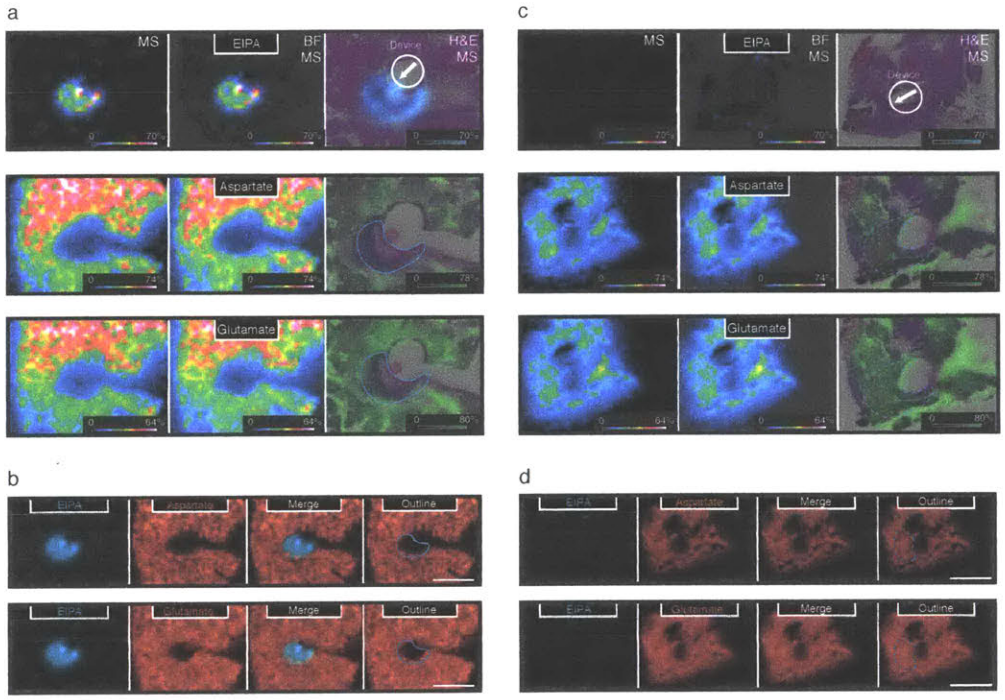

Figure 3.4. Like endocytosis and autophagy, macropinocytosis can deliver material to the lysosome. Local depletion of amino acids following inhibition of macropinocytosis in $Kras^{G12D}$-driven pancreatic tumors *in vivo*. (A) Devices containing EIPA were implanted directly into pancreatic tumors of KP mice. 24 hours after device implantation, serial sections from the tumor were analyzed by matrix assisted laser desorption ionization coupled to imaging mass-spectrometry (MALDI-IMS). Positive ion mode was used to detect the macropinocytosis inhibitor, EIPA (top panels; EIPA diffused approximately 400-500μM). Negative ion mode used to detect the amino acids aspartate and glutamate (middle and bottom panels respectively). A scale bar representing the intensity range of ions detected for each image is included in the lower right of each panel and the length of this bar corresponds to 1mm. The left panels (MS) show the mass spectrometry signal only, the center panels (BF, MS) show an overlay of the mass spectrometry signal with a bright field image of an adjacent tissue section, and the right panels (H & E, MS) show an overlay of the mass spectrometry signal and an H & E stain of an adjacent tissue section. Schematic demonstrating device placement is included in the upper right as a white circle with an arrow indicating direction of EIPA release. A blue line indicates the extent of the EIPA signal in the H & E, MS images. Images are representative of n = 2 KP mice with triplicate reservoirs. (B) Qualitative signal for EIPA (blue) and signal from the amino acids aspartate (top) and glutamate (bottom) (red) are shown as separate and overlaid images as indicated. Also shown is an outline (blue line) of the extent of EIPA signal overlaid on the aspartate and glutamate signal as indicated. White scale bar corresponds to 1mm. (C) Devices containing vehicle control (polyethylene glycol) were implanted directly into pancreatic tumors of KP mice. 24 hours after device implantation, serial sections from the tumor were analyzed by matrix assisted laser desorption ionization coupled to imaging mass-spectrometry (MALDI-IMS). Positive ion mode was used to demonstrate the absence of the macropinocytosis inhibitor, EIPA (top panels; No EIPA observed, vehicle). Negative ion mode used to detect the amino acids aspartate and glutamate (middle and bottom panels respectively). A scale bar representing the intensity range of ions detected for each image is included in the lower right of each panel and the length of this bar corresponds to 1mm. The left panels (MS) show the mass spectrometry signal only, the center panels (BF, MS) show an overlay of the mass spectrometry signal with a bright field image of an adjacent tissue section, and the right panels (H & E, MS) show an overlay of the mass spectrometry signal and an H & E stain of an adjacent tissue section. Schematic demonstrating device placement is included in the upper right as a white circle with an arrow indicating direction of vehicle release. A blue dashed line indicates the approximate extent of diffusion based on diffusion of EIPA in A. Images are representative of n = 2 KP mice with triplicate reservoirs. (D) Qualitative signal for EIPA (blue) and signal from the amino acids aspartate (top) and glutamate (bottom) (red) are shown as separate and overlaid images as indicated. Also shown is an outline (blue dashed line) of the expected extent of EIPA diffusion if it were included in the reservoir. White scale bar corresponds to 1mm.

Figure 3.4

scales this process was studied in mice. However, increased turnover of whole body protein stores and albumin consumption by tumors may eventually affect circulating albumin levels in patients with pancreatic cancers (Gupta and Lis, 2010).

We report two methods to interrogate albumin catabolism that could be extended to other solid tumors. Labeling of albumin on specific amino acids could also enable finer mapping of the fate of protein-derived amino acids in central carbon metabolism. Using albumin as a carrier for chemotherapeutics has been a successful therapeutic strategy in the clinic (Schilling et al., 1992; Von Hoff et al., 2013), possibly owing to the propensity of some tumors to use macropinocytosis. Albumin conjugation and preferential albumin-uptake can allow for both better solubility and improved tumor delivery (Wosikowski et al., 2003). The approaches used here to study local protein catabolism may also allow for direct testing of therapeutic hypotheses in an individual tumor, and could be used at the time of biopsy to identify patients that might benefit from treatments that take advantage of increased protein catabolism by tumors.

Experimental Procedures

Animal Statement

All animal studies were approved by the MIT Committee on Animal Care. Mice were housed under standard 12-hr light/dark cycles and fed RMH 3000 (Prolab) ad-libitum until experiments were conducted. All experimental groups were assigned based on genotype and experiments conducted blinded. Plasma exchange experiments were conducted at the same time of day. Cohort sizes were based on anticipated results from previous studies in vitro8.

Production of [^{15}]MSA

The MSA cDNA was cloned from the liver of a wild-type mouse using the following PCR primers: (F-GAAGCACACAAGAGTGAGATCGC; R-TTAGGCTAAGGCGTCTTTGCATCTA). The cDNA was cloned into an expression vector containing α-factor and a GAPDH promoter (pGAPZα) for subsequent transformation and expression in *Pichia pastoris* (Invitrogen). *P. pastoris* expressing MSA was cultured in a glucose fed-batch bioreactor (Sartorius) at 30°C for 7 days with [^{15}N]labeled nutrients using conditions described previously (Cregg et al., 2000). Media containing MSA was separated from the cellular fraction after centrifugation at 15,000xg for 3 hours at 4°C and supernatant containing MSA was concentrated using a rotary evaporator. Concentrated supernatant was dialyzed using a 45,000 Dalton molecular weight cutoff dialysis cassette (Thermo-Fisher) and further purified using a Q-Sepharose High Performance anion exchange column (GE). Purified MSA were subsequently lyophilized and resuspended in PBS and filtered through 0.45μM filters for use in animal experiments. Additional [^{15}N]MSA was acquired from Albumin Biosciences, INC.

Microfluidic Plasmapheresis Device

The plasma exchange microfluidic device is based on the concept of cell margination and was previously developed for bacterial clearance in a mouse model of sepsis (Hou et al., 2010, 2012). The device is made of polydimethylsiloxane (PDMS) (Sylgard 184, Dow Corning, Midland, MI) and consists of 3 channels; each 6 mm long, 20μm × 40μm (W×H) with 3 stages of bifurcation at 2 mm channel interval. A filter region with an array of square pillars (100μm gap) is added upstream of the margination channels to trap large thrombi or cell clusters to ensure smooth flow within the device. As blood flows through the margination channel, deformable RBCs migrate axially towards the channel center, leaving a layer of plasma next to the channel wall which is removed via the smaller side channels. To minimize RBC loss, the side channel skimming volume is progressively lower (15%, 10%, 5%) at each bifurcation stage with a total volume of 30%. Therefore, the microdevice is capable of exchanging up to 30% of plasma from the incoming blood with labeled albumin, which is infused to the filtered blood with a separate syringe pump. During the extracorporeal plasma exchange in mice, blood is drawn from an arterial (carotid) catheter using a peristaltic pump (P720, Instech Laboratories, Inc., Plymouth Meeting, PA) for 25 minutes ($30\mu L min^{-1}$) into the device which would partially replace the filtered blood with labelled albumin ($10\ \mu L min^{-1}$) prior returning to the animal through a venous (jugular) catheter.

Mouse Pancreatic Cancer Models

For the autochthonous genetically engineered mouse model of pancreatic ductal adenocarcinoma (PDAC), tumors were initiated using a pancreas-restricted Pdx1 promoter to express Cre-recombinase (Pdx1-Cre) in $Kras^{LSL\text{-}G12D/+}$; $p53^{loxP/loxP}$ animals from a mixed 129/Sv and C57Bl6/J background. For imaging studies, mice harboring a $tdTomato^{LSL/+}$ allele were used to

allow visualization of individual cells where Cre was expressed. Chronic catheters were implanted in the jugular vein and carotid artery when male mice were between 6-8 weeks of age with detectable tumors. For xenograft studies: two to four-month old male C57Bl6/J or nu/nu mice were used. Briefly, $2.5x10^5$ established cell lines derived from C57Bl6/J KP mice, or $5x10^5$ MIA PaCa2 or BxPC-3 human pancreatic cancer cell lines, were injected into the flanks of recipient mice and experiments performed when total tumor volume was approximately $1cm^3$. All human cell lines were acquired from ATCC and cultured in 21% oxygen in DMEM containing 10% FBS and penicillin/streptomycin.

Metabolite Extraction

Tissues were weighed (wet tissue weight) and homogenized cryogenically (Retsch Cryomill). Metabolites were extracted from tissues weighing between 10-40mg in a chloroforom:methanol:water extraction solution at a volume ratio of 400:600:300. Samples were vortexed and centrifuged at 10,000xg for 10min to separate aqueous and organic layers. Polar metabolites were dried under nitrogen gas and frozen at -80°C for subsequent and analysis by gas-chromatography mass-spectrometry.

Measurement of Labeled Albumin Peptides

Mouse tissue was extracted and homogenized in ice cold 8 M urea. Proteins were quantified using BCA assay (Pierce). Proteins were reduced (10 mM dithiothreitol, 56 °C for 45 min) and alkylated (50 mM iodoacetamide, room temperature in the dark for 1 h), then were subsequently digested with trypsin (sequencing grade, Promega, Madison, WI) at an enzyme/substrate ratio of 1:50 at room temperature overnight in 100 mM ammonium acetate pH 8.9. Trypsin activity was quenched by adding formic acid to a final concentration of 5%. Peptides were desalted using C18 SpinTips

(Protea, Morgantown, WV) then lyophilized and stored at -80°C. After being resuspended in 0.1% formic acid, each sample (1 µg of tissue or 100 ng of serum) was separated by reverse phase HPLC using an EASY-nLC1000 (Thermo) over a 75-minute gradient before nanoelectrospray using a QExactive mass spectrometer (Thermo). The mass spectrometer was operated in a data-dependent mode. The parameters for the full scan MS were: resolution of 70,000 across 350-2000 m/z, AGC 3e6, and maximum IT 50 ms. The full MS scan was followed by MS/MS for the top 10 precursor ions in each cycle with a NCE of 28 and dynamic exclusion of 30 s. Raw mass spectral data files (.raw) were searched using Proteome Discoverer (Thermo) and Mascot version 2.4.1 (Matrix Science). Mascot search parameters were: 10 ppm mass tolerance for precursor ions; 0.8 Da for fragment ion mass tolerance; 2 missed cleavages of trypsin; fixed modification was carbamidomethylation; variable modification was oxidized methionine. We analyzed the following peptides and all possible isotopomers to determine plasma enrichment and quantity of labeled albumin present in each tissue: AADKDTcFSTEGPNLVTR (+2), AADKDTcFSTEGPNLVTR (+3), APQVSTPTLVEAAR (+2), ENYGELADccTK (+2), LVQEVTDFAK (+2), SLHTLFGDK (+2), TcVADESAANcDK (+2) (c = carbamidomethylation). Fractional enrichment was determined for each peptide and each measurement represents the mean of the 7 peptides. The average fractional enrichment in plasma and tissues were normalized to the average fractional plasma enrichments of [^{15}N]MSA post plasma-exchange.

Gas-Chromatography Mass-Spectrometry Measurement of Free Amino Acids

Dried tissue metabolites were dissolved in 10 µL/10mg of 2% methoxyamine hydrochloride in pyridine (Sigma) and held at 37°C for 1.5h. Tert-butyldimethylsilyl derivatization was initiated by adding 15µL/10mg of N-methyl-N-(tert-butyldimethylsilyl)trifluoroacetamide + 1% tert-butyldimethylchlorosilane (Sigma) and incubated at 37°C for 1hr. GC-MS analysis was

performed using an Agilent 7890 GC equipped with 30m DB-35MS capillary column connected to an Agilent 5975B MS operating under electron impact ionization at 70eV. One microliter of sample was injected in splitless mode at 270°C, using helium as a carrier gas at a flow rate of 1mL min^{1}. For measurement of polar metabolites, the GC oven temperature was held at 100°C for 3 minutes and increased to 300°C at 3.5C min^{-1}. The MS source and quadrupole were held at 230°C and 150°C, respectively, and the detector was run in scanning mode, recording ion abundance in the range of 100-605m/z. MIDs were determined by integrating the appropriate ion fragments and correct for natural isotope abundance using in house algorithms adapted as previously reported (METRAN, Matlab 2013b)8. Labeled amino acids are defined as the M+1 (one nitrogen labeled) and M+2 (two nitrogens labeled) isotopomers of examined amino acids for ^{15}N labeled studies or M+n (where n= total carbon atoms composing each amino acid) for ^{13}C labeled studies.

Albumin Measurements in Plasma

Plasma was collected in EDTA-coated tubes, aliquoted, and frozen at -80°C for further analysis. Plasma mouse albumin levels were determined using a mouse albumin ELISA assay according to manufacturers' specification (Abcam #ab108791).

Device to Deliver FITC DQ-BSA, Rh-Dextran, FITC-Dextran, TRITC-Fibronectin, EIPA, and Hydroxychloroquine

Microdose drug delivery devices were manufactured as described previously18. In short, cylindrical, micro-scale devices with 820μm (diameter) × 4mm (length) were manufactured from medical-grade Delrin acetyl resin blocks (DuPont) by micro-machining (CNC Micromachining Center, Cameron). Circular reservoirs (2-6 per device) were shaped on the outer surface of devices in dimensions of 300μm (diameter) × 250μm (depth). DQ-BSA, Dextran, Fibronectin and/or hydroxychloroquine or

EIPA (1µg per reservoir) were packed into device reservoirs using a tapered, metal needle (Electron Microscopy Sciences). Devices were implanted directly into the mouse tumor using a 19-gauge spinal biopsy needle (Angiotech) using the retractable needle obturator to push the device into tissue. Devices remained in situ for 6-48h. The tumor was then excised and the tissue containing the device was snap-frozen. Tissue was sectioned using a standard cryotome and tissue slices of 20µm thickness were collected from each reservoir and imaged on an EVOS microscope.

Multi-photon Imaging of DQ-BSA, FITC-Dextran, Rh-Dextran, TRITC-Fibronectin

Intravital multiphoton imaging was performed as described previously39,40 using a 25 x 1.05NA water immersion objective with correction lens. Ninety-minute long time-lapse movies were analyzed for measuring and quantifying fluorescence intensity and cell characteristics in 3D and through time using NIH ImageJ41. Data were pooled from at least 3 mice per tumor group, with 4-8 fields imaged per mouse. Macropinocytic index was determined as previously described for xenograft tumors (Commisso et al., 2014).

MALDI Imaging experiments

Samples were cryosectioned at 20 µm, thaw-mounted on glass slides, and serial sections analyzed. The orientation of specimens was shifted for serial sections analyzed in positive versus negative ion mode, with device location used to orient the sample in each serial section. Slides were then coated with HCCA (7 mg/mL, 50% methanol, 0.1% TFA) or 9-aminoacridine (10 mg/mL, 70% ethanol, 0.1% TFA) using a TM sprayer (HTX Technologies, Carrboro, NC, USA). Serial sections were prepared for imaging analysis in both positive and negative ion modes on a 7T solariX-XR FTMS (Bruker, Billerica, MA, USA) equipped with dual ESI/MALDI source, SmartBeam II 2 kHz Nd:YAG (355 nm) laser, and paracell. Samples were analyzed with a raster width of 125 µm in

positive ion mode and 100 um in negative ion mode in the mass range of 80 – 2000 m/z at 2MW acquisition size. Images contained between 7200 and 10500 pixels. Data was visualized and co-registration of H& E images performed using FlexImaging 4.1. Compound identifications were made on the basis of accurate mass (<1ppm) and isotopic peak matching.

Cell Culture

Cell lines from murine KP pancreatic tumors were established by standard protocols24. Cells were cultured in complete DMEM with 10% fetal bovine serum and 5% penicillin/streptomycin. For BCAA deprivation, DMEM with 5% dialyzed serum with or without BCAAs (leucine, valine, and isoleucine) was used in the presence or absence of 3% albumin and in the presence or absence of 20μM EIPA. Where indicated, 2mg/mL of a fully labeled ^{15}N or ^{13}C labeled amino acid mixture (Cambridge Isotopes Laboratories) was included for 6 hours prior to metabolite extraction.

Statistical Analysis

Two-tailed unpaired Student's T-test was performed for all experiments and data were normally distributed for all analyses conducted. Variances were not statistically different in any of the data. Results for independent experiments are presented as mean ± SD.

Acknowledgements

The authors wish to dedicate this paper to the memory of Katherine Kellersberger. We thank the MIT Department of Chemical Engineering and Jean Francois-Hamel for access to bioreactor equipment, Roderick Bronson for pathological grading of tumors, and Allison Lau for providing tumor-bearing animals. S.M.D. and A.L. received support from a National Science Foundation Graduate Research Award Fellowship, and support from T32 GM007287 is also acknowledged. O.J received support from

the Koch Institute Frontier Grant and the Prostate Cancer Foundation. JRM acknowledges support from grant F30CA183474 from the NCI and T32GM007753 from NIGMS. MAK and GS acknowledge support from NIH grants 1R01DK075850-01 and 1R01CA160458-01A1. M.G.V.H acknowledges support from the Lustgarten Foundation, the Ludwig Center at MIT, the Broad Institute SPARC program, the Burroughs Wellcome Fund, SU2C, and the NIH (P30CA1405141, R01CA168653).

References

Andersson C, Iresjö BM, Lundholm K. Identification of tissue sites for increased albumin degradation in sarcoma-bearing mice. *The Journal of Surgical Research* **50**, 156 (1991).

Andersson C, Lönnroth C, Moldawer LL, Ternell M, Lundholm K. Increased degradation of albumin in cancer is not due to conformational or chemical modifications in the albumin molecule. *The Journal of Surgical Research* **49**, 23 (1990).

Bardeesy N, Aguirre AJ, Chu GC, Cheng Kh, Lopez LV, et al. Both p16Ink4a and the p19Arf-p53 pathway constrain progression of pancreatic adenocarcinoma in the mouse. *Proceedings of the National Academy of Sciences* **103**, 5947 (2006).

Commisso C, Davidson SM, Soydaner-Azeloglu RG, Parker SJ, Kamphorst JJ, et al. Macropinocytosis of protein is an amino acid supply route in Ras-transformed cells. *Nature* **497**, 633 (2013).

Commisso C, Flinn RJ, Bar-Sagi D. Determining the macropinocytic index of cells through a quantitative image-based assay. *Nature Protocols* **9**, 182 (2014).

Cregg JM, Cereghino JL, Shi J, Higgins DR. Recombinant protein expression in Pichia pastoris. *Molecular Biotechnology* **16**, 23 (2000).

Daly R, Hearn MTW. Expression of heterologous proteins in Pichia pastoris: a useful experimental tool in protein engineering and production. *Journal of Molecular Recognition* **18**, 119 (2005).

Fearon KC, Falconer JS, Slater C, McMillan DC, Ross JA, et al. Albumin synthesis rates are not decreased in hypoalbuminemic cachectic cancer patients with an ongoing acute-phase protein response. *Annals of Surgery* **227**, 249 (1998).

Gupta D, Lis CG. Pretreatment serum albumin as a predictor of cancer survival: a systematic review of the epidemiological literature. *Nutrition Journal* **9**, 69 (2010).

Hou HW, Hou HW, Bhagat AAS, Bhagat AAS, Lin Chong AG, et al. Deformability based cell margination–a simple microfluidic design for malaria-infected erythrocyte separation. *Lab on a Chip* **10**, 2605 (2010).

Hou HW, Hou HW, Gan HY, Gan HY, Bhagat AAS, et al. A microfluidics approach towards high-throughput pathogen removal from blood using margination. *Biomicrofluidics* **6**, 24115 (2012).

Jewell WR, Krishnan EC, Schloerb PR. Apparent cellular ingress of albumin in Walker 256 tumor and rat muscle. *Cancer Research* **35**, 405 (1975).

Jonas O, Landry HM, Fuller JE, Santini JT, Baselga J, et al. An implantable microdevice to perform high-throughput in vivo drug sensitivity testing in tumors. *Science Translational Medicine* **7**, 284ra57 (2015).

Kamphorst JJ, Nofal M, Commisso C, Hackett SR, Lu W, et al. Human pancreatic cancer tumors are nutrient poor and tumor cells actively scavenge extracellular protein. *Cancer Research* **75**, 544 (2015).

Klionsky DJ. Autophagy in mammalian systems, Part B. Preface. *Methods in Enzymology* **452**, xxi (2009).

Locasale JW. Serine, glycine and one-carbon units: cancer metabolism in full circle. *Nature Reviews. Cancer* **13**, 572 (2013).

Mahadevan D, Von Hoff DD. Tumor-stroma interactions in pancreatic ductal adenocarcinoma. *Molecular Cancer Therapeutics* **6**, 1186 (2007).

Manic G, Obrist F, Kroemer G, Vitale I, Galluzzi L. Chloroquine and hydroxychloroquine for cancer therapy. *Molecular & Cellular Oncology* **1**, e29911 (2014).

Mayers JR, Vander Heiden MG. Famine versus feast: understanding the metabolism of tumors in vivo. *Trends in Biochemical Sciences* (2015).

Mayers JR, Wu C, Clish CB, Kraft P, Torrence ME, et al. Elevation of circulating branched-chain amino acids is an early event in human pancreatic adenocarcinoma development. *Nature Medicine* **20**, 1193 (2014).

Merlot AM, Kalinowski DS, Richardson DR. Unraveling the mysteries of serum albumin-more than just a serum protein. *Frontiers in Physiology* **5**, 299 (2014).

Metallo CM, Vander Heiden MG. Understanding metabolic regulation and its influence on cell physiology. *Molecular Cell* **49**, 388 (2013).

Palm W, Park Y, Wright K, Pavlova NN, Tuveson DA, et al. The utilization of extracellular proteins as nutrients is suppressed by mTORC1. *Cell* **162**, 259 (2015).

Racoosin EL, Swanson JA. Macropinosome maturation and fusion with tubular lysosomes in macrophages. *Journal of Cell Biology* **121**, 1011 (1993).

Rothschild MA, Oratz M, Schreiber SS. Regulation of albumin metabolism. *Medicine* **26**, 91 (1975).

Schilling U, Friedrich EA, Sinn H, Schrenk HH, Clorius JH, et al. Design of compounds having enhanced tumour uptake, using serum albumin as a carrier–Part II. In vivo studies. *International journal of radiation applications and instrumentation. Part B, Nuclear medicine and biology* **19**, 685 (1992).

Steinfeld JL. I131 albumin degradation in patients with neoplastic diseases. *Cancer* **13**, 974 (1960).

Swanson JA, Watts C. Macropinocytosis. *Trends in Cell Biology* **5**, 424 (1995).

Tolner B, Smith L, Begent RHJ, Chester KA. Production of recombinant protein in Pichia pastoris by fermentation. *Nature Protocols* **1**, 1006 (2006).

Vander Heiden MG, Cantley LC, Thompson CB. Understanding the Warburg effect: the metabolic requirements of cell proliferation. *Science* **324**, 1029 (2009).

Von Hoff DD, Ervin T, Arena FP, Chiorean EG, Infante J, et al. Increased survival in pancreatic cancer with nab-paclitaxel plus gemcitabine. *The New England Journal of Medicine* **369**, 1691 (2013).

Whatcott CJ, Diep CH, Jiang P, Watanabe A, LoBello J, et al. Desmoplasia in primary tumors and metastatic lesions of pancreatic cancer **21**, 3561 (2015).

White E. Exploiting the bad eating habits of Ras-driven cancers. *Genes & Development* **27**, 2065 (2013).

Wise DR, Thompson CB. Glutamine addiction: a new therapeutic target in cancer. *Trends in Biochemical Sciences* **35**, 427 (2010).

Wosikowski K, Biedermann E, Rattel B, Breiter N, Jank P, et al. In vitro and in vivo antitumor activity of methotrexate conjugated to human serum albumin in human cancer cells. *Clinical Cancer Research: An Official Journal of the American Association for Cancer Research* **9**, 1917 (2003).

4

Pkm1 expression is tumor suppressive in a mouse model of prostate cancer

Author statement

This work has not yet been submitted for publication.

Authors

The following authors contributed to this work:
Shawn M. Davidson[1,2,3], Julia E. Heyman+1, James P O'Brien[+1], Amy C. Liu[+1], Talya Dayton[1], William J. Israelsen[1], Rachel Kelly[4], Francesca Giunchi[5], Roderick Bronson[1], Elizaveta Freinkman, Howard Mak[1], Scott Malstrom[1], Gary Bellinger[6], Arkaitz Carracedo[6], Pier P. Pandolfi[6], Kevin Courtney[6], John Frangioni[6], Ronald A. DePinho[6], James Horner[8], Matt Boxer[7], Craig J. Thomas[7], Lewis C. Cantley[6], Massimo Loda[8], Matthew G. Vander Heiden[1,2,3,8]

Author affilations

1. Koch Institute for Integrative Cancer Research, Massachusetts Institute of Technology, Cambridge, Massachusetts, USA
2. Department of Biology, Massachusetts Institute of Technology, Cambridge, Massachusetts, USA.
3. Broad Institute of MIT and Harvard University, Cambridge, Massachusetts, USA.
4. Department of Epidemiology, Harvard T.H. Chan School of Public Health (RK)
5. University of Bologna, Italy (FG)
6. Beth Israel Deaconess Medical Center, Cambridge, MA
7. National Center for Advancing Translational Sciences, NIH, Bethesda, Maryland, USA.
8. Dana-Farber Cancer Institute, Boston, Massachusetts, USA.

+These authors contributed equally to this work.

Author contributions

Conceptualization: S.M.D., M.G.V.H. Methodology: S.M.D., J.E.H., J.P.O., A.C.L., T.D., W.J.I., R.K., E.F., H.M., S.M., G.B., A.C. Formal Analysis: S.M.D., R.B., F.G. Investigation: S.M.D., M.G.V.H. Writing: S.M.D., M.G.V.H. Visualization: S.M.D. Supervision: M.G.V.H. Funding Acquisition: S.M.D., L.C.C., M.G.V.H.

Abstract

Most cancers express the M2 isoform of pyruvate kinase (*Pkm2*) and pyruvate kinase isoform selection can promote anabolic metabolism to support tumor growth. However, *Pkm2* expression is dispensable for some cancers and whether expression of the pyruvate kinase M1 isoform (*Pkm1*) impacts cancer initiation or progression remains unknown. To test how differential pyruvate kinase isoform expression affects prostate cancer, we generated a mouse harboring a conditional allele of *Pkm1* and crossed this allele as well as a *Pkm2* conditional allele to a *Pten*-loss driven model of prostate cancer. We found that loss of *Pkm1* expression accelerates prostate cancer initiation and progression, while deletion of *Pkm2* leads to increased *Pkm1* expression and tumor suppression. Tumors with high *Pkm1* expression are depleted for essential metabolites involved in nucleotide biosynthesis and display features consistent with cellular senescence. Prostate cancers with low *Pkm1* expression overcome *Pten*-loss induced senescence, and when *Pkm2* is expressed, small molecule *Pkm2* activation can suppress tumor growth. These data argue that *Pkm1* expression suppresses cancer formation in susceptible tissues and that the pharmacological activation of *Pkm2* may be beneficial in some patients with prostate cancer.

Introduction

Prostate cancer is the second leading cancer-related cause of death in men, and most aged men will develop benign prostatic hyperplasia (BPH) or frank cancer (Siegel et al., 2015). The loss of the phosphatase and tensin homolog (*Pten*) tumor suppressor is strongly associated with abnormal prostate growth found in both BPH and prostate cancer, and 70-80% of primary prostate cancers harbor mutations in *Pten* that result in loss of function of one or both copies of *Pten* (Gray et al., 1998; Whang et al., 1998; Monn et al., 2016). Loss-of-function mutations in *Pten* frequently occur

in the lipid phosphatase domain, and this results in accumulation of phosphatidylinositol-(3,4,5)-triphosphate (PIP3) and activation of AKT signaling to drive inappropriate proliferation and survival (Song et al., 2012; Testa and Tsichlis, 2005). The signaling events that promote cancer phenotypes in prostate cancer have been extensively studies, as have the ways in which increased growth signaling can affect cell metabolism. However, less well characterized are which metabolic alterations are required for tumor initiation and progression.

Changes in cellular metabolism are necessary to sustain rapid cellular proliferation, and oncogene activation can drive glucose uptake (Cairns et al., 2011; Deberardinis and Chandel, 2016). Many cancer cells exhibit increased levels of glucose uptake with elevated lactate production even in the presence of oxygen (also known as aerobic glycolysis or the "Warburg effect") (Vander Heiden et al., 2009) and the increased consumption of glucose by tumors relative to normal tissues is exploited clinically to detect malignancies through utilization of ^{18}FDG-PET (Plathow and Weber, 2008); however, while FDG-PET is frequently used in the clinic to detect frank tumors and late stage metastases, early lesions such as neoplasias are also frequently PET-positive (Reske and Kotzerke, 2001). These observations suggest that elevated glucose uptake can be an early event in tumorigenesis, but whether increased glucose uptake alone accompanies tumor formation, or is sufficient to drive cancer initiation, is not known.

Oncogene activation can also drive cellular senescence as a mechanism to suppress cancer development (Pérez-Mancera et al., 2014; Kuilman et al., 2010; Collado et al., 2007). *Pten* inactivation results in the prostate results in a p53-dependent senescence response by prostate epithelial cells (Chen et al., 2005) and suppresses tumor formation in this organ (Campisi, 2013; Collado and Serrano, 2010; Pérez-Mancera et al., 2014). Cellular senescence is classically defined as irreversible, however mechanisms exist that allow a subset of cell to escape senescence (Patel et al., 2016). Changes in metabolism can promote senescence in some tissues (Kaplon et al., 2013) and

senescent lesions can be hypermetabolic (Dörr et al., 2013), however the relationship between glucose metabolism and the induction and maintenance of the senescent state remains controversial (Ashrafian, 2006; Dörr et al., 2013; Favaro et al., 2012; Lunt and Vander Heiden, 2011; Levine and Puzio-Kuter, 2010).

The metabolism of senescent cells has been shown to involve high levels of glucose oxidation, decreased anaplerotic flux into the tricarboxylic acid (TCA) cycle, and low levels of nucleotides. Increasing oxidative glucose metabolism through pharmacological inhibition of Pdk1 promotes oxidative flux through pyruvate dehydrogenase (PDH) and is critical in maintaining senescence in a BrafV600E model of melanoma (Kaplon et al., 2013). p53 expression represses the expression of malic enzymes 1 and 2 (ME), the enzyme that converts malate to pyruvate, leading to speculation that ME-derived pyruvate is essential for maintaining TCA cycle flux or promoting anabolic metabolism (Jiang et al., 2013). Nucleotide deficiencies caused by mutations in Rrm2 or other mechanisms trigger a p53-mediated DNA damage response, leading to p21 transcription, cell cycle arrest, and senescence (Aird et al., 2013; Aird and Zhang, 2015). A recently discovered mechanism exploring the link between nucleotide metabolism and senescence uncovered the transcription factor, HEXIM1, which prevents transcription elongation in response to depleted nucleotide conditions through the direct binding of the small nucleolar ribonucleoprotein (S7K), which sequesters Ptef-b (Tan et al., 2016). Taken together, these data suggest that high oxidative and low anaplerotic TCA metabolism, in addition to nucleotide deficiency, can aid in promoting or maintaining cellular senescence.

The pyruvate kinase muscle (Pkm) gene encodes an RNA product and undergoes mutually exclusive alternative exon splicing to generate mRNAs that encode two different protein products: *Pkm1* and *Pkm2* (Chen et al., 2012; Wang et al., 2012). *Pkm1* has been associated with promoting oxidative flux (Christofk et al., 2008b) and *Pkm2* has been associated with elevated flux into

nucleotide synthetic and other anabolic pathways (Lunt et al., 2015). In mouse embryonic fibroblasts (MEFs) in culture, the genetic deletion of *Pkm2* results in *Pkm1* expression and induces quiescence. These *Pkm1* expressing cells exhibit both increased oxidative metabolism and depletion of nucleotide precursors and nucleotides, and the quiescent phenotype can be rescued by addition of exogenous nucleotide bases (Lunt et al., 2015). These findings strongly suggest that nucleotides are limiting for proliferation in the context of high *Pkm1* expression, and are further consistent with the observations between high oxidative flux and depleted nucleotide levels as a means to suppress cell proliferation (Lehmann et al., 2008; Lunt et al., 2015; Puzio-Kuter, 2011; Michaloglou et al., 2005; Aird and Zhang, 2015).

While most tissues in the body express either the *Pkm1* or *Pkm2* isoform of pyruvate kinase (Dayton et al., 2016)) cancer cells preferentially express *Pkm2* (Christofk et al., 2008b,a; Mazurek, 2011). Our lab and others have suggested that the preferential expression of the M2 isoform allows cancer cells to adapt pyruvate kinase activity and glucose metabolism to different cell conditions (Chaneton et al., 2012; Gui et al., 2013). As an enzyme, *Pkm1* is a constitutively active tetramer, while *Pkm2* can exist in a low-activity state (monomers and dimers) and can be allosterically activated to assume a high-activity state (tetramer). *Pkm2* activators include metabolite products that allow pyruvate kinase activity to respond to cellular nutrient status. Serine (Chaneton et al., 2012), SAICAR (Gui et al., 2013; Keller et al., 2012), fructose-1,6,-bisphosphate (Murcott et al., 1992), have been shown to promote *Pkm2* activation. As low *Pkm2* activity has been correlated with being advantageous for anabolic metabolism and proliferation and high *Pkm2* activity being advantageous for oxidative metabolism (David et al., 2010), small molecules that promote *Pkm2* activation by inducing tetramerization have been identified (Yacovan et al., 2012; Parnell et al., 2013; Walsh et al., 2011). One such *Pkm2* activator, TEPP-46, can reduce xenograft tumor growth and phenocopy the constitutive tetrameric activity found with *Pkm1* with respect to metabolic flux

and proliferation (Anastasiou et al., 2012). However, the finding that *Pkm2* expression is dispensable for tumor formation in some settings (Israelsen, 2014; Cortés-Cros et al., 2013) has suggested that loss of *Pkm2* expression might limit the efficacy of pyruvate kinase activators. It has also been suggested that *Pkm2* might play a role in cell proliferation outside of its function as a glycolytic enzyme, however whether *Pkm2* has non-glycolytic functions remains controversial. Determining where *Pkm2* expression is important, and situations where differential pyruvate kinase isoform expression has an effect on cancer is critical to selecting patients that might respond to PK activators.

The function of *Pkm1* in cancer is unknown. In normal tissues that express Pkm2, genetic deletion results in compensatory Pkm1 expression with surprisingly few systemic phenotypes. One strong phenotype is the promotion of hepatocellular carcinoma and this occurs with high penetrance, though this likely occurs through a non-cell autonomous mechanism related to whole animal metabolic stress as the liver expresses neither *Pkm1* nor *Pkm2* (Dayton et al., 2016). It has also been observed that tumors can form with *Pkm1* expression, raising the question of the importance of differential isoform expression cancer (Israelsen, 2014). In most tumors, however, *Pkm2* is the isoform that is associated with proliferating cells (Israelsen, 2014), and the function of *Pkm1* in normal and malignant tissues remains unclear.

To study the impact of differential Pkm isoform expression in mice, we generated mice harboring a conditional allele of *Pkm1* to complement mice with a conditional *Pkm2* allele. We crossed animals harboring the *Pkm1* and *Pkm2* conditional alleles to a *Pten*-driven mouse model of prostate cancer and found that Pkm isoform expression profoundly impacts prostate tumor initiation and progression. Deletion of *Pkm1* and *Pten* in the prostate decreases organismal survival and increases tumor progression. In contrast, deletion of *Pkm2* and *Pten* in the prostate results in high *Pkm1* expression and suppresses tumor formation. Tumor suppression is accompied by in

decreased nucleotide levels and senescence, These findings are consistent with previous data suggesting Pkm isoform expression impacts proliferation via affecting nucleotide synthesis (Lunt et al., 2015). We show *Pkm2* activation can also slow growth in this model, arguing that *Pkm1* expression and high pyruvate kinase activity functions suppress tumor formation in the prostate.

Results

Pten deletion increases glucose uptake independent of the formation of invasive prostate cancer

To better understand the temporal metabolic changes that occur with prostate tumor formation, we first asked whether acute genetic silencing of *Pten* is sufficient to promote glucose uptake. Knockdown of *Pten* using small-interfering RNA (siRNA) was sufficient to increase glucose uptake in the absence of cellular transformation in fibroblasts in culture (Figure 4.1A), consistent with published data suggesting increased PI(3)K signaling can drive glucose uptake (Dibble and Cantley, 2015). To ask whether increased glucose uptake was also an early consequence of *Pten* loss in the prostate, mice homozygous for a conditional allele with flanking loxP sites around the lipid phosphatase domain (exon 5) of *Pten* ($Pten^{fl}$) (Trotman et al., 2003; Wang et al., 2003) were crossed to mice with prostate-specific Probasin-Cre-recombinase (PbCre4) expression, giving rise to adult animals with prostate-restricted deletion of *Pten* ($Pten^{pc-/-}$) (Birbach, 2013). Loss of *Pten* in the mouse prostate results in prostatic intraepithelial neoplasia (PIN) at approximately 3 months of age, that can progress to invasive cancer by 6 months of age (Curry et al., 2013).

Assessment of pyruvate kinase isoform expression in the prostate and prostate cancer

To assess the effect of *Pten* loss on glucose uptake prior to the development of invasive cancers, we assessed ^{18}FDG uptake in the prostate of $Pten^{pc-/-}$ mice at 10 weeks of age, a time point well before

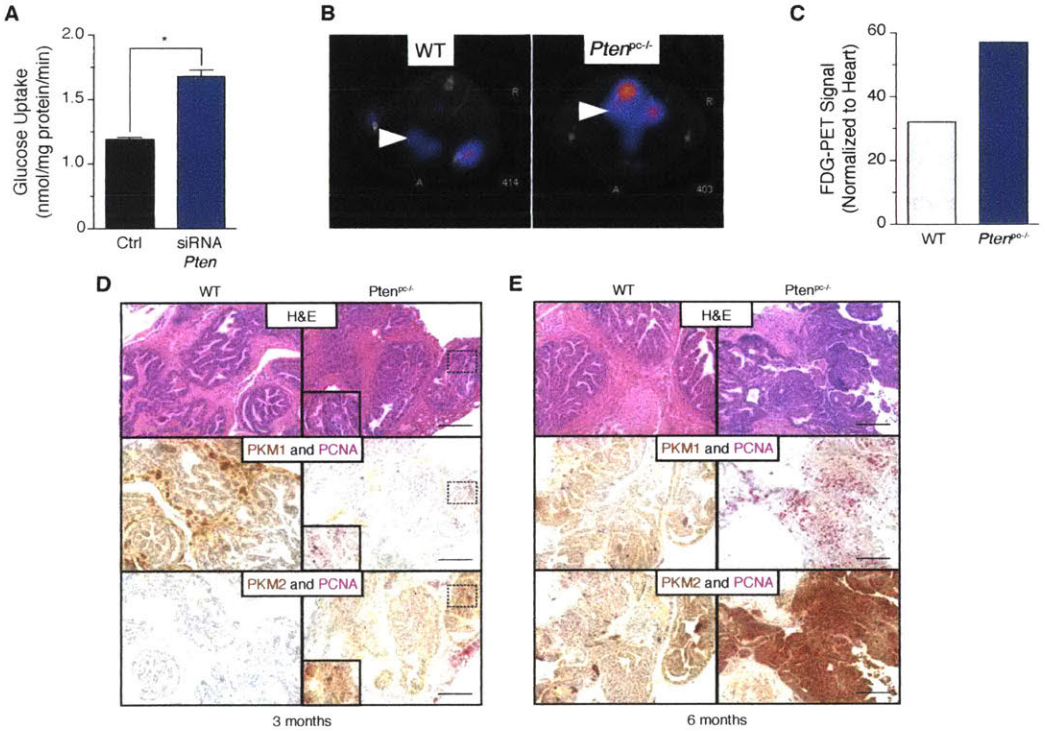

Figure 4.1. Increased glucose uptake upon *Pten* silencing or prostate-restricted deletion of *Pten* in the mouse prostate with changes in Pkm isoform expression from *Pkm1* to *Pkm2*. (A) Quantification of [^{14}C] glucose uptake in NIH 3T3 cells with siRNA scramble (Ctrl) and siRNA *Pten*. Counts per minute (cpm) were normalized to total cellular protein content after 30 minutes of uptake. Significance determined by Student's t-test, *p<0.05. Each bar represents the mean +/- the SD of three replicates. (n=3). (B) Representative [^{18}F]fluoro-2-deoxyglucose positron emission tomography (FDG-PET) in wild-type (WT) and *Pten* (*Pten*$^{pc-/-}$) at 12 weeks. Anterior prostate location inidicated by the white arrows. (C) Representative quantification of maximum intensity of [18F]fluoro-2-deoxyglucose emission spectra in wild-type (WT) and *Pten* (*Pten*$^{pc-/-}$) mouse prostates normalized to the intensity of the emission spectra in the heart. (D) Representative immunohistochemical staining of *Pkm1* (brown, left) or *Pkm2* (brown, right) or PCNA (pink) in wild-type (WT) in the anterior mouse prostate at 3 months of age (n=6). (E) Representative immunohistochemical staining of *Pkm1* (brown, left) or *Pkm2* (brown, right) PCNA (pink) in wild-type (WT) in the anterior mouse prostate at 6 months of age (n=6).

Figure 4.1

the onset of invasive cancer, when animals have normal pathology or low-grade PIN (Trotman et al., 2003; Chen et al., 2005; Wu and Pandolfi, 2001). We observed that even at this early time point, glucose uptake was elevated in the prostate of these mice as compared to control animals (Figure 4.1 B,C). These findings suggest that loss of *Pten* expression is sufficient to increase glucose uptake in cells, but that increased glucose uptake alone is not sufficient to cause cancer. They also suggest that additional events are needed beyond increased glucose uptake to develop invasive prostate cancer.

Because *Pkm1* expression is sufficient to suppress proliferation in some cells despite high glucose uptake (Lunt et al., 2015), we questioned whether changes in pyruvate kinase isoform expression might be associated with tumor initiation or progression in the prostate. To assess which Pkm isoform is expressed in the normal mouse prostate, we used antibodies specific for *Pkm1* or *Pkm2* by immunohistochemistry (IHC). While the human has one prostate organ with three distinct but developmentally related zones (peripheral, central, and transition zones), the mouse has three anatomically distinct and developmentally different lobes (anterior (AP), dorsolateral (DLP), and ventral (VP)) (Valkenburg and Williams, 2011). In wild-type (WT) 6-month-old animals, *Pkm1* is the dominant pyruvate kinase isoform expressed in the basal and luminal epithelial cells in the AP and is also prominent in the surrounding stromal cells, with no detectable *Pkm2* expression (Figure 4.2A). The dorsolateral prostate (DLP) exhibits *Pkm1* expression similar to the anterior lobe, however, low level *Pkm2* expression is also observed in luminal epithelial cells (Figure 4.2B). In contrast, the ventral prostate (VP) expresses approximately equal levels of each isoform in epithelial cells and preferentially expresses *Pkm1* in basal cells (Figure 4.1 C; Figure 4.1D,E shown as IHC antibody controls for all other panels in Figure 4.2).

Despite expression of *Pb-Cre4* in all lobes of the mouse prostate (Valkenburg and Williams, 2011), the AP forms tumors with the fastest kinetics in $Pten^{pc-/-}$ mice and is also frequently the

cause of mortality (Wang et al., 2003; Trotman et al., 2003; Zhang et al., 2000), Therefore we focused on the characterization of tumors arising in this lobe in the remainder of our studies. By 3 months of age when PIN was present, we observed some expression of both *Pkm1* and *Pkm2* in the epithelial cells of the AP of $Pten^{pc-/-}$ mice, although *Pkm2* staining was more prominent (Figure 4.1 D). To assess the relationship between *Pkm1* and *Pkm2* expression, and cell proliferation, we co-stained for expression of proliferating cell nuclear antigen (PCNA), and noted that overlap between PCNA staining and *Pkm1* expression was minimal (Figure 4.1 D). By 6 months of age, there was evidence of invasive cancer in $Pten^{pc-/-}$ mice (primarily adenocarcinoma) and observed robust *Pkm2* expression with increased PCNA staining and further loss of *Pkm1* expression in the tumors. These results demonstrate that a shift from *Pkm1* to *Pkm2* isoform expression occurs with the onset and progression of *Pten*-driven prostate cancer, and that loss of *Pkm1* expression is correlated with cell proliferation.

Generation and characterization of Pkm1 conditional allele

The Pkm pre-mRNA is transcribed from the Pkm gene and undergoes mutually exclusive splicing of a single exon to generate two alternatively spliced gene products, *Pkm1* (exon 9 inclusion, exon 10 exclusion) or *Pkm2* (exon 10 inclusion, exon 9 exclusion). To control *Pkm1* isoform expression in mouse tissues, we introduced loxP site flanking exon 9 into the Pkm genomic locus of mouse embryonic stem (ES) cells using homologous recombination (Figure 4.3A). ES cells were screened for integration of the targeting construct at the endogenous genomic locus by positive (NeoR) and negative selection (Diptheria Toxin) (Figure 4.3A). Targeted ES cells were used to generate chimeric mice, which were subsequently bred to achieve germline transmission of the conditional allele and then crossed to FLP recombinase transgenic mice to delete the NeoR gene. Expected targeting of the PKM genomic locus was assessed by Southern blot, with the predicted size products of 9.3 kb

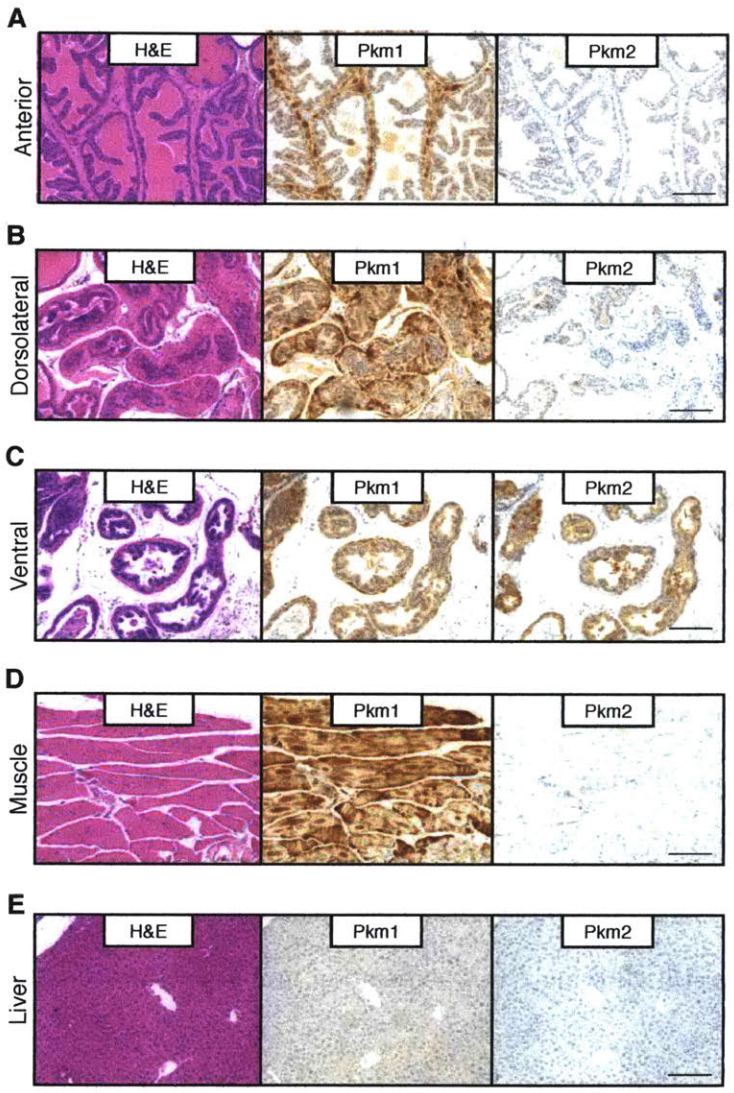

Figure 4.2. Increased glucose uptake upon *Pten* silencing or prostate-restricted deletion of *Pten* in the mouse prostate with changes in Pkm isoform expression from *Pkm1* to *Pkm2*. (A) Representative H&E immunohistochemical staining of *Pkm1* (brown, left) or *Pkm2* (brown, right) in wild-type (WT) in the anterior mouse prostate at 3 months of age. (B) Representative H&E immunohistochemical staining of *Pkm1* (brown, left) or *Pkm2* (brown, right) in wild-type (WT) in the dorsolateral mouse prostate at 3 months of age. (C) Representative H&E immunohistochemical staining of *Pkm1* (brown, left) or *Pkm2* (brown, right) in wild-type (WT) in the ventral mouse prostate at 3 months of age. (D) Representative H&E immunohistochemical staining of *Pkm1* (brown, left) or *Pkm2* (brown, right) in wild-type (WT) in the smooth muscle (quadriceps) at 3 months of age. (E) Representative H&E immunohistochemical staining of *Pkm1* (brown, left) or *Pkm2* (brown, right) in wild-type (WT) in the liver (negative control for PKM1 and PKM2) at 3 months of age.

Figure 4.2

observed from mice that were homozygous for the conditional allele (*Pkm1*fl), 11.3kb from animals with that were wild-type (*Pkm1*+), and both 9.3 and 11.3 kb products for heterozygous mice (Figure 4.3B). A PCR-based stragety was developed for genotyping that was analogous to the one used for *Pkm2* conditional mice ((Israelsen, 2014) (Figure 4.3A, C and Experimental Methods) and the predicted PCR products were observed from animals harboring two copies of the floxed allele (577 bp band); for wild-type animals (509 bp band); two bands for heterozygous mice. Intercrossing *Pkm1* conditional mice yielded progeny born in the expected Mendelian ratios, and displayed no overt phenotypes (not shown).

To determine the effect of *Pkm1* deletion in the prostate, we crossed *Pkm1* conditional mice to animals with *Pb-Cre4* allele to achieve animals homozygous for *Pkm1* ($Pkm1^{fl/fl}$ *Pb-Cre4*). Examination of *Pkm1* RNA expression and protein expression in the AP from these animals showed decreased *Pkm1* transcript levels by quantitative reverse-transcriptase PCR (RT-qPCR) (Figure 4.3D), and the absence of *Pkm1* protein expression by Western blot in all lobes of the mouse prostate without altering *Pkm1* protein levels in other *Pkm1*-expressing tissues (Figure 4.3E). Of note, all lobes of the prostate (AP, DLP, AP) exhibited an increase in *Pkm2* protein in mice with *Pkm1* deletion (Figure 4.3E). These results confirm that Cre expression results in loss of *Pkm1* while still allowing *Pkm2* expression in mouse tissues *in vivo*.

Pkm1 deletion promotes prostate cancer progression

To determine the effect of *Pkm1* deletion on prostate tumor initiation and progression, we crossed *Pkm1* conditional mice to $Pten^{pc-/-}$. Surprisingly, we noted that *Pten;*$Pkm1^{pc-/-}$ animals developed large palpable pelvic masses as early as 3-months of age, a finding that was never observed in $Pten^{pc-/-}$ littermates. The lifespan of the *Pten;*$Pkm^{pc-/-}$ animals was reduced compared with both $Pten^{pc-/-}$ or $Pten^{pc+/+}$ (Ctrl) (Figure 4.4A). Tumors were also never observed in $Pkm1^{pc-/-}$ mice

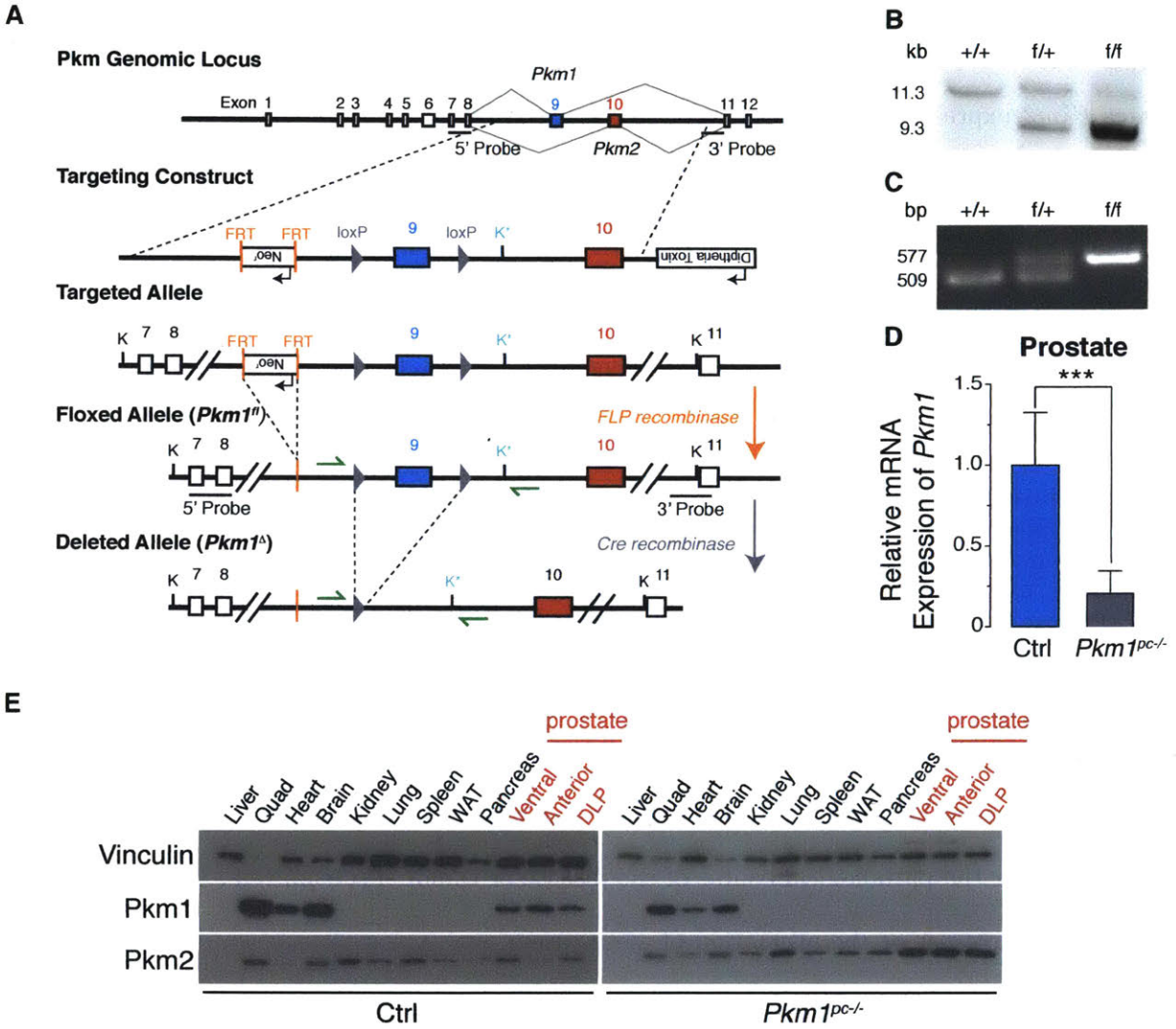

Figure 4.3. Generation and validation of *Pkm1* conditional mice. (A) The mouse Pkm locus, targeting construct, and resulting targeted, floxed, and deleted alles. The KpnI sites used for Southern blot analysis are marked with "K," and the new KpnI site introduced by the targeting vec tor is marked with "K*". The locations of the 5' and 3' probes used for southern blot analysis are also shown. Genotyping primers are indicated by green arrows to detect the floxed allele and the deleted allele. (B) South blot analysis of KpnI-digested genome DNA using the 5' probe shown in (A). Digestion of the genomic DNA for the wild-type allele yields an 8.3 kb fragment, and the floxed allele yields a 6.0 kb fragment. (C) PCR genotyping of the genomic DNA from $Pkm1+/+$, $Pkm1^{+/\mathrm{LoxP}}$, and $Pkm1^{LoxP/LoxP}$ mice. Genotyping primers anneal outside of the LoxP sites as indicated by the arrows in (A) to produce amplicons of 509 bp from the Pkm wild-type allele (Pkm+) and 577 bp from the Pkm allele with flanking LoxP sites ($Pkm2^{LoxP}$). (D) *Pkm1* mRNA levels in $Pkm1^{+/+}$ and $Pkm1^{LoxP/LoxP}$ anterior prostate tissue by quantitative RT-PCR, (n=5 animals per genotype, Significance determined by Student's t-test, *** $p < 0.001$.). (E) Representatitve Western blot analysis of *Pkm1*, *Pkm2*, and vinculin in normal mouse tissues (black) and different lobes of the mouse prostate (red) in wild-type and $Pkm1^{LoxP/LoxP}$; $Pkm1^{pc-/-}$ ($Pkm1^{pc-/-}$).

Figure 4.3

aged to 15 months, and these mice did not show a decreased lifespan. Histological assessment of the pelvic masses arising in *Pten;Pkm1*$^{pc-/-}$ mice was consistent with prostate cancer. We confirmed *Pkm1* loss in the tumors arising in these animals by IHC, and noted that in the *Pkm1* null prostates *Pkm2* expression was observed (Figure 4.4B). To quantitate the differences in growth kinetics between tumors arising in *Pten;Pkm1*$^{pc-/-}$ and *Pten*$^{pc-/-}$ animals, we examined longitudinal cohorts by magnetic resonance imaging (MRI) from 4 to 8 months. Tumors from *Pten;Pkm1*$^{pc-/-}$ animals arose earlier, and grew faster than tumors in *Pten*$^{pc-/-}$ animals (Figure 4.4C, 3D). Dissection of these tumors from 6-months old mice confirmed that tumors from *Pten;Pkm1*$^{pc-/-}$ animals were increased in size compared to tumors from *Pten*$^{pc-/-}$ controls (Figure 4.4E and F). To assess proliferation in the tumors, we examined Ki-67 staining and noticed an increase in staining in both the stromal and epithelial compartments in the *Pten;Pkm1*$^{pc-/-}$ tumors relative to the *Pten*$^{pc-/-}$ tumors (Figure 4.4G, H). At both 6 and 12 months, we noted no significant histological difference in the appearance of tumors arising in *Pten*$^{pc-/-}$ and *Pten;Pkm1*$^{pc-/-}$ animals and no evidence of macroscopic metastases was noted in the mice (data not shown). These data demonstrate that deletion of *Pkm1* together with *Pten* dramatically accelerates prostate cancer initiation and growth, but does not alter the pathological course of the disease or tumor spectrum (e.g. shift in distribution to sarcomas or the promotion of metastases).

Pkm2 deletion suppresses prostate cancer formation

To determine the effect of *Pkm2* deletion on prostate tumor initiation and progression, we crossed a *Pkm2* conditional mice that is analogous to the *Pkm1* conditional allele to *Pten*$^{pc-/-}$ mice. Strikingly, 6 month old *Pten;Pkm2*$^{pc-/-}$ animals had nearly normal prostate tissue that was similar to wild-type tissue, despite the fact that littermates with *Pten* deletion in the prostate and no *Pkm2* conditional allele had prostate tumors. These animals live relatively normal lifespans, and given

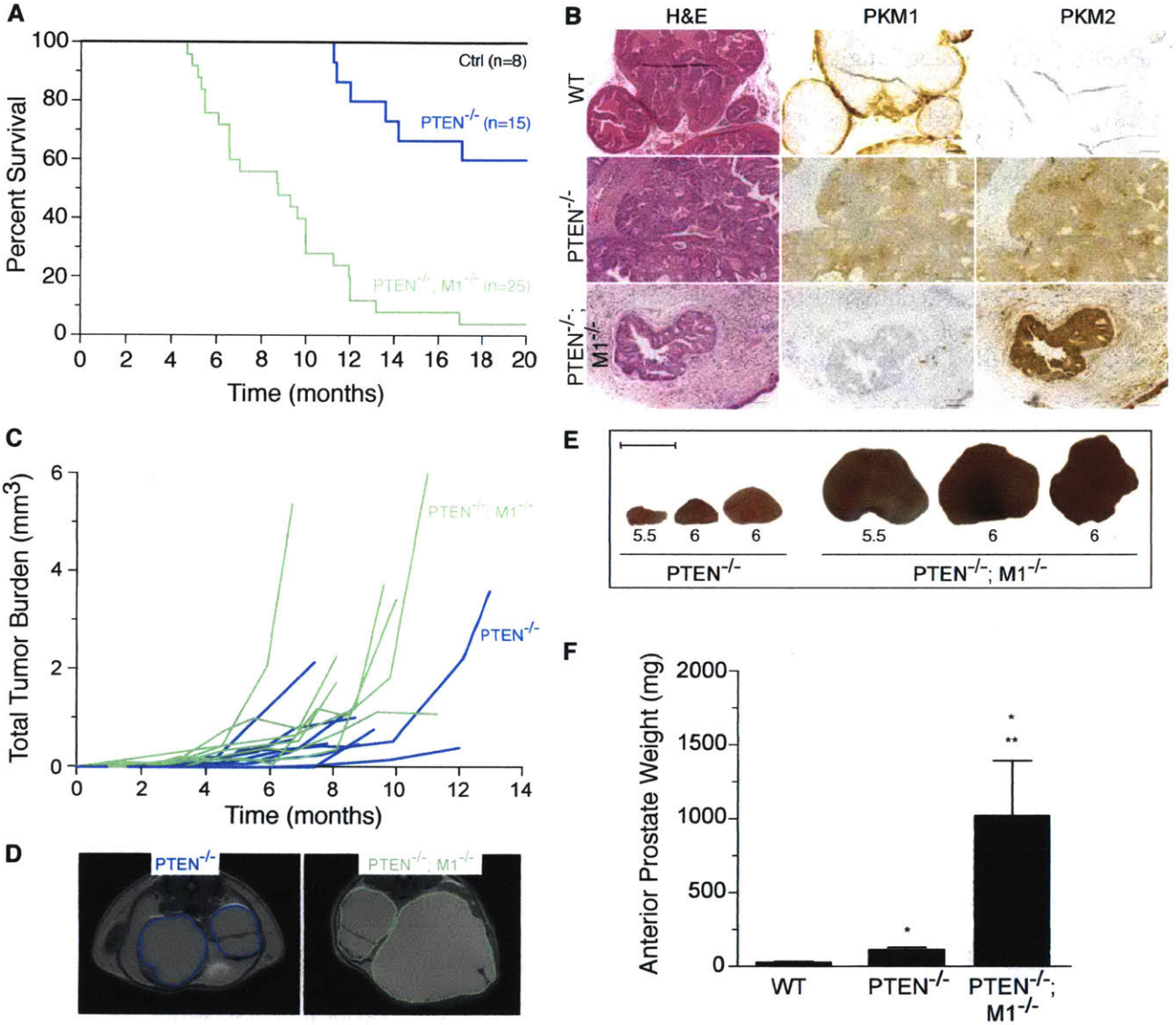

Figure 4.4. Prostate-restricted *Pkm1* on a *Pten*$^{pc-/-}$ genetic background results in decreased survival, increased tumor burden and growth, and increased proliferative index of both the tumor and stromal compartments. (A) Kaplan-Meier curve demnonstrating reduced sruvival in the *Pten;Pkm1*$^{pc-/-}$ cohort, compared with *Pten*$^{pc-/-}$ mice (n displayed, P < 0.001, log-rank test). (B) Representative H&E and immunohistochemical staining of *Pkm1* and *Pkm2* expression in wild-type (WT), *Pten*$^{pc-/-}$, and *Pten*$^{pc-/-}$; *Pkm1*$^{pc-/-}$ at 3 months of age. (C) Tumor volumes estimated from dimensions acquired in a longitudinal magnetic resnonance imaging (MRI) scans, taken at approximately 2-week intervals until tumor burden. (D) Representative MRI image of littermates of *Pten*$^{pc-/-}$- and *Pten;Pkm1*$^{pc-/-}$ mice at 6 months of age. Outlines of left and right anterior prostates (blue and green). (E) Normal weight for WT, *Pten*$^{pc-/-}$ and *Pten;Pkm1*$^{pc-/-}$ at 6 months of age. Significance determined by Student's t-test, *p<0.05 or p<0.001. Each bar represents the mean +/- the SD (WT, n=6; *Pten*$^{pc-/-}$, n=7, and *Pten;Pkm1*$^{pc-/-}$ n=6). (F) Representative macroscopic images of anterior prostate tissue taken at the indicated age from *Pten*$^{pc-/-}$ or *Pten;Pkm1*$^{pc-/-}$. Ages from littermate mice of indicated genotype in months below individual tumors. Scale bar 1cm.

Figure 4.4

that these animals had no significant risk of mortality due to primary prostate burden, we decided instead to examine whether *Pten*;*Pkm2*$^{pc-/-}$ exhibit any changes in growth kinetics as compared to *Pten*$^{pc-/-}$ only. Using longitudinal MRI to measure prostate volumes of *Pten*;*Pkm2*$^{pc-/-}$ and *Pten*$^{pc-/-}$ only, we monitored animals bi-weekly. If 2-consecutive measurements of increased tumor volume, or a difference of >10% in tumor volume after a single measurement were noted, this was scored as abnormal growth. We observed a strong and significant reduction in prostate tissue growth of the *Pten*;*Pkm2*$^{pc-/-}$ as compared to animals with the genotype *Pten*$^{pc-/-}$ (Figure 4.5A) observed deletion of *Pkm2* resulted in the high expression of *Pkm1* in these tissues after 6-months (Figure 4.5B). To quantitate the differences in growth kinetics from tumors arising from *Pten*;*Pkm2*$^{pc-/-}$ and *Pten*$^{pc-/-}$ animals, we examined cohorts of animals with these genotypes by longitudinal magnetic resonance imaging (MRI), using littermates when possible, and observed that tumors from animals with the *Pten*;*Pkm2*$^{pc-/-}$ genotype rarely grew to present an appreciable size and significantly slower than animals *Pten*$^{pc-/-}$ only genotype (Figure 4.5C,D). Upon dissection and macroscopic observation, prostate tissue from *Pten*;*Pkm2*$^{pc-/-}$ animals at an age of > 14 months exhibited dramatically smaller size, even when compared to tumors from *Pten*$^{pc-/-}$ only animals at 6 months (Figure 4.5E). Tissue from *Pten*;*Pkm2*$^{pc-/-}$ further exhibits significantly decreased tumor weight as compared to tumors from *Pten*$^{pc-/-}$ only littermate controls at 6-months, consistent with observations from longitudinal MRI imaging (Figure 4.5F). To determine whether the small size tissue resulting *Pten*;*Pkm2*$^{pc-/-}$ was a result of decreased proliferation, we quantitated Ki-67 staining. We noticed an a significant decrease in proliferation in tumors *Pten*;*Pkm2*$^{pc-/-}$ by Ki-67 staining (Figure 4.5G,H). We further observed significant pathological differences at both 6 and 12 months in tissues and tumors from *Pten*;*Pkm2*$^{pc-/-}$ and *Pten*$^{pc-/-}$ animals. Specifically we observed that prostate tissue from *Pten*;*Pkm2*$^{pc-/-}$ had not progressed past high-grade PIN, even after 12 months, a time point that we observed 100% penetrance of adenocarcinoma or sarcoma-like pathology in

Pten$^{pc-/-}$ animals. Impressively, most animals with the *Pten;Pkm2*$^{pc-/-}$ genotype were healthy and many lived with a normal lifespan. These data, taken together with the data from Figure 4.4, provide formal possibilities that either *Pkm2* expression is necessary for tumorigenesis, or *Pkm1* is tumor suppressive, or both.

Nucleotide depletion and maintenance of cellular senescence is found in Pkm2 null, Pkm1-expressing Pten null prostate tissue

Pten-deletion in the prostate initially results in cellular senescence that is overcome with time, or with deletion of p53. To determine whether *Pkm2* loss suppressed tumorigenesis by promoting maintence of senescence, we performed β-gal staining on tissues from *Pten;Pkm2*$^{pc-/-}$ and *Pten*$^{pc-/-}$ animals. We observed strikingly elevated β-gal staining at 6-months in prostate epithelial cells from tissue from *Pten;Pkm2*$^{pc-/-}$ animals as compared to *Pten*$^{pc-/-}$ only animals (Figure 4.6A). Importantly, prostate tissue from mice with *Pkm2*$^{pc-/-}$ deletion alone did not exhibit a senescent phenotype, suggesting that loss of *Pkm2*, without *Pten*-loss, in the prostate is not sufficient to induce cellular senescence (data not shown). These data suggest that high *Pkm1* expression may promote senescence in the setting of *Pten* loss, and consistent with this decreased β-gal staining is observed in tumors arising at early time points in *Pkm1*. *Pkm1*-mediated suppression of cell proliferation have been shown previously to involve a depletion of nucleotides that limits DNA replication, but whether this is also a feature of senescent cells *in vivo* has not been determined.

To determine whether the nucleotide levels were altered in mouse prostate with *Pkm2* loss, we examined metabolite levels in the anterior prostates from 6-month old *Pten;Pkm2*$^{pc-/-}$ and *Pten*$^{pc-/-}$ mice. We observed significant decreases in intermediates of the pyrimidine and purine biosynthesis pathways as well as intermediates that contribute to the carbon or nitrogen content of nucleobases (Figure 4.6C, D), including deoxy-thymidine monophosphate (dTMP), adenosine monophosphate

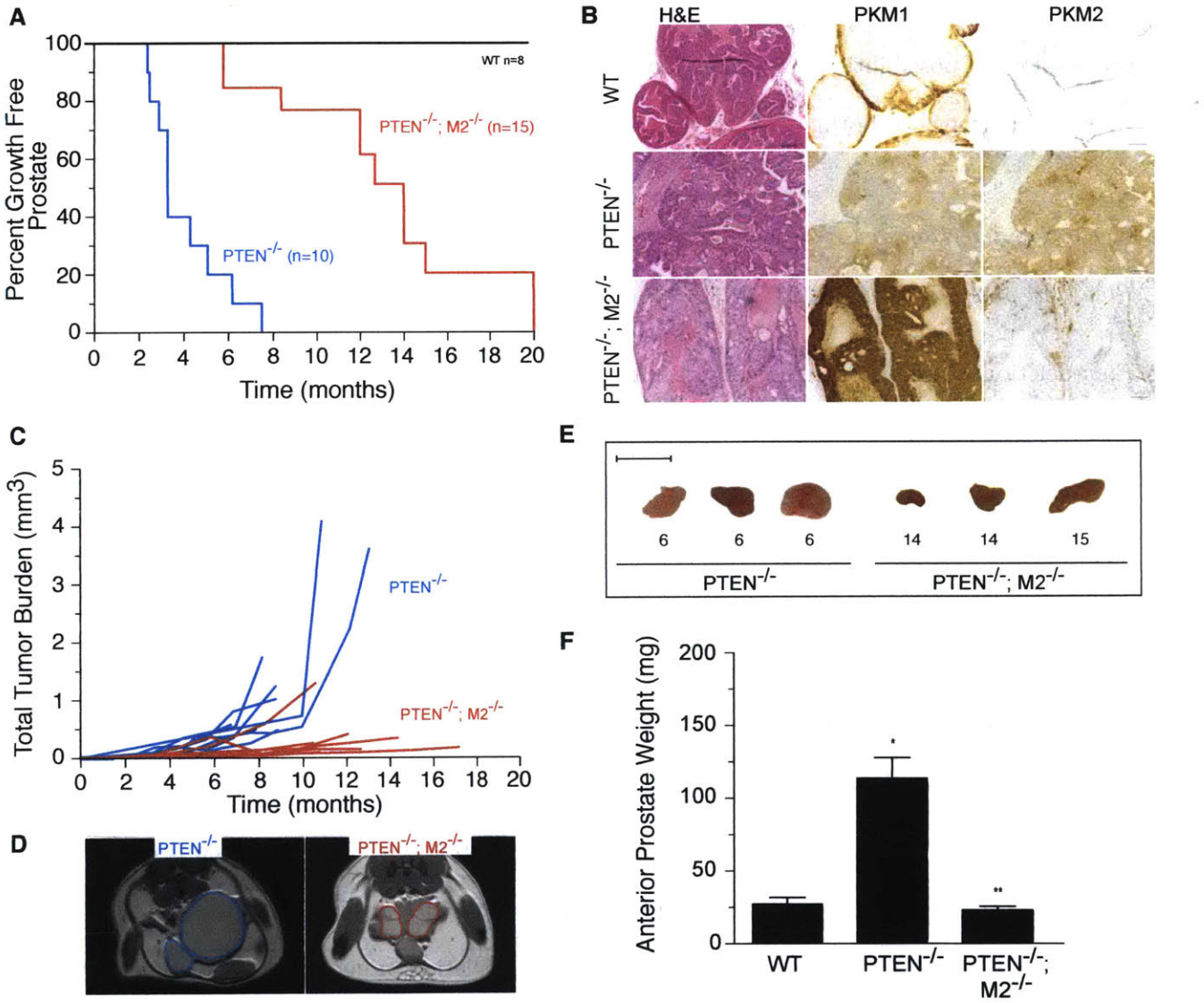

Figure 4.5. Prostate-restricted *Pkm2* deletion on a $Pten^{pc-/-}$ genetic background results in decreased time until abnormal prostate growth, decreased tumor burden and growth, and decreased proliferative index of the prostate epithelium. (A) Kaplan-Meier (log-rank) curve demonstrating reduced survival in the $Pten;Pkm2^{pc-/-}$ cohort, compared with $Pten^{pc-/-}$ mice (n displayed, $P < 0.001$). (B) Representative H& E and immunohistochemical staining of *Pkm1* and *Pkm2* expression in wild-type (WT), $Pten^{pc-/-}$, and $Pten^{pc-/-}$; $Pkm1^{pc-/-}$ at 3 months of age. (C) Tumor volumes estimated from dimensions acquired in a longitudinal magnetic resnonance imaging (MRI) scans, taken at approximately 2-week intervals until tumor burden. (D) Representative MRI image of littermates of $Pten^{pc-/-}$ and $Pten;Pkm1^{pc-/-}$ mice at 6 months of age. Outlines of left and right anterior prostates (blue and green). (E) Normal weight for WT, $Pten^{pc-/-}$ and $Pten;Pkm2^{pc-/-}$ at 6 months of age and 14-15 months of age, respectively. Significance determined by Student's t-test, *$p<0.05$ or $p<0.001$. Each bar represents the mean +/- the SD (WT, n=5; $Pten^{pc-/-}$, n=5, and $Pten;Pkm2^{pc-/-}$ n=7). (F) Representative macroscopic images of anterior prostate tissue taken at the indicated age from $Pten^{pc-/-}$ or $Pten;Pkm2^{pc-/-}$. Ages from littermate mice of indicated genotype in months below tumor. Scale bar 1cm.

Figure 4.5

(AMP), guanosine monophosphate (GMP), uridine monophosphate (UMP), ribose-5-phosphate (R5P), inosine monophosphate (IMP), aspartate, glutamine, and glycine (Figure 4.6E). Furthermore, with respect to purine metabolism, we noted an increased levels of guanosine and adenosine, suggesting that nucleotide salvage pathway activity may also be decreased, which might further contribute to decreased nucleotide pools (Figure 4.6E). To determine whether glucose uptake was different in prostate from *Pten*;*Pkm2*$^{pc-/-}$ and *Pten*$^{pc-/-}$ mice, we used FDG-PET. Prostates from *Pten*;*Pkm2*$^{pc-/-}$ mice exhibited glucose uptake that was similar to prostates wild-type animals and prostate from both wild-type and *Pten*;*Pkm2*$^{pc-/-}$ mice take up less glucose than prostates from *Pten*$^{pc-/-}$ mice that harbor invasive cancers (Figure 4.6F, G). These data suggest that loss of *Pkm2* leads to nucleotide depletion and decreased glucose uptake despite *Pten* deletion and suppresses tumor formation.

Pharmacological activation of Pkm2 in Pten mice delays prostate tumor growth

Because *Pkm1* exhibits high consitutive activity, while *Pkm2* enzyme activity is regulated, we hypothesized that high pyruvate kinase activity associated with high *Pkm1* expression is sufficient to suppress prostate tumors following *Pten* deletion. To test this hypothesis, we asked whether TEPP-46, a pharmacological activator of *Pkm2* with reasonable pharmacokinetics and tissue distribution *in vivo* (Anastasiou et al., 2011) would effect tumor growth in *Pten*$^{pc-/-}$ mice. Prostate in *Pten*$^{pc-/-}$ animals were monitored by MRI until tumors were $> 2mm^3$ prior to initation of treatment. Animals were treated with TEPP-46 orally twice a day, or with vehicle control, for one month and assessed tumor growth bi-weekly using MRI. As expected, nearly all (7/8) tumors from *Pten*$^{pc-/-}$ that were treated with vehicle exhibited growth over the one-month period of treatment. However, only 2/8 tumors arising from *Pten*$^{pc-/-}$ grew after one month of treatment (data not shown). These data suggest that pharmacological activation of *Pkm2* can also suppress prostate

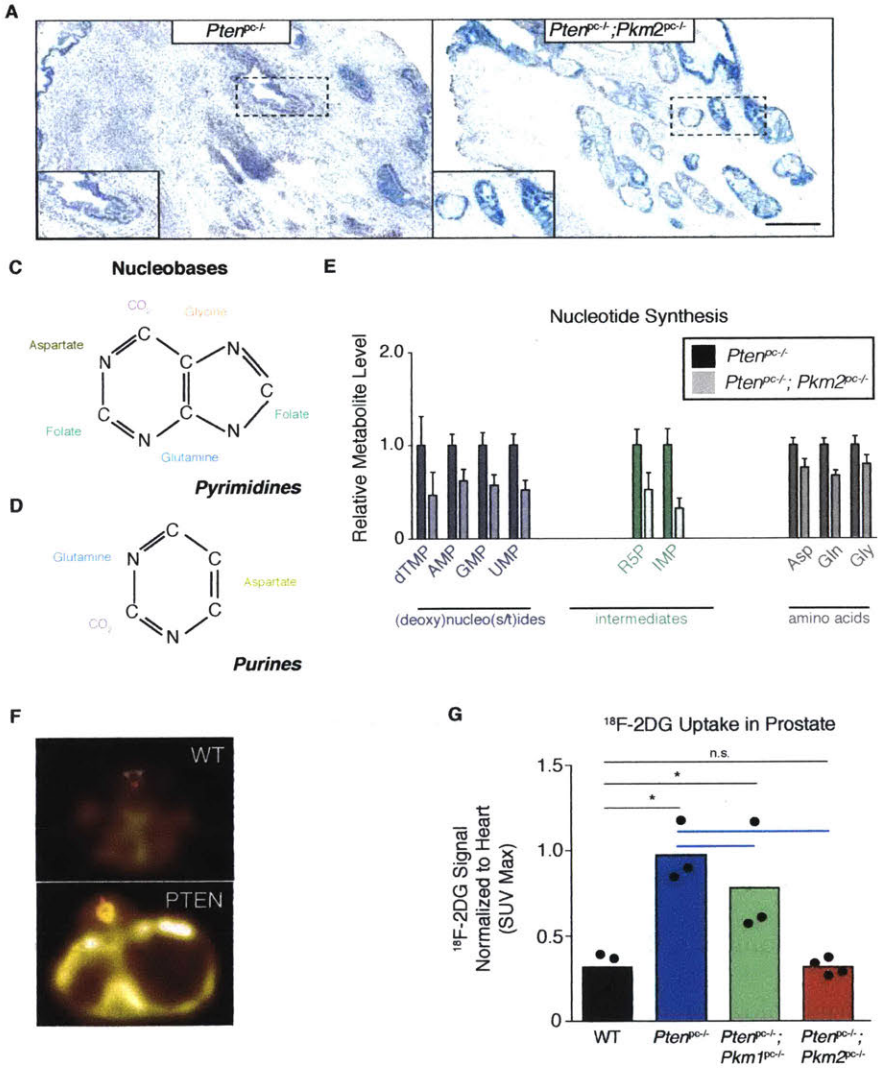

Figure 4.6. *Pten;Pkm2*$^{pc-/-}$ tumors exhibit prolonged senescence, decreased glucose uptake, and decreased metabolites involved in nucleotide synthesis relative to *Pten*$^{pc-/-}$ tumors in the mouse prostate. (A) Representative β-gal senescence staining of the anterior prostate in WT, Pten$^{pc-/-}$; or *Pten;Pkm2*$^{pc-/-}$ at 6 or 12 months of age. (D) Metabolite contribution to purine nucleobases. Indicated atom positions colored according to origin of carbon or nitrogen constituent. (D) Metabolite contribution to pyrimidine nucleobases. Indicated atom positions colored according to origin of carbon or nitrogen constituent. (F) Normalized total ion counts from liquid-chromatography mass-spectrometry (LC/MS) of the purine and pyrimidine biosynthetic intermediate pathway. (Pten$^{pc-/-}$ n=x; or *Pten;Pkm2*$^{pc-/-}$ n=6-8 mice per genotype, * $P < 0.05$, ** $P<0.01$, *** $P<0.001$, Bonferroni corrected for multiple hypothesis testing). (F) Representative [18F]fluoro-2-deoxyglucose positron emission tomography (FDG-PET) in wild-type (WT), *Pten* (*Pten*$^{pc-/-}$) , and *Pten;Pkm2*$^{pc-/-}$ at 6 months of age. Anterior prostate location indicated by the white arrows (n=4). (G) Quantification of maximum intensity of [^{18}F]fluoro-2-deoxyglucose emission spectra in wild-type (WT) and *Pten* (*Pten*$^{pc-/-}$) mouse prostates normalized to the intensity of the emission spectra in the heart.

Figure 4.6

tumor growth, and supports the notion that *Pkm1* expression is tumor suppressive in this tissue.

Human prostate cancer exhibit moderate to high levels of Pkm2 expression

Because variable *Pkm2* expression has been observed in cancer, we aimed to better understand *Pkm2* expression in human prostate cancer in order to provide a context where activators might be employed for therapeutic value. For this analysis, a tumor microarray containing specimens from 150 patients with prostate cancer was examined (Figure 4.7). In contrast to breast cancers, we observed that most human prostate tumors exhibit moderate to robust *Pkm2* expression. However, similar to findings in breast cancer, there was a high degree of heterogeneity of *Pkm1* and *Pkm2* expressoin in the human prostate tumors. We also quantified *Pkm1* and *Pkm2* relative staining in different cell types in adjacent normal prostate of these patients to determine whether there was isoform exclusivity (Figure 4.7). In patients with high expression of *Pkm2* isoform in many tumors, *Pkm1* expression was often high. In an orthogonal examination that may have implications for PKM expression , we next turned to examine genomic data from deep-sequencing efforts from the Cancer Genome Atlas (TCGA). In further contrast to endometrial cancers where loss-of-function mutations resulting in early truncation of PKM were identified in exon 10 (Israelsen, 2014), few such mutations were observed in prostate cancer. From this prostate TCGA analysis, only 2/333 revealed deletions (homozygous) in the total PKM gene (cbioportal). The mutational data that mutations or deletions in *Pkm2* are infrequent in human prostate cancer, and combined with our data from the tumor microarray, suggest that *Pkm2* may be an actionable target in this disease.

Discussion

Our studies show that loss of Pkm1 isoform expression and activity is critical for *Pten*-driven prostate tumor initiation and progression. We show data to suggest that silencing or genetic

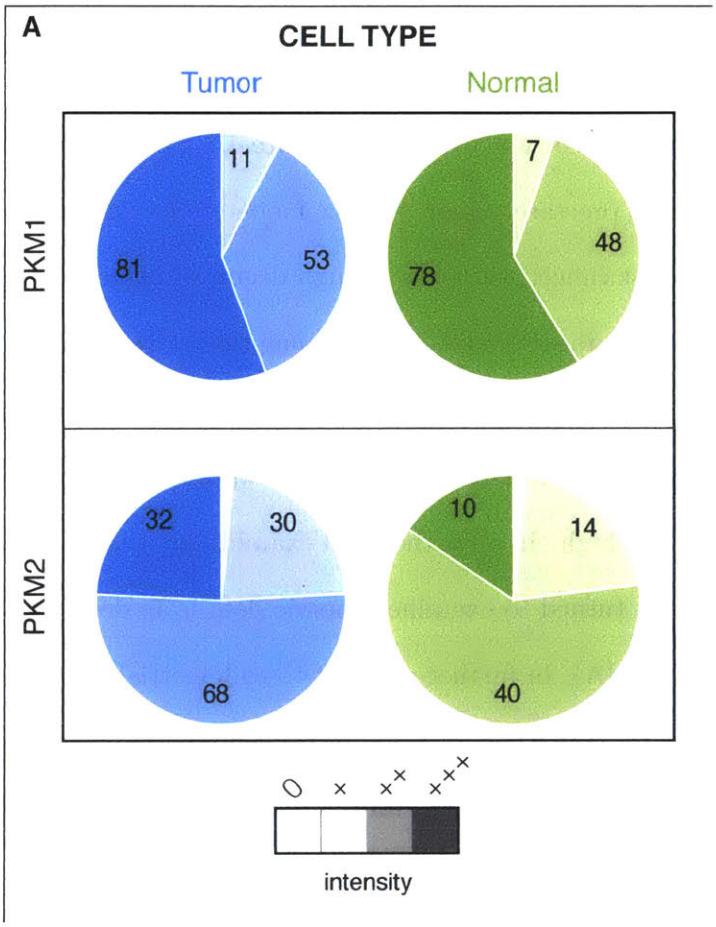

Figure 4.7. *Pkm2* expression is retained in most human tumors examined. Quantification of immunohistochemical staining for *Pkm1* and *Pkm2* isoform expression in tumor (blue) and normal adjacent (green) sections from a tumor microarray. Staining intensity is marked from dark to light, number of positive tumors per intensity displayed.

Figure 4.7

deletion of *Pten* promotes increased glucose uptake in the absence of cellular transformation and that genetic deletion of *Pten* results in an isoform switch from *Pkm1* (normal prostate) to *Pkm2* (tumors) *in vivo*. We further demonstrate that prostate-restricted genetic deletion of *Pkm1* and *Pten* results in decreased animal survival, accelerated tumor progression, and tumors with an increased proliferative index as compared to animals with prostate-restricted *Pten* deletion alone. In contrast, prostate-restricted genetic deletion of *Pkm2* and *Pten* exhibit lesions that rarely progress past neoplasias, minimal or no change in prostate size, and prostate tissue with a proliferative index that is normal tissue from control wild-type animals. These data, taken together, suggest that in additional to glucose uptake, one element of additional downstream metabolic coordination required for the development of prostate cancer is isoform switching from *Pkm1* to *Pkm2*.

The prostate is a metabolically distinct organ and focuses most of its energy on biosynthesis of citrate and fructose for seminal fluid (Costello et al., 2005; Costello and Franklin, 2000, 2006). Indeed, *Pkm1* expression has been correlated in other settings with promoting metabolism that favors high flux into the TCA cycle, supporting a possible role for *Pkm1* expression in citrate production in normal tissue. In the human disease, it has been observed that citrate production declines with increasing tumor progression, and this may be a result of mutations in *Pten* or other genes that drive prostate cancer and promote isoform switching from *Pkm1* to *Pkm2*, corroborating our observations in the mouse model. Since tumors derived from *Pten*;*Pkm2*$^{pc-/-}$ animals significantly lower levels of nucleotides, in part owing to reduced of glucose uptake. Because cells exhibit sensitivity to nucleotide levels through a number of mechanisms to preserve genomic integrity, we suggest that decreases in these metabolites contribute to the maintenence of the *Pten*-induced senescence observed in this model. Taken together, the trends in isoform expression and the metabolic programs they promote are consistent with all themes for previous studies examining metabolism and senescence, with high *Pkm1* activity promoting high oxidative flux and

low levels of nucleotides and biosynthetic intermediates.

We also demonstrate decreases in tumor growth in animals with *Pten*-driven prostate cancer that were treated with the small-molecule *Pkm2* activator, TEPP-46, as compared to those treated with a vehicle control. Whether *Pkm2* activators can be used to treat prostate cancer is an open question. That *Pkm1* expression and high Pkm activity is correlated with depletion of nucleotides makes the possibilities of using *Pkm2* activators in combination with existing therapies that further reduce available nucleotide pools. Additionally, if combined with radiation, decreased nucleotide pools could make DNA repair from these regions of focal radiation less efficient and therefore synergize with this therapeutic modality, provided *Pkm2* is expressed.

While recent work from our lab and others have demonstrated that *Pkm2* is dispensable for the formation of certain tumor types, including breast tumors in Brcafl/fl; p53fl/+ mouse models and in colon cancer cell lines and resulting xenografts (Israelsen, 2014; Cortés-Cros et al., 2013). In human prostate cancer, our analysis of a tumor microarray revealed heterogeneity in the levels of *Pkm2* expressions, but most tumors exhibit moderate to high levels of *Pkm2* expression. As this has only been demonstrated in some settings, it will be further important to analyze different tumor types and further understand the molecular bases that promote *Pkm2* expression to determine which events are most predictive of isoform expression.

Experimental Procedures

Animal Statement

All animal studies were approved by the MIT Committee on Animal Care. Prostate tumor volumes were assessed using a Varian MRI and OsiriX (OsiriX-Viewer) was used for image analysis.

[18F]-2-Deoxyglucose Positron Emission Tomography (PET)

Animals were fasted overnight before administration of 100μCi of FDG F18 via Tail Catheter. Animals were kept warm using a heated water pad and under 2% anesthesia during the 1hr uptake time to lower background uptake signal. Animals were then imaged for 10 mins in PET and 1 min in CT using 720 projections at 50kv and 200μA using Sofie G8 PET/CT. Images were CT attenuation corrected and MLEM3D reconstructed. All images were decay corrected to time of injection.

Glucose Uptake Assays and Cell Culture

NIH 3T3 cells were cultured in DMEM with 10% FBS with 4 mM of glucose and 2.5 mM glutamine and transfected with siRNAs containing anti-sense sequences against *Pten* or the scrambled sequence of *Pten.* Cells were then plated in a 6-well dish in serum-containing medium (DMEM) and washed three times with room temperature saline. Media containing 1 μCi/mL of 2-deoxy-D-[^{3}H] glucose was added to the cells and allowed to incubate for five minutes. Cells were washed with ice-cold PBS and solubilized in 1% SDS. Intracellular ^{3}H-glucose was measured from cell lysates using a Beckman scintillation counter. Blank wells were run to subtract non-specific glucose uptake.

Generation and Breeding of Pkm1 Conditional Mice and Mouse Strains

The conditional allele for *Pkm1* was generated using standard protocols to introduce loxP sites in the intronic region flanking exon 9 of the *Pkm1* gene. *Pb-Cre4* allele was maintained in males due to previously observed mosaic recombination when transmitted through females (Birbach, 2013). Males harboring $Pkm1^{pc-/-}$ and *Pten*, *Pkm1*, or *Pkm2* floxed alleles were crossed to females harboring *Pten*, *Pkm1*, or *Pkm2* floxed alleles to generate prostate restricted deletion of these genes and splice products. All animals were maintained on a mixed background and littermates were used for direct comparisons.

Southern Blot

Asp718 (Roche)-digested genomic DNA was analyzed by Southern blot using standard protocols and probe binding was visualized by autoradiography.

PCR Genotyping

PCR genotyping was developed to detect and amplify the targeted Pkm genetic locus and performed using forward (5'-CACGCAACCATTCCAGGAGCATAT-3') and reverse (5'-TGGTGACCTTGGCTGTCTTCCTGA-3') primers. For all primers used for genotyping in this study, see Extended Experimental Procedures.

Tumor Microarray Analysis

Pkm1 and *Pkm2* expression in human prostate cancer was determined as described above. We analyzed one tumor microarray from the Gelb Study with over 150 unique patients (3 cores per region of tumor, with two adjacent cores of normal tissue per patient).

Western Blot and Immunohistochemistry

Western blots were performed using primary antibodies against *Pkm1* (Sigma SAB4200094), *Pkm2* (Cell Signaling Technology #4053), PKM (Cell Signaling Technology #3190; Abcam ab6191), Vinculin (Sigma, V4505, clone VIN-11-5). Fixed sections were stained with the following primary antibodies after antigen retrieval: *Pkm1* (Cell Signaling Technology #7067), *Pkm2* (Cell Signaling Technology #4053), PCNA (Cell Signaling Technology #2586), Ki-67 (BD Pharmingen 556003), cleaved-caspase 3 (Cell Signaling Technology #9661). *Pkm1*/PCNA and *Pkm1*/Ki-67 dual staining was q4uantified by scoring cells as PCNA positive or negative and *Pkm1* high or low/none.

β-Galactosidase Senescence Staining of Tissues

β-gal staining was conducted as previously reported in (Dimri et al., 1995). In brief, fresh frozen-sections were cut to 8um thickness and fixed in 4% paraformaldehyde. A solution containing 1 mg of 5-bromo-4-chloro-3-indoyl β-D-galactoside (X-gal) per mL (stock = 20mg of dimethylformamide per mL) with 40 mM critic acid/sodium phosphate pH 5.5, 5 mM potassium ferricyanide in 150 mM NaCl/2 mM MgCl2 was applied to the tissue and sections were incubated in a CO2 free incubator at 37°C for 12-16 hours and visualized by conventional light microscopy.

Magnetic Resonance Imaging (MRI)

Animals were randomized following genotypes into the following cohorts: WT, Ptenpc-/-; *Pkm1* or *Pkm2* littermates. Animals were monitored bi-weekly for tumor growth using a Varian 7T MRI imaging system. Image sequences were acquired using the proton imaging FSEMS sequence (fast spin echo multiple slice) with TR: 4000 ms; TE: 12 ms in the axial orientation. Additional settings were as follows: 256X256 data matrix; 45X45 mm region; 1 mm thick slice; for 20 slices.

Metabolite Measurement

For metabolite extraction, 10-40mg tissue was weighed and homogenized cryogenically (Retsch Cryomill) prior to extraction in chloroforom:methanol:water (400:600:300). Samples were centrifuged to separate aqueous and organic layers, and polar metabolites dried under nitrogen gas for subsequent analysis by mass-spectrometry. For liquid chromatography mass spectrometry (LC-MS), dried metabolites were resuspended in water based on tissue weight with valine-D8 included as an injection control.

TEPP-46 Dosing

Animals were imaged until tumors were observed and randomized prior to the beginning treatment with either *Pkm2* activator (TEPP-46) or a vehicle control. TEPP-46 was formulated in 0.5% carboxy methyl cellulose with 0.1% v/v Tween 80 as previously reported in (Anastasiou et al., 2011) and delivered via oral gavage to a final dosage of 10 mg/kg in a volume less than 250µL.

Statistical Analysis

Log-rank tests were performed to determine significance in survival or tumor incidence (SPSS Statistics). Two-tailed paired and unpaired Student's T-test were performed for all other experiments unless otherwise specified (GraphPad PRISM 7). Results for independent experiments are presented as mean ±SEM; results for technical replicates are presented as mean ±SD.

Acknowledgements

We thank the Swanson Biotechnology Center for mouse tissue processing and the Vander Heiden Laboratory for thoughtful discussions. S.M.D. was supported by an NSF Graduate Research Fellowship and T32GM007287. M.G.V.H acknowledges support from the Ludwig Center at MIT, the Burroughs

Wellcome Fund, the NIH (P30CA1405141, R01CA168653), and SPORE NCI/NIH (2P50CA090381-11A1).

References

Aird KM, Zhang G, Li H, Tu Z, Bitler BG, et al. Suppression of nucleotide metabolism underlies the establishment and maintenance of oncogene-induced senescence. *Cell Reports* **3**, 1252 (2013).

Aird KM, Zhang R. Nucleotide metabolism, oncogene-induced senescence and cancer. *Cancer Letters* **356**, 204 (2015).

Anastasiou D, Poulogiannis G, Asara JM, Boxer MB, Jiang Jk, et al. Inhibition of pyruvate kinase M2 by reactive oxygen species contributes to cellular antioxidant responses. *Science* **334**, 1278 (2011).

Anastasiou D, Yu Y, Israelsen WJ, Jiang JK, Boxer MB, et al. Pyruvate kinase M2 activators promote tetramer formation and suppress tumorigenesis. *Nature Chemical Biology* **8**, 839 (2012).

Ashrafian H. Cancer's sweet tooth: the Janus effect of glucose metabolism in tumorigenesis. *Lancet* **367**, 618 (2006).

Birbach A. Use of PB-Cre4 mice for mosaic gene deletion. *PLoS ONE* **8**, e53501 (2013).

Cairns R, Harris I, Mak T. Regulation of cancer cell metabolism. *Nature Reviews Cancer* **11**, 85 (2011).

Campisi J. Aging, Cellular Senescence, and Cancer. *Annual Review of Physiology* **75**, 685 (2013).

Chaneton B, Hillmann P, Zheng L, Martin ACL, Maddocks ODK, et al. Serine is a natural ligand and allosteric activator of pyruvate kinase M2. *Nature* **491**, 458 (2012).

Chen M, David CJ, Manley JL. Concentration-dependent control of pyruvate kinase M mutually exclusive splicing by hnRNP proteins. *Nature Structural & Molecular Biology* **19**, 346 (2012).

Chen Z, Trotman LC, Shaffer D, Lin HK, Dotan ZA, et al. Crucial role of p53-dependent cellular senescence in suppression of Pten-deficient tumorigenesis. *Nature* **436**, 725 (2005).

Christofk HR, Vander Heiden MG, Harris MH, Ramanathan A, Gerszten RE, et al. The M2 splice isoform of pyruvate kinase is important for cancer metabolism and tumour growth. *Nature* **452**, 230 (2008a).

Christofk HR, Vander Heiden MG, Wu N, Asara JM, Cantley LC. Pyruvate kinase M2 is a phosphotyrosine-binding protein. *Nature* **452**, 181 (2008b).

Collado M, Blasco MA, Serrano M. Cellular senescence in cancer and aging. *Cell* **130**, 223 (2007).

Collado M, Serrano M. Senescence in tumours: evidence from mice and humans. *Nature Reviews Cancer* **10**, 51 (2010).

Cortés-Cros M, Hemmerlin C, Ferretti S, Zhang J, Gounarides JS, et al. M2 isoform of pyruvate kinase is dispensable for tumor maintenance and growth. *Proceedings of the National Academy of Sciences* **110**, 489 (2013).

Costello LC, Franklin RB. The intermediary metabolism of the prostate: a key to understanding the pathogenesis and progression of prostate malignancy. *Oncology* **59**, 269 (2000).

Costello LC, Franklin RB. The clinical relevance of the metabolism of prostate cancer; zinc and tumor suppression: connecting the dots. *Molecular Cancer* **5**, 17 (2006).

Costello LC, Franklin RB, Feng P. Mitochondrial function, zinc, and intermediary metabolism relationships in normal prostate and prostate cancer. *Mitochondrion* **5**, 143 (2005).

Curry NL, Mino-Kenudson M, Oliver TG, Yilmaz mH, Yilmaz VO, et al. Pten -null tumors cohabiting the same lung display differential AKT activation and sensitivity to dietary restriction. *Cancer Discovery* **3**, 908 (2013).

David CJ, Chen M, Assanah M, Canoll P, Manley JL. HnRNP proteins controlled by c-Myc deregulate pyruvate kinase mRNA splicing in cancer. *Nature* **463**, 364 (2010).

Dayton TL, Gocheva V, Miller KM, Israelsen WJ, Bhutkar A, et al. Germline loss of PKM2 promotes metabolic distress and hepatocellular carcinoma. *Genes & Development* **30**, 1 (2016).

Deberardinis RJ, Chandel NS. Fundamentals of cancer metabolism. *Science Advances* **2**, e1600200 (2016).

Dibble CC, Cantley LC. Regulation of mTORC1 by PI3K signaling. *Trends in Cell Biology* **25**, 545 (2015).

Dimri GP, Lee XH, Basile G, Acosta M, Scott C, et al. A biomarker that identifies senescent human-cells in culture and in aging skin in-vivo. *Proceedings of the National Academy of Sciences of the United States of America* **92**, 9363 (1995).

Dörr JR, Yu Y, Milanovic M, Beuster G, Zasada C, et al. Synthetic lethal metabolic targeting of cellular senescence in cancer therapy. *Nature* **501**, 421 (2013).

Favaro E, Bensaad K, Chong MG, Tennant DA, Ferguson DJP, et al. Glucose utilization via glycogen phosphorylase sustains proliferation and prevents premature senescence in cancer cells. *Cell Metabolism* **16**, 751 (2012).

Gray IC, Stewart LM, Phillips SM, Hamilton Ja, Gray NE, et al. Mutation and expression analysis of the putative prostate tumour-suppressor gene PTEN. *British Journal of Cancer* **78**, 1296 (1998).

Gui DY, Lewis Ca, Vander Heiden MG. Allosteric regulation of PKM2 allows cellular adaptation to different physiological states. *Science Signaling* **6**, 1 (2013).

Israelsen WJ. *The Role of Pyruvate Kinase Regulation in Tumor Growth and Metabolism.* Ph.D. thesis, Massachusetts Institute of Technology (2014).

Jiang P, Du W, Mancuso A, Wellen KE, Yang X. Reciprocal regulation of p53 and malic enzymes modulates metabolism and senescence. *Nature* **493**, 689 (2013).

Kaplon J, Zheng L, Meissl K, Chaneton B, Selivanov VA, et al. A key role for mitochondrial gatekeeper pyruvate dehydrogenase in oncogene-induced senescence. *Nature* **498**, 109 (2013).

Keller KE, Tan IS, Lee YS. SAICAR stimulates pyruvate kinase isoform M2 and promotes cancer cell survival in glucose-limited conditions. *Science* **1069**, 1 (2012).

Kuilman T, Michaloglou C, Mooi WJ, Peeper DS. The essence of senescence. *Genes & Development* **24**, 2463 (2010).

Lehmann BD, Paine MS, Brooks AM, McCubrey JA, Renegar RH, et al. Senescence-associated exosome release from human prostate cancer cells. *Cancer Research* **68**, 7864 (2008).

Levine AJ, Puzio-Kuter AM. The control of the metabolic switch in cancers by oncogenes and tumor suppressor genes. *Science* **330**, 1340 (2010).

Lunt SY, Muralidhar V, Hosios AM, Israelsen WJ, Gui DY, et al. Pyruvate kinase isoform expression alters nucleotide synthesis to impact cell proliferation. *Molecular Cell* **57**, 95 (2015).

Lunt SY, Vander Heiden MG. Aerobic glycolysis: meeting the metabolic requirements of cell proliferation. *Annual Review of Cell and Developmental Biology* **27**, 441 (2011).

Mazurek S. Pyruvate kinase type M2: a key regulator of the metabolic budget system in tumor cells. *International Journal of Biochemistry and Cell Biology* **43**, 969 (2011).

Michaloglou C, Vredeveld LCW, Soengas MS, Denoyelle C, Kuilman T, et al. BRAFE600-associated senescence-like cell cycle arrest of human naevi. *Nature* **436**, 720 (2005).

Monn MF, Flack CK, Koch MO. High-intensity focused ultrasound. *Prostate Cancer* 551–562 (2016).

Murcott TH, Gutfreund H, Muirhead H. The cooperative binding of fructose-1,6-bisphosphate to yeast pyruvate kinase. *The EMBO Journal* **11**, 3811 (1992).

Parnell KM, Foulks JM, Nix RN, Clifford A, Bullough J, et al. Pharmacologic activation of PKM2 slows lung tumor xenograft growth. *Molecular Cancer Therapeutics* **12**, 1453 (2013).

Patel PL, Suram A, Mirani N, Bischof O, Herbig U. Derepression of hTert gene expression promotes escape from oncogene-induced cellular senescence. *Proceedings of the National Academy of Sciences* **113**, 201602379 (2016).

Pérez-Mancera PA, Young ARJ, Narita M. Inside and out: the activities of senescence in cancer. *Nature Reviews Cancer* **14**, 547 (2014).

Plathow C, Weber WA. Tumor cell metabolism imaging. *Journal of Nuclear Medicine* **49**, 43S (2008).

Puzio-Kuter AM. The role of p53 in metabolic regulation. *Genes & Cancer* **2**, 385 (2011).

Reske SN, Kotzerke J. FDG-PET for clinical use: results of the 3rd German Interdisciplinary Consensus Conference, "Onko-PET III", 21 July and 19 September 2000. *European Journal of Nuclear Medicine* **28**, 1707 (2001).

Siegel R, Miller K, Jemal A. Cancer statistics, 2015. *CA Cancer Journal for Clinicians* **65**, 5 (2015).

Song MS, Salmena L, Pandolfi PP. The functions and regulation of the PTEN tumour suppressor. *Nature Reviews Molecular Cell Biology* **13**, 283 (2012).

Tan JL, Fogley RD, Flynn RA, Ablain J, Yang S, et al. Stress from nucleotide depletion activates the transcriptional regulator HEXIM1 to suppress melanoma. *Molecular Cell* **62**, 34 (2016).

Testa JR, Tsichlis PN. AKT signaling in normal and malignant cells. *Oncogene* **24**, 7391 (2005).

Trotman LC, Niki M, Dotan ZA, Koutcher JA, Di Cristofano A, et al. Pten dose dictates cancer progression in the prostate. *PLoS Biology* **1**, e9 (2003).

Valkenburg KC, Williams BO. Mouse models of prostate cancer. *Prostate Cancer* **2011**, 895238 (2011).

Vander Heiden MG, Cantley LC, Thompson CB. Understanding the Warburg effect: the metabolic requirements of cell proliferation. *Science* **324**, 1029 (2009).

Walsh MJ, Brimacombe KR, Veith H, Bougie JM, Daniel T, et al. 2-Oxo-N-aryl-1,2,3,4-tetrahydroquinoline-6-sulfonamides as activators of the tumor cell specific M2 isoform of pyruvate kinase. *Bioorganic & Medicinal Chemistry Letters* **21**, 6322 (2011).

Wang S, Gao J, Lei Q, Rozengurt N, Pritchard C, et al. Prostate-specific deletion of the murine Pten tumor suppressor gene leads to metastatic prostate cancer. *Cancer Cell* **4**, 209 (2003).

Wang Z, Chatterjee D, Jeon HY, Akerman M, Vander Heiden MG, et al. Exon-centric regulation of pyruvate kinase M alternative splicing via mutually exclusive exons. *Journal of Molecular Cell Biology* **4**, 79 (2012).

Whang YE, Wu X, Suzuki H, Reiter RE, Tran C, et al. Inactivation of the tumor suppressor PTEN/MMAC1 in advanced human prostate cancer through loss of expression. *Proceedings of the National Academy of Sciences* **95**, 5246 (1998).

Wu X, Pandolfi PP. Mouse models for multistep tumorigenesis. *Trends in Cell Biology* **11**, 2 (2001).

Yacovan A, Ozeri R, Kehat T, Mirilashvili S, Sherman D, et al. 1-(sulfonyl)-5-(arylsulfonyl)indoline as activators of the tumor cell specific M2 isoform of pyruvate kinase. *Bioorganic and Medicinal Chemistry Letters* **22**, 6460 (2012).

Zhang J, Thomas TZ, Kasper S, Matusik RJ. A small composite probasin promoter confers high levels of prostate-specific gene expression through regulation by androgens and glucocorticoids in vitro and in vivo. *Endocrinology* **141**, 4698 (2000).

5

Critical functions of the lysosome in cancer biology

Author statement

Some passages and figures have been adapted or quoted verbatim from the following published articles:
Davidson, SM, & Vander Heiden, MG (2017). Critical Functions of the Lysosome in Cancer Biology. Annual Review of Pharmacology and Toxicology, 57(1), 481-507.

Authors

Shawn M. Davidson[1,2,3] and Matthew G. Vander Heiden[1,2,3,4]

Author affilations

1. Koch Institute for Integrative Cancer Research, Massachusetts Institute of Technology, Cambridge, Massachusetts, USA
2. Department of Biology, Massachusetts Institute of Technology, Cambridge, Massachusetts, USA.
3. Broad Institute of MIT and Harvard University, Cambridge, Massachusetts, USA.
4. Dana-Farber Cancer Institute, Boston, Massachusetts, USA.

Author contributions

Writing: S.M.D., M.G.V.H.

Abstract

Lysosomes (or "lytic bodies") were so named because they contain high levels of hydrolytic enzymes. Lysosome function and dysfunction have been found to play important roles in human disease, including cancer; however, the ways in which lysosomes contribute to tumorigenesis and cancer progression are still being uncovered. Beyond serving as a cellular recycling center, recent evidence suggests that the lysosome is involved in energy homeostasis, generating building blocks for cell growth, mitogenic signaling, priming tissues for angiogenesis and metastasis formation, and activating transcriptional programs. This review examines how emerging knowledge of lysosomal processes contribute to the "Hallmarks of Cancer" and highlights vulnerabilities that might be exploited for cancer therapy.

Introduction

Lysosomes are cellular organelles that arise from the Golgi and endoplasmic reticulum (ER) network that have a well-established role in recycling cellular material. The vacuolar ATPase (V-ATPase) pumps protons into the lysosome to create an acidic (pH 4.5-5.0) compartment enclosed by a phospholipid membrane. The lysosome contains many pH-sensitive enzymes including lipases, peptidases, nucleases, glycosidases, phosphatases, and sulfatases that hydrolyze macromolecules (Holtzman, 2013). Cargo from both outside and inside the cell are trafficked to the lysosome for degradation by these enzymes. While lysosomal enzymes function optimally in the low pH conditions present within this organelle, some of the enzymes retain activity when released from lysosomes. This extralysosomal enzyme activity, particularly the cathepsin class of protein hydrolases, can affect many aspects of cell biology (Saftig et al., 2010). In addition, emerging evidence suggests that the lysosome can stimulate transcriptional programs and impact cells in ways

that do not involve the release of lysosomal enzymes (Settembre et al., 2011, 2013, 2012).

Mutations in genes encoding lysosomal components can cause decreased production or mislocalization of resident enzymes and accumulation of cellular waste, underscoring the importance of regulating the activity of this organelle (for review see (Scriver, 2001)). In cancer, cell transformation increases the requirement for new biomass production and lysosome function can contribute precursors for macromolecular synthesis. The lysosome is also important for adaptation to nutrient stress, another challenge encountered by cancer cells to survive in inappropriate tissue environments, and autophagy plays a critical role in allowing progression of some tumors (Levine and Kroemer, 2008; Kimmelman, 2011). Elevated lysosomal enzyme activity is observed in many tumors compared to adjacent normal tissue (Kirkegaard and Jäättelä, 2009), and lysosomal changes in cancer have been noted for decades. In fact, many "Hallmarks of Cancer" cause, or are the consequence of, lysosomal function or dysfunction (Hanahan and Weinberg, 2011) (Figure 5.1). Understanding the lysosome changes that occur in cancer will be critical to developing therapies that target this organelle.

Lysosome involvement in the hallmarks of cancer

The role of the lysosome in sustaining proliferative signaling

Mammalian cell proliferation relies on exogenous signals to regulate tissue size (Raff, 1996). These signals are provided by growth factors that impinge on mitogenic signaling pathways to direct a proliferative program in cells. In addition to driving cell cycle progression, mitogenic signaling controls other processes needed for cell growth and division including anabolic metabolism to accumulate biomass (Cairns et al., 2011; Boroughs and DeBerardinis, 2015). Cancer cells gain the ability to proliferate in the absence of normal cell signaling that otherwise limits the number of cells

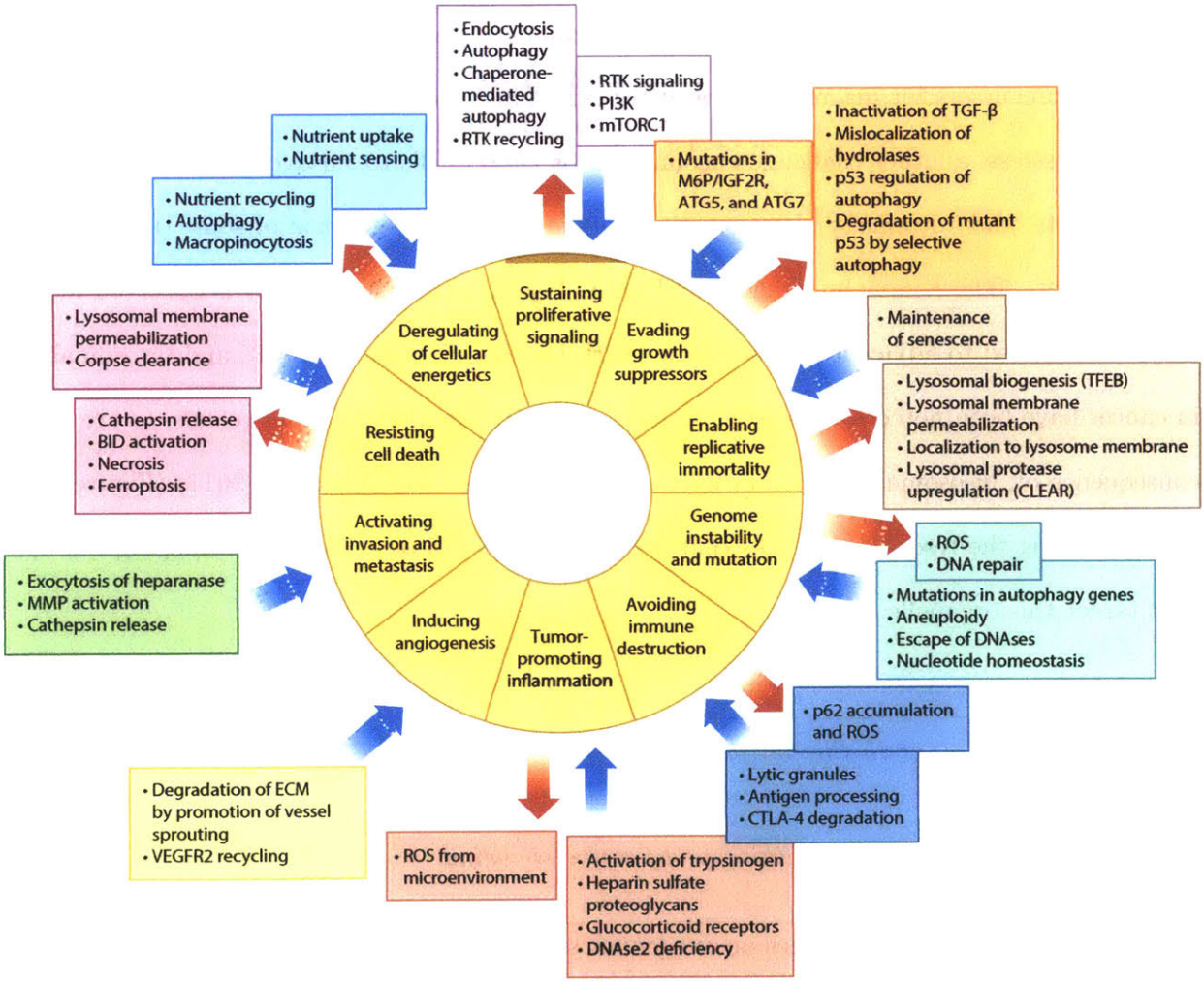

Figure 5.1. Relationship of the lysosome to the classic "Hallmarks of Cancer." Lysosome changes are a consequence of many classic cancer hallmarks (outward pointing arrows), and lysosomal changes can also drive cancer hallmarks (inward pointing arrows).

Figure 5.1

within a tissue. The lysosome affects growth factor signaling by mediating turnover of cell surface receptors and associated signaling proteins. This occurs primarily through endocytic degradation of growth factors, their receptors, or signal transduction mediators to modulate signaling output (Goh and Sorkin, 2013).

Receptor tyrosine kinases (RTKs) are a large class of plasma membrane proteins and proper localization is necessary to gain access to extracellular ligands (Gschwind et al., 2004). Cell surface expression of RTKs is governed in large part by vesicular trafficking that involves either clathrin-mediated endocytosis (CME) or clathrin-independent endocytosis (CIE), and the lysosome helps limit the number of receptors available for signaling (Goh and Sorkin, 2013; Mellman and Yarden, 2013). While the exact mechanisms controlling cell surface localization and recycling kinetics are distinct for each RTK and context-dependent across different cancer types, lysosomal degradation of RTKs plays a role in controlling proliferative processes (Sorkin and Fortian, 2014). RTKs and their ligands can reciprocally stimulate endocytic pathways to increase lysosomal degradation of the receptors, suggesting that lysosomal degradation is part of a feedback mechanism to limit RTK signaling.

The use of endocytic trafficking to control RTK signaling has been best demonstrated for the epidermal growth factor receptor (EGFR). EGFR is a member of the ErbB family of receptors, many of which are mutated or overexpressed in cancer. While several factors govern cell surface EGFR levels, multiple endocytic mechanisms leading to lysosome-mediated degradation are important (Goh and Sorkin, 2013). One mechanism requires ubiquitination via the Cbl E3 ubiquitin ligase, with Cbl being recruited to EGFR by binding to the adaptor protein Grb2 (Yamazaki et al., 2002). Ubiquitinated EGFR is then trafficked to the lysosome for degradation. Because ligand binding recruits Grb2, this is one way in which ligand binding can promote receptor degradation by the lysosome (Yamazaki et al., 2002). Blocking endocytosis to increase activated receptor signaling

has also been reported following ligand binding. In this case, ligand binding recruits two proteins that interact with Cbl, Sts-1 (p70) and Sts-2 (Clip4) (Kowanetz et al., 2004). Sts-1 and Sts-2 interact with ubiquitinated EGFR and interfere with the endosomal sorting machinery to block EGFR degradation in the lysosome. The same process can also control levels of the platelet-derived growth factor receptor (PDGFR), another RTK (Kowanetz et al., 2004).

Lysosomal trafficking downstream of CIE also can promote receptor turnover and decrease signaling from PDGFR and fibroblast growth factor receptor (FGFR) (Elfenbein et al., 2012; Schmees et al., 2012). Decreased CIE increases PDGFR signaling and promotes anchorage-independent growth and proliferation (Schmees et al., 2012). CIE also controls FGFR levels through Syndecan-4 driven receptor internalization as a predominant process to control human vein umbilical cord (HUVEC) cell proliferation (Elfenbein et al., 2012). In both cases, lysosomal trafficking limits pro-proliferative signals emanating from the RTKs.

Autophagy pathways also regulate intracellular RTK signaling mediators. Autophagy is a process conserved across eukaryotes to deliver intracellular material to the lysosome, and allows cells to adapt to starvation and recycle damaged material (reviewed extensively in (White, 2015; Goldsmith et al., 2014; Bergeron et al., 2016; Goldenring, 2013; Mah and Ryan, 2012)). The sequestration of intracellular materials in double-membrane autophagosomes is a characteristic feature of macroautophagy and allows delivery of bulk material to the lysosome for degradation. This is a way for cells to use intracellular material as a source of nutrients under starvation conditions. In contrast, microautophagy and chaperone-mediated autophagy involve directed uptake of particular cell cargo such as damaged organelles or specific proteins/protein complexes via invagination of the lysosome membrane (Mah and Ryan, 2012), (Cuervo and Wong, 2014), with the lysosome ultimately degrading the cargo. Genes encoding the machinery for macroautophagy such as Ulk1, Beclin1, Atg5, and Atg7 are important in a broad spectrum of malignancies (Liang et al.,

1999; Feng et al., 2014; Mathew et al., 2007). Autophagy is active in many types of cancer (31, 32) and is required for cancer progression by both promoting survival during nutrient stress and allowing recycling of cell components to support a transformed phenotype (White, 2015).

Suppressing autophagy is an additional mechanism by which mutant EGFR exploits endocytosis to increase RTK signaling. This occurs through the phosphorylation and inactivation of Beclin-1 to reduce VPS34 kinase activity. VPS34 kinase is a positive inducer of autophagy and promotes endosome trafficking to lysosomes (Wei et al., 2013). While EGFR turnover was not directly interrogated in relation to autophagy, it has been posited that this mechanism of autophagy suppression blocks EGFR degradation to maintain surface expression and growth signaling (Wei et al., 2013; Matsunaga et al., 2009).

Multiple other growth signaling mediators regulate autophagy and lysosome function including phosphoinositide-3-kinase (PI3K), Protein Kinase B (PKB)/Akt, and the mammalian target of rapamycin complex 1 (mTORC1), proteins that are at the intersection of many oncogenic processes (Manning and Cantley, 2007; Shanware et al., 2013). PI3K activity can increase endomembrane trafficking through RAB proteins (Wheeler et al., 2015) and chemical inhibition of PI3K impairs late endosome fusion with the lysosome to produce hybrid endosome-lysosome organelles that fail to mature into true lysosomes (Mousavi et al., 2003; Luzio et al., 2003; Liu et al., 2016). Inhibition of PI3K/Akt signaling also increases NOTCH1 signaling in T-cell acute lymphoblastic leukemia (T-ALL) to directly activate mTORC1 at the lysosome (Dibble and Cantley, 2015; Hales et al., 2014). mTORC1 is a master regulator of cell growth that is linked to lysosome function and integrates amino acid availability with proliferative signals downstream of RTKs and PI3K. To form an active signaling complex, mTORC1 must localize to the lysosome membrane surface in an amino acid-dependent manner where it encounters Rheb, an effector that mediates mTORC1 activation by growth signals (Laplante and Sabatini, 2012).

One major challenge to exploiting lysosome-mediated regulation of proliferative signaling for therapy is an incomplete understanding of how ligand binding affects signaling molecule turnover. Theoretically, promoting lysosomal degradation of signaling proteins presents an opportunity to reduce oncogenic signaling. In the case of EGFR, the EGF-EGFR complex is degraded at near-saturable levels that are proportional to EGFR expression and limited by lysosomal capacity and trafficking rates (Goh and Sorkin, 2013) but whether this is true for all growth receptors and their ligands is unknown. Recent advances in cell imaging provide an opportunity for kinetic analysis to understand the rate limiting steps in endolysosomal trafficking from CME and CIE (Wang et al., 2014; Valley et al., 2014). Additionally, understanding how endocytosis is altered in cancer (Wang et al., 2015a) and whether agents such as amiloride, chloroquine (CQ), or hydroxychloroquine (HCQ) that change endolysosomal pH will affect proliferative signaling remains to be determined.

Deregulation of cellular energetics

Sustained proliferation comes at a bioenergetic cost and imposes a large requirement for nutrients to support macromolecular synthesis. Cancer cells adapt metabolism to fulfill the increased demands that accompany biomass accumulation (Cairns et al., 2011). Aerobic glycolysis (also known as the "Warburg Effect") is commonly observed across different types of cancer and other proliferative tissues and may reflect an anabolic program (Vander Heiden et al., 2009). In addition to glucose, cancer cells in culture also rely on glutamine consumption to fuel the TCA cycle and support cell growth (Son et al., 2013; DeBerardinis et al., 2008). However, relatively little glucose- and glutamine-derived carbon is directly incorporated into biomass (Hosios et al., 2016). Instead, other nutrients such as amino acids and lipids are consumed in lesser quantities but contribute more to cancer cell mass (Hosios et al., 2016). This argues that the relationship between individual

nutrient consumption and mass accumulation is not necessarily direct and that acquiring nutrients such as non-glutamine amino acids and lipids can also play a role in tumor growth.

One way that cancer cells can acquire lipids and amino acids is by scavenging macromolecules. Recycling of intracellular materials or uptake and catabolism of extracellular protein can act as sources of these nutrients (Commisso et al., 2013). The lysosome is the final destination for extracellular material obtained through phagocytosis, endocytosis, and macropinocytosis; and the lysosome also enables the breakdown of intracellular material captured by autophagy. Thus, another core function of the lysosome in cancer is to recycle endogenous or exogenous macromolecules to provide energy, and to provide metabolic precursors for the synthesis of new cell mass. Pinocytosis pathways and autophagy are both elevated in many cancers and can be stimulated by growth factor signaling (Haigler et al., 1979; Lewis, 1937; Mosesson et al., 2008).

Macropinocytosis is an F-actin-dependent, CIE mechanism that allows bulk uptake of extracellular material. It was first observed that membrane ruffling and pinocytosis could be stimulated in lung carcinoma cell lines by the addition of EGF to cells (Haigler et al., 1979). Later studies examining fibroblasts demonstrated that expression of oncogenic H-rasG12V was sufficient to stimulate membrane ruffling and pinocytosis (Bar-Sagi and Feramisco, 1986). While the phenomenon had been observed in many cancer types for decades, the functional importance of macropinocytosis remained unclear until recent studies demonstrated that this process allows for protein and lipid scavenging (Commisso et al., 2013). Macropinocytosis appears to be a feature of many RAS-transformed cells, and protein derived from macropinocytosis can contribute to intracellular amino acid pools in cultured cells. These free amino acids can be re-incorporated into protein or further catabolized to provide energy or metabolite precursors for biosynthetic pathways (Commisso et al., 2013). Recent data suggests that this process is active in some human tumors (Kamphorst et al., 2013). Macropinocytosis is also to used to scavenge lipids in Kras-driven cancer

cells or cells grown in hypoxia, but the pathways used to scavenge lipids are incompletely defined (Young et al., 2013; Kamphorst et al., 2013). Unsaturated fatty acids can also become limiting under hypoxic conditions (Young et al., 2013), and the extent to which protein, lipids, and other macromolecules derived from the extracellular environment contribute to metabolism in different environmental conditions is an area of active investigation.

Interestingly, activation of mTORC1 suppresses autophagy and macropinocytosis. This regulation fits with a pivotal role for mTORC1 in amino acid sensing, and the ability of the lysosome to provide amino acids from the breakdown of either intra- or extra-cellular material. Mammalian cells are composed largely of protein (Hosios et al., 2016), and catabolism of endogenous or exogenous cell material can be a source of amino acids. It has been reported that mTORC1 inhibition is required for macropinosome trafficking to the lysosome to provide amino acids and support growth of some tumors (Palm et al., 2015), although mTORC1 activity loss is inconsistent with growth and proliferation in other systems (Guertin et al., 2006).

Autophagy also delivers intracellular material to the lysosome for catabolism and is necessary to provide bioenergetics substrates when nutrients are limiting (Goldsmith et al., 2014; Mathew et al., 2007; Lum et al., 2005). Many genes involved in autophagy are essential. Mice lacking Atg5 or Atg7 die from perinatal amino acid starvation, further underscoring the importance of autophagy-lysosome pathways to provide nutrients during metabolic stress (Kuma et al., 2004). While cells must adapt more rapidly to survive acute nutrient stress (Hecht et al., 2016), autophagy-mediated catabolism of intracellular stores can enable cell survival for weeks (Lum et al., 2005). Autophagy contribution to cellular nutrition can be significant, but distinguishing between autophagy and other endocytic pathways that utilize similar components remains experimentally challenging. In addition to recycling macromolecules, lysosomes are capable of fusing and catabolizing entire organelles. This process is best described for mitochondria via a distinct process

termed mitophagy (Chourasia et al., 2015; Youle and Narendra, 2011). Turnover, maintenance, and renewal of mitochondrial may also be relevant under metabolic stress conditions, as the number of functional mitochondria must match substrate availability to work efficiently. In addition, failure to clear damaged mitochondria can impair tumor progression leading to an oncocytoma phenotype that is associated with the accumulation of damaged mitochondria and less malignant tumors (Guo et al., 2013). In yeast, vacuolar pH decreases with age and affects amino acid storage and mitochondrial function (Hughes and Gottschling, 2012). How changes in lysosome physiology in cancer impact mitochondria function, number, and turnover remain to be determined however lysosomal acidification has been demonstrated to be particularly important in Kras-Lkb1 mutant lung tumors. These tumors become addicted to endolysosomal trafficking and inhibition of lysosomal activity in this context causes mitochondrial defects and subsequent cell death (Kim et al., 2013).

The extent to which other forms of "organellophagy" occur in cancer remains to be determined. Two recent studies demonstrated receptor-mediated degradation of the endoplasmic reticulum (ER) and portions of the nucleus in yeast (Mochida et al., 2015), and mammals (Khaminets et al., 2015), but the relevance of ER/nucleophagy in cancer has not been examined. While these organellophagy pathways are still being elucidated in the mammalian setting, recent work from Levine and colleagues demonstrates a novel role for tumor suppressor Fanconi anemia (FA) complementation group C (FANCC) in mitophagy. FANCC typically is known for its role in genomic DNA damage repair, but FANCC and two other FA genes, FANCF and FANCL were identified in a genetic screen as autophagy factors. FA genes are required for selective autophagy to remove cytoplasmic contents. The pleiotropic effects observed through the FA proteins' interaction with Parkin, including clearance of mitochondria, decreased ROS, and activation of the inflammasome likely impact many cancer cell-types, and indeed many cancers have hypomorphic

alleles of FA proteins (Sumpter et al., 2016).

The lysosome plays a pivotal role in how nutrients are sensed in cells. Cellular sensing of at least some amino acids are thought to occur within the lysosomal lumen, although some amino acids are sensed by cytoplasmic proteins (Wang et al., 2015b). It has been demonstrated that localization of the mTORC1 complex to lysosomal membranes is induced by amino acid-mediated recruitment of Rag-GTPases. mTORC1 is subsequently activated by the resident Rheb protein and Rag GTPases. The specific amino acid sensors governing this localization and activation have been recently proposed. Glutamine, leucine, and a are putatively sensed by SLC38A9.1 and affect mTORC1 activation through mechanisms involving lysosomal V-ATPase activity and the Ragulator complex (Wang et al., 2015b; Rebsamen et al., 2015). A mechanism for how leucine and arginine facilitates mTORC1 localization to the lysosome is better understood (Wolfson et al., 2016). The GATOR complex containing GATOR1 and -2 interacts with Rags to promote mTORC1 translocation to the lysosomal surface where it can be activated. Leucine binding to the amino acid sensor Sestrin2 causes dissociation of Sestrin2 from GATOR2, allowing activation of the mTORC1. In addition to potentially being sensed by SLC38A9.1, arginine is sensed in the cytosol, and through an analogous mechanism to Sestrin2 causes dissociation of the CASTOR and GATOR2 complex which subsequently allows for the activation of mTORC1 (Chantranupong et al., 2016). Finally, it has been posited that lysosomal signaling stimulates transcriptional programs that regulate lipid catabolism under starvation conditions, but whether the lysosome directly senses lipid levels is not known (Settembre and Ballabio, 2014).

Nutrient sensing also occurs at the organismal level (Efeyan et al., 2015) and is often dysregulated in cancer. Many patients with diverse malignancies experience cachexia, a poorly understood state where up to 80% of muscle and fat stores are depleted. While the mechanisms driving cachexia are incompletely understood, mobilization of protein and other nutrient stores can

begin years before the some cancers become clinically apparent (Mayers et al., 2014). Whether autophagy and lysosome function in specific tissues impact whole-body nutrient sensing is an area of active investigation.

Understanding the source and contents of the cargo trafficked to the lysosome in cancer cells could help determine differential amino acid requirements between tumor and normal tissue that might be exploited therapeutically with drugs or dietary manipulation (Covini et al., 2012). Exposure of pancreatic cancer cells, or pancreatic tumors in mice, to the Na+/H+ exchange inhibitor 5-(N-Ethyl-N-isopropyl)amiloride (EIPA) blocks macropinocytosis and limits proliferation, potentially by starving cells of amino acid (Koivusalo et al., 2010; Vander Heiden, 2013). Use of EIPA for this purpose in patients is limited by poor pharmacokinetics, and better inhibitors are needed to determine whether blocking macropinocytosis will be effective in patients. The lysosomotropic anti-malarial drugs CQ and HCQ prevent lysosomal acidification and can slow PDAC progression in mice, but to date have shown mixed results in early stage trials. The use of CQ, HCQ, and other CQ derivatives, such as Lys05 is still being investigated in patients as single-agent and in combination with existing chemotherapeutic strategies (Piao and Amaravadi, 2015). Exactly how these drugs perturb lysosome function and how to best use them to deprive tumors of nutrients is an open question. Both the lack of available compounds and an incomplete understanding of nutrient sensing mechanisms have limited efforts to target lysosomes and prevent the acquisition of essential nutrients.

Enabling replicative immortality

Pre-malignant cells must evade oncogene-induced senescence (OIS) to replicate indefinitely (McDuff and Turner, 2011). A role for senescence in tumor suppression has been demonstrated in many tissues, but cell senescence is an incompletely understood program involving the expression of cell

cycle checkpoint genes and activation of senescence-associated secretory phenotype (SASP) to prevent continued proliferation of neighboring cells (Braig et al., 2005; Chen et al., 2005; Collado et al., 2005; Courtois-Cox et al., 2006; Dankort et al., 2007; Michaloglou et al., 2005; Sarkisian et al., 2007). Interestingly, senescent cells display a host of lysosome-specific phenotypes including increased expression of lysosomal genes and increased lysosome number and size (Lee et al., 2006; Kurz et al., 2008).

It was initially thought that senescence cells were less metabolically active than proliferating cells; however, senescent cells are in fact hypermetabolic, perhaps explaining why they have increased demand for lysosome-derived nutrients (Pérez-Mancera et al., 2014; Ros and Schulze, 2012; Aird and Zhang, 2015). Senescent cells have increased oxidative metabolism, and pushing cells toward oxidative metabolism can drive OIS. Senescent cells also frequently have altered chromatin structure that manifests as senescence-associated heterochromatin foci (SAHF) which can extrude out of the nucleus and into the cytoplasm. It has also been suggested that senescent cells process cytoplasmic chromatin fragments (CCFs) through an autophagy-dependent lysosomal process and that this processing is essential for maintenance of senescence-mediated tumor suppression (Ivanov et al., 2013).

Replicative immortality induced by proto-oncogene activation or tumor-suppressor gene loss can elicit additional lysosome changes. Oncogene expression results in increased lysosome biogenesis and increased lysosomal hydrolase expression. Specifically, SV40 transformation, MYC expression, and mutant KRAS expression increase expression of cathepsins and glycosidases including Cathepsin D and Cathepsin E (Allison, 1974). In contrast, inactivation of p53 in murine fibroblasts results in lysosomal features that are not observed following oncogenic transformation, such as the lack of cathepsin activation (Kroemer and Jäättelä, 2005). These findings suggest that different cancer-associated mutations may result in distinct lysosomal phenotypes.

Increased lysosome biogenesis is a general response to cell stress, such as that experienced during cellular transformation. Lysosome biogenesis can be stimulated by mTORC1 activation and mTORC1 activation in turn promotes cytoplasmic to nuclear translocation of transcription factor "EB" (TFEB) (for complete review see (Settembre et al., 2011)). TFEB upregulation is correlated with autophagy, and is associated with several cancers including renal cell carcinoma, non-small cell lung cancer, and pancreatic ductal adenocarcinoma (Roczniak-Ferguson et al., 2012; Perera and Bardeesy, 2015; Giatromanolaki et al., 2014). TFEB binds to a palindromic 10-base pair motif, GTCACGTGAC, termed the Coordinated Lysosome Expression and Regulation element (CLEAR), a highly enriched promoter sequence found in 68 of 96 known lysosomal genes (Giatromanolaki et al., 2014). This signaling mechanism may support increased autophagy to help malignant cells cope with nutrient stress. Apart from an increased number of lysosomes observed in cancer, these organelles are also frequently delocalized from the perinuclear space to the periphery of the cell. The peripheral localization of lysosome can play a role in maintaining cell membrane integrity and repair during rapid cell division (Andrews et al., 2014).

The idea of "pro-senescence" cancer therapy is appealing (Nardella et al., 2011); however, the mechanisms by which transformed cells overcome senescence are only partially characterized. Inducing senescence for therapy is controversial, in part because senescent cells secrete exosomes containing factors that can cause inflammation and promote a local environment that is conducive to malignancy (Krtolica et al., 2001; Parrinello et al., 2005). Targeting the autophagy-lysosomal pathway to inhibit chromatin remodeling was effective in a Braf-driven model of melanoma, driving the formation of senescent nevi that failed to progress to cancer (Michaloglou et al., 2005). While senescence is classically defined to be an irreversible cell state, some cells may escape senescence to form malignancies (McDuff and Turner, 2011; Kuilman et al., 2010). Nevertheless, it has been suggested that lysosome membrane integrity changes associated with senescence sensitizes cells to a

host of pro-death stimuli, including tumor necrosis factor alpha (TNFα) and oxidative damage, and targeting cells in the senescent state with altered lysosomes could present a therapeutic window.

Evading growth suppressors

Tumor suppressor gene inactivation is a common genetic event in cancer. One tumor suppressor gene responsible for maintaining proper lysosome function is the mannose-6-phosphate/insulin growth factor 2 receptor (M6P/IGF2R), a cell surface protein that binds multiple ligands associated with carcinogenesis, including IGF2 and retinoic acid (De Souza et al., 1995b,a; Mills et al., 1998). M6P/IGFR2 is responsible for the proper trafficking of lysosomal hydrolase enzymes. Glycosylation of asparagine residues on the hydrolases is needed for hydrolase delivery to lysosomes where signaling factors are processed that can play a role in tumor suppression (Kornfeld and Kornfeld, 1992). M6P/IGF2R was identified as a possible tumor suppressor gene upon observing decreased expression in hepatocellular carcinoma (HCC) (Mills et al., 1998). Further examination of M6P revealed loss-of-function mutations, and loss of heterozygosity was noted for the mutated alleles in HCC (De Souza et al., 1995b). Some mutations in M6P have also been demonstrated to confer dominant-negative sequestration of wild-type M6P protein (Kreiling et al., 2012), and M6P is mutated in other malignancies including colon, breast, prostate, kidney, and lung cancers (Hoyo et al., 2012; Cheng et al., 2009; Tian et al., 2014).

Mislocalization of hydrolases caused by M6P/IGFR2R mutation results in an inability to activate members of the transforming growth factor-β(TGF-β) family (Kreiling et al., 2012). TGF-$\beta$is a class of conserved cytokines that suppress cell proliferation. Members of the TGF-βfamily are synthesized in a pre-pro form that requires proteolytic activation in the lysosome to activate tumor suppressive TGF-βreceptor signaling. Thus, in the absence of proteolytic cleavage of TGF-$\beta$by lysosomal proteases, this check on tumorigenesis is relieved.

Other tumor suppressors, such as p53, PTEN, TSC1 and TSC2, regulate lysosome activity by governing autophagic flux (Levine and Kroemer, 2008). A dual role of p53 in regulating autophagy has been described for several cancers (Tasdemir et al., 2008; Rosenfeldt et al., 2013). On one hand, activation of p53 through either genotoxic stress or cytotoxic drugs lead to a p53-dependent activation of autophagy (118). Conversely, in a mouse model of pancreatic cancer driven by activation of oncogenic KrasG12D, deletion of either ATG5 or ATG7, two essential autophagy genes, prevents the development of invasive cancers (Yang et al., 2014). However, if p53 loss is combined with Kras activation, deletion of ATG7 accelerates progression to frank adenocarcinoma. These data suggest that p53 plays two roles in governing autophagy during pancreatic tumorigenesis (Rosenfeldt et al., 2013). In addition to the regulation of autophagy by p53 and other tumor suppressor genes, autophagy genes have been implicated as tumor suppressor genes. This line of investigation began with the initial observation that that Beclin1 heterozygous mice developed tumors more frequently (Liang et al., 1999), and the involvement of autophagy genes as tumor suppressors is a topic that has been reviewed in depth elsewhere (Liang and Jung, 2010). Inhibiting autophagy may be of value to treat cancer, but the context-dependent tumor suppressive nature of autophagy with respect to p53 mutational status complicates the use of autophagy inhibitors in this disease.

Genome instability and mutation

As introduced above, there is a role for autophagy and lysosome activity in the maintenance of genome stability. Kidney cells isolated from Beclin+/- ATG5-/- mice show accumulation of p62/SQSTM1 (p62), an autophagy adaptor responsible for guiding damaged or misfolded proteins to the lysosome for degradation (Mathew et al., 2007). Serial passage of these cells leads to altered cell ploidy, and it has been postulated that autophagy inhibition in the setting of aneuploidy causes

genomic instability for three reasons. First, damage to proteins required for mitosis and centrosome function accumulates in the cells. Second, a high level of DNA-damaging reactive oxygen species (ROS) can prevent clearance of defective mitochondria through mitophagy. Third, the loss of autophagy can impair DNA damage signaling. The connection between the loss of autophagy and genomic instability was further supported by studies examining ATG7 null cells. Following ATG7 deletion, cells are unable to degrade the checkpoint kinase Chk1 in the lysosome (Liu et al., 2015). A lower level of Chk1 decreases reliance on high-fidelity homologous recombination for DNA repair, and increased use of error-prone non-homologous end joining (NHEJ). In fact, deletion of NHEJ components is synthetic lethal with autophagy inhibition (Liu et al., 2015). Promoting genome instability through autophagy inhibition may render cells more sensitive to inhibitors of NHEJ DNA repair, a situation analogous to the synthetic lethality and dependency on NHEJ observed with aberrant Chk1 degradation (Mathew et al., 2007).

Interestingly, autophagy defective iBMK cells are significantly more sensitive to the depletion of pyrimidines by N-phosphonacetyl-l-aspartate (PALA), an inhibitor of pyrimidine biosynthesis (Mathew et al., 2007). While speculative, it is possible that the inability to maintain sufficient autophagic flux to recycle nucleic acids can lead to nucleotide depletion in cells. Impaired de novo nucleotide synthesis can lead to DNA damage in replicating cells (Lunt et al., 2015; Cunningham et al., 2014). The finding that autophagy is upregulated in nucleotide depleted cells further suggests that this may be an adaptive strategy to salvage nucleotides.

Regardless of whether lysosomal nucleases enable salvage and recycling of endogenous and exogenous nucleic acids, the mislocalization of DNAses to the cytoplasm places an enzyme activity that cleaves double-stranded DNA in a location where it can promote DNA damage. When lysosomal integrity is compromised, leakage of DNAses from the lysosome can contribute to carcinogenesis (Kroemer and Jäättelä, 2005). While most lysosomal enzymes function optimally at

low pH, the pH of tumors is frequently lower than that of many normal tissues, making the cytosol of cancer cells a more permissive environment for lysosomal enzymes to be active (Webb et al., 2011).

Cancer cells are frequently aneuploid. Untransformed aneuploid cells exhibit decreased autophagy that correlates with the degree of karyotypic imbalance. Interestingly, imbalanced protein stoichiometry caused by the aneuploid state increases the requirement to degrade excess proteins and exceeds lysosome capacity (Santaguida and Amon, 2015b,a; Santaguida et al., 2015). As a result, autophagic cargo is either trapped in lysosomes or late endosomes without undergoing degradation. Aneuploid cells can sense the defects in lysosomal degradation causing activation of the TFEB-mediated transcriptional program to stimulate lysosome biogenesis and increase autophagic gene expression.

Resisting cell death

Lysosomal enzymes can stimulate programmed cell death (PCD) via several mechanisms. Activation of autophagy can eventually lead to cell death; however, release of lysosomal proteases can directly activate caspases to kill cells (Aits and Jäättelä, 2013). For example, cathepsin D can cleave and activate the BH3-domain containing protein Bid that in turn activates the intrinsic apoptosis pathway (Repnik et al., 2013). The autophagic machinery is also required for another type of PCD termed "autosis" that is reported to be mediated by the Na+, K+-ATPase pump (Liu and Levine, 2015). Robust lysosomal cathepsin activity that degrades cell material faster than apoptosis can be initiated might result in cell death via necrosis. The inability to clear dead cell debris because of defective lysosomes in surviving cancer cells may lead to the survival of neighboring cells (Huang et al., 2013). There is crosstalk between the autophagy and apoptosis pathways in cancer. For instance, it has been demonstrated that overexpression of the

anti-apoptotic gene Bcl-2 can inhibit Beclin 1-mediated autophagy and help promote cell survival by limiting autophagy and preventing autosis (Pattingre et al., 2005).

Additionally, lysosomes have been reported to stimulate their own programmed cell death pathway, and immortalization renders cells more susceptible to lysosome-mediated cell death through destabilization of the lysosomal membrane (Kroemer and Jäättelä, 2005). This less stable membrane is thought to be caused by increased organelle biogenesis that exceeds the rate of sphingolipid synthesis along with accumulation of ROS frequently seen in transformed cells. The resulting permeabilized lysosomal membranes are prone to leakage of cathepsins which activate caspases to kill cells (Fehrenbacher and Jäättelä, 2005). Finally, the engulfment of dead cells and debris is an essential feature of programmed cell death first described in C. elegans, and lysosome function is required for the clearance of this material (Wu and Horvitz, 1998; Hengartner, 2001). The extent to which inhibition of cell engulfment promotes tumorigenesis is unknown, but the failure to do so can contribute to an inflammatory microenvironment (Hochreiter-Hufford and Ravichandran, 2013).

Lysosome function is also involved in a form of cell death termed ferroptosis (Dixon et al., 2012). While the mechanism of iron transport into the lysosome is unknown, iron can accumulate in lysosomes and create favorable conditions for ROS formation through Fenton reactions (Kurz et al., 2008). Therapies such as desferoxamine and other iron or copper chelating agent used to treat iron-overload in patients may be beneficial for cancer through the reduction of reactive oxygen species (ROS) (Wiggins et al., 2015; Yamasaki et al., 2011).

Activating invasion and metastasis

Tumor cell invasion and metastasis *in vivo* require extracellular matrix degradation (Westermarck and Kähäri, 1999). Thus, direct cathepsin action or indirect cathepsin-mediated activation of

extracellular matrix-degrading matrix metalloproteases (MMPs) may play a role in metastasis of some tumors. Gene expression profiling in tumors arising from a Rip2-Tag mouse model of pancreatic islet cancer showed increased expression of cysteine cathepsins, and broad-spectrum pharmacological inhibition of cysteine cathepsins in pancreatic cancer yields less invasive tumors (McCarthy et al., 2004). Lysosome function is also involved in membrane remodeling to allow cell shape changes that enable invasion through the basement membrane. Exocytosis of lysosome-derived heparanase, cathepsins, and Neu1 affect cell shape as well as favor degradation of extracellular matrix to prime local invasion (Machado et al., 2015).

Different cathepsins may have a role in metastatic tropism. In a mouse model of pancreatic cancer, loss of Cathepsin B was found to decrease metastasis to the liver and increase overall survival. However, these tumors appeared to have compensatory Cathepsin L activity, which instead promoted lung metastasis. Other studies examining Cathepsin L suggest that this enzyme may also play a role in bone metastasis (Arvatz et al., 2011). Targeting cathepsins has challenges, owing to the fact that various cathepsins often have redundant activities, and inhibition of one cathepsin type can be compensated by elevated activity of another cathepsin. Nevertheless, understanding the relationship between specific cathepsins and their ability to degrade specific extracellular matrix composition of different tissue sites may help to limit metastasis in some settings. Multiple cathepsin inhibitors exist and are in clinical trials, but their impact in cancer has yet to be determined (Mohamed and Sloane, 2006).

Inducing angiogenesis

Remodeling the extracellular matrix and basement membrane is also essential for vessel sprouting and the initiation of angiogenesis (Carmeliet, 2003; Folkman et al., 1989). The lysosome is involved in exocytosis, with the secretion of lytic granules containing lysosomal cathepsins serving to break

down basement membrane components even at physiological pH (McCarthy et al., 2004). As such, cathepsins D, B, S, K, and L have all been implicated in promoting angiogenesis. Activation of MMP by cathepsins can similarly enable angiogenesis, and there are data to support a role for cathepsins as direct mitogens to stimulate angiogenesis with the pro-form of Cathepsin D reported to stimulate MAPK signaling and angiogenic gene expression (Kallunki et al., 2013). Cathepsin K has also been determined to have a role in neovascularization under hypoxic conditions through activating NOTCH1 signaling, and knockdown of cathepsins K in endothelial cells caused decreased invasion, proliferation, and tube formation (Jiang et al., 2015). Similarly, Cathepsin B overexpression results in a reduced VEGF-dependent tube response in endothelial cells (Im et al., 2005).

The lysosome also plays a role in regulating the turnover of endothelial cell migration factors. Rab GTPases are essential for blood vessel formation and are involved in endosome-to-plasma membrane recycling of VEGFR2 (Jopling et al., 2014). Genetic deletion of Rab4a and Rab11a or inhibition of lysosomal activity with chloroquine results in defective endosome-to-plasma membrane recycling of VEGFR and inhibits the migration of endothelial cells (Jopling et al., 2014). A better understanding of lysosomal function in endothelial cells and cancer cells is required to understand how treatment with CQ, HCQ, and other lysosomotropic drugs will affect both cancer and non-cancer cells and impact the efficacy of these drugs to treat cancer.

Tumor promoting inflammation

The lysosome plays a role in inflammatory responses that can drive proliferation, DNA damage, and angiogenesis (Kobayashi et al., 2013). Release of lysosomal enzymes can promote inflammation in several settings. First, Cathepsin B can cleave tryspinogen-1 in the pancreas and cause pancreatitis (Lindkvist et al., 2006), a chronic inflammatory state correlated with increased pancreatic cancer

risk (156). Defects in essential autophagy genes ATG7 and Beclin1 also cause chronic inflammation in many settings (Choi and Ryter, 2011), and appear to promote spontaneous cancers in the lung, liver, and lymphocytes through incompletely understood mechanisms (White et al., 2010). Therapy-related lysosomal membrane permeabilization might also contribute to inflammation preceding cell death (Aits and Jäättelä, 2013).

The lysosome plays pivotal roles in modulating glucocorticoid levels and anti-inflammatory responses in diseases such as lupus erythematosus and rheumatoid arthritis (He et al., 2011). Cancer cells often exhibit high expression of the glucocorticoid receptor (Kach et al., 2015; Abduljabbar et al., 2015; Kassi and Moutsatsou, 2011), and inhibition of lysosome function with chloroquine or the vacuolar ATPase inhibitor bafilomycin A1 reduces inflammation while knockdown of TFEB increases glucocorticoid level and represses transcription of pro-inflammatory cytokines (He et al., 2011). Heparin sulfate proteoglycans (HSPGs) are one of the main components of the extracellular matrix and can modulate the activity of cytokines and growth factors, such as TGF-β(164). HSPGs can additionally promote inflammatory responses through activation of toll-like receptor 4 (TLR4) signaling and leukocyte recruitment (165). Heparanase, the only known mammalian endoglycosidase capable of degrading HSPGs (Nakajima et al., 1984), is synthesized as an inactive pro-enzyme and is proteolytically activated in the lysosome. Heparanase inhibitors, such as the heparin sulfate mimetics PG545, PI-88, M402, and SST0001 are being studied in clinical trials and have shown moderate efficacy in preventing progression and metastasis in ovarian cancer and hepatocellular carcinoma (Dredge et al., 2011; Winterhoff et al., 2015)). Inhibiting inflammation mediated by heparanase, cathepsins and their targets, or glucocorticoid receptor modulation may impact different tumor initiation programs that are stimulated by chronic inflammation.

The loss of lysosomal Dnase2a can promote inflammation through the failure to degrade exported nuclear DNA in the cytosol, leading to accumulation of DNA and activation of the Sting

cytosolic DNA-sensing pathway (Lan et al., 2014). Interestingly, Dnase2a null mice develop autoantibodies that are thought to contribute to autoimmune disease. It has also been proposed that DNA-damaging agents can induce antitumor immunity and may contribute to innate immune system activation (Lan et al., 2014). While the extent to which cytosolic DNA accumulates in the cytosol in cancer is unknown, there is evidence for micronuclei in human cancer cells and it stands to reason that autophagy changes may also result in cytosolic DNA accumulation and subsequent inflammation through this mechanism.

Avoiding immune destruction

Interactions between tumor cells and cells of the innate and adaptive immune system are influenced by lysosomal activity. The lysosome is critical for processing of tumor antigens and antigen presentation (Münz, 2013; Mah and Ryan, 2012). A role for lysosome function in the immune response to cancer has been best studied in hepatocellular carcinoma. In this setting, autophagy deficiency results in p62 accumulation, which promotes the generation of ROS through the dampening of NF-κB signaling in hepatocytes (Chen and White, 2011). Autophagy deficiency affects the anti-tumor immune response by inhibiting NF-κB and causing hepatocyte cell death and inflammation to promote tumorigenesis. p62 accumulation and formation of inclusion bodies can also sequester Kelch-Like ECH-Associated Protein 1 (Keap1) and cause non-canonical activation of the Nrf2 antioxidant transcriptional program (Lau et al., 2010). Finally p62 accumulation and subsequent ROS generation promotes an oxidative environment that inhibits local dendritic cell function and impairs anti-tumor immune responses (Saitoh and Akira, 2010).

Recent successes involving immune checkpoint blockade demonstrates the power of the immune system in cancer therapy (Intlekofer and Thompson, 2013). It has been proposed that the cytoplasmic domain of the cytotoxic glycoprotein, T lymphocyte antigen-4 (CTLA-4) cell surface

receptor functions to dictate the correct localization of this T cell inhibitory protein (Walker and Sansom, 2015). CTLA-4 expression and presentation is largely dictated by lysosomal regulation; it is degraded in the lysosome and secretory lysosomes are used to traffic CTLA-4 to the membrane. Expression of other inhibitory receptors on T cells, such as PD-1, may also be similarly regulated by lysosomal processing, although the impact of these lysosomal pathways in controlling immune responses has yet to be determined.

Secreted vesicles containing lysosome enzymes (also termed lytic granules) can impact the function of immune cells (Blott and Griffiths, 2002). Secretory lysosomes are involved in natural killer cell function (Blott and Griffiths, 2002), and secretory lysosomes can contain clotting factors and chemoattractants that affect immune responses (Blott and Griffiths, 2002). Regulation of metabolism in cells during an immune response can also change cell fate, with the mTORC1-mediated nutrient sensing playing a prominent role. Emerging data suggests that the localization of mTOR during asymmetric T cell division can have a significant impact on cell fate and influence T cell differentiation.

Challenges in targeting lysosomal processes for cancer therapy

Many strategies to deliver drugs to the lysosome have been proposed based on unique characteristics of this organelle and have been extensively reviewed (Sakhrani and Padh, 2013) (Figure 5.2). These strategies include agents that permeabilize lysosome membranes, small-molecule cathepsins inhibitors that exploit the low pH environment to activate or catalyze drug release, or molecules that become protonated to increase drug concentration within the organelle. To date, clinical data are limited on whether these approaches can be successful.

Tumors that rely on increased macropinocytosis for nutrients might be more vulnerable to lysosomal targeting agents that use macropinocytosis to deliver active molecules to the lysosome.

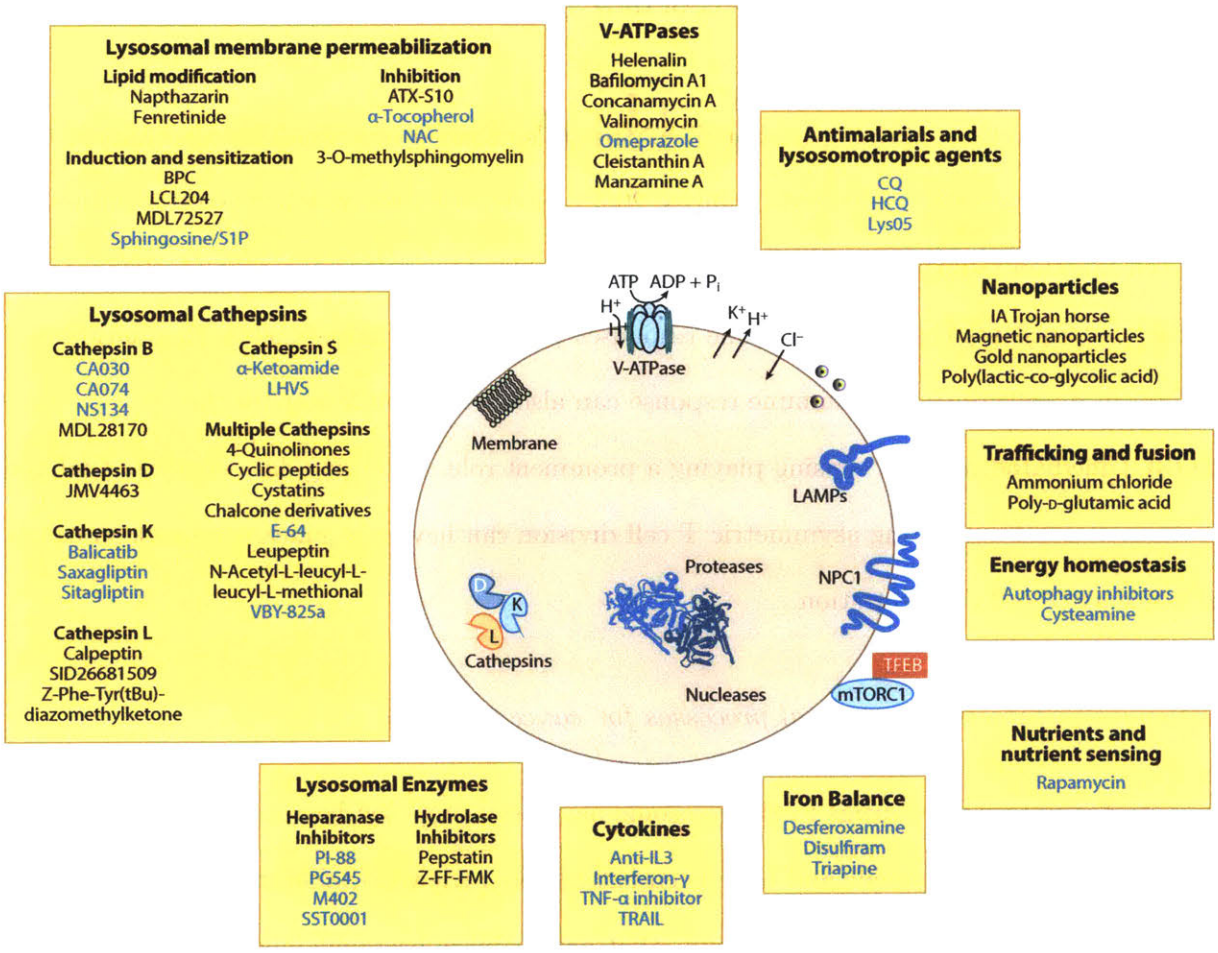

Figure 5.2. Approaches to target the lysosome. Many therapeutics with lysosomal targets are being considered for lysosomal storage diseases, rheumatoid arthritis, osteoporosis, and other conditions. See also Table 5.1.

Figure 5.2

Cells of the immune system, such as dendritic cells, undergo constitutive macropinocytosis and it remains to be determined whether this can be exploited for improved immunotherapy (Lim and Gleeson, 2011). A complete list of lysosomal proteins is lacking, and proteomic studies have recently identified several lysosomal proteins and transporters of unknown function (Chapel et al., 2013), some of which may become good targets for cancer therapy. Emerging probe-based techniques used to interrogate chemical properties of this organelle in real-time will improve the understanding of how endolysosomal trafficking is regulated during tumor progression (Wang et al., 2014).

Because the lysosome sits at the intersection of numerous endosomal trafficking pathways, understanding how targeting the lysosome will affect the action of existing drugs will be important. For example, lysosomal sequestration of sunitinib and other chemotherapeutics is a mechanism of drug resistance, and therefore, it has been proposed that chemosensitivity could be increased by using drugs that inhibit lysosomal function (Gotink et al., 2011). How to best exploit lysosomal transport to prevent chemotherapeutic sequestration and understanding changes in the largely uncharacterized specific lysosomal transporters channels in the normal and cancer setting will be important (Xu and Ren, 2015). Additionally, understanding the mechanisms by which currently approved chemotherapeutics have unexpected lysosomal consequences could lead to more effective lysosomal targeting.

Because rapid cell division requires maintenance of organelle homeostasis the emerging roles played by the lysosome in nucleophagy, pexophagy, and other forms of organellophagy are also of potential therapeutic interest (Okamoto, 2014). It is clear that the lysosome is more than just the cellular recycling center for the cell, and improved understanding of how this organelle participates in tumor initiation and progression will be an exciting area of biology that could lead to the development of new therapeutic strategies for cancer.

Disclosure Statement

M.G.V.H. is a consultant and scientific advisory board member for Agios Pharmaceuticals and Evelo Therapeutics. The authors acknowledge support from the National Science Foundation Graduate Research Fellowship Program (NSF-GRFP), Ludwig Center at MIT, the Burrough's Wellcome Fund, the Lustgarten Foundation, SU2C, and the National Cancer Institute.

Acknowledgements

We regret that we were unable to cite many excellent papers. We thank Kendall Condon, Kristin Knouse, Rachel Wolfson, Stefano Santaguida, Jared Mayers and members of the Vander Heiden Lab for critical reading of the manuscript.

Summary Points

1. The lysosome has sensing properties and can have an impact on cellular physiology.
2. The lysosome plays a role in metabolic homeostasis of cells.
3. Autophagy pathways are involved in the cell response to nutrient stress.
4. Transcriptional programs regulated in response to lysosomal activity are still being described.
5. The lysosome plays a functional role in chemotherapy resistance.
6. Targeting lysosomes may play a role in cancer therapy.

Future Issues

1. Are additional lysosome components involved in nutrient sensing?
2. How do existing chemotherapies alter lysosomal physiology?
3. Can macropinocytosis be targeted to interrupt the nutrient supply of cancers or for delivery of

other effective therapy?

4. Can we improve existing therapies using a combination of lysosomotropic agents and lysosomal membrane permeabilizing agents?

5. Will cataloging the contents of lysosomes contents provide further insight into function?

6. To what extent does "organellophagy" contribute to oncogenesis?

Drug or genetic target (abbreviation)	Molecule class or cellular product	Proposed lysosomal target	Effected cell type or disease tested	Hallmark(s) effected	Reference
Balicatib	small-molecule	Cathepsin K	Breast cancer	Activating invasion and metastasis	-184
Saxagliptin	small-molecule	Cathepsin K	Melanoma, lung cancer	Activating invasion and metastasis	(185-187)
Sitagliptin	small-molecule	Cathepsin K	Melanoma, lung cancer	Activating invasion and metastasis	(185-187)
a-ketoamide	small-molecule	Cathepsin S	A2058	Activating invasion and metastasis	-188
Leelamine	small-molecule	RTK-AKT/STAT/MAPK	Melanoma	Activating invasion and metastasis	-188
N-acetyl cysteine	metabolite	ROS	multiple cell types	Resisting cell death	-189
a-tocopherol	vitamin	ROS	prostate carcinoma	Resisting cell death	-189
Vitamin C	vitamin	ROS	multiple cell types	Resisting cell death	-189
Ciclopirox	fungicide	autophagy induction	Cervical cancer	Resisting cell death	-188
CD20 (Tositumomab)	antibody	Cathepsin B	Lymphoma	Resisting cell death	-190
HLA-DR (L243)	antibody	Cathepsin B	Lymphoma	Resisting cell death	-190
Interferon g	cytokine	Cathepsin B	Cervical carcinoma and leukemia	Resisting cell death	-190
Imatinib (Bcr-Abl)	kinase inhibitors	Cathepsin B	Leukemia	Resisting cell death	-190
Discodermolide	microtubules	Cathepsin B	NSCLC	Resisting cell death	-190
Docetaxel	microtubules	Cathepsin B	Prostate carcinoma	Resisting cell death	-190
Epithilone B	microtubules	Cathepsin B	NSCLC	Resisting cell death	-190
Paclitaxel	microtubules	Cathepsin B	NSCLC	Resisting cell death	-190
Triptolide	natural product	Cathepsin B	MCF-7, foreskin, lung fibroblasts	Resisting cell death	-188
Camptothecin	chemotherapy	Cathepsin B/D	Leukemia and lymphoma	Resisting cell death	-190
TRAIL	cytokine	Cathepsin B/D	Leukemia, HCC, SQCC	Resisting cell death	-190
Etoposide	chemotherapy	Cathepsin B/D/L	Leukemia and MEFs	Resisting cell death	-190
Sphingosine	lysosomotropic	Cathepsin B/D/L	Leukemia	Resisting cell death	-190
Cisplatin	chemotherapy	Cathepsin B/L	MEFs	Resisting cell death	-190
TNF-a inhibitor	cytokine	Cathepsin B/L	Breast, cervical carcinoma	Resisting cell death	-190
LeuLeuOMe	lysosomotropic	Cathepsin B/L	Cervical carcinoma	Resisting cell death	-190
Siramesine	lysosomotropic	Cathepsin B/L	Breast carcinoma, HaCaT, U-87MG	Resisting cell death	-190
Nanomycin & Siomycin A	antibiotics	Cathepsin D	Colon carcinoma	Resisting cell death	-190
Staurosporine (Protein kinase C)	kinase inhibitors	Cathepsin D	Activated T-lympocytes and fibroblasts	Resisting cell death	-190
Vincristine	microtubules	Cathepsin L	Cervical carcinoma	Resisting cell death	-190
Resveratrol	natural product	Cathepsin L	Cervical carcinoma	Resisting cell death	-190
Calpeptin	small-molecule	Cathepsin L	Breast carcinoma, MCF7, MDA-MB-231	Resisting cell death	-191
Leupeptin	small-molecule	Cathepsins	HT-29	Resisting cell death	-192
Adriamycin	DNA-damaging agent	DNA damage	MEF	Resisting cell death	-130
Anti-Fas	antibody	Fas and Cathepsin D	Cervical carcinoma and leukemia	Resisting cell death	-190
Anti-IL3	antibody	IL3	multiple cell types	Resisting cell death	-130
3-aminopyridine-2-carboxaldehyde thiosemicarbazone (Triapine)	small-molecule	iron homeostasis	multiple cell types	Resisting cell death	-188
Deferasirox	small-molecule	iron homeostasis	multiple cell types	Resisting cell death	-188
Desferoxamine (DFO)	small-molecule	iron homeostasis	multiple cell types	Resisting cell death	-188
Paclitaxel	microtubules	lysosome membrane	multiple cell types	Resisting cell death	-189
Vinblastine	microtubules	lysosome membrane	multiple cell types	Resisting cell death	-189
Vinorelbine	microtubules	lysosome membrane	multiple cell types	Resisting cell death	-189
NPe6	photodamaging agent	lysosome membrane	Breast carcinoma, MG-63	Resisting cell death	-189
Fenretinide	vitamin	lysosome membrane	multiple cell types	Resisting cell death	-189
EGCG	natural product	lysosome membrane	HepG2, MEF	Resisting cell death	-188
Cipro & norfloxacin	antibiotics	unknown	Cervical carcinoma	Resisting cell death	-190
3,6-bis(1-methyl-4-vinylpyridinium) carbazole diiodide (BMVC)	small-molecule	unknown	MCF-7, foreskin, lung fibroblasts	Resisting cell death	-188
Omeprazole	V-ATPase inhibitors	V-ATPase inhibitors, Cathepsin B/L	Leukemia and lymphoma	Resisting cell death	-190
Geldanamycin	natural product	Hsp90	HTB-26, MDA-MB-231, HEK293T, HL-60, fibroblasts	Sustaining proliferative signaling	-188
Vildagliptin	small-molecule	Cathepsin K	mc38, Colorectal cancer lung metastases	Activating invasion and metastasis, Resisting cell death	-193
Epoxysuccinyl-based inhibitor (E-64, CA030, CA074, NS134, LHVS)	small-molecule	Cathepsins	multiple cell types	Activating invasion and metastasis, Avoiding the immune system	-194
Cysteamine	small-molecule	autophagy, cystine levels	Breast cancer, melanoma	Inducing angiogenesis and Activating invasion and metastasis	(195, 196)
VBY-825	small-molecule	Cathepsins B, L, S, V	Breast carcinoma	Sustaining proliferative signaling and Activating of invasion and metastasis	-197
M402	small-molecule	heparanase	Breast carcinoma 4T1	Inducing angiogenesis and Activating invasion and metastasis	-198
PG454	small-molecule	heparanase	Lymphoma, NK cells	Inducing angiogenesis and Activating invasion and metastasis	-199
PI-88	small-molecule	heparanase	HCC	Inducing angiogenesis and Activating invasion and metastasis	(200, 201)
SST0001	small-molecule	heparanase	Multiple myeloma	Inducing angiogenesis and Activating invasion and metastasis	-202
Chloroquine/hydroxychloroquine	antimalarials	lysosomal pH	multiple cell types	multiple hallmarks	(130, 203)
Lys05	chloroquine formulation	lysosomal pH	multiple cell types	multiple hallmarks	-204
Rapamycin	small-molecule	mTORC1/autophagy	multiple cell types	multiple hallmarks	-205

Table 5.1

References

Abduljabbar R, Negm OH, Lai CF, Jerjees DA, Al-Kaabi M, et al. Clinical and biological significance of glucocorticoid receptor (GR) expression in breast cancer. *Breast Cancer Research and Treatment* **150**, 335 (2015).

Aird KM, Zhang R. Nucleotide metabolism, oncogene-induced senescence and cancer. *Cancer Letters* **356**, 204 (2015).

Aits S, Jäättelä M. Lysosomal cell death at a glance. *Journal of cell science* **126**, 1905 (2013).

Allison AC. Lysosomes in cancer cells. *Journal of Clinical Pathology. Supplement (Royal College of Pathologists)* **7**, 43 (1974).

Andrews NW, Almeida PE, Corrotte M. Damage control: cellular mechanisms of plasma membrane repair. **24**, 734 (2014).

Arvatz G, Shafat I, Levy-Adam F, Ilan N, Vlodavsky I. The heparanase system and tumor metastasis: is heparanase the seed and soil? *Cancer Metastasis Reviews* **30**, 253 (2011).

Bar-Sagi D, Feramisco JR. Induction of membrane ruffling and fluid-phase pinocytosis in quiescent fibroblasts by ras proteins. *Science* **233**, 1061 (1986).

Bergeron JJM, Di Guglielmo GM, Dahan S, Dominguez M, Posner BI. Spatial and temporal regulation of receptor tyrosine kinase activation and intracellular signal transduction. *Annual Review of Biochemistry* (2016).

Blott EJ, Griffiths GM. Secretory Lysosomes **3**, 122 (2002).

Boroughs LK, DeBerardinis RJ. Metabolic pathways promoting cancer cell survival and growth. *Nature* **17**, 351 (2015).

Braig M, Lee S, Loddenkemper C, Rudolph C, Peters AHFM, et al. Oncogene-induced senescence as an initial barrier in lymphoma development. *Nature* **436**, 660 (2005).

Cairns RA, Harris IS, Mak TW. Regulation of cancer cell metabolism. *Nature Reviews Cancer* **11**, 85 (2011).

Carmeliet P. Angiogenesis in health and disease. *Nature Medicine* **9**, 653 (2003).

Chantranupong L, Scaria SM, Saxton RA, Gygi MP, Shen K, et al. The CASTOR proteins are arginine sensors for the mTORC1 pathway. *Cell* **165**, 153 (2016).

Chapel A, Kieffer-Jaquinod S, Sagne C, Verdon Q, Ivaldi C, et al. An extended proteome map of the lysosomal membrane reveals novel potential transporters. *Molecular & Cellular Proteomics* **12**, 1572 (2013).

Chen HY, White E. Role of autophagy in cancer prevention. *Cancer Prevention Research* **4**, 973 (2011).

Chen Z, Trotman LC, Shaffer D, Lin HK, Dotan ZA, et al. Crucial role of p53-dependent cellular senescence in suppression of Pten-deficient tumorigenesis. *Nature* **436**, 725 (2005).

Cheng I, Stram DO, Burtt NP, Gianniny L, Garcia RR, et al. IGF2R missense single-nucleotide polymorphisms and breast cancer risk: the multiethnic cohort study. *Cancer Epidemiology, Biomarkers & Prevention: A Publication of the American Association for Cancer Research, cosponsored by the American Society of Preventive Oncology* **18**, 1922 (2009).

Choi AJS, Ryter SW. Autophagy in inflammatory diseases. *International Journal of Cell Biology* **2011**, 1 (2011).

Chourasia AH, Boland ML, Macleod KF. Mitophagy and cancer. *Cancer & Metabolism* **3**, 4 (2015).

Collado M, Gil J, Efeyan A, Guerra C, Schuhmacher AJ, et al. Tumour biology: senescence in premalignant tumours. *Nature* **436**, 642 (2005).

Commisso C, Davidson SM, Soydaner-Azeloglu RG, Parker SJ, Kamphorst JJ, et al. Macropinocytosis of protein is an amino acid supply route in Ras-transformed cells. *Nature* **497**, 633 (2013).

Courtois-Cox S, Genther Williams SM, Reczek EE, Johnson BW, McGillicuddy LT, et al. A negative feedback signaling network underlies oncogene-induced senescence. *Cancer Cell* **10**, 459 (2006).

Covini D, Tardito S, Bussolati O, Chiarelli LR, Pasquetto MV, et al. Expanding targets for a metabolic therapy of cancer: L-asparaginase. *Recent patents on anti-cancer drug discovery* **7**, 4 (2012).

Cuervo AM, Wong E. Chaperone-mediated autophagy: roles in disease and aging. *Cell research* **24**, 92 (2014).

Cunningham JT, Moreno MV, Lodi A, Ronen SM, Ruggero D. Protein and nucleotide biosynthesis are coupled by a single rate-limiting enzyme, PRPS2, to drive cancer. *Cell* **157**, 1088 (2014).

Dankort D, Filenova E, Collado M, Serrano M, Jones K, et al. A new mouse model to explore the initiation, progression, and therapy of BRAFV600E-induced lung tumors. *Genes & Development* **21**, 379 (2007).

De Souza AT, Hankins GR, Washington MK, Fine RL, Orton TC, et al. Frequent loss of heterozygosity on 6q at the mannose 6-phosphate/insulin-like growth factor II receptor locus in human hepatocellular tumors. *Oncogene* **10**, 1725 (1995a).

De Souza AT, Hankins GR, Washington MK, Orton TC. M6P/IGF2R gene is mutated in human hepatocellular carcinomas with loss of heterozygosity. *Nature* **11**, 447 (1995b).

DeBerardinis RJ, Lum JJ, Hatzivassiliou G, Thompson CB. The biology of cancer: metabolic reprogramming fuels cell growth and proliferation. *Cell Metabolism* **7**, 11 (2008).

Dibble CC, Cantley LC. Regulation of mTORC1 by PI3K signaling. *Trends in Cell Biology* **25**, 545 (2015).

Dixon SJ, Lemberg KM, Lamprecht MR, Skouta R, Zaitsev EM, et al. Ferroptosis: an iron-dependent form of nonapoptotic cell death. *Cell* **149**, 1060 (2012).

Dredge K, Hammond E, Handley P, Gonda TJ, Smith MT, et al. PG545, a dual heparanase and angiogenesis inhibitor, induces potent anti-tumour and anti-metastatic efficacy in preclinical models. *British Journal of Cancer* **104**, 635 (2011).

Efeyan A, Comb WC, Sabatini DM. Nutrient-sensing mechanisms and pathways. *Nature* **517**, 302 (2015).

Elfenbein A, Lanahan A, Zhou TX, Yamasaki A, Tkachenko E, et al. Syndecan 4 regulates FGFR1 signaling in endothelial cells by directing macropinocytosis. *Science Signaling* **5**, ra36 (2012).

Fehrenbacher N, Jäättelä M. Lysosomes as targets for cancer therapy. *Cancer Research* **65**, 2993 (2005).

Feng Y, He D, Yao Z, Klionsky DJ. The machinery of macroautophagy. *Cell Research* **24**, 24 (2014).

Folkman J, Watson K, Ingber D, Hanahan D. Induction of angiogenesis during the transition from hyperplasia to neoplasia. *Nature* **339**, 58 (1989).

Giatromanolaki A, Sivridis E, Mitrakas A, Kalamida D, Zois CE, et al. Autophagy and lysosomal related protein expression patterns in human glioblastoma. *Cancer Biology & Therapy* **15**, 1468 (2014).

Goh LK, Sorkin A. Endocytosis of receptor tyrosine kinases. **5**, a017459 (2013).

Goldenring JR. A central role for vesicle trafficking in epithelial neoplasia: intracellular highways to carcinogenesis. *Nature Reviews Cancer* **13**, 813 (2013).

Goldsmith J, Levine B, Debnath J. Autophagy and cancer metabolism. *Methods in Enzymology* **542**, 25 (2014).

Gotink KJ, Broxterman HJ, Labots M, de Haas RR, Dekker H, et al. Lysosomal sequestration of sunitinib: a novel mechanism of drug resistance. *Clinical Cancer Research* **17**, 7337 (2011).

Gschwind A, Fischer OM, Ullrich A. The discovery of receptor tyrosine kinases: targets for cancer therapy. *Nature Reviews Cancer* **4**, 361 (2004).

Guertin DA, Stevens DM, Thoreen CC, Burds AA, Kalaany NY, et al. Ablation in mice of the mTORC components raptor, rictor, or mLST8 reveals that mTORC2 is required for signaling to Akt-FOXO and PKCalpha, but not S6K1. *Developmental Cell* **11**, 859 (2006).

Guo JY, Karsli-Uzunbas G, Mathew R, Aisner SC, Kamphorst JJ, et al. Autophagy suppresses progression of K-ras-induced lung tumors to oncocytomas and maintains lipid homeostasis. *Genes & Development* **27**, 1447 (2013).

Haigler HT, McKanna JA, Cohen S. Rapid stimulation of pinocytosis in human carcinoma cells A-431 by epidermal growth factor. *Journal of Cell Biology* **83**, 82 (1979).

Hales EC, Taub JW, Matherly LH. New insights into Notch1 regulation of the PI3K–AKT–mTOR1 signaling axis: targeted therapy of γ-secretase inhibitor resistant T-cell acute lymphoblastic leukemia. *Cellular Signalling* **26**, 149 (2014).

Hanahan D, Weinberg RA. Hallmarks of cancer: the next generation. *Cell* **144**, 646 (2011).

He Y, Xu Y, Zhang C, Gao X, Dykema KJ, et al. Identification of a lysosomal pathway that modulates glucocorticoid signaling and the inflammatory response. *Science Signaling* **4**, ra44 (2011).

Hecht VC, Sullivan LB, Kimmerling RJ, Kim DH, Hosios AM, et al. Biophysical changes reduce energetic demand in growth factor-deprived lymphocytes. *Journal of Cell Biology* **212**, 439 (2016).

Hengartner MO. Apoptosis: corralling the corpses. *Cell* **104**, 325 (2001).

Hochreiter-Hufford A, Ravichandran KS. Clearing the dead: apoptotic cell sensing, recognition, engulfment, and digestion. *Cold Spring Harbor Perspectives Biology* **5**, a008748 (2013).

Holtzman E. *Lysosomes.* Springer Science & Business Media, Boston, MA (2013).

Hosios AM, Hecht VC, Danai LV, Johnson MO, Rathmell JC, et al. Amino acids rather than glucose account for the majority of cell mass in proliferating mammalian cells. *Developmental Cell* **36**, 540 (2016).

Hoyo C, Murphy SK, Schildkraut JM, Vidal AC, Skaar D, et al. IGF2R genetic variants, circulating IGF2 concentrations and colon cancer risk in African Americans and Whites. *Disease Markers* **32**, 133 (2012).

Huang S, Jia K, Wang Y, Zhou Z, Levine B. Autophagy genes function in apoptotic cell corpse clearance during C. elegans embryonic development. *Autophagy* **9**, 138 (2013).

Hughes AL, Gottschling DE. An early age increase in vacuolar pH limits mitochondrial function and lifespan in yeast. *Nature* **492**, 261 (2012).

Im E, Venkatakrishnan A, Kazlauskas A. Cathepsin B regulates the intrinsic angiogenic threshold of endothelial cells. *Molecular Biology of the Cell* **16**, 3488 (2005).

Intlekofer AM, Thompson CB. At the bench: preclinical rationale for CTLA-4 and PD-1 blockade as cancer immunotherapy. *Journal of Leukocyte Biology* **94**, 25 (2013).

Ivanov A, Pawlikowski J, Manoharan I, van Tuyn J, Nelson DM, et al. Lysosome-mediated processing of chromatin in senescence. *Journal of Cell Biology* **202**, 129 (2013).

Jiang X, Overholtzer M, Thompson CB. Autophagy in cellular metabolism and cancer. *Journal of Clinical Investigation* **125**, 47 (2015).

Jopling HM, Odell AF, Pellet-Many C, Latham AM, Frankel P, et al. Endosome-to-plasma membrane recycling of VEGFR2 receptor tyrosine kinase regulates endothelial function and blood vessel formation. *Cells* **3**, 363 (2014).

Kach J, Conzen SD, Szmulewitz RZ. Targeting the glucocorticoid receptor in breast and prostate cancers. *Science Translational Medicine* **7**, 305ps19 (2015).

Kallunki T, Olsen OD, Jäättelä M. Cancer-associated lysosomal changes: friends or foes? *Oncogene* **32**, 1995 (2013).

Kamphorst JJ, Cross JR, Fan J, de Stanchina E, Mathew R, et al. Hypoxic and Ras-transformed cells support growth by scavenging unsaturated fatty acids from lysophospholipids. *Proceedings of the National Academy of Sciences of the United States of America* **110**, 8882 (2013).

Kassi E, Moutsatsou P. Glucocorticoid receptor signaling and prostate cancer. *Cancer Letters* **302**, 1 (2011).

Khaminets A, Heinrich T, Mari M, Grumati P, Huebner AK, et al. Regulation of endoplasmic reticulum turnover by selective autophagy. *Nature* **522**, 354 (2015).

Kim HS, Mendiratta S, Kim J, Pecot CV, Larsen JE. Systematic identification of molecular subtype-selective vulnerabilities in non-small-cell lung cancer. *Cell* **36**, 65 (2013).

Kimmelman AC. The dynamic nature of autophagy in cancer. *Genes & Development* **25**, 1999 (2011).

Kirkegaard T, Jäättelä M. Lysosomal involvement in cell death and cancer. *Biochimica et Biophysica Acta (BBA) - Molecular Cell Research* **1793**, 746 (2009).

Kobayashi T, Tanaka T, Toyama-Sorimachi N. How do cells optimize luminal environments of endosomes/lysosomes for efficient inflammatory responses? *Journal of Biochemistry* **154**, 491 (2013).

Koivusalo M, Welch C, Hayashi H, Scott CC, Kim M, et al. Amiloride inhibits macropinocytosis by lowering submembranous pH and preventing Rac1 and Cdc42 signaling. *Journal of Cell Biology* **188**, 547 (2010).

Kornfeld S, Kornfeld S. Structure and function of the mannose 6-phosphate/insulinlike growth factor II receptors. *Annual Review of Biochemistry* **61**, 307 (1992).

Kowanetz K, Crosetto N, Haglund K, Schmidt MHH, Heldin CH, et al. Suppressors of T-cell receptor signaling Sts-1 and Sts-2 bind to Cbl and inhibit endocytosis of receptor tyrosine kinases. *The Journal of Biological Chemistry* **279**, 32786 (2004).

Kreiling JL, Montgomery MA, Wheeler JR, Kopanic JL, Connelly CM, et al. Dominant-negative effect of truncated mannose 6-phosphate/insulin-like growth factor II receptor species in cancer. *FEBS* **279**, 2695 (2012).

Kroemer G, Jäättelä M. Lysosomes and autophagy in cell death control. *Nature Reviews Cancer* **5**, 886 (2005).

Krtolica A, Parrinello S, Lockett S, Desprez PY, Campisi J. Senescent fibroblasts promote epithelial cell growth and tumorigenesis: a link between cancer and aging. *Proceedings of the National Academy of Sciences* **98**, 12072 (2001).

Kuilman T, Michaloglou C, Mooi WJ, Peeper DS. The essence of senescence. *Genes & Development* **24**, 2463 (2010).

Kuma A, Hatano M, Matsui M, Yamamoto A, Nakaya H, et al. The role of autophagy during the early neonatal starvation period. *Nature* **432**, 1032 (2004).

Kurz T, Terman A, Gustafsson B, Brunk UT. Lysosomes in iron metabolism, ageing and apoptosis. *Histochemistry and Cell Biology* **129**, 389 (2008).

Lan YY, Londoño D, Bouley R, Rooney MS, Hacohen N. Dnase2a deficiency uncovers lysosomal clearance of damaged nuclear DNA via autophagy. *Cell Reports* **9**, 180 (2014).

Laplante M, Sabatini DM. mTOR signaling in growth control and disease. *Cell* **149**, 274 (2012).

Lau A, Wang XJ, Zhao F, Villeneuve NF, Wu T, et al. A noncanonical mechanism of Nrf2 activation by autophagy deficiency: direct interaction between Keap1 and p62. *Molecular and Cellular Biology* **30**, 3275 (2010).

Lee BY, Han JA, Im JS, Morrone A, Johung K, et al. Senescence-associated beta-galactosidase is lysosomal beta-galactosidase. *Aging Cell* **5**, 187 (2006).

Levine B, Kroemer G. Autophagy in the pathogenesis of disease. *Cell* **132**, 27 (2008).

Lewis WH. Pinocytosis by malignant cells. *Cancer Research* **29**, 666 (1937).

Liang C, Jung JU. Autophagy genes as tumor suppressors. *Current Opinion in Cell Biology* **22**, 226 (2010).

Liang XH, Jackson S, Seaman M, Brown K, Kempkes B, et al. Induction of autophagy and inhibition of tumorigenesis by Beclin 1. *Nature* **402**, 672 (1999).

Lim JP, Gleeson PA. Macropinocytosis: an endocytic pathway for internalising large gulps. *Immunology and Cell Biology* **89**, 836 (2011).

Lindkvist B, Fajardo I, Pejler G, Borgström A. Cathepsin B activates human trypsinogen 1 but not proelastase 2 or procarboxypeptidase B **6**, 224 (2006).

Liu EY, Xu N, O'Prey J, Lao LY, Joshi S, et al. Loss of autophagy causes a synthetic lethal deficiency in DNA repair. *Proceedings of the National Academy of Sciences of the United States of America* **112**, 773 (2015).

Liu K, Jian Y, Sun X, Yang C, Gao Z, et al. Negative regulation of phosphatidylinositol 3-phosphate levels in early-to-late endosome conversion. *Journal of Cell Biology* **212**, 181 (2016).

Liu Y, Levine B. Autosis and autophagic cell death: the dark side of autophagy. *Cell Death and Differentiation* **22**, 367 (2015).

Lum JJ, Bauer DE, Kong M, Harris MH, Li C, et al. Growth factor regulation of autophagy and cell survival in the absence of apoptosis. *Cell* **120**, 237 (2005).

Lunt SY, Muralidhar V, Hosios AM, Israelsen WJ, Gui DY, et al. Pyruvate kinase isoform expression alters nucleotide synthesis to impact cell proliferation. *Molecular Cell* **57**, 95 (2015).

Luzio JP, Poupon V, Lindsay MR, Mullock BM, Piper RC, et al. Membrane dynamics and the biogenesis of lysosomes. *Molecular Membrane Biology* **20**, 141 (2003).

Machado E, White-Gilbertson S, van de Vlekkert D, Janke L, Moshiach S, et al. Regulated lysosomal exocytosis mediates cancer progression. *Science Advances* **1**, e1500603 (2015).

Mah LY, Ryan KM. Autophagy and cancer. *Cold Spring Harbor Perspectives in Biology* **4**, a008821 (2012).

Manning BD, Cantley LC. AKT/PKB signaling: navigating downstream. *Cell* **129**, 1261 (2007).

Mathew R, Karantza-Wadsworth V, White E. Role of autophagy in cancer. *Nature Reviews Cancer* **7**, 961 (2007).

Matsunaga K, Saitoh T, Tabata K, Omori H, Satoh T, et al. Two Beclin 1-binding proteins, Atg14L and Rubicon, reciprocally regulate autophagy at different stages. *Nature Cell Biology* **11**, 385 (2009).

Mayers JR, Wu C, Clish CB, Kraft P, Torrence ME, et al. Elevation of circulating branched-chain amino acids is an early event in human pancreatic adenocarcinoma development. *Nature Medicine* **20**, 1193 (2014).

McCarthy N, Joyce JA, Baruch A, Chehade K, Meyer-Morse N, et al. Cathepsin cysteine proteases are effectors of invasive growth and angiogenesis during multistage tumorigenesis. *Cancer Cell* **5**, 443 (2004).

McDuff FKE, Turner SD. Jailbreak: oncogene-induced senescence and its evasion. *Cellular Signalling* **23**, 6 (2011).

Mellman I, Yarden Y. Endocytosis and cancer. **5**, a016949 (2013).

Michaloglou C, Vredeveld LCW, Soengas MS, Denoyelle C, Kuilman T, et al. BRAFE600-associated senescence-like cell cycle arrest of human naevi. *Nature* **436**, 720 (2005).

Mills JJ, Falls JG, De Souza AT, Jirtle RL. Imprinted M6p/Igf2 receptor is mutated in rat liver tumors. *Oncogene* **16**, 2797 (1998).

Mochida K, Oikawa Y, Kimura Y, Kirisako H, Hirano H, et al. Receptor-mediated selective autophagy degrades the endoplasmic reticulum and the nucleus. *Nature* **522**, 359 (2015).

Mohamed MM, Sloane BF. Cysteine cathepsins: multifunctional enzymes in cancer. *Nature Reviews Cancer* **6**, 764 (2006).

Mosesson Y, Mills GB, Yarden Y. Derailed endocytosis: an emerging feature of cancer. *Nature Reviews Cancer* **8**, 835 (2008).

Mousavi SA, Brech A, Berg T, Kjeken R. Phosphoinositide 3-kinase regulates maturation of lysosomes in rat hepatocytes. *The Biochemical Journal* **372**, 861 (2003).

Münz C. Autophagy in cellular transformation, survival and communication with the tumor microenvironment. *Seminars in Cancer Biology* **23**, 299 (2013).

Nakajima M, Irimura T, Di Ferrante N, Nicolson GL. Metastatic melanoma cell heparanase. Characterization of heparan sulfate degradation fragments produced by B16 melanoma endoglucuronidase. *The Journal of Biological Chemistry* **259**, 2283 (1984).

Nardella C, Clohessy JG, Alimonti A, Pandolfi PP. Pro-senescence therapy for cancer treatment. *Nature Reviews Cancer* **11**, 503 (2011).

Okamoto K. Organellophagy: eliminating cellular building blocks via selective autophagy. *Journal of Cell Biology* **205**, 435 (2014).

Palm W, Park Y, Wright K, Pavlova NN, Tuveson DA, et al. The utilization of extracellular proteins as nutrients is suppressed by mTORC1. *Cell* **162**, 259 (2015).

Parrinello S, Coppe JP, Krtolica A, Campisi J. Stromal-epithelial interactions in aging and cancer: senescent fibroblasts alter epithelial cell differentiation. *Journal of Cell Science* **118**, 485 (2005).

Pattingre S, Tassa A, Qu X, Garuti R, Liang XH, et al. Bcl-2 antiapoptotic proteins inhibit Beclin 1-dependent autophagy. *Cell* **122**, 927 (2005).

Perera RM, Bardeesy N. Pancreatic cancer metabolism: breaking it down to build it back up. *Cancer Discovery* **5**, 1247 (2015).

Pérez-Mancera PA, Young ARJ, Narita M. Inside and out: the activities of senescence in cancer. *Nature Reviews Cancer* **14**, 547 (2014).

Piao S, Amaravadi RK. Targeting the lysosome in cancer. *Annals of the New York Academy of Sciences* n/a–n/a (2015).

Raff MC. Size control: the regulation of cell numbers in animal development. *Cell* **86**, 173 (1996).

Rebsamen M, Pochini L, Stasyk T, de Araújo MEG, Galluccio M, et al. SLC38A9 is a component of the lysosomal amino acid sensing machinery that controls mTORC1. *Nature* **519**, 477 (2015).

Repnik U, Cesen MH, Turk B. The endolysosomal system in cell death and survival. *Cold Spring Harbor Perspectives in Biology* **5**, a008755 (2013).

Roczniak-Ferguson A, Petit CS, Froehlich F, Qian S, Ky J, et al. The transcription factor TFEB links mTORC1 signaling to transcriptional control of lysosome homeostasis. *Science Signaling* **5**, ra42 (2012).

Ros S, Schulze A. Linking glycogen and senescence in cancer cells. *Cell Metabolism* **16**, 687 (2012).

Rosenfeldt MT, O'Prey J, Morton JP, Nixon C, MacKay G, et al. p53 status determines the role of autophagy in pancreatic tumour development. *Nature* **504**, 296 (2013).

Saftig P, Schröder B, Blanz J. Lysosomal membrane proteins: life between acid and neutral conditions. *Biochemical Society Transactions* **38**, 1420 (2010).

Saitoh T, Akira S. Regulation of innate immune responses by autophagy-related proteins. *Journal of Cell Biology* **189**, 925 (2010).

Sakhrani NM, Padh H. Organelle targeting: third level of drug targeting. *Drug Design, Development and Therapy* **7**, 585 (2013).

Santaguida S, Amon A. Aneuploidy triggers a TFEB-mediated lysosomal stress response. *Autophagy* **11**, 2383 (2015a).

Santaguida S, Amon A. Short- and long-term effects of chromosome mis-segregation and aneuploidy. *Nature Reviews Molecular and Cellular Biology* **16**, 473 (2015b).

Santaguida S, Vasile E, White E, Amon A. Aneuploidy-induced cellular stresses limit autophagic degradation. *Genes & Development* **29**, 2010 (2015).

Sarkisian CJ, Keister BA, Stairs DB, Boxer RB, Moody SE, et al. Dose-dependent oncogene-induced senescence in vivo and its evasion during mammary tumorigenesis. *Nature Cell Biology* **9**, 493 (2007).

Schmees C, Villaseñor R, Zheng W, Ma H, Zerial M, et al. Macropinocytosis of the PDGF β-receptor promotes fibroblast transformation by H-RasG12V. *Molecular Biology of the Cell* **23**, 2571 (2012).

Scriver CR. *The Metabolic & Molecular Bases of Inherited Disease.* New York ; Montreal : McGraw-Hill (2001).

Settembre C, Ballabio A. Lysosome: regulator of lipid degradation pathways. *Trends in Cell Biology* **24**, 743 (2014).

Settembre C, Di Malta C, Polito VA, Garcia Arencibia M, Vetrini F, et al. TFEB links autophagy to lysosomal biogenesis. *Science* **332**, 1429 (2011).

Settembre C, Fraldi A, Medina DL, Ballabio A. Signals from the lysosome: a control centre for cellular clearance and energy metabolism. *Nature Reviews Molecular and Cellular Biology* **14**, 283 (2013).

Settembre C, Zoncu R, Medina DL, Vetrini F, Erdin S, et al. A lysosome-to-nucleus signalling mechanism senses and regulates the lysosome via mTOR and TFEB. *The EMBO Journal* **31**, 1095 (2012).

Shanware NP, Bray K, Abraham RT. The PI3K, metabolic, and autophagy networks: interactive partners in cellular health and disease. **53**, 89 (2013).

Son J, Lyssiotis CA, Ying H, Wang X, Hua S, et al. Glutamine supports pancreatic cancer growth through a KRAS-regulated metabolic pathway. *Nature* **496**, 101 (2013).

Sorkin A, Fortian A. Endocytosis and endosomal sorting of receptor tyrosine kinases. *Receptor Tyrosine Kinases: Structure, Functions and Role in Human Disease*, Springer New York, New York, NY, 133–161 (2014).

Sumpter R, Sumpter Jr R, Sirasanagandla S, Fernández ÁF, Wei Y, et al. Fanconi anemia proteins function in mitophagy and immunity. *Cell* **165**, 867 (2016).

Tasdemir E, Maiuri MC, Morselli E, Criollo A. A dual role of p53 in the control of autophagy. *Autophagy* (2008).

Tian Z, Yao G, Song H, Zhou Y, Geng J. IGF2R expression is associated with the chemotherapy response and prognosis of patients with advanced NSCLC. *Cellular Physiology and Biochemistry: International Journal of Experimental Cellular Physiology, Biochemistry, and Pharmacology* **34**, 1578 (2014).

Valley CC, Lidke KA, Lidke DS. The spatiotemporal organization of ErbB receptors: insights from microscopy. *Cold Spring Harbor Perspectives in Biology* **6**, a020735 (2014).

Vander Heiden MG. Exploiting tumor metabolism: challenges for clinical translation. *The Journal of Clinical Investigation* **123**, 3648 (2013).

Vander Heiden MG, Cantley LC, Thompson CB. Understanding the Warburg effect: the metabolic requirements of cell proliferation. *Science* **324**, 1029 (2009).

Walker LSK, Sansom DM. Confusing signals: recent progress in CTLA-4 biology. *Trends in Immunology* **36**, 63 (2015).

Wang C, Wang Y, Li Y, Bodemann B, Zhao T, et al. A nanobuffer reporter library for fine-scale imaging and perturbation of endocytic organelles. *Nature Communications* **6**, 8524 (2015a).

Wang S, Tsun ZY, Wolfson RL, Shen K, Wyant GA, et al. Metabolism. Lysosomal amino acid transporter SLC38A9 signals arginine sufficiency to mTORC1. *Science* **347**, 188 (2015b).

Wang Y, Gao J, Guo X, Tong T, Shi X, et al. Regulation of EGFR nanocluster formation by ionic protein-lipid interaction. *Cell Research* **24**, 959 (2014).

Webb BA, Chimenti M, Jacobson MP, Barber DL. Dysregulated pH: a perfect storm for cancer progression. *Nature Reviews Cancer* **11**, 671 (2011).

Wei Y, Zou Z, Becker N, Anderson M, Sumpter R, et al. EGFR-mediated Beclin 1 phosphorylation in autophagy Suppression, tumor progression, and tumor chemoresistance. *Cell* **154**, 1269 (2013).

Westermarck J, Kähäri VM. Regulation of matrix metalloproteinase expression in tumor invasion. *FASEB Journal: Official Publication of the Federation of American Societies for Experimental Biology* **13**, 781 (1999).

Wheeler DB, Zoncu R, Root DE, Sabatini DM, Sawyers CL. Identification of an oncogenic RAB protein. *Science* **350**, 211 (2015).

White E. The role for autophagy in cancer. *Journal of Clinical Investigation* **125**, 42 (2015).

White E, Karp C, Strohecker AM, Guo Y, Mathew R. Role of autophagy in suppression of inflammation and cancer. *Current Opinion in Cell Biology* **22**, 212 (2010).

Wiggins HL, Wymant JM, Solfa F, Hiscox SE, Taylor KM, et al. Disulfiram-induced cytotoxicity and endo-lysosomal sequestration of zinc in breast cancer cells. *Biochemical Pharmacology* **93**, 332 (2015).

Winterhoff B, Freyer L, Hammond E, Giri S, Mondal S, et al. PG545 enhances anti-cancer activity of chemotherapy in ovarian models and increases surrogate biomarkers such as VEGF in preclinical and clinical plasma samples. *European Journal of Cancer* **51**, 879 (2015).

Wolfson RL, Chantranupong L, Saxton RA, Shen K, Scaria SM, et al. Sestrin2 is a leucine sensor for the mTORC1 pathway. *Science* **351**, 43 (2016).

Wu YC, Horvitz HR. C. elegans phagocytosis and cell-migration protein CED-5 is similar to human DOCK180. *Nature* **392**, 501 (1998).

Xu H, Ren D. Lysosomal physiology. *Annual Review of Physiology* **77**, 57 (2015).

Yamasaki T, Terai S, Sakaida I. Deferoxamine for advanced hepatocellular carcinoma. *The New England Journal of Medicine* **365**, 576 (2011).

Yamazaki T, Zaal K, Hailey D, Presley J, Lippincott-Schwartz J, et al. Role of Grb2 in EGF-stimulated EGFR internalization. *Journal of Cell Science* **115**, 1791 (2002).

Yang A, Rajeshkumar NV, Wang X, Yabuuchi S, Alexander BM, et al. Autophagy is critical for pancreatic tumor growth and progression in tumors with p53 alterations. *Cancer Discovery* **4**, 905 (2014).

Youle RJ, Narendra DP. Mechanisms of mitophagy. *Nature* **12**, 9 (2011).

Young RM, Ackerman D, Quinn ZL, Mancuso A, Gruber M, et al. Dysregulated mTORC1 renders cells critically dependent on desaturated lipids for survival under tumor-like stress. *Genes & Development* **27**, 1115 (2013).

6

Conclusion

Summary

In this thesis, we developed and implemented methods to study cancer metabolism in mouse models. Our results highlight the importance of studying cancer metabolism in a physiological setting. In contrast to cells in culture with the same oncogenic mutations, glucose and glutamine metabolism in tumors arising in a mouse model of lung cancer preferentially utilize glucose for anaplerosis and oxidative metabolism as compared to adjacent normal lung tissue. Surprisingly, glutamine is not preferentially used by the lung tumors studied as compared to adjacent tissue. These data further dispel the notion that one oncogene causes a single metabolic phenotype and instead strongly suggests that the metabolic phenotype of cancer cells is not only determined by the mutational status of specific oncogenes, but also by the microenvironment. Importantly, the mouse models of lung cancer we examined faithfully recapitulate metabolic features of the human disease, particularly concerning the fate of glucose in human lung cancer (Hensley et al., 2016; Hensley and DeBerardinis, 2015; Sellers et al., 2015; Fan et al., 2009), and also metabolic phenotypes of tumors in other settings *in vivo* (Maher et al., 2012; Marin-Valencia et al., 2012).

We next studied macropinocytosis of extracellular protein in a mouse model of pancreatic cancer *in vivo*. Consistent with previous work *in vitro* (Commisso et al., 2013), we demonstrate that

cell-autonomous macropinocytosis occurs in pancreatic cancer cells *in vivo* at a high rate and free amino acids derived from extracellular protein are critical for tumor proliferation. We also demonstrate that fibronectin, a high molecular weight and abundant extracellular matrix (ECM) protein, is internalized at high rates by pancreatic cancer cells. These data indicate that fibronectin and other proteins of the ECM may be particularly important nutrients in pancreatic cancer. Taken together with data suggesting a link between hypoxia and elevated macropinocytosis from Kamphorst et al. (2013), we further speculate that proteins found in the local microenvironment may be utilized in poorly vascularized regions of the tumor where circulating nutrients (such as glucose, glutamine, and free amino acids) may not be available. The microdevice used in Chapter 3 can also be used in the clinic at the time of biopsy to determine whether tumors in patients perform macropinocytosis. As inhibitors of macropinocytosis are being investigated, use of this device could be further tested in pre-clinical models using a similar local delivery strategy. In sum, our data suggest that tumor-autonomous protein catabolism is a significant source of free amino acids for some tumors and targeting macropinocytosis may be a viable therapeutic strategy in pancreatic cancer.

Finally, we demonstrate that expression of the M1 isoform of the glycolytic enzyme pyruvate kinase (*Pkm1*) is tumor suppressive in a mouse model of prostate cancer. Genetic deletion of *Pkm2* and forced expression of *Pkm1* suppresses formation of prostate adenocarcinoma in a *Pten*-driven mouse model. This tumor suppression appears to occur through the induction or maintenance of cellular senescence and is consistent with a mechanism whereby nucleotide biosynthesis is limiting for replication (Lunt et al., 2015). In contrast to mouse models of breast and colon cancer, these data are further consistent with earlier observations that low PK activity is required for cell growth (Christofk et al., 2008b,a; Gui et al., 2013) and with more recent observations that high *PKM1* expression and activity promote quiescence (Lunt et al., 2015). We also demonstrate that tumors

resected from patients with prostate cancer express PKM2. Therefore, we propose prostate cancer may be one type of cancer that may benefit from the pharmacological activation of PKM2.

Targeting metabolism for cancer therapy

Further examination of the genetic, environmental, and yet to be identified determinants that contribute to changes observed in the metabolism of cancer cells *in vivo* will provide insight into our basic understanding of proliferation and will facilitate the development of new therapeutic strategies. More answers will be provided by metabolic phenotyping studies in mouse models models of cancer *in vivo* using different nutrients or tracers labeled with different stable-isotope atoms (e.g. ^{15}N, ^{13}C, ^{2}H, ^{18}O). Advances in somatic genome editing technology will hasten the process of establishing the causality of aberrant metabolic processes and enable rapid testing of metabolic requirements that contribute to tumor initiation, progress, maintenance, and metastasis. Further indexing of the "metabolome" will enhance discovery efforts and a growing interest in using untargeted metabolomics for this purpose. As our results have implications for cancer therapy, we conclude here by discussing some possibilities that arise from our observations. We also propose several questions that remain unanswered for future studies in cancer metabolism.

Lung cancer

At the conclusion of the study examining glucose and glutamine metabolism in lung tumors driven by oncogenic *Kras* and *p53* in Chapter 2, we hypothesized that cell of origin or possible local nutrient concentrations might play a role in dictating the metabolic program that is not governed by oncogenic signaling. Other studies examining brain, liver, and lung cancer in mice and humans also observed similar metabolic phenotypes (Maher et al., 2012; Marin-Valencia et al., 2012; Hensley et al., 2016; Hensley and DeBerardinis, 2015; Yuneva et al., 2012). To understand whether the

metabolic phenotypes we observed were a general feature of lung cancer, we began to examine other mouse models of lung cancer and have generated preliminary data.

KP mouse model In Chapter 2, we demonstrated that cancer cells generated from the KP mouse model exhibit a phenotype that is consistent with the Warburg effect, but the tumors they originate from *in vivo* exhibit a metabolic program that requires anaplerosis and oxidative metabolism of glucose carbon through the enzymes pyruvate carboxylase and the pyruvate dehydrogenase complex, respectively. We speculate that pyruvate carboxylase supports both anaplerosis and the production of aspartate, a nutrient that has been recently shown to be essential to for proliferation (Birsoy et al., 2015; Gui et al., 2016; Sullivan et al., 2015). Surprisingly, oxidative metabolism through the PDH complex is critical for tumor initiation and progression in Kras-driven lung cancer. We also determined that KP-driven lung cancers do not preferentially utilize glutamine, a contrast to those cells *in vitro*. With numerous efforts underway to inhibit glutaminolysis (Gross et al., 2014) and to visualize tumors with glutamine PET probes (Venneti et al., 2015), these data are disappointing. Nevertheless, in addition to the genetic and pathophysiological features that are consistent with the human disease, the KP mouse model faithfully recapitulates metabolic features as well, especially with respect to pyruvate carboxylase (Pcx) activity (Sellers et al., 2015; Cheng et al., 2011). We conclude that the *KP* mouse model performs metabolism similar to human lung tumors, and therefore, the KP mouse model represents a starting point to identify metabolic targets that may be translational to the human disease.

KP Keap1-driven lung cancer Kelch-like associated protein 1 (*Keap1*) is mutated in approximately 15% of all non-small cell lung adenocarcinoma (Collisson et al., 2014). *Keap1* is a negative regulator of nuclear factor, erythroid 2-like 2 (*Nrf2*), a master transcriptional regulator of the antioxidant

response program. As a consequence of increased mitochondrial metabolism, deficiencies in Complex I activity as seen with p53 mutations, along with other cancer metabolism processes, reactive oxygen species (ROS) accumulate in the cell. The presence of ROS stimulates the upregulation genes for the synthesis of glutathione and other antioxidant response programs. Levels of ROS are critical for tumor formation, and there is a balance of ROS levels required for tumorigenesis. This is best demonstrated by one study where lung tumor acceleration is observed when animals are administered the anti-oxidants, vitamin E and N-acetylcysteine (Sayin et al., 2014).

In ongoing work to examine metabolic dependencies of various lung tumors, we have discovered a sensitivity of KP lung tumors with Keap1 (KPK) mutations to glutamine deprivation and the glutaminase inhibitor CB839 *in vivo* and *in vitro* (Figure 6.1). In this Keap1 knockout, the reasons for sensitization to glutamine deficiency remain unknown. Glutathione (γ-L-glutamyl-L-cysteinyl glycine) is a tripeptide synthesized in the cytosol. The ligation of cysteine to glutamate by glutamate cysteine ligase (GCL) is the rate limiting step in glutathione biosynthesis. GSH synthase (GS) catalyzes the condensation of γ-glutamyl-cysteine with glycine to complete the synthesis. It is possible that glutamate derived from glutamine is limiting for glutathione synthesis. However, as discussed in Chapter 1, glutamine plays many roles in the cell, and many other possibilities for the glutaminase sensitivity observed in this model exist. This work further highlights the great variation in metabolic requirements in tumors and, once more, places an important emphasis on genetic regulation of metabolic processes. Importantly, and in contrast to data in KP lung tumor metabolism described in Chapter 2, this data further suggests that glutaminase inhibitors may be used in this setting. Further characterization of tumors from patients with KEAP1 mutations, along with a retrospective analysis examining KEAP1 status in patients in the ongoing clinical trial for glutaminase inhibitor may provide additional insight.

EML4-ALK-driven lung cancer The fusion transcript of echinoderm microtubule-associated

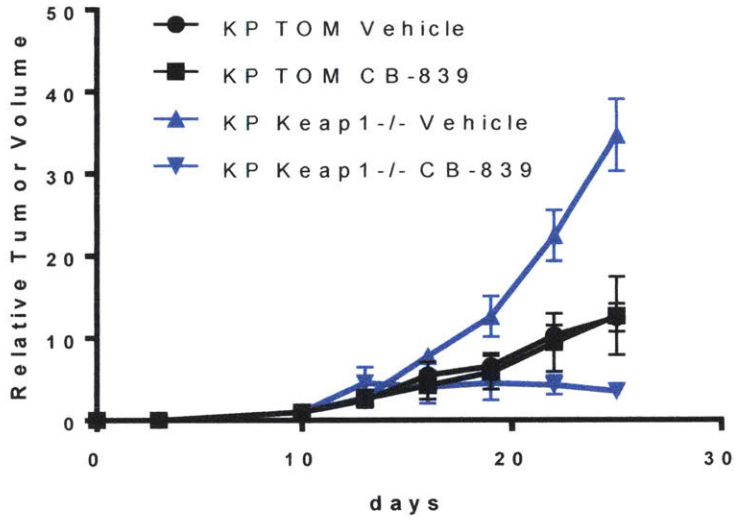

Figure 6.1. KP-Keap1$^{-/-}$ tumors are sensitive to glutaminase inhibition Animals harboring cells with KP with guide RNAs targeting tdTomato (Control, KP Tomato) or targeting Keap1 (KP Keap1) were treated for 4 weeks with vehicle or CB-839 as indicated. Each point represents data from an independently derived tumor, and the mean ±SEM is indicated. KP-Keap1$^{-/-}$ tumors are sensitive to the glutaminase inhibitor CB-839 inhibition.

Figure 6.1

protein-like 4 (*EML4*) gene and the anaplastic lymphoma kinase (*ALK*) gene were identified as a molecular driver event in approximately 7% of non-small cell lung cancers (NSCLC) (Soda et al., 2007). In addition to testing gene function at the time of initiation, the CRISPR/Cas9 genome editing machinery can also be used to create mutations that lead to oncogenic fusion proteins that mimic those found in human disease (Maddalo et al., 2014). The implementation of CRISPR/Cas9 technology highlights the utility and versatility of somatic genome editing for rapid cancer modeling.

Through similar metabolic phenotyping approaches, we observed that tumors are driven by *EML4-ALK* exhibit two to three times the levels of glycolytic serine production as compared to the KP mouse model (data not shown). Current studies are examining whether *EML4-ALK*-driven lung tumors require enzymes in the serine biosynthesis pathway through pharmacological and genetic means. While many therapies targeting *EML4-ALK* exist, resistance to these therapies is frequently developed within 1-2 years (Awad and Shaw, 2014). If glycolytic serine synthesis is

important for these tumors, this may be one type of cancer that could benefit from existing small molecule inhibitors of *PHGDH* (Pacold et al., 2016; Mullarky et al., 2016) or a by implementing a similar regimen targeting the serine biosynthesis pathway (Mattaini et al., 2016).

Open questions The metabolic program of each type of NSCLC is likely to be dictated by a combination of oncogenic driver, cell-of-origin, tissue-of-origin, and local microenvironment. This conclusion is not necessarily surprising given other reports describing the overall heterogeneity in NSCLC (Chen et al., 2014). An important next step is to confirm whether those driver mutations also exhibit the same metabolic consequences in patients. It will further be important to determine if patient-derived xenografts can be used to model individual subtypes of tumors and create systems that will facilitate the development and rapid screening of therapeutics that target metabolic processes.

Further studies to dissect the genetic interaction of Kras and p53 independently in these models would be useful. These include assessing the metabolic phenotypes of inducible Kras allele (iKras) to understand better metabolic changes that occur as a function of oncogene expression in normal tissues, independent of pathological disease. Few experiments have delineated differences between complete loss of function or point mutations that result in dominant-negative alleles. Characterizing metabolic consequences of the loss-of-function p53 mutation as compared to the dominant-negative gain-of-function mutation will also be informative in tumors and normal tissue. It is of significant importance to understand how the dominant negative allele that is the more frequently occurring mutation in cancer affects metabolism, and to what extent this is similar to complete loss-of-function. Understanding this difference may, in part, account for the differences in tumor latency observed in mouse models as a result of gain-of-function and loss-of-function mutations. Another similar experiment would involve utilizing a mouse model harboring a

restorable p53 allele (Donehower and Lozano, 2009).

Many unanswered questions about the essentiality of glutamine as a nutrient source for tumors remain, although most data currently suggests a significant degree of context-dependency. While some of this context-dependency seems to arise from different culture conditions, glutamine requirements as a function of microenvironmental differences require better characterization. Several lines of work have attempted to address these environmental differences to assess the effects they exert on the metabolic program. One of these environmental differences is best demonstrated by a recent study examining a xenograft mouse model of breast cancer (murine 4T1 cells). Christen et al. (2016) demonstrated that 4T1 cells that metastasized from the breast tissue to the lung had higher pyruvate carboxylase expression and activity in the lung. The authors conclude that the relative ratio of pyruvate to glutamate in the breast as compared to the lung may be responsible for these differences (Christen et al., 2016). It would be of further interest to determine whether the pyruvate to glutamate ratio varies across other known sites of metastasis. Extending this concept, how does local nutrient availability or the ratio of different nutrients impact metabolism in general? A second possible explanation for differences in glutamine metabolism comes from a recent study which demonstrated that the local concentration of glutamine could result in dictating the differentiation status by altering α-ketoglutarate levels and subsequently histone methylation (Pan et al., 2016). Other differences in glutamine metabolism could be in response for the requirements to maintain glutathione levels or high rates of protein synthesis, two areas not directly interrogated in our work in Chapter 2. The underlying mechanisms to explain the *in vitro* and *in vivo* metabolic preferences remain largely unknown.

Pancreatic cancer

In a mouse model of pancreatic cancer, we observed tumor-autonomous catabolism and preferential uptake of albumin and showed that blocking macropinocytosis in these cells with the inhibitor of macropinocytosis, EIPA, resulted in reduced levels of free amino acids. Many questions remain unanswered for understanding the role macropinocytosis plays in cancer. Examination of albumin catabolism has remained elusive due to the lack of a reliable tracer (Rothschild et al., 1975). Further studies employing the use of both nitrogen- and carbon- labeled albumin in normal and disease settings may further aid identification of metabolic vulnerabilities and macropinocytic substrates that are essential for the nutrient supply of tumors (including micronutrients, such as vitamins and other co-factors). It remains of great interest to understand if there are genetic determinants are to stimulate macropinocytosis in cancer besides those exhibited by RAS and v-Src. There is significant value in understanding how cells can preferentially uptake different substrates with high affinity, and research in this area could facilitate the delivery of therapeutic agents specifically to the tumor.

Inhibition of macropinocytosis What other substrates do tumor cells eat? Besides protein and lipids, it is unknown whether tumors internalize other circulating nutrients through the macropinocytotic pathway. Another study demonstrated that NSCLC could acquire ATP through endocytosis and macropinocytosis (Qian et al., 2016). A rigorous and systematic account study will be required to dissect the relative contribution of endocytic and intracellular recycling pathways in cancer cells. The experimental strategy for such a study is not entirely straightforward and critical to the success of such an effort will be clever use of stable isotope tracers, fine kinetic analyses of the constituents of biomass, and modern genome editing technologies to ablate machinery of these intertwined trafficking pathways. Furthermore, advances that enable the rapid isolation of

organelles and the cataloging of the contents as a function of transformation and oncogenesis in both cell and animal models will be critical.

The development of macropinocytosis inhibitors with improved pharmacokinetic and pharmacodynamic properties may work to starve pancreatic cancer cells. Adaptation of the microdevice used in Chapter 3 will aid in characterizing macropinocytosis in animal models and can be used clinically to determine which tumors use macropinocytosis to monitor therapeutic regimens in patient-derived xenografts. The device could also be used in tumors in patients and provide novel means for which we will be able to assess existing therapeutics rapidly. The ability to further assess which oncogenic drivers and which solid tumors perform macropinocytosis will be essential to devising therapeutic strategies.

Exploiting macropinocytosis for delivery of therapeutics It has been observed that tumors preferentially internalize albumin since the 1970s (Schilling et al., 1992), and albumin conjugated therapies have been appealing for this reason. Cancer cells that perform constitutive macropinocytosis may be especially vulnerable to these therapies. We were surprised by two findings regarding the nature of macropinocytosis in the pancreatic tumors we observed. First, the kinetics at which macropinocytosis occur in *Kras*-driven tumor cells in the autochthonous or xenograft setting is remarkable and similar to Lewis' initial observations in macrophages (Lewis, 1937). In fact, the constitutive nature of Ras-driven macropinocytosis results in near instantaneous uptake and trafficking to the lysosome. Second, the size of the cargo taken up by these tumors is striking. Macropinocytic vesicles have a range of 0.2μM to 2μM. Understanding whether uptake of substrates other than albumin and fibronectin through the macropinocytic pathway, such as other ECM protein components, will also be important.

Mutations in *RAS* seem to promote constitutive macropinocytosis, possibly through

constitutive PI3K signaling. However, other cells, including normal cells can undergo inducible macropinocytosis (Swanson and Watts, 1995). Can we simulate normal biological stimuli to increase macropinocytosis levels in normal cells and cancer cells? This may be one viable approach toward killing cancer cells. Varmus and colleagues suggest that increasing macropinocytosis levels to high rates results in cell death, as demonstrated by the synthetic lethality observed between mutant Kras and mutant EGFR (Unni et al., 2015). This approach may suggest that there is a therapeutic index that is dependent on levels of macropinocytosis.

Prostate cancer

Prostate cancer has recently been classified into seven primary subtypes (Abeshouse et al., 2015). There is a wealth of data from sequencing primary tumors that have recently delineated the molecular drivers, in addition to sequencing data available from advanced metastatic prostate cancer (Robinson et al., 2015; Cho et al., 2016). Further determination of *PKM2* expression as a function of oncogenic driver mutations in patients with prostate cancer may enable determination of those patients who may benefit from pharmacological efforts attempting to target this enzyme. It is expected that these activators would be relatively well tolerated based the phenotype of the *Pkm2*-null mouse (*Pkm1* expressing, high activity).

The road ahead

The causal determinants that are responsible for observed differences in metabolism in cancer cells *in vitro* and *in vivo* remain incompletely understood. With emerging techniques and log-fold improved sensitivity for mass-spectrometric and imaging platforms, further development of methods will be critical to continue to understand the most challenging questions in metabolism, specifically examining tumor heterogeneity and further understanding compartmentalized reactions at the

single cell level. A straightforward but critical component will be characterizing mouse models and understanding how these are similar to the human disease at the level of metabolism. This thesis concludes with potential methodology and directions for future studies.

Finding physiological conditions for in vitro studies.

In Warburg's seminal 1956 paper, "On the Origin of Cancer Cells," he describes two lines of cultured cells that grew with similar (if not identical) kinetics, yet had significantly different malignant effects when engrafted in C3H/He mice *in vivo* (Warburg, 1956). By design, cell culture medias have been selected for the growth properties they engender, beginning with Basal Medium Eagle (BME) to the modern day Dulbecco's modified Eagle medium (DMEM). A calculation determined that upon isolating cells from a tumor, any cell with only a 5% proliferative advantage will completely overtake a slower growing clone in only 65 generations (Mayers and Vander Heiden, 2015). Therefore, by the time one has established a cell line, it is likely that a small number of the rapidly growing population has been selected.

Development of media that represents that simulate the *in vivo* setting will be critical for future studies. Indeed, an implementation such as those from Birsoy et al. (2014) using nutristatic conditions to maintain levels of nutrients in media represent a movement in this direction. However, this system is currently limited to cells grown in suspension. Other efforts to grow cells in more physiological conditions are underway and represent an important direction for future metabolic studies. These studies should be facilitated by having the answer key in hand from studies *in vivo* combined with robust analytical methods.

Compartmentalized metabolism

Most metabolic studies conducted to date involve the use of a destructive method by which a cell is lysed in a way that is destructive and indiscriminate for quantitating the contents of specific sub-cellular compartments. These methods are typically performed in a mixture of methanol and water or methanol, chloroform, and water termed the Folch extraction (Folch et al., 1956). As a result of limited methodology, studying the contents of specific organelles and their involvement in cancer has been challenging.

Two organelles that have the profound implications on cellular metabolism are the mitochondria and the lysosome. Clever studies using isotope tracing and knowledge of atom transitions between metabolites along with known localization of specific isoforms of IDH1/2 have been implemented to elucidate the relative contribution of mitochondrial versus cytosolic enzymatic activity to the production NADPH (Lewis et al., 2014). Studies employing a similar strategy will continue to define further components of compartmentalized reactions to assess relative contributions of enzymes in different compartments, where redundant catalytic activity exists. While powerful, the strategy above relies on fractional labeling patterns of isotopomers of metabolites of interest and the conclusions are drawn from these observations, which do not allow for interpretation of absolute levels of compartmentalized metabolites.

Further development of methods is required to study compartmentalized metabolism at the systems level. A recent strategy has emerged to address this problem, which involves the rapid affinity purification of cells expressing an HA-EGFP tag (Chen et al., 2016). Emerging methods to study sub-cellular structure would be highly beneficial to understand more about not only compartmentalization of metabolites but also about the catabolism and trafficking of certain drugs, particularly in the case of resistance. As discussed in Chapter 5, an emerging mechanism of drug

resistance is lysosomal sequestration of the drug. To what extent does sequestration of metabolites occur in other settings?

Mouse models

Genetic approaches to examine cancer in mouse models have relied on siRNA and shRNA. This is a particular problem for studies in metabolism as small amounts of residual protein can have near-normal levels of total activity. CRISPR/Cas9 technology enables complete ablation of enzymatic activity and enables fast and powerful functional analysis of critical metabolic enzymes. While the work in this thesis employed a strategy of somatic genome editing to knockout metabolic enzymes from the time of tumor initiation, studies using inducible systems will be able to assess the function of metabolic enzymes during different parts of oncogenesis (e.g. tumor maintenance, progression, and metastasis). Further, performing genetic screens using libraries with sgRNAs against metabolic enzymes in cells *in vivo* and *in vitro* in parallel would enable rapid detection of differential dependencies in these two contexts. It will also be important to extend these studies to other organ systems. Strategies employing all-in-one genome editing, such as pSECC utilized in Chapter 2, are now being used to target the colon, pancreas, liver and numerous other somatic tissues. The use of these would also be feasible in the mouse prostate, and we have performed preliminary experiments to establish this possibility (Figure 6.2).

Aging and cancer metabolism

> *If a large enough number of cells is allowed a sufficiently long period, gene mutations will necessarily occur in some of them. If the cells propagate–in other words, if the tissue in question grows or renews itself–it is possible that the mutated cells will multiply in great number. In this case, it is probably that some of the already mutated cells will mutate again and thus become provided with two abnormal genes. This process of mutation, propagation, mutation, and so on may, of course, continue incessantly during the life of the individual. If the propagation of cells is rapid, the whole process will take place more rapidly; and if the cells are influenced by mutation agents such as X-rays or mustard gas, there will also be an acceleration of the process as a whole.*
> -C.O. Nordling, 1953

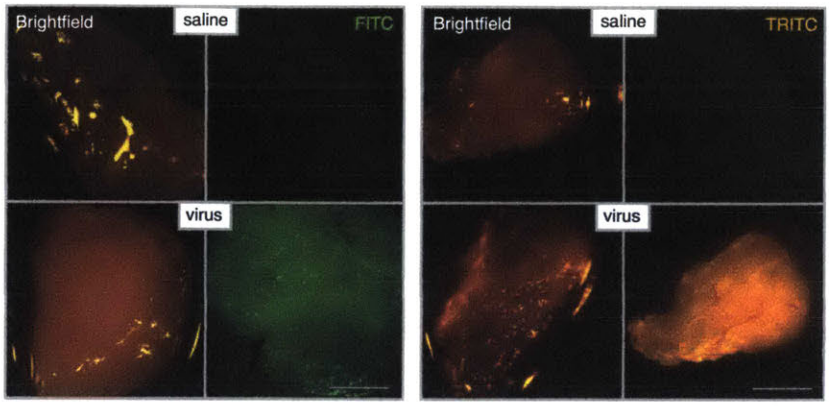

Figure 6.2. Viral delivery to the murine prostate epithelium. Microsurgery was performed to expose the seminal vesicles and mouse prostate. A fine needle was inserted into the prostate ducts under a microscope and 5 µM of Lenti-EFS-Cre-P2A-mNeonGreen (left) or AAV5-CMV-Cre (right) were injected into wild-type mice or mice harboring an allele for tdTomato, respectively. Anterior prostate lobes were visualized under a conventional fluorescence microscope with FITC and TRITC filters. No evidence for viral backflow into other organs or lobes of the prostate was detected.

Figure 6.2

Is cancer just bad luck? Alfred Knudson dispelled Nordling's multi-gene theory by keen observations through his examination of the probability that a child inherits retinoblastoma. He noted that the frequency of events that children who have inherited retinoblastoma followed a Poisson distribution. This allowed the estimation of a mean number of tumors to be estimated per gene carrier (Knudson, 1971). From this study, Knudson concluded that the first mutation in the later discovered Rb gene occurred in the germline, while the second occurs in the somatic cells (Knudson, 1971).

Many theories have been put forth to explain the higher incidence of cancer. Theories involving error rate (mutation) and the number of divisions of stem cells at certain tissue sites are appealing and there is also strong evidence for high mutation rates in certain tissues or after exposure to environmental toxins.

Adjusted for age, however, benign prostate hyperplasia and frank prostate cancer still appear to be an outlier regarding cancer incidence. That prostate cancer is nearly a fact of life, rather than a coincidence or due to the statistical probability of mutation rate, for men over the age of 70 remains

puzzling. In one paper attempting to model the stem-cell theory, there is an astonishing absence of the mention of prostate cancer (Tomasetti and Vogelstein, 2015). In a follow-up study, prostate and breast cancer were included and similarly modeled. Based on the model developed by Tomasetti and Vogelstein (2015), the authors concluded that the frequency of occurrence of these two cancers could not be explained by the intrinsic factors and suggested that extrinsic factors may be at play (Wu et al., 2015). It has further been proposed that prostate cancer not be selected against as it is typically a slow growing cancer with late onset. This idea is consistent with the theory of antagonist pleiotrophy put forth by Williams (1957), the theory that evolution by natural selection favors certain favor traits during the reproductive years at the expense of organismal integrity.

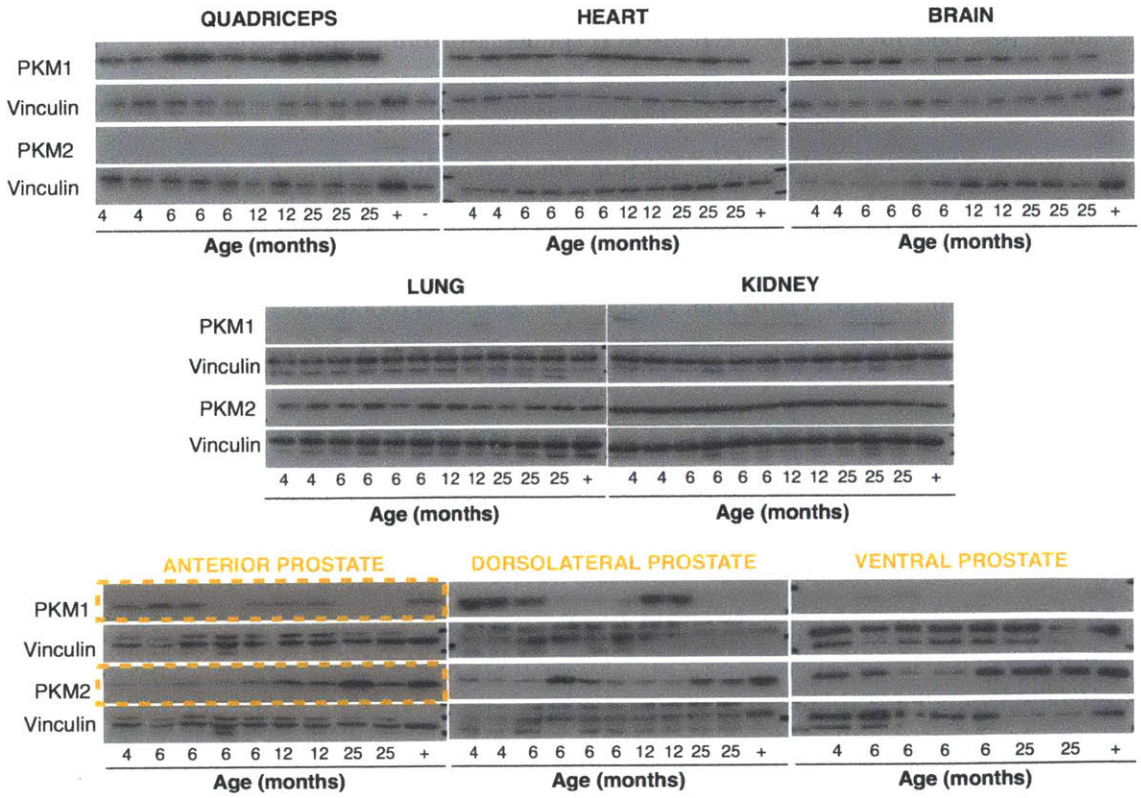

Figure 6.3. PK isoform expression as a function of age in mouse tissues. Western blot with antibodies to isoforms of pyruvate kinase. Antibody to vinculin used as a loading control. Individual lanes are from the tissue of an individual animal in the indicated tissue time point.

The synthesis of Nordling's and Williams' hypotheses forms the basis of a question to address prostate cancer prevalence in aged males: do natural physiological processes change as a function of the normal aging process to promote specific cancers? Central to Nordling's hypothesis was that age-related changes in hormone levels could also be responsible for altered physiology and could be mutagenic, such as in menopause and, in this case, andropause. The prostate is a highly specialized metabolic organ which produces citrate at a millimolar level. The degree of specialization that occurs in this organ from the metabolic perspective is remarkable, and there are few examples of tissues that have such high-affinity transporters to move nutrients against a 1000-fold concentration difference (Costello and Franklin, 2000; Costello et al., 2005; Costello and Franklin, 2006). Is this metabolic specialization detrimental, or even carcinogenic, over time?

Interestingly, we observed that the prostate undergoes switching of isoform expression from Pkm1 to Pkm2 as a function of normal age (Figure 6.3). This data was striking and unexpected. In fact, isoform switching of pyruvate kinase from Pkm1 to Pkm2 with increasing organism age was noted in the prostate only. Whether this change in isoform expression is epiphenomenal or has a more causal role in prostate cancer frequency as a function of age connection requires more rigorous examination. However, the discordance in prostate cancer as compared to nearly any other tumor as a function of age has no current explanation and few other hypotheses exist to explain such a strong correlation. Taking advantage of the temporal control of *Pten* deletion using adeno-Cre and other genetic manipulations (Figure 6.2) could begin to address this question.

Systems approaches to whole animal physiology

Studies and modifications to isotope tracing methods *in vivo* will provide a powerful basis to answer questions that are not addressed by any existing methods. Textbook biochemistry does not apply to the physiological setting, and most enzymes are limited by reactants and products inside of the cell.

Complementary genetic manipulations to alter enzymatic activity in candidate enzymes based on predictions made from tracing patterns are essential to enable determination of causality.

The wealth of information in the post-genome sequencing era is astounding and ever-growing. There is surprisingly little known about the relationship between gene expression, metabolic fluxes, and metabolite concentrations at the organismal level (Figure 6.4 (Eissing et al., 2011; Uhlen et al., 2016)). Additionally, continued profiling efforts in mouse models and the effort to move towards rigorous quantitative physiology approaches will depend on a more complete understanding of metabolic pathways and networks at the whole organism level.

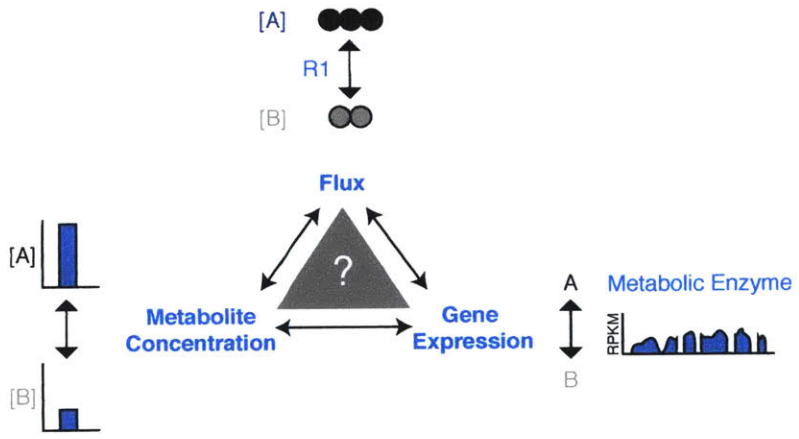

Figure 6.4. Integrating "-omics" information. Integrating information to better understand correlations between expression levels of enzymes, concentrations of metabolites, and fluxes in a the physiological setting is necessary. RNA-sequencing studies and expression levels at the RNA or protein level are not necessarily indicative of enzymatic activity, metabolite concentrations, or metabolic flux.

Figure 6.4

Circadian rhythm disruption

Epidemiological studies demonstrate that shift-workers exhibit higher incidences of cancer or exhibit worse prognosis (Megdal et al., 2005; Truong et al., 2014; Lis et al., 2003). In collaboration with Thales Papagiannakopolous and Tyler Jacks, we demonstrated that disruption of circadian rhythm causes both cell autonomous and non-cell autonomous changes in metabolism that ultimately lead

to accelerated cancer in the KP mouse model (Papagiannakopoulos et al., 2016). Experiments performed here demonstrate the importance of understanding the consequences of systemic changes in metabolism on the oncophenotypes of cancer. It is further interesting to speculate how circadian gene ablation in tumors themselves can cause this phenotype. We propose that circadian genes govern metabolic processes in coordination with c-Myc to exacerbate the tumor phenotype. Recent work further suggests that *CRY2*, a critical circadian gene, cooperates with FBXL3 to regulate degradation of c-Myc through ubiquitylation (Huber et al., 2016).

Beyond informing risk or prognosis, it is also apparent that circadian biology plays a role in determining cancer treatment regimens (Sahar and Sassone-Corsi, 2009). The importance of therapeutic timing has been best modeled in the setting radiation treatment (Leder et al., 2014). As metabolism is known to oscillate, and this has been extensively characterized through genetic knockout models in organs such as the liver (Eckel-Mahan and Sassone-Corsi, 2013; Adamovich et al., 2014; Van Potter et al., 1966), determining times of day where metabolite level changes may sensitize cancer cells to a treatment modality of interest could be exploited to optimize the therapeutic index.

Lifestyle and nutrition

Warburg and Schoeller proposed that cancer might be a nutritional problem and that cancer might be avoided by eating a natural diet (Otto, 2016). There is supporting evidence for this idea from a series of modern epidemiological and experimental studies. In one direction, high-fat diets seem almost universally to be correlated with worse cancer prognosis (Deslypere, 2012). In another, more complicated direction, calorie restriction appears to play opposing roles in different cancers (Hursting et al., 2009).

The increased relative risk of developing cancer has been observed to be elevated in overweight

and obese individuals, yet a paucity of generalized mechanistic bases for these correlations exist. We know little about the adipose organ (Rosen and Spiegelman, 2014). Large depots of adipose tissue found in obesity are often poorly vascularized and, similar to tumors, also exhibit HIF-1α (Ye, 2009; Trayhurn, 2013). These adipose depots also promote a high degree of inflammation which secretes cytokines. Other factors exist that inhibit the immune function or simply present a physical barrier that interferes with immune responses (Wellen and Hotamisligil, 2005; Hosogai et al., 2007). In line with this are findings in colon cancer from recent work from Beyaz et al. (2016) that demonstrates that high-fat diets maintain cells in a more stem-like state (Beyaz et al., 2016).

The specific sources of nutrients in tumors with respect to whole animal metabolism is poorly defined. Lipid synthesis in some contexts has been demonstrated to be limiting and indeed some tumors that are more dependent on scavenging lipids from the environment (Kamphorst et al., 2013). Careful *in vivo* metabolic accounting efforts that test cancer progression would be useful to establish a more causal relationship.

Calorie restriction is the only current known dietary intervention to extend lifespan in a conserved way from worms to mammals (Anderson et al., 2009). Studies in animals undergoing calorie restriction reveal opposing roles in tumor development or progression (Longo and Fontana, 2010). The mechanisms by which calorie restriction exert their life-extending benefits and prevent tumor initiation and progression in some instances are poorly understood (Tannenbaum, 1987). A recent review of this literature by the International Agency for Research on Cancer (IARC) concluded that evidence for this is sufficient to prevent either tumor initiation or progression in numerous cancers including breast, colon, liver, pancreas, skin, and pituitary but there was an inverse association (observation of worse prognosis) in models of prostate cancer, lymphomas, and leukemias (Secretan et al., 2016). All calories are not created equally and systematic studies to better understand this connection would require the examination of calorie restriction with defined

macronutrient profiles for each tumor type (Lee et al., 2015).

Metabolic link to metastatic cancer

Why is it that certain tumors exhibit a preference for distant sites? Of all processes in oncogenesis, metastatic colonization remains poorly described (Shibue and Weinberg, 2011). Two major hypotheses exist for the expansion of tumor cells to frank metastases that have extravasated, survived in circulation, and embedded themselves in a distant site. First, it is possible that metastatic tropisms arise as a result of physical constraints (e.g. blood or lymph vessel structure and physiology tending to concentrate cells at certain sites). Second, the "seed and soil" hypothesis, originally conceived by Stanley Paget (Paget, 1889). This hypothesis focuses on the biological and physical properties of the target organ (the "soil") rather than the metastatic cell (the "seed"). Paget hypothesized that the destination organ or environment of the metastatic cell has favorable conditions for the growth. While the first hypothesis is likely true for certain cases, particularly concerning sites where circulating tumor cells travel that may be immunoprotected (such as the brain, certain parts of the lung, and other distant sites) it fails to explain the majority of tropisms observed.

There is early evidence for a metabolic version of the seed and soil hypothesis at the level of metabolism, and this is best exemplified in an ovarian cancer model. They noted that ovarian metastases frequently colonize the omental fat and that this omental fat mobilizes fatty acids which serve as a nutrient source to the resulting metastasis (Nieman et al., 2011; Currie et al., 2013). To extend these findings, we ask how are tumor cells taking advantage of their environment? Do certain pathological features, such as desmoplasia is observed in pancreatic cancer (Schober et al., 2014), have any bearing on tumor metabolism? From the metabolic standpoint, and our demonstration that these cancer cells internalize fibronectin raises the possibility that these fibrotic

regions are potential contributors nutrient depots created by cancer cells, possibly in response to the absence of vasculature. The "seed and soil" hypothesis remains an attractive one that will require a rigorous and systematic study of modern-day analytical methods. This line of investigation will require an understanding of local nutrient concentrations at the metastatic organ and nutrient requirements of the eventual metastatic tumor.

Tumor heterogeneity

In the course of studying disaggregated breast tumors, Heppner and colleagues observed and isolated four distinct populations of cells based on morphology (Heppner, 1984) and this formed the basis of a hypothesis around the existence of tumor heterogeneity. Tumor heterogeneity can be used to describe different cell populations and also to describe spatial variations of oxygen and nutrients (Hensley et al., 2016). Examining tumor heterogeneity has proven to be a long-standing challenge in cancer biology and metabolism studies are no exception to these limitations (Alizadeh et al., 2015). Metabolic studies are further plagued by the rapid reactions that occur in central carbon metabolism. The instability of these metabolites results in quantitative changes on the order of seconds to minutes. These limitations have hindered the exploration of different cell populations in the tumor using conventional methodology such as FACS based assays. Therefore, there is a necessity to develop approaches and tools to understand the differences between cell types within a tumor at the level of metabolism. Recent efforts have shown great therapeutic promise in targeting not only malignant cells and cancer stem cells within a tumor, but other distinct cell populations (such as cancer associated fibroblasts and immune cells) that contribute to the overall plasticity and architecture of these cells.

The use of "retrobiosynthetic" approaches have been used extensively to study plant metabolism and recently has been extended in a flux modeling framework to study the consequences

of oncogenic *Myc* (Werner et al., 1997; Wiechert et al., 2001; Murphy et al., 2013). This approach interrogates the incorporation of labeled precursor substrates such as glucose or amino acids into macromolecules (Botezatu et al., 2011; Werner et al., 1997) and will allow for the utilization of tracing techniques as these macromolecular pools that are stable over an adequate period. Reverse engineering the labeling patterns in these stable macromolecular pools will allow for the use of traditional techniques, such as FACS, to separate populations from heterogeneous tumors containing multiple distinct populations of cells.

Given that solid tumors have a wide range of perfusion and that regional metabolic differences and dependencies may exist within these solid tumors (Alizadeh et al., 2015; Hickman et al., 2014), additional methods that expand the tracing studies presented here are required. The continued development of imaging mass spectrometry and other ambient ionization methods will enable more rigorous profiling of tumor heterogeneity.

Oncometabolites

Since the determination and involvement of 2-HG, succinate, and fumarate in cancer, few other *bona fide* oncometabolites or mutations in enzymes that result in neomorphic activity have been discovered (Yang et al., 2013; Sullivan et al., 2016). Are there other mutations similar to those found for IDH or mutations that cause altered levels of metabolites? A clear place to look would be to further characterize frequent mutations in metabolic enzymes in the cancer genome. This analysis would be best accompanied by a systematic determination of how different genetic variants impact enzymatic activity levels. Another possible approach includes the use of untargeted metabolomic techniques to determine whether there are metabolite species in cancer cells that do not exist in adjacent normal tissue. Strikingly, when we capture metabolite information from a single sample, there are tens-of-thousands of masses that represent individual metabolites or

metabolite species detected. Determining the identities and cataloging the number of chemical species in any given sample may enable further discovery of oncometabolites.

Do metabolites accumulate in cancer cells, which are frequently hypermetabolic? Of the more than 300 hypotheses that attempt to explain the biology of organismal aging, an interesting area of research that falls under the "wear and tear" hypothesis comes from a study by Gladyshev and colleagues (Avanesov et al., 2014). In this study, flies were fed equivalent nutrient sources and analyzed when they were young and when they were old. The generation of "un-metabolizable" products was observed, and it is postulated that these are error products that accumulate as a function of age. This accumulation of products that cannot be processed has been speculated to contribute to cellular damage over time. This hypothesis, and further understanding of which of these unprocessed metabolites are most damaging remain untested. This work has broad implications, as the spontaneous formation of metabolites is an area that has been under-explored due to limitations in technology.

To extend this idea to cancer, how many of these error products are carcinogenic or otherwise deleterious in the normal setting? A reasonable extension of the hypothesis by Gladyshev and colleagues would be that the accumulation of un-metabolizable products could occur preferentially in cancer cells as a function of hyper-consumption of glucose or other nutrients. A simple analysis to perform would be to determine how many different metabolites are in tumors at different stages of tumorigenesis. Whether or not the cancer metabolome is distinct from the normal metabolome regarding unique metabolite species and whether, if present, these contribute to oncogenic processes could be an exciting area of investigation.

Therapeutic synergy

A recent systematic review by Vernieri et al. (2016) discusses the connection between genetics, tumor metabolism, and systemic metabolism. The mechanism of action of many chemotherapies is unclear, and in many cases, how these drugs impact metabolic processes is unknown. While expression and activity can be different, few enzymes are unique to cancer cells. Therefore, it is essential to continue the development of studies that will enable us to modulate levels of key metabolites that will result in selective inhibition of the growth of cancer cells. Careful studies to determine the metabolic phenotypes in cancer cells and normal cells upon treatment with existing drugs may provide an additional therapeutic opportunity. Studies that harness both the physiologically appropriate conditions of a to-be-defined set of culture conditions will allow for the testing of nutrient combinations with drug combinations. These studies could manifest as therapeutic regimens by either identifying specific vulnerabilities and target them directly with small molecules or other agents or indirectly by manipulating diet or dosing regimens in combination with the conventional treatment.

Conclusion

Studies in metabolism have become a powerful tool for cancer research. Metabolomic efforts and stable isotope tracer studies are becoming more prevalent tools in the clinic and enable a better understanding of the metabolic vulnerabilities of individual tumors. To improve our understanding of cancer metabolism in a meaningful way, it will be critical to continue to develop and validate mouse models that recapitulate features of the human disease. With this information, new therapeutic strategies can be devised and tested rapidly and mechanisms of resistance more easily understood. Integrative approaches and cooperative efforts between scientists, engineers, and

physicians have enabled studying metabolism in real-time, and this knowledge is currently used to aid diagnosis, therapy, and procedures. These interdisciplinary approaches and continued cooperation are the true paths forward for finding cures for cancer.

References

Abeshouse A, Ahn J, Akbani R, Ally A, Amin S, et al. The molecular taxonomy of primary prostate cancer. *Cell* **163**, 1011 (2015).

Adamovich Y, Rousso-Noori L, Zwighaft Z, Neufeld-Cohen A, Golik M, et al. Circadian clocks and feeding time regulate the oscillations and levels of hepatic triglycerides. *Cell Metabolism* **19**, 319 (2014).

Alizadeh AA, Aranda V, Bardelli A, Blanpain C, Bock C, et al. Toward understanding and exploiting tumor heterogeneity. *Nature Medicine* **21**, 846 (2015).

Anderson RM, Shanmuganayagam D, Weindruch R. Caloric restriction and aging: studies in mice and monkeys. *Toxicological Pathology* **37**, 47 (2009).

Avanesov AS, Ma S, Pierce KA, ee Yim SH, heon Lee BC, et al. Age- and diet-associated metabolome remodeling characterizes the aging process driven by damage accumulation. *eLife* **3**, e02077 (2014).

Awad MM, Shaw AT. ALK inhibitors in non-small cell lung cancer: Crizotinib and beyond. *Clinical Advances in Hematology and Oncology* **12**, 429 (2014).

Beyaz S, Mana MD, Roper J, Kedrin D, Saadatpour A, et al. High-fat diet enhances stemness and tumorigenicity of intestinal progenitors. *Nature* **531**, 53 (2016).

Birsoy K, Possemato R, Lorbeer FK, Bayraktar EC, Thiru P, et al. Metabolic determinants of cancer cell sensitivity to glucose limitation and biguanides. *Nature* **508**, 108 (2014).

Birsoy K, Wang T, Chen WW, Freinkman E, Abu-Remaileh M, et al. An essential role of the mitochondrial electron transport chain in cell proliferation is to enable aspartate synthesis. *Cell* **162**, 540 (2015).

Botezatu L, Sievers S, Gama-Norton L, Schucht R, Hauser H, et al. Genetic Aspects of Cell Line Development from a Synthetic Biology Perspective. *Genomics and Systems Biology of Mammalian Cell Culture* 251–284 (2011).

Chen WW, Freinkman E, Wang T, Birsoy K, Sabatini DM. Absolute quantification of matrix metabolites reveals the dynamics of mitochondrial metabolism. *Cell* **166**, 1324 (2016).

Chen Z, Fillmore CM, Hammerman PS, Kim CF, Wong KK. Non-small-cell lung cancers: a heterogeneous set of diseases. *Nature Reviews Cancer* **14**, 535 (2014).

Cheng T, Sudderth J, Yang C, Mullen AR, Jin ES, et al. Pyruvate carboxylase is required for glutamine-independent growth of tumor cells. *Proceedings of the National Academy of Sciences* **108**, 8674 (2011).

Cho WJ, Oliveira DS, Najy AJ, Mainetti LE, Aoun HD, et al. Gene expression analysis of bone metastasis and circulating tumor cells from metastatic castrate-resistant prostate cancer patients. *Journal of Translational Medicine* **14**, 72 (2016).

Christen S, Lorendeau D, Schmieder R, Broekaert D, Metzger K, et al. Breast cancer-derived lung metastases show increased pyruvate carboxylase-dependent anaplerosis. *Cell Reports* **17**, 837 (2016).

Christofk HR, Vander Heiden MG, Harris MH, Ramanathan A, Gerszten RE, et al. The M2 splice isoform of pyruvate kinase is important for cancer metabolism and tumour growth. *Nature* **452**, 230 (2008a).

Christofk HR, Vander Heiden MG, Wu N, Asara JM, Cantley LC. Pyruvate kinase M2 is a phosphotyrosine-binding protein. *Nature* **452**, 181 (2008b).

Collisson EA, Campbell JD, Brooks AN, Berger AH, Lee W, et al. Comprehensive molecular profiling of lung adenocarcinoma. *Nature* **511**, 543 (2014).

Commisso C, Davidson SM, Soydaner-Azeloglu RG, Parker SJ, Kamphorst JJ, et al. Macropinocytosis of protein is an amino acid supply route in Ras-transformed cells. *Nature* **497**, 633 (2013).

Costello LC, Franklin RB. The intermediary metabolism of the prostate: a key to understanding the pathogenesis and progression of prostate malignancy. *Oncology* **59**, 269 (2000).

Costello LC, Franklin RB. The clinical relevance of the metabolism of prostate cancer; zinc and tumor suppression: connecting the dots. *Molecular Cancer* **5**, 17 (2006).

Costello LC, Franklin RB, Feng P. Mitochondrial function, zinc, and intermediary metabolism relationships in normal prostate and prostate cancer. *Mitochondrion* **5**, 143 (2005).

Currie E, Schulze A, Zechner R, Walther TC, Farese RV. Cellular fatty acid metabolism and cancer. *Cell Metabolism* **18**, 153 (2013).

Deslypere JP. Obesity and cancer outcome. *The Lancet* **379**, 1366 (2012).

Donehower LA, Lozano G. 20 years studying P53 functions in genetically engineered mice. *Nature Reviews Cancer* **9**, 831 (2009).

Eckel-Mahan K, Sassone-Corsi P. Metabolism and the circadian clock converge. *American Physiological Society* **93**, 107 (2013).

Eissing T, Kuepfer L, Becker C, Block M, Coboeken K, et al. A computational systems biology software platform for multiscale modeling and simulation: integrating whole-body physiology, disease biology, and molecular reaction networks. *Frontiers in Physiology* **FEB**, 4 (2011).

Fan TWM, Lane AN, Higashi RM, Farag MA, Gao H, et al. Altered regulation of metabolic pathways in human lung cancer discerned by (13)C stable isotope-resolved metabolomics (SIRM). *Molecular Cancer* **8**, 41 (2009).

Folch J, Lees M, Slone Stanley G. A simple method for the isolation and purification of total lipides from animal tissues. *Journal of Biological Chemistry* **226**, 497 (1956).

Gross MI, Demo SD, Dennison JB, Chen L, Chernov-Rogan T, et al. Antitumor activity of the glutaminase inhibitor CB-839 in triple-negative breast cancer. *Molecular Cancer Therapeutics* **13**, 890 (2014).

Gui DY, Lewis Ca, Vander Heiden MG. Allosteric regulation of PKM2 allows cellular adaptation to different physiological states. *Science Signaling* **6**, 1 (2013).

Gui DY, Sullivan LB, Luengo A, Hosios AM, Bush LN, et al. Environment dictates dependence on mitochondrial complex I for NAD+ and aspartate production and determines cancer cell sensitivity to metformin. *Cell Metabolism* **24**, 716 (2016).

Hensley CT, DeBerardinis RJ. In vivo analysis of lung cancer metabolism: nothing like the real thing. *Journal of Clinical Investigation* **125**, 495 (2015).

Hensley CT, Faubert B, Yuan Q, Lev-Cohain N, Jin E, et al. Metabolic heterogeneity in human lung tumors. *Cell* **164**, 681 (2016).

Heppner GH. Tumor heterogeneity. *Cancer Research* **44**, 2259 (1984).

Hickman JA, Graeser R, de Hoogt R, Vidic S, Brito C, et al. Three-dimensional models of cancer for pharmacology and cancer cell biology: Capturing tumor complexity in vitro/ex vivo. *Biotechnology Journal* **9**, 1115 (2014).

Hosogai N, Fukuhara A, Oshima K, Miyata Y, Tanaka S, et al. Adipose tissue hypoxia in obesity and its impact on adipocytokine dysregulation. *Diabetes* **56**, 901 (2007).

Huber AL, Papp SJ, Chan AB, Henriksson E, Jordan SD, et al. CRY2 and FBXL3 cooperatively degrade c-MYC. *Molecular Cell* **64**, 774 (2016).

Hursting SD, Smith SM, Lashinger LM, Harvey AE, Perkins SN. Calories and carcinogenesis: lessons learned from 30 years of calorie restriction research. *Carcinogenesis* **31**, 83 (2009).

Kamphorst JJ, Cross JR, Fan J, de Stanchina E, Mathew R, et al. Hypoxic and Ras-transformed cells support growth by scavenging unsaturated fatty acids from lysophospholipids. *Proceedings of the National Academy of Sciences* **110**, 8882 (2013).

Knudson AG. Mutation and cancer: statistical study of retinoblastoma. *Proceedings of the National Academy of Sciences* **68**, 820 (1971).

Leder K, Pitter K, Laplant Q, Hambardzumyan D, Ross BD, et al. Mathematical modeling of pdgf-driven glioblastoma reveals optimized radiation dosing schedules. *Cell* **156**, 603 (2014).

Lee D, Hwang W, Artan M, Jeong DE, Lee SJ. Effects of nutritional components on aging. *Aging Cell* **14**, 8 (2015).

Lewis CA, Parker SJ, Fiske BP, McCloskey D, Gui DY, et al. Tracing compartmentalized NADPH metabolism in the cytosol and mitochondria of mammalian cells. *Molecular cell* **55**, 253 (2014).

Lewis WH. Pinocytosis by malignant cells. *Cancer Research* **29**, 666 (1937).

Lis CG, Grutsch JF, Wood P, You M, Rich I, et al. Integrative cancer therapies circadian timing in cancer treatment: for an integrative approach. *Integrative Cancer Therapies* **2**, 105 (2003).

Longo VD, Fontana L. Calorie restriction and cancer prevention: metabolic and molecular mechanisms. *Trends in Pharmacological Sciences* **31**, 89 (2010).

Lunt SY, Muralidhar V, Hosios AM, Israelsen WJ, Gui DY, et al. Pyruvate kinase isoform expression alters nucleotide synthesis to impact cell proliferation. *Molecular Cell* **57**, 95 (2015).

Maddalo D, Manchado E, Concepcion CP, Bonetti C, Vidigal JA, et al. In vivo engineering of oncogenic chromosomal rearrangements with the CRISPR/Cas9 system. *Nature* **516**, 423 (2014).

Maher EA, Marin-Valencia I, Bachoo RM, Mashimo T, Raisanen J, et al. Metabolism of [U-13C]glucose in human brain tumors in vivo. *NMR in Biomedicine* **25**, 1234 (2012).

Marin-Valencia I, Yang C, Mashimo T, Cho S, Baek H, et al. Analysis of tumor metabolism reveals mitochondrial glucose oxidation in genetically diverse human glioblastomas in the mouse brain in vivo. *Cell Metabolism* **15**, 827 (2012).

Mattaini KR, Sullivan MR, Vander Heiden MG. The importance of serine metabolism in cancer. *Journal of Cell Biology* **214**, 249 (2016).

Mayers JR, Vander Heiden MG. Famine versus feast: understanding the metabolism of tumors in vivo. *Trends in Biochemical Sciences* **40**, 130 (2015).

Megdal SP, Kroenke CH, Laden F, Pukkala E, Schernhammer ES. Night work and breast cancer risk: a systematic review and meta-analysis. *European Journal of Cancer* **41**, 2023 (2005).

Mullarky E, Lucki NC, Beheshti R, Anglin JL, Gomes AP, et al. Identification of a small molecule inhibitor of 3-phosphoglycerate dehydrogenase to target serine biosynthesis in cancers. *Proceedings of the National Academy of Sciences* **113**, E1585 (2016).

Murphy TA, Dang CV, Young JD. Isotopically nonstationary 13C flux analysis of Myc-induced metabolic reprogramming in B-cells. *Metabolic Engineering* **15**, 206 (2013).

Nieman KM, Kenny HA, Penicka CV, Ladanyi A, Buell-Gutbrod R, et al. Adipocytes promote ovarian cancer metastasis and provide energy for rapid tumor growth. *Nature Medicine* **17**, 1498 (2011).

Otto AM. Warburg effect(s)-a biographical sketch of Otto Warburg and his impacts on tumor metabolism. *Cancer & Metabolism* **4**, 5 (2016).

Pacold ME, Brimacombe KR, Chan SH, Rohde JM, Lewis CA, et al. A PHGDH inhibitor reveals coordination of serine synthesis and one-carbon unit fate. *Nature Chemical Biology* **12**, 452 (2016).

Paget S. The distribution of secondary growths in cancer of the breast. *The Lancet* **133**, 571 (1889).

Pan M, Reid MA, Lowman XH, Kulkarni RP, Tran TQ, et al. Regional glutamine deficiency in tumours promotes dedifferentiation through inhibition of histone demethylation. *Nature Cell Biology* **18**, 1090 (2016).

Papagiannakopoulos T, Bauer MR, Davidson SM, Heimann M, Subbaraj L, et al. Circadian rhythm disruption promotes lung tumorigenesis. *Cell Metabolism* **24**, 324 (2016).

Qian Y, Wang X, Li Y, Cao Y, Chen X. Extracellular ATP a new player in cancer metabolism: NSCLC cells internalize ATP in vitro and in vivo using multiple endocytic mechanisms. *American Association for Cancer Research* **14**, 1087 (2016).

Robinson D, Van Allen EM, Wu YM, Schultz N, Lonigro RJ, et al. Integrative clinical genomics of advanced prostate cancer. *Cell* **161**, 1215 (2015).

Rosen ED, Spiegelman BM. What we talk about when we talk about fat. *Cell* **156**, 20 (2014).

Rothschild MA, Oratz M, Schrieber SS. Regulation of albumin metabolism. *Annual Review of Medicine* **26**, 91 (1975).

Sahar S, Sassone-Corsi P. Metabolism and cancer: the circadian clock connection. *Nature Reviews Cancer* **9**, 886 (2009).

Sayin VI, Ibrahim MX, Larsson E, Nilsson Ja, Lindahl P, et al. Antioxidants accelerate lung cancer progression in mice. *Science Translational Medicine* **6**, 221ra15 (2014).

Schilling U, Friedrich EA, Sinn H, Schrenk HH, Clorius JH, et al. Design of compounds having enhanced tumour uptake, using serum albumin as a carrier. Part I. *Nuclear Medicine and Biology* **19**, 685 (1992).

Schober M, Jesenofsky R, Faissner R, Weidenauer C, Hagmann W, et al. Desmoplasia and chemoresistance in pancreatic cancer. *Cancers* **6**, 2137 (2014).

Secretan BL, Ph D, Scoccianti C, Ph D, Loomis D, et al. Body fatness and cancer — viewpoint of the IARC working group. *The New England Journal of Medicine* **375**, 794 (2016).

Sellers K, Fox MP, Ii MB, Slone SP, Higashi RM, et al. Pyruvate carboxylase is critical for non-small-cell lung cancer proliferation. *The Journal of Clinical Investigation* **125**, 687 (2015).

Shibue T, Weinberg RA. Metastatic colonization: settlement, adaptation, and propagation of tumor cells in a foreign tissue environment. *Seminars in Cancer Biology* **21**, 99 (2011).

Soda M, Choi YL, Enomoto M, Takada S, Yamashita Y, et al. Identification of the transforming EML4-ALK fusion gene in non-small-cell lung cancer. *Nature* **448**, 561 (2007).

Sullivan LB, Gui DY, Heiden MGV. Altered metabolite levels in cancer: implications for tumour biology and cancer therapy. *Nature Reviews Cancer* **16**, 680 (2016).

Sullivan LB, Gui DY, Hosios AM, Bush LN, Freinkman E, et al. Supporting aspartate biosynthesis is an essential function of respiration in proliferating cells. *Cell* **162**, 552 (2015).

Swanson JA, Watts C. Macropinocytosis. *Trends in Cell Biology* **5**, 424 (1995).

Tannenbaum A. The initiation and growth of tumors. *Nutrition Reviews* **45**, 20 (1987).

Tomasetti C, Vogelstein B. Variation in cancer risk among tissues can be explained by the number of stem cell divisions. *Science* **347**, 78 (2015).

Trayhurn P. Hypoxia and adipose tissue function and dysfunction in obesity. *Physiological Reviews* **93**, 1 (2013).

Truong T, Liquet B, Menegaux F, Plancoulaine S, Laurent-Puig P, et al. Breast cancer risk, nightwork, and circadian clock gene polymorphisms. *Endocrine-Related Cancer* **21**, 629 (2014).

Uhlen M, Hallstro m BM, Lindskog C, Mardinoglu A, Ponten F, et al. Transcriptomics resources of human tissues and organs. *Molecular Systems Biology* **12**, 862 (2016).

Unni AM, Lockwood WW, Zejnullahu K, Lee-Lin SQ, Varmus H. Evidence that synthetic lethality underlies the mutual exclusivity of oncogenic KRAS and EGFR mutations in lung adenocarcinoma. *eLife* **4**, 1 (2015).

Van Potter R, Gebert RA, Pitot HC, Peraino C, Lamar C, et al. Systematic oscillations in metabolic activity in rat liver and in hepatomas I. Morris hepatoma No. 7793. *Cancer Research* **26**, 1547 (1966).

Venneti S, Dunphy MP, Zhang H, Pitter KL, Zanzonico P, et al. Glutamine-based PET imaging facilitates enhanced metabolic evaluation of gliomas in vivo. *Science Translational Medicine* **7**, 1 (2015).

Vernieri C, Casola S, Foiani M, Pietrantonio F, de Braud F, et al. Targeting cancer metabolism: dietary and pharmacologic interventions. *Cancer Discovery* **6**, 1315 (2016).

Warburg O. On the origin of cancer cells. *Science* **123**, 309 (1956).

Wellen KE, Hotamisligil GS. Inflammation, stress, and diabetes. *The Journal of Clinical Investigation* **115**, 1111 (2005).

Werner I, Bacher A, Eisenreich W. Retrobiosynthetic NMR studies with C-labeled glucose. *Journal of Biological Chemistry* **272**, 25474 (1997).

Wiechert W, Mo M, Petersen S, de Graaf Aa. A universal framework for 13C metabolic flux analysis. *Metabolic engineering* **3**, 265 (2001).

Williams GC. Pleiotroy, natural-selection, and the evolution of senescence (1957).

Wu S, Powers S, Zhu W, Hannun YA. Substantial contribution of extrinsic risk factors to cancer development. *Nature* **529**, 43 (2015).

Yang M, Soga T, Pollard PJ, Yang M, Soga T, et al. Oncometabolites: linking altered metabolism with cancer. *Journal of Clinical Investigation* **123**, 3652 (2013).

Ye J. Emerging role of adipose tissue hypoxia in obesity and insulin resistance. *International Journal of Obesity* **33**, 54 (2009).

Yuneva MO, Fan TWM, Allen TD, Higashi RM, Ferraris DV, et al. The metabolic profile of tumors depends on both the responsible genetic lesion and tissue type. *Cell Metabolism* **15**, 157 (2012).

Appendix A

Supplementary Figures

This section contains supplementary details for Chapter 2. Supplemental tables omitted for space consideration.

Author statement

Some passages and figures have been adapted or quoted verbatim from the following published article:
Davidson, SM, Papagiannakopoulos, T, Olenchock, BA, Heyman, JE, Keibler, MA, Luengo, A, Vander Heiden, MG (2016). Environment impacts the metabolic dependencies of ras-driven non-small cell lung cancer. Cell Metabolism, 23(3), 517–528.

Authors

Shawn M. Davidson[1,2,3], Thales Papagiannakopoulos[1], Benjamin A. Olenchock[1,3,4], Julia E. Heyman[1], Mark A. Keibler[5], Alba Luengo[1,2], Matthew R. Bauer[1], Abhishek K. Jha[6], James P. O'Brien[1], Kerry A. Pierce[3], Dan Y. Gui[1], Lucas B. Sullivan[1], Thomas M. Wasylenko[5], Lakshmipriya Subbaraj[1], Christopher R. Chin[1], Gregory Stephanopolous[5], Bryan T. Mott[7], Tyler Jacks[1,2], Clary B. Clish[3], and Matthew G. Vander Heiden[1,2,3,8]

Author affilations

1. Koch Institute for Integrative Cancer Research, Massachusetts Institute of Technology, Cambridge, Massachusetts, USA
2. Department of Biology, Massachusetts Institute of Technology, Cambridge, Massachusetts, USA.
3. Broad Institute of MIT and Harvard University, Cambridge, Massachusetts, USA.
4. Division of Cardiovascular Medicine, Department of Medicine, The Brigham and Women's Hospital, Boston, MA 02115, USA
5. Department of Chemical Engineering, Massachusetts Institute of Technology, Cambridge, Massachusetts, USA.
6. Elucidata Corporation, Cambridge MA 02139.
7. National Center for Advancing Translational Sciences, NIH, Bethesda, Maryland, USA.
8. Dana-Farber Cancer Institute, Boston, Massachusetts, USA.

Author contributions

Conceptualization: S.M.D, T.P., B.A.O., M.G.V.H. Methodology: S.M.D, T.P., B.A.O., M.A.K., A.L., Formal Analysis: S.M.D., T.P., A.L. Investigation: J.E.H., A.L., J.P.O, M.R.B., A.K.J., J.P.O., K.A.P., D.Y.G., L.B.S., T.M.W., L.S., C.R.C. Writing: S.M.D., M.G.V.H. Visualization: S.M.D. Supervision: T.J., C.B.C., M.G.V.H. Funding Acquisition: S.M.D., B.A.O., M.G.V.H.

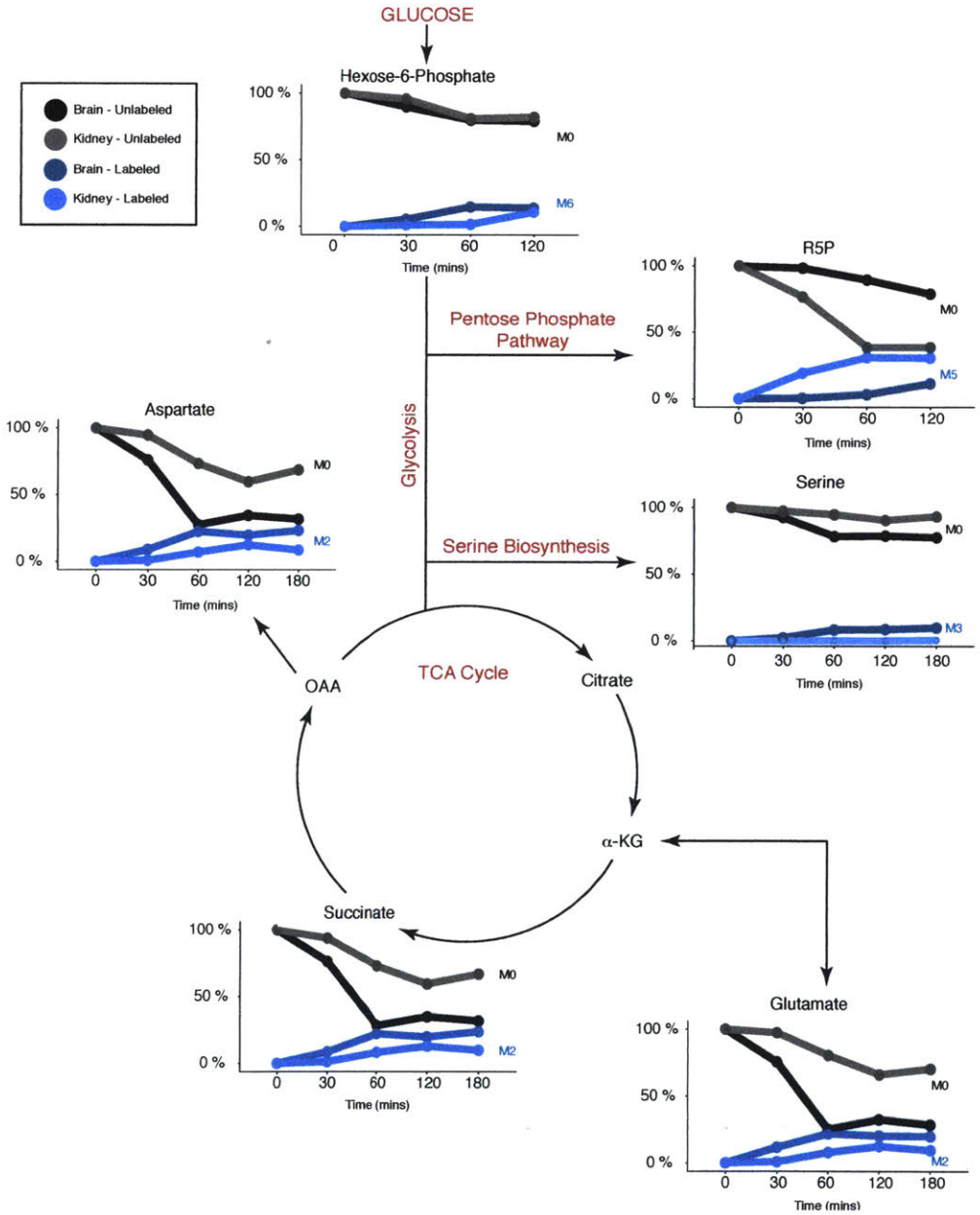

Figure A1. Infusion of stable isotope labeled glucose results in isotopic steady state across pathways in the indicated tissue samples, related to Figure 2.1. Tissue metabolites of time from animals infused with [U-^{13}C]glucose. The unlabeled species and the dominant expected isotopomer of the indicated metabolite from brain and kidney are displayed.

Figure A1

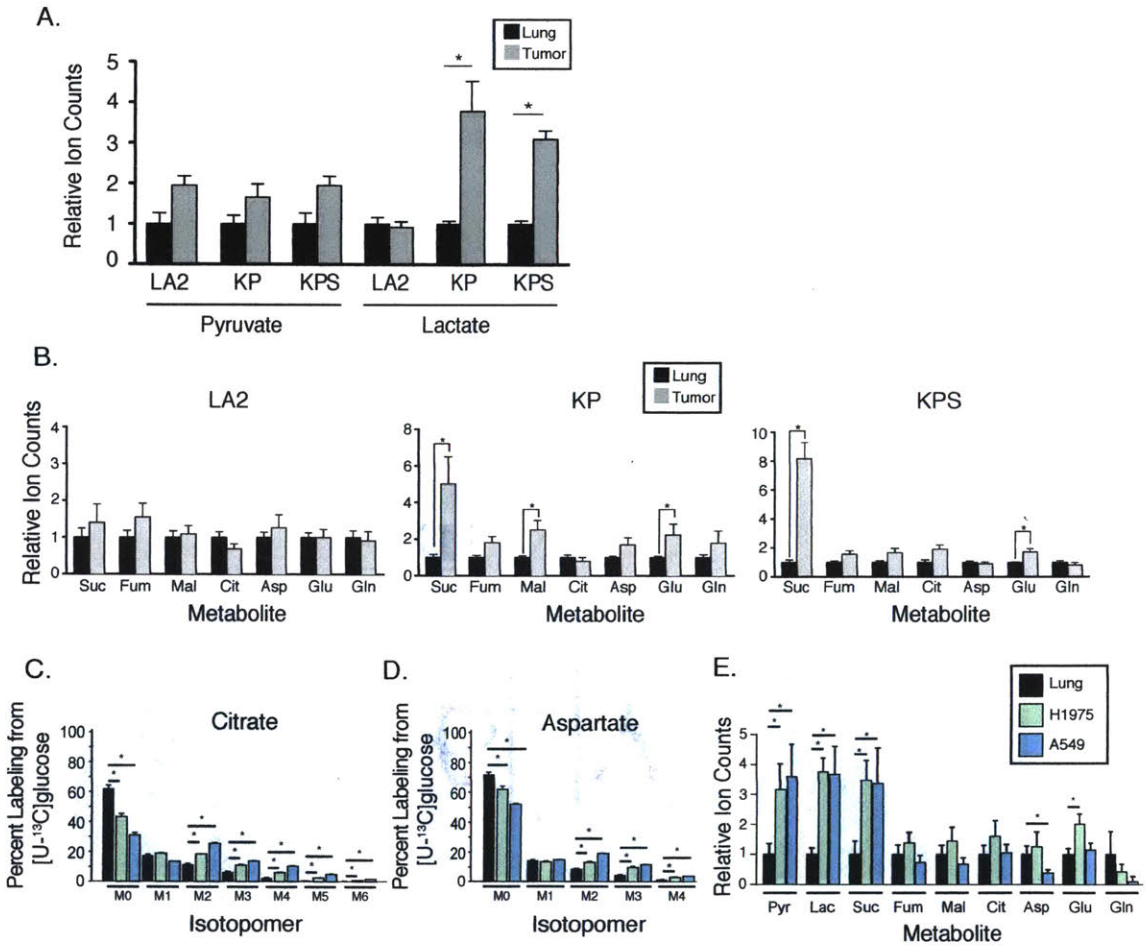

Figure A2. Relative metabolite concentrations and extended isotopomer distributions of xenograft tumors, related to Figure Figure 2.2 (A) Relative abundance of intracellular pyruvate and lactate in lung (black) and adjacent tumor (grey) for the indicated lung tumor models (LA2, n = 8; KP, n = 12; KPS, n = 12). Significantly different values as determined by two-tailed T-test are marked with a *, $p < 0.05$. All values shown represent mean ±SEM. (B) Relative abundance of measured intracellular metabolites in lung (black) and adjacent tumor (grey) for the indicated lung tumor models (LA2, n = 8; KP, n = 12; KPS, n = 12). Significantly different values as determined by two-tailed T-test are marked with a *, $p < 0.05$. All values shown represent mean ±SD. (C, D) Mass-isotopomer distribution of metabolites of citrate (Cit) and aspartate (Asp) following 6-hour [U-^{13}C]glucose infusion in lung (black) and xenografted tumors H1975 (green) and A549 (blue). (Lung, n = 8; H1975, n = 8; A549, n = 8). Significantly different values as determined by two-tailed unpaired T-test are marked with a *, $p < 0.05$. All values are mean ±SEM. (E) Relative abundance of measured intracellular metabolites in lung (black) and xenografted tumors H1975 (green) and A549 (blue). (Lung, n = 8; H1975, n = 8; A549, n = 8). Significantly different values as determined by two-tailed T-test are marked with a *, $p < 0.05$. All values shown represent mean ±SD unless otherwise indicated.

Figure A2

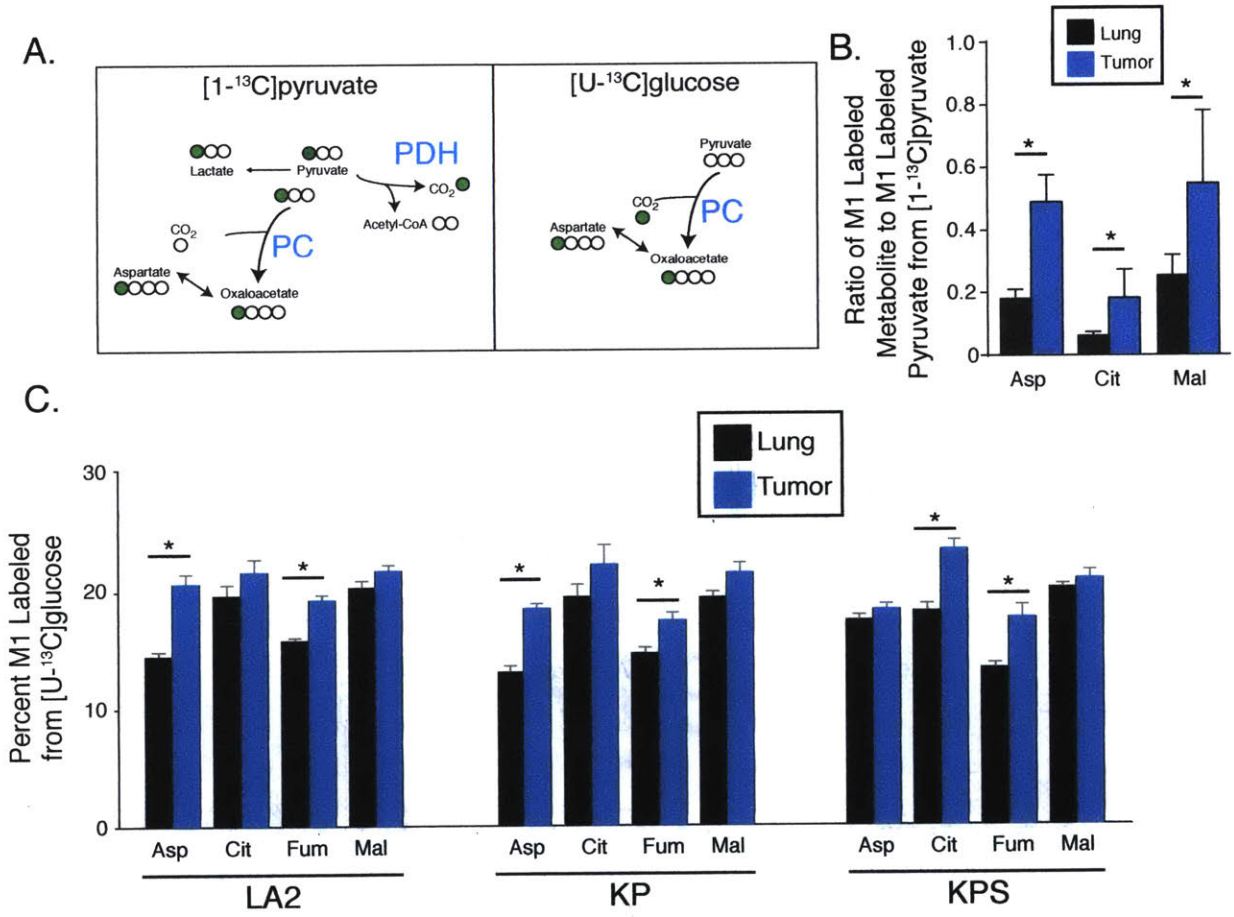

Figure A3. Assessment of pyruvate carboxylase flux into the TCA cycle using U-^{13}C glucose and 1-^{13}C pyruvate tracers, related to Figure 2.4 (A) Schematic showing isotope transitions expected from [1-^{13}C]pyruvate to oxaloacetate and from unlabeled pyruvate incorporating a labeled CO2 derived from [U-^{13}C]glucose through PC. (B) Ratio of intratumoral M1 isotopomers of aspartate (Asp), citrate (Cit), and malate (Mal) to M1 labeled pyruvate in lung (black) and KP tumor (blue) following infusion of [1-^{13}C]pyruvate. (Lung, n = 3; KP tumor n=4). Significantly different values as determined by two-tailed unpaired T-test are marked with a *, $p < 0.05$. All values are mean ±SD. (C) M1 mass-isotopomers of metabolites of aspartate (Asp), citrate (Cit), fumarate (Fum) and malate (Mal) in lung tissue (black) and tumor tissue (blue) following 6-hour [U-^{13}C]glucose infusion. (LA2, n = 4; KP, n = 6; KPS, n = 5). Significantly different values as determined by two-tailed unpaired T-test are marked with a *, $p < 0.05$. All values are mean ±SEM.

Figure A3

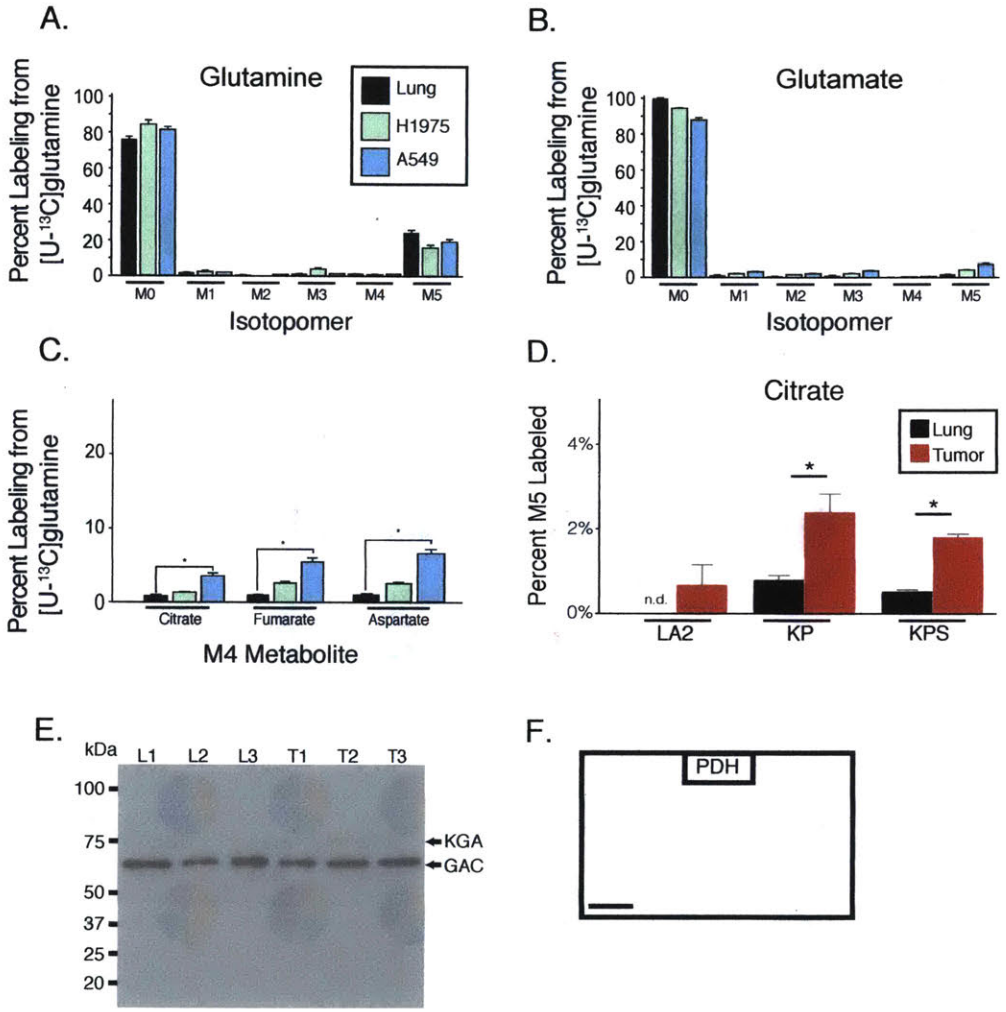

Figure A4. Limited glutamine catabolism by xenografted tumors and evidence for reductive carboxylation in tumors from ^{13}C glutamine infusion, related to Figure 2.6 (A,B) Mass-isotopomer distribution of glutamine and glutamate in lung tissue (black) and xenograft tissue (H1975, green; A549, blue) following 6-hour [U-^{13}C]glutamine infusion. (Lung n=7, A549 n=6, H1975 n=8). Mean glutamine enrichment was 34.3 (±3.7%). Significantly different values as determined by two-tailed paired T-test are marked with a *, $p < 0.05$. All values are mean ±SEM. (C) Labeled M4 mass-isotopomer of citrate, fumarate, and aspartate in lung (black) and tumor tissue (H1975, green; A549, blue) following 6-hour [U-^{13}C]glutamine infusion. Significantly different values as determined by two-tailed paired T-test are marked with a *, $p < 0.05$. All values are mean ±SEM. (D) Labeled M5 mass-isotopomer of citrate in lung tissue (black) and the indicated tumor tissue (red) following 6-hour [U-^{13}C]glutamine infusion. n.d. indicates that the isotopomer was not detected. (LA2, n = 4; KP, n = 4; KPS, n = 4). Significantly different values as determined by two-tailed paired T-test are marked with a *, $p < 0.05$. All values are mean ±SEM. (E) Western blot analysis of glutaminase (Gls1) expression in three representative KP lung tumors (Tumor) and normal lung tissue from three mice (Lung). Full blot presented to determine if either splice isoform of Gls1, KGA (predicted MW: 75kDa) and GAC (predicted MW: 65kDa), is expressed. (F) Representative IHC analysis of Pdha1 expression in KP lung tumors and adjacent normal lung tissue.

Figure A4

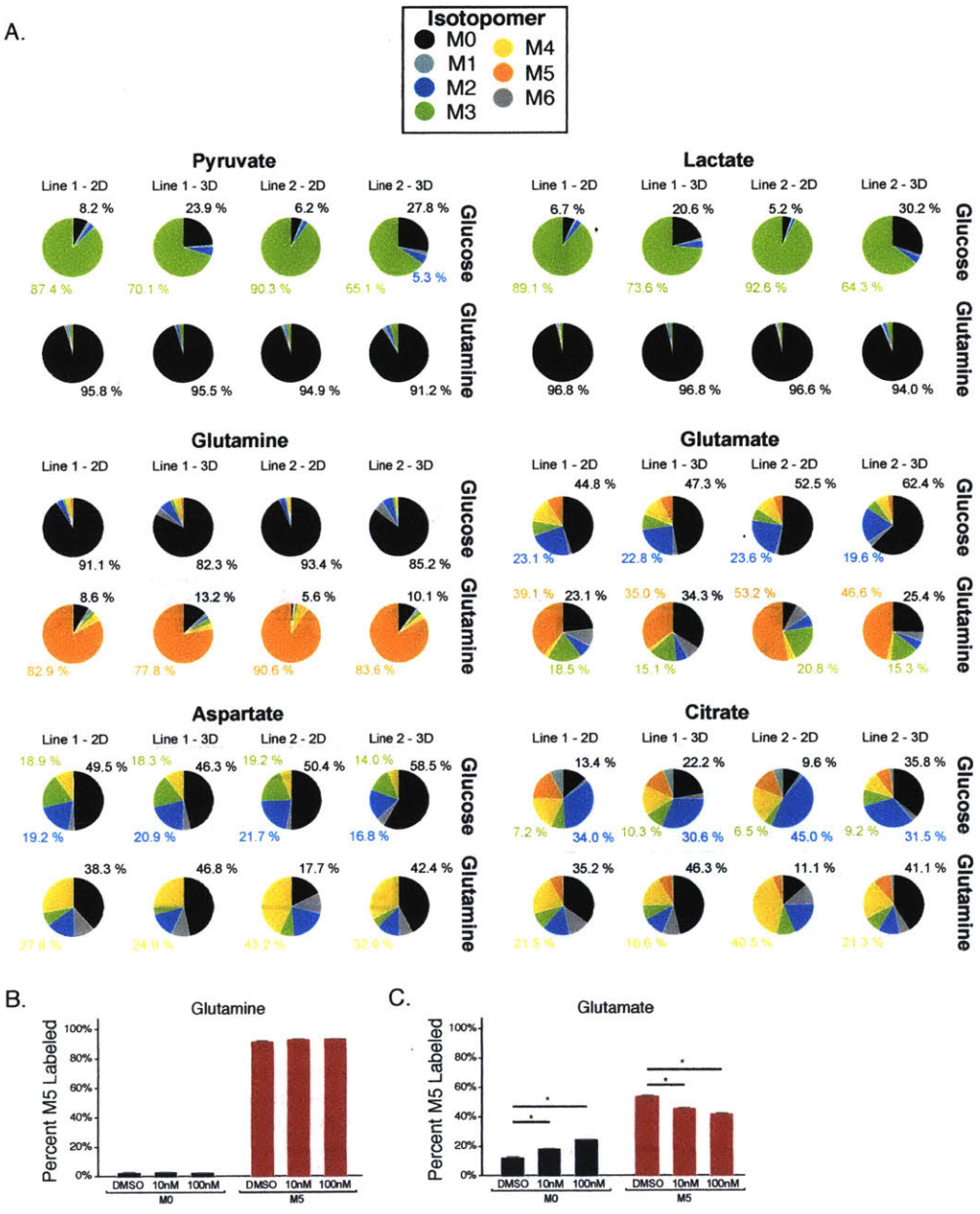

Figure A5. Glucose and glutamine metabolism by lung cancer cells in 3D culture, related to Figure 2.4. (A) Labeling of central carbon metabolites from [U-^{13}C]glucose or [U-^{13}C]glutamine (rows) from KP lung cancer cells cultured in standard cell culture conditions (2D) or in matrigel (3D). The numerical percent labeling is color coded by isotopomer for major isotopomer species, (n=3). (B,C) The unlabeled M0 and fully labeled M5 isotopomers of glutamine (B) and glutamate (C) from KP-derived lung cancer cells treated with DMSO, 10 nM CB-839 (10 nM), or 100 nm CB-839 (100 nM) are shown.

Figure A5

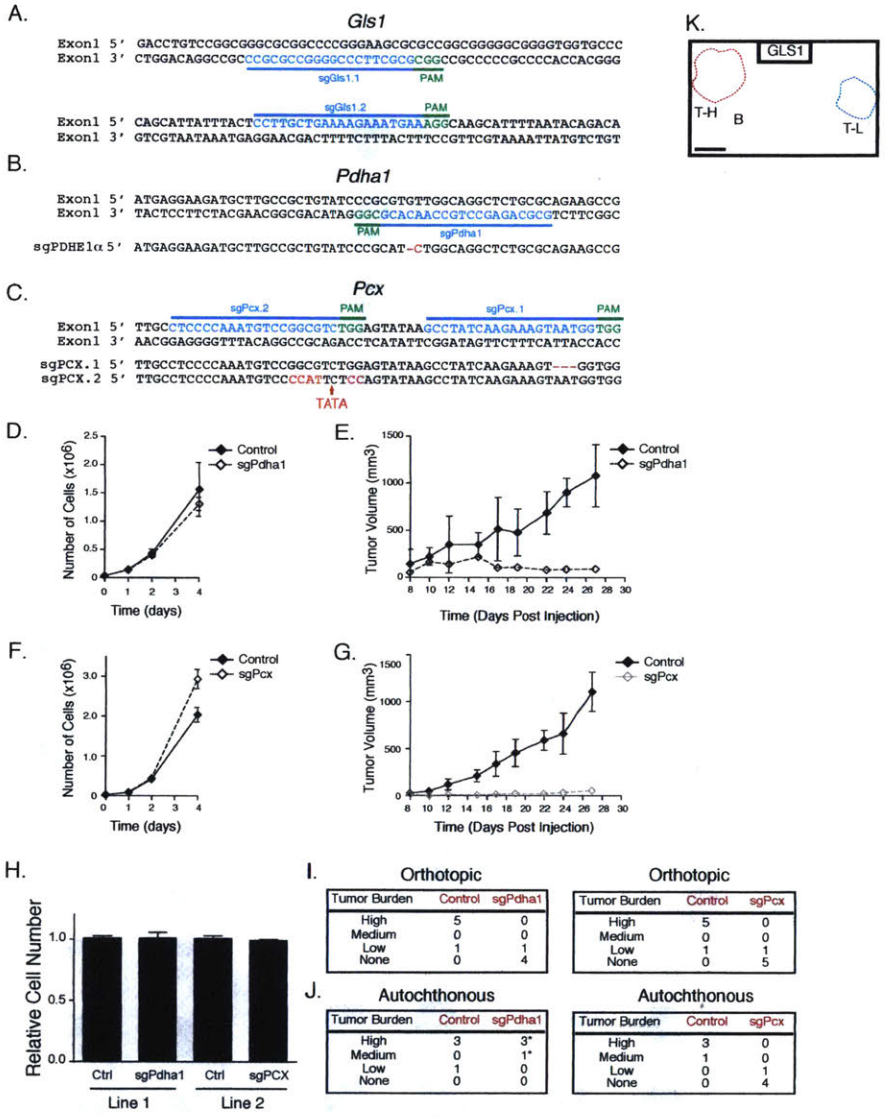

Figure A6. Targeted gene disruption with CRISPR/Cas9 and effect on cell proliferation and tumor growth, related to Figure 2.6 (A-C), sgRNA design and representative sequencing results showing mutations introduced into isogenic cell lines where Pdha1, Pcx, Gls1 are disrupted (guide sequence, blue; protospacer adjacent motif (PAM), green; mutations, red). (D-E) Cell numbers over time of a Control and sgPdha1 targeted KP cell line in culture (F) and tumor volume measurements over time of the same cell lines allografted into the flanks of C57Bl/6J mice (G). Data shown are the mean ±SEM (n = 4/cell line). (F-G) Cell numbers over time of a Control and sgPcx targeted KP cell line in culture (D) and tumor volume measurements over time of the same cell lines allografted into the flanks of C57Bl/6J mice (E). Data shown are the mean ±SEM (n = 4/cell line). (H) Relative tumor burden from orthotopic transplants from control, sgPdha1, and sgPcx or cell lines in the lungs of nu/nu and C57Bl/6J mice. Data are based on relative tumor area. (I) KP lung cancer cells with or without disruption of Pdha1 or Pcx were cultured in matrigel and relative cell numbers assessed after 48 hours (n=3). (J) Relative tumor burden from autochthonous pSECC experiments from control, sgPdha1 and sgPcx. Data are based on relative tumor area. * denotes that Pdha1 knockout was not observed and that the tumors responsible for the high burden observed in these models retained Pdha1 expression. (K) Representative IHC analysis of Gls1 expression after delivery of pSECC containing sgGls1 in KP lung tumors and adjacent normal lung tissue. Scale bar = 300μm. (T-H = Tumor High Gls1 Expression, T-L = Tumor Low Gls1 Expression, B = Bronchiole)..

Figure A6

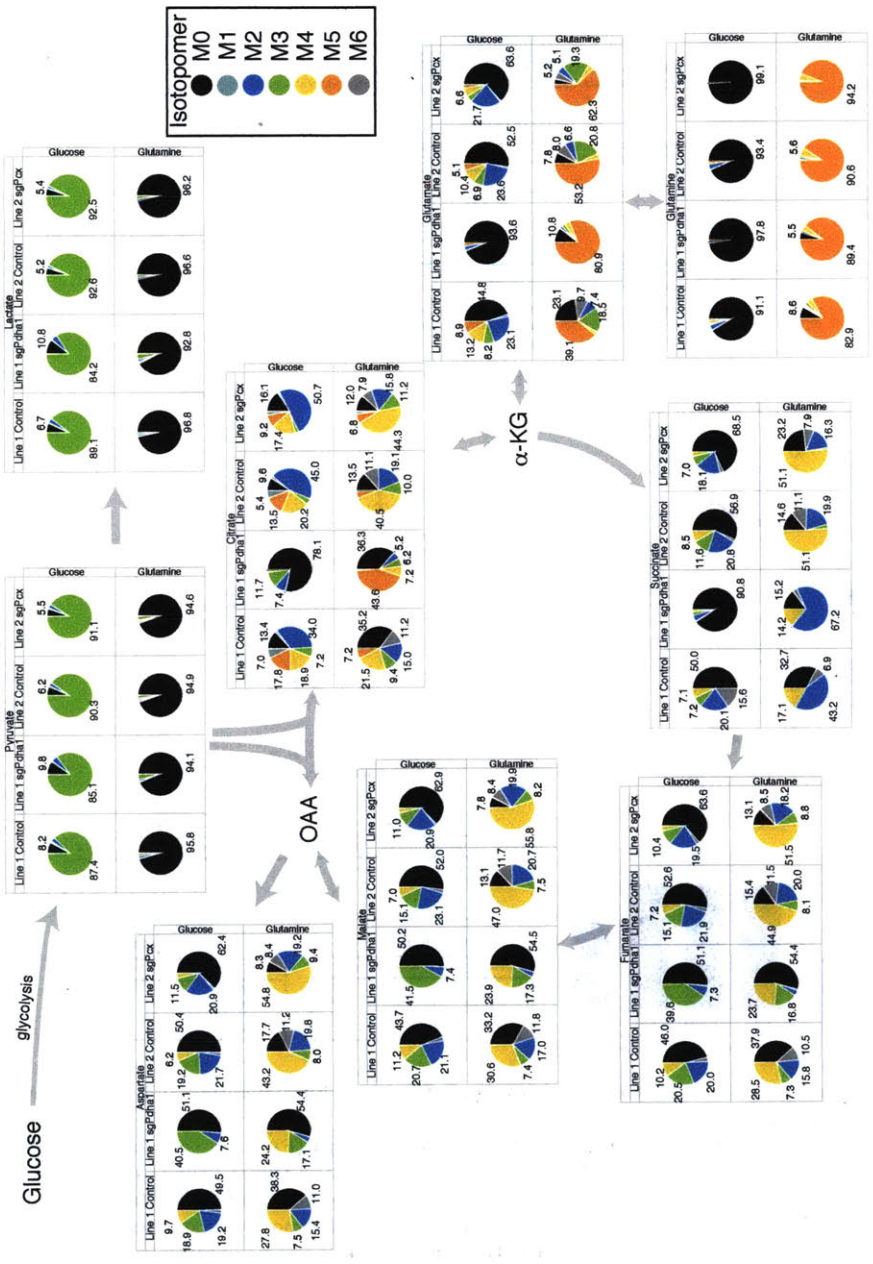

Figure A7. Targeted gene disruption with CRISPR/Cas9 and effect on cell proliferation and tumor growth, related to Figures Figure 2.6 and Figure 2.7. [U-^{13}C]glucose- and glutamine- isotopomers labeling of central carbon metabolites (columns, genetic alterations of either Control, sgPcx, or sgPdha1 cell lines; rows, stable isotope tracer of labeled glucose or glutamine and resulting isotopomers, n=3).

Figure A7

Supplementary Experimental Procedures

Mouse Lung Cancer Models

All animal studies were approved by the MIT Committee on Animal Care. For all studies, animals were placed randomly into groups before collecting data or administering treatments. Mice were housed under standard 12-hr light/dark cycles and fed RMH 3000 (Prolab) ad-libitum until 6-hours before infusions. For the LA2 model (Johnson et al., 2001) we used four to six-month old mice from a mixed 129/Sv and B6 genetic background. For KP mouse studies, we initiated tumors in two to six-month old mice from a mixed 129/Sv and B6 genetic background by intratracheal administration of $2.5x10^7$ PFU of adenovirus with Cre-recombinase (Gene Transfer Vector Core, University of Iowa). For allograft and xenograft studies, two to four month old C57Bl/6J or nu/nu mice were used.

Orthotopic/Allograft Induction in Mice

For orthotopic transplant tumors, cells were grown to 70 % confluence and resuspended in PBS. Cells were injected at a concentration of 7x104 cells/50µL intratracheally through a 25-gauge catheter to seed cell in the lung directly in 12 week C57Bl/6J (Line 1) or nu/nu (Line 2) mice. For allograft tumors, cells were grown to 70 % confluence and resuspended in PBS. These were injected at $2x10^5$/100µL in flanks of C57Bl/6J (Line 1) or nu/nu (Line 2) mice. Tumor growth in allograft flanks were measured with calipers and volumes estimated with the formula $(\pi/6)(L \times W2)$. Graphs with identical control curves represent experiments performed in parallel in the same cohort of mice.

Glucose and Glutamine Infusions in Mice

Arterial and venous catheters were surgically implanted into the jugular veins and/or carotid artery of normal or tumor bearing animals 3-4 days prior to infusions. Animals were fasted for 6-hrs

(morning fast) and infusions were performed in free-moving, conscious animals at 1:00pm for all studies to minimize metabolic changes associated with circadian rhythm. A constant infusion of [U-^{13}]glucose (30mg/kg/min, unless otherwise specified to be 20mg/kg/min) or [U-^{13}]glutamine (LA2 tumor-bearing mice infused at 2.0mg/kg/min, KP, KPS, and xenografted A549 and H1975 tumor-bearing mice infused at 3.7mg/kg/min) (Cambridge Isotopes Laboratories) was administered for a 6-hour duration. Animals were terminally anesthetized with 120mg/kg sodium pentobarbital and all tissues were harvested in less than 5 minutes. Following microdissection, tumors and adjacent lung tissue was rapidly frozen using a BioSqueezer (BioSpec Products) to ensure rapid quenching of metabolism. Tissues were stored at -80° and subsequently processed for metabolite extraction and analysis.

Cell Culture

Cell lines from tumors arising from the KP lung cancer model were established by digestion of tumors in collagenase IV/dispase for 30 min at 37°C in 1mL of trypsin and propagated in DMEM without pyruvate containing 10 % FBS, 2mM glutamine, 100U/mL penicillin, 100µg/uL streptomycin at 21 % oxygen. Isogenic clones were selected for comparison of CRISPR cell lines. For labeling studies and MFA, cells were seeded at an initial density of 150,000 cells/well in DMEM and changed to glucose or glutamine-free DMEM and grown for 24 hours in media containing 17.5mmol/L [U-^{13}C]glucose, [1,2-^{13}C]glucose, or 4mmol/L [U-^{13}C]glutamine (Cambridge Isotopes Laboratories). For labeling in 3D culture, cells were seeded at an initial density of 150,000 cells/well of Low Adherence plates (Corning) in DMEM + 2 % matrigel and changed to glucose or glutamine-free DMEM and grown for 24 hours in media containing 17.5mmol/L [U-^{13}C]glucose, [1,2-^{13}C]glucose, or 4mmol/L [U-^{13}C]glutamine (Cambridge Isotopes Laboratories). Cells in 3D were quantified using CellTiter-Glo (Promega) after establishing intracellular ATP concentration is linear with cell number.

Metabolite Extractions

Tissues were weighed (wet tissue weight) and homogenized cryogenically (Retsch Cryomill). Metabolites were extracted from tissues weighing between 10-40mg in a chloroforom:methanol:water extraction solution at a volume ratio of 400:600:300. Samples were vortexed and centrifuged at 10,000 xg for 10min to separate aqueous and organic layers. Polar metabolites were dried under nitrogen gas and frozen at -80C for subsequent analysis by liquid or gas-chromatography mass-spectrometry.

LC-MS Measurements from [U-^{13}]glucose, [U-^{13}]glutamine, and CB-839 labeling experiments

Frozen and dried metabolites were resuspended in water based on tissue weight with valine-D8 included as an injection control. Liquid chromatography tandem mass spectrometry (LC-MS) metabolomics profiling plasma and tissue profiles were measured using a combination of two LC-MS methods designed to measure polar metabolites. Negative and positive ionization mode analyses of polar metabolites were acquired using an LC-MS system comprised of a Nexera X2 U-HPLC (Shimadzu, Marlborough, MA) and a Q-Exactive hybrid quadrupole orbitrap mass spectrometer (Thermo Fisher Scientific; Waltham, MA). Samples for positive ion mode, polar metabolite analyses were prepared and separated using the same hydrophobic interaction liquid chromatography method (HILIC) as described previously (Townsend et al., 2013; Wang et al., 2011) and MS data were acquired over m/z 70-800. Samples for negative ion mode analyses of polar metabolites were achieved using a HILIC method under basic conditions as described previously (Avanesov et al., 2014) and MS data were acquired over m/z 70-750. MS data were processed using Tracefinder (version 3.2, Thermo Fisher Scientific; Waltham, MA). Two LC-MS methods were used to measure polar metabolites in plasma and tissues. All data were acquired using an LC-MS system comprised of a Nexera X2 U-HPLC (Shimadzu, Marlborough, MA) and a Q Exactive hybrid quadrupole orbitrap mass spec-

trometer (Thermo Fisher Scientific; Waltham, MA). Hydrophilic interaction liquid chromatography (HILIC) analyses of water soluble metabolites in the positive ionization mode were carried out by extracting 10 µl homogenate using 90 µl of 74.9:24.9:0.2 vol/vol/vol acetonitrile/methanol/formic acid containing stable isotope-labeled internal standards (valine-d8, Isotec; and phenylalanine-d8, Cambridge Isotope Laboratories; Andover, MA). The samples were centrifuged (10 min, 9000 x g, 4°C) and the supernatants were injected directly onto a 150 x 2 mm Atlantis HILIC column (Waters; Milford, MA). The column was eluted isocratically at a flow rate of 250 µl/min with 5% mobile phase A (10 mM ammonium formate and 0.1% formic acid in water) for 1 min followed by a linear gradient to 40% mobile phase B (acetonitrile with 0.1% formic acid) over 10 min. The electrospray ionization voltage was 3.5 kV and data were acquired using full scan analysis over m/z 70–800 at 70,000 resolution and a 3 Hz data acquisition rate. Negative ion mode analyses of polar metabolites were achieved using a HILIC method under basic conditions. Briefly, 30µl homogenate was extracted using 120 µl of 80% methanol containing [^{15}N]inosine, thymine-d4, and glycocholate-d4 internal standards (Cambridge Isotope Laboratories; Andover, MA). The samples were centrifuged (10 min, 9000 x g, 4°C) and the supernatants were injected directly onto a 150 x 2.0 mm Luna NH2 column (Phenomenex; Torrance, CA) that was eluted at a flow rate of 400 µl/min with initial conditions of 10% mobile phase A (20 mM ammonium acetate and 20 mM ammonium hydroxide in water) and 90% mobile phase B (10 mM ammonium hydroxide in 75:25 vol/vol acetonitrile/methanol) followed by a 10 min linear gradient to 100% mobile phase A. MS full scan data were acquired over m/z 70–750. The ionization source voltage is -3.0 kV and the source temperature is 325°C.

GC-MS Measurements of [U-^{13}]glucose and [U-^{13}]C-glutamine labeled metabolites

Frozen and dried tissue metabolites were dissolved in 10µL/10mg of wet weight of tissue extracted of 2% methoxyamine hydrochloride in pyridine (Sigma) and held at 37°C for 1.5h. Tert-

butyldimethylsilyl derivatization was initiated by adding 15µL/10mg of wet weight of extracted tissue of N-methyl-N-(tert-butyldimethylsilyl)-trifluoroacetamide + 1 % tert-butyldimethylchlorosilane (Sigma) and incubated at 37C for 1hr. GC-MS analysis was performed using an Agilent 7890 GC equipped with 30m DB-35MS capillary column connected to an Agilent 5975B MS operating under electron impact ionization at 70eV. One microliter of sample was injected in splitless mode at 270°C, using helium as a carrier gas at a flow rate of 1mL min-1. For measurement of polar metabolites, the GC oven temperature was held at 100C for 3mins and increased to 300°C at 3.5°C $^{min-1}$. The MS source and quadrupole were held at 230°C and 150°C, respectively, and the detector was run in scanning mode, recording ion abundance in the range of 100-605m/z. MIDs were determined by integrating the appropriate ion fragments and correct for natural isotope abundance using in house algorithms adapted as previously reported using norvaline as an internal injection control (Commisso et al., 2013).

Extracellular Flux Measurements

Extracellular flux measurements were calculated by extracting fresh and spent medium supernatant from tracing experiments after 24 hours of growth. Cells were assumed to grow exponentially over the culture period. Glucose, lactate, glutamine, and glutamate were measured using YSI biochemistry analyzer (Yellow Springs Instruments, Yellow Springs, OH).

Enzyme-linked Immunosorbent Assay (ELISA) and Glucometer Measurements

Plasma was collected from an arterial catheter during venous glucose infusions in EDTA-coated tubes, aliquoted, and frozen at -80°C for further analysis. Plasma insulin levels were determined using an ultrasensitive mouse insulin ELISA kit (Crystal Chem, #90080). Blood glucose levels from the same mice were measured using a handheld glucometer (One Touch).

Micro Computed Tomography Imaging

Animals were anesthetized with 2 % isofluorane, oxygen mixture and underwent μCT scanning in a eXplore CT120-whole mouse μCT (GE Healthcare). Volume measurements were quantified using MicroView 3D Image Viewing (Parallax-Innovations) and representative coronal Z-stacks were extracted using OsiriX (OsiriX-Viewer).

Metabolic Flux Analysis

^{13}C-assisted metabolic flux analysis (MFA) was used to estimate the fates of intracellular pyruvate in KP-derived mouse lung cancer cell lines. An in-house, elementary-metabolite-unit-based software (Antoniewicz et al., 2006, 2007) was used to generate a set of flux values and 95 % confidence intervals corresponding to a simplified model of central carbon metabolism. The software, which was run in Matlab v2009b (Mathworks), minimizes the lack of fit between measured data (extracellular fluxes and intracellular metabolite labeling patterns) and simulated data corresponding to potential flux distributions, as described elsewhere (Antoniewicz et al., 2006; Wiechert and de Graaf, 1996). Flux estimation was performed 500 times, each with randomly chosen initial values, and the flux distribution with the lowest weighted sum of squared errors was that corresponding to the global minimum. Measured glucose consumption, lactate production, glutamine consumption, and proliferation were used to constrain the flux distribution. The intracellular metabolite fragment labeling patterns used in the analysis were Pyr174, Lac233, Lac261, Ala260, Mal419, Asp302, Asp390, Asp418, Glu330, Glu432, Cit459, and Cit591, as these were found to give sufficient resolution for estimating pyruvate-consuming fluxes with a [U-^{13}C]glutamine tracer. In addition, the Lac261 labeling pattern from a [1,2-^{13}C]glucose tracer was used to resolve pentose phosphate pathway fluxes (Metallo et al., 2012) The following assumptions were made for the analysis:

1. Cells were cultured in media containing the ^{13}C tracer for 24 h before harvesting, at which point the system was assumed to be at pseudo-steady state for both metabolic fluxes and isotopic-labeling patterns of metabolites were attained, enabling the use of steady state MFA (Wiechert and de Graaf, 1996). Changes in TCA cycle metabolite or lactate labeling patterns following 24-h culture in [U-^{13}C]glutamine or [1,2-^{13}C]glucose, respectively, have previously been shown to be negligible (Ahn and Antoniewicz, 2011, 2013; Metallo et al., 2012). Cells were in the exponential growth phase during the labeling period.

2. Dissolved CO2 freely exchanges with gaseous CO2. Unlabeled CO2 can be used in carboxylation reactions, but evolved CO2 resulting from loss of ^{13}C atoms can also be reincorporated for carboxylation reactions, if necessary.

3. Pyruvate, malate, citrate, α-ketoglutarate, and aspartate exist in separate mitochondrial and cytosolic pools, where they participate in distinct chemical reactions and become differentially labeled, but can be transported freely between intracellular compartmental. The measured metabolite labeling patterns results from the mixture of these two pools. Other metabolites may exist in both pools, but rapid equilibration between the pools in a manner that precludes distinct labeling patterns was assumed.

4. Succinate and fumarate are symmetric metabolites, so their interconversion scrambles the first- and second-carbon labeling states with the third- and fourth-carbon labeling states, respectively.

5. Because anabolic fluxes that contribute to biomass fluxes are small relative to others in central carbon metabolism, the expected flux distribution is largely insensitive to the assumed biomass composition (Folger et al., 2011; Frezza et al., 2011). Correspondingly, the biomass equation used here is only approximate. Dry cell weight is predominantly protein, so the core biomass equation

was assumed to consist of nonessential amino acids primarily synthesized by intracellular central carbon metabolites in DMEM culture conditions; this led to the inclusion of aspartate, glutamate, glutamine, and alanine. Asparagine (which is synthesized from aspartate) and proline (which is synthesized from glutamate) were included with aspartate and glutamate respectively. Serine, glycine, and cysteine were not included as they were assumed to be derived primarily from the media. Dihydroxyacetone phosphate (DHAP) and cytosolic acetyl CoA were also considered to account for lipid synthesis, and pentose 5-phosphate (P5P) was considered to account for nucleotide synthesis. Literature reports of biomass composition for hybridoma cells was used as an estimate for the relative sizes of these demands (Sheikh et al., 2005), and these were scaled to give units of fmol/cell by assuming each cell weighs 150 pg (Murphy et al., 2013).

6. The uncertainties of extracellular fluxes were set to their measured standard deviations. The uncertainties of metabolite isotopomer mole fractions were set to 0.35 mol %, which is consistent with typical measurement and modeling errors (Wasylenko et al., 2015a,b)

sgRNAs and Primers Used for the Generation of Knockout Cell Lines and Tumors

sgRNAs and Primers Used for the Generation of Knockout Cell Lines and Tumors sgRNAs were designed using E-CRISP (e-crisp.org) to Pdha1, Pcx, and Gls1 with restriction enzyme compatible sites and a G was added to the +1 position where not already present for U6 transcription. sgRNAs were introduced into the U6-sgRNA-EFS-Cas9-2A-Puro vector for generation of cell lines or U6-sgRNA-EFS-Cas9-2A-Cre (pSECC) for use in vivo using BsmBI as previously described (Sánchez-Rivera et al., 2014). Lentivirus was produced by co-transfection of 293T cells with packaging constructs (delta8.2 and VSV-G) using TransIT-LT1 (Mirus Bio). Supernatant was concentrated by ultracentrifugation, resuspended in OptiMEM (Gibco), and animals were infected with pSECC to disrupt

Gls1, Pcx, or Pdha1 concomitantly with Cre activation to initiate tumors as described previously (Sánchez-Rivera et al., 2014).

Table 6.1

Target Gene	sgRNA ID	Sequence of sgRNA	Strand	Exon
Pdha1	sgPdha1	GCGCAGAGCCTGCCAACACGCGG	-	1
Pcx	sgPcx.1	GCCTATCAAGAAAGTAATGGTGG	+	1
Pcx	sgPcx.2	CTCCCCAAATGTCCGGCGTCTGG	+	1
Gls1	sgGls1.1	CCGCGCCGGGGCCCTTCGCGCGG	+	1
Gls1	sgGls1.2	CCTTGCTGAAAAGAAATGAAAGG	+	1

References

Ahn WS, Antoniewicz MR. Metabolic flux analysis of CHO cells at growth and non-growth phases using isotopic tracers and mass spectrometry. *Metabolic Engineering* (2011).

Ahn WS, Antoniewicz MR. Parallel labeling experiments with [1,2-(13)C]glucose and [U-(13)C]glutamine provide new insights into CHO cell metabolism. *Metabolic Engineering* (2013).

Antoniewicz MR, Antoniewicz MR, Kelleher JK, Kelleher JK, Stephanopoulos G, et al. Elementary metabolite units (EMU): a novel framework for modeling isotopic distributions. *Metabolic Engineering* (2007).

Antoniewicz MR, Kelleher JK, Stephanopoulos G. Determination of confidence intervals of metabolic fluxes estimated from stable isotope measurements. *Metabolic Engineering* (2006).

Johnson L, Mercer K, Greenbaum D, Bronson RT, Crowley D, et al. Somatic activation of the K-ras oncogene causes early onset lung cancer in mice. *Nature* (2001).

Metallo CM, Gameiro PA, Bell EL, Mattaini KR, Yang J, et al. Reductive glutamine metabolism by IDH1 mediates lipogenesis under hypoxia. *Nature* (2012).

Sánchez-Rivera FJ, Papagiannakopoulos T, Romero R, Tammela T, Bauer MR, et al. Rapid modelling of cooperating genetic events in cancer through somatic genome editing. *Nature* (2014).

Sheikh K, Förster J, Nielsen LK. Modeling hybridoma cell metabolism using a generic genome-scale metabolic model of Mus musculus. *Biotechnology Progress* (2005).

Wasylenko TM, Ahn WS, Stephanopoulos G. The oxidative pentose phosphate pathway is the primary source of NADPH for lipid overproduction from glucose in Yarrowia lipolytica. *Metabolic Engineering* (2015a).

Wasylenko TM, Wasylenko TM, Stephanopoulos G, Stephanopoulos G. Metabolomic and (13)C-metabolic flux analysis of a xylose-consuming Saccharomyces cerevisiae strain expressing xylose isomerase. *Biotechnology and Bioengineering* (2015b).

Wiechert W, de Graaf AA. In vivo stationary flux analysis by 13C labeling experiments. *Advances in Biochemical Engineering/Biotechnology* (1996).

Appendix B

Supplementary Figures

This section contains supplementary details for Chapter 3.

Author statement

Some passages and figures have been adapted or quoted verbatim from the following published articles:
Davidson, SM, Jonas, O, Keibler, MA, Hou, HW, Luengo, A, Vander Heiden, MG (2016). Direct evidence for cancer-cell-autonomous extracellular protein catabolism in pancreatic tumors. Nature Medicine, (December). *in press*

Authors

Shawn M. Davidson[1,2,3+], Oliver Jonas[1+], Mark A. Keibler[4], Han Wei Hou[5], Alba Luengo[1,2], Jared R. Mayers[1,2], Jeffrey Wyckoff[1], Amanda Del Rosario[1], Matthew Whitman[1], Christopher R. Chin[1], Kendall J. Condon[1,2], Alex Lammers[1], Katherine A. Kellersberger[6], Brian J. Stall[6], Gregory Stephanopoulos[4], Dafna Bar-Sagi[7], Jongyoon Han[4], Joshua D. Rabinowitz[8], Michael Cima[1], Robert Langer[1,4], and Matthew G. Vander Heiden[1,2,3,9*]

Author affilations

1. Koch Institute for Integrative Cancer Research, Massachusetts Institute of Technology, Cambridge, Massachusetts, USA
2. Department of Biology, Massachusetts Institute of Technology, Cambridge, Massachusetts, USA.
3. Broad Institute of MIT and Harvard University, Cambridge, Massachusetts, USA.
4. Department of Chemical Engineering, Massachusetts Institute of Technology, Cambridge, Massachusetts, USA.
5. Department of Electrical Engineering and Computer Science, Massachusetts Institute of Technology, Cambridge, Massachusetts, USA.
6. Bruker Daltronics, Inc. 40 Manning Rd, Billerica, MA 01821.
7. Department of Biochemistry and Molecular Pharmacology, New York University, New York, New York, USA.
8. Department of Chemistry and Integrative Genomics, Princeton University, Princeton, New Jersey, USA.
9. Department of Medical Oncology, Dana-Farber Cancer Institute and Harvard Medical School, Boston, Massachusetts, USA.
+ These authors contributed equally to this work.

Author contributions

Conceptualization: S.M.D, O.J., and M.G.V.H. Methodology: S.M.D., O.J., M.A.K., H.W.H., A.L., J.R.M., J.W., A.M.D., M.W., C.R.C., K.J.C., A.L., K.A.K., B.K.S., G.S., J.H. and D.B.-S.., Formal Analysis S.M.D., O.J., A.M.D. Investigation S.M.D. and O.J. Writing Original Draft: S.M.D., O.J., and M.G.V.H. Visualization S.M.D., O.J., and M.G.V.H. Supervision M.J.C., R.L., and M.G.V.H. Funding Acquisition O.J., J.D.R., R.L. and M.G.V.H.

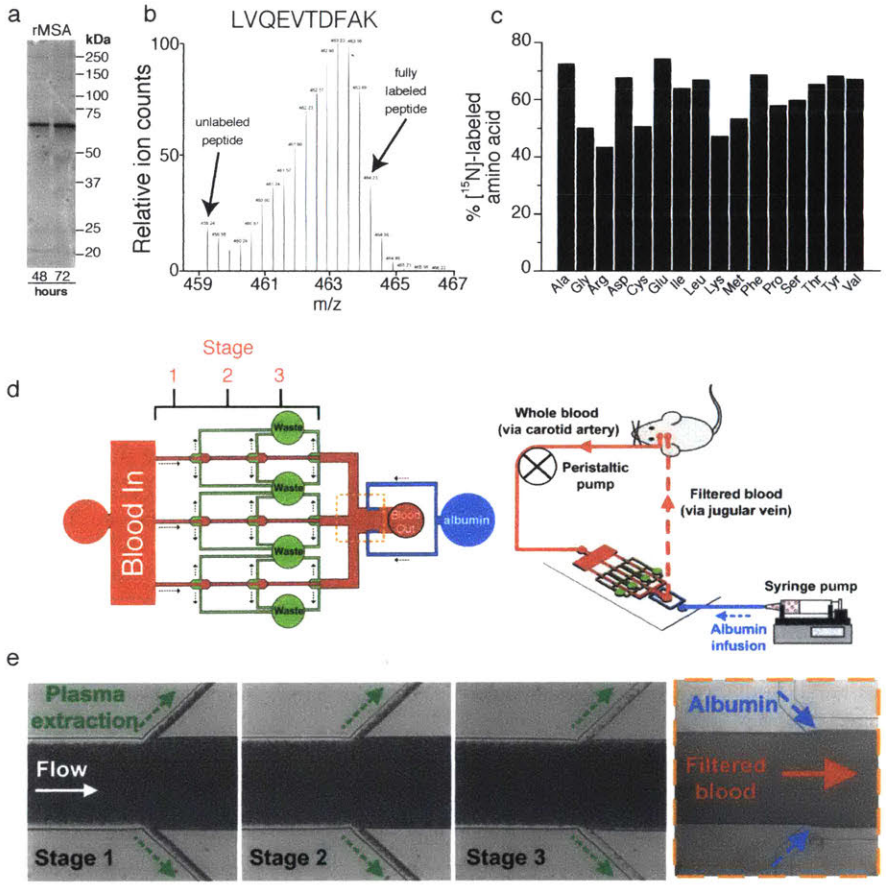

Figure B1. Production and purification of msAlbumin and miniaturized plasmapheresis, Related to Figure 3.1 (A) Recombinant mouse serum albumin (MSA) was produced in P. pastoris. Supernatant from the culture was collected at 48- and 72-hours post inoculation and analyzed by SDS-PAGE and Coomassie-stain as shown. The predicted molecular weight of MSA is 69kDa. (B) [^{15}N]-MSA generated was generated in P. pastoris, purified, and a representative analysis of the LVQEVTDFAK tryptic peptide by LC-MS/MS is shown (This preparation corresponds to the infusate used to generate the data presented in Fig. 1). (C) To determine the extent of albumin amino acid labeling, ^{15}N-labeled MSA produced in P. pastoris was subjected to acid hydrolysis and amino acids assessed by GC-MS. The % ^{15}N isotopomer labeling for the indicated amino acid is shown. (Ala = alanine; Asp = aspartate; Cys = cysteine; Gln = glutamine; Glu = glutamate; Gly = glycine; Ile = isoleucine; Leu = leucine; Lys = lysine; Met = methionine; Phe = phenylalanine; Ser = serine; Thr = threonine; Val = valine). (D) Schematic representation of a miniaturized multiplexed 4-channel plasmapheresis device fabricated from PDMS as well as a schematic depicting the use of the plasmapheresis device to perform albumin exchange in mice. Blood from the carotid artery is pumped into the device using a miniaturized peristaltic pump, plasma removed, and the cellular component of blood is then re-mixed with labeled albumin and returned to the mouse via a venous catheter. (E) Microscopic image of a single channel in a functioning miniaturized plasmapheresis device showing plasma skimming from arterial blood based on axial migration of red blood cells towards the center of the microchannel at Stage 1, Stage 2, and Stage 3 (see schematic in panel d). The concentrated red blood cells are then mixed with labeled albumin (right panel) prior to reinfusion into mice.

Figure B1

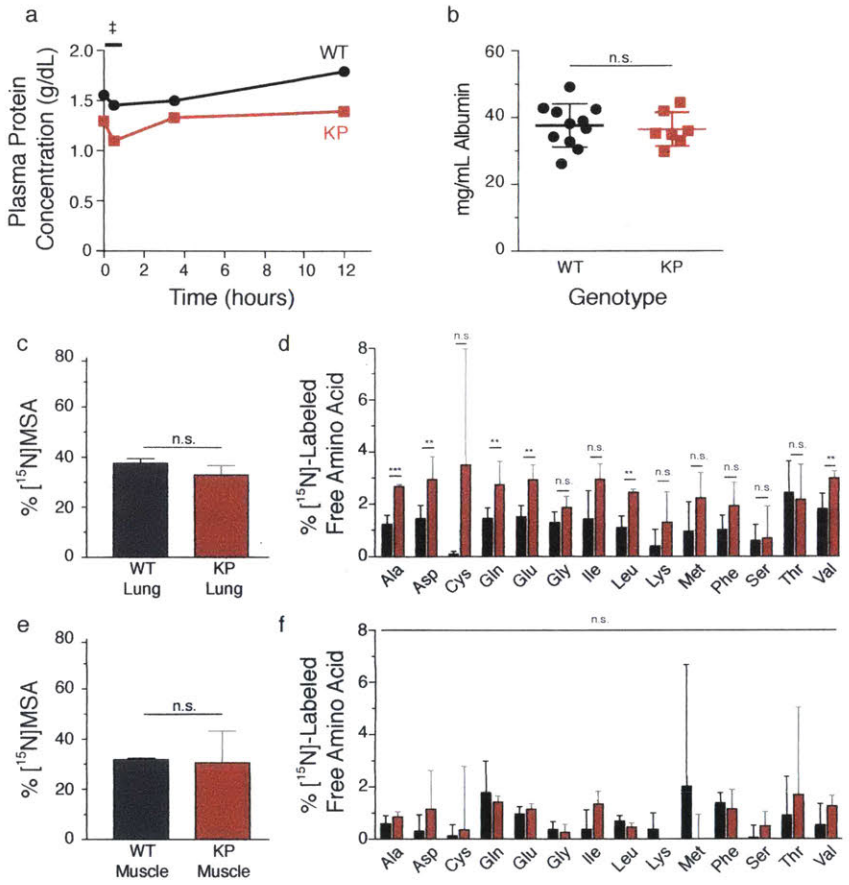

Figure B2. Labeled albumin fate in plasma, lung and muscle of WT and KP animals, Related to Figure 3.1 (A) Representative plasma protein levels from a plasma exchange experiment to deliver labeled mouse serum albumin (MSA). Plasma was collected longitudinally before, during and after the plasma exchange period in WT and KP mice. The time period indicated by the double dagger corresponds to the 30-minute plasma exchange period (n = 5). (B) Enzyme linked immunoadsorption assay (ELISA) to assess MSA levels in 7-8 week old WT and KP mice, a time point when the KP mice have late stage pancreatic cancer. No significant difference (n.s.) in albumin levels was measured between WT and KP mice (WT n = 11; KP n = 7). (C) Following plasma exchange of [^{15}N]-labeled MSA for endogenous MSA in WT and KP mice, the presence of [^{15}N]-labeled MSA in tissue was determined by analysis of labeled peptides from lungs of animals with pancreatic tumors (KP) or without pancreatic tumors (WT) by LC-MS/MS. No significant difference (n.s.) in albumin levels was measured between WT and KP mice. (D) The presence of labeled free amino acids in the lungs of WT or KP mice 12 hours after plasma exchange of [^{15}N]-labeled MSA for endogenous MSA. Labeled amino acids were determined by GC-MS. (E) Following plasma exchange of [^{15}N]-labeled MSA for endogenous MSA in WT and KP mice, the presence of [^{15}N]-labeled MSA in tissue was determined by analysis of labeled peptides from muscle of animals with pancreatic tumors (KP) or without pancreatic tumors (WT) by LC-MS/MS. No significant difference (n.s.) in albumin levels was measured between WT and KP mice. (F) The presence of labeled free amino acids in the muscle of WT or KP mice 12 hours after plasma exchange of [^{15}N]-labeled MSA for endogenous MSA. Labeled amino acids were determined by GC-MS (Ala = alanine; Asp = aspartate; Cys = cysteine; Gln = glutamine; Glu = glutamate; Gly = glycine; Ile = isoleucine; Leu = leucine; Lys = lysine; Met = methionine; Phe = phenylalanine; Ser = serine; Thr = threonine; Val = valine). (for panels c-f: * $p<0.05$; ** $p<0.01$, *** $p<0.001$ by Students t-test, n.s. differences not significant, n = 5 per genotype).

Figure B2

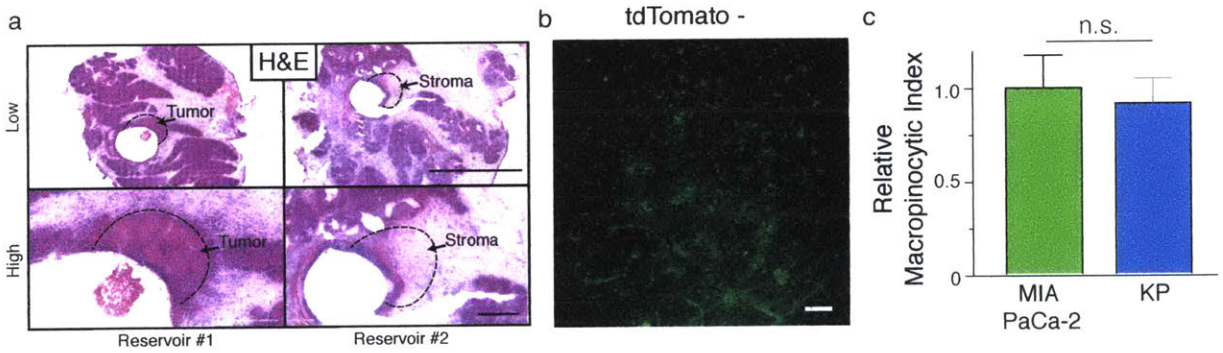

Figure B3. Device placement in autochthonous pancreatic tumors and intravital imaging of DQ-BSA in tdTomato-negative pancreatic tumors, Related to Figure 3.3 (A) Representative hematoxylin and eosin (H& E) staining of devices with reservoirs adjacent to tumor tissue (left, Reservoir #1) and non-tumor tissue (right, Reservoir #2). Dotted black lines indicate the diffusion distance for EIPA observed by MALDI-IMS. Scale bar, 2mm for upper panels (low magnification) and 200µm for lower panels (high magnification). (B) Devices containing DQ-BSA were implanted into the pancreas of tomato-negative KP mice with pancreatic tumors. Multiphoton imaging of DQ-BSA fluorescence in the pancreatic tissue of live mice is shown (images are representative of n = 2 mice per genotype with triplicate reservoirs). Scale bar, 50 µm. (D) Quantification of macropinocytic index of tomato-negative autochthonous KP tumors based on fluorescence from DQ-BSA as shown in a. The macropinocytic index of MIA PaCa-2 xenograft tumors based on fluorescence from DQ-BSA is shown for comparison (n=5 distinct fields were used to quantify macropinocytic index per condition).

Figure B3

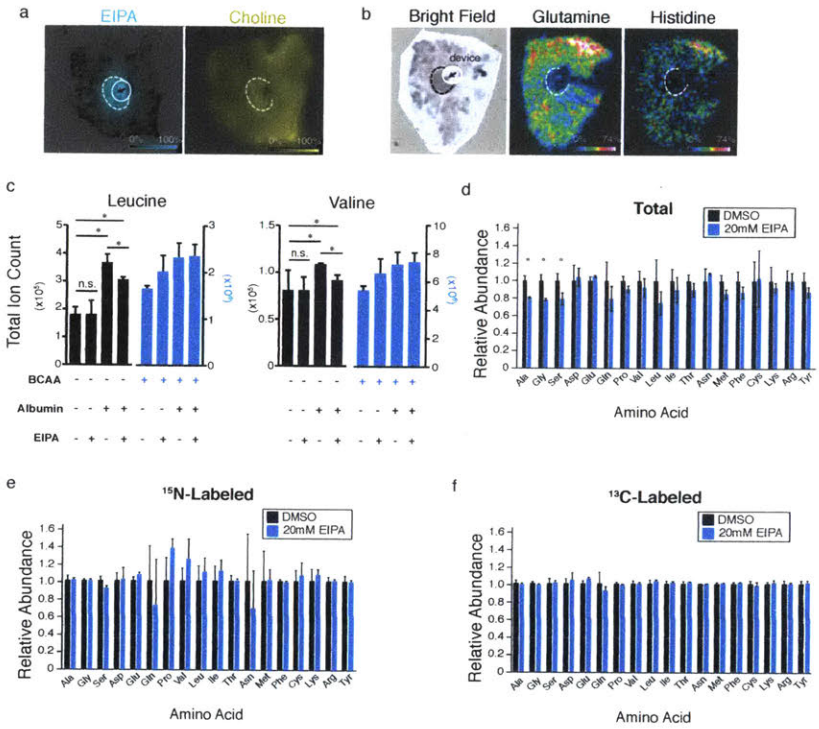

Figure B4. Local depletion of amino acids by EIPA in $Kras^{G12D}$-driven pancreatic tumors and affect of EIPA on amino acid levels in cells in culture. Related to Figure 3.4 (A) Devices containing EIPA were implanted directly into pancreatic tumors of KP mice. The position of the device and direction of the arrow indicate orientation and direction of EIPA delivery (white circle and black arrow, respectively). 24 hours after device implantation, serial sections from the tumor were analyzed by matrix assisted laser desorption ionization coupled to imaging mass-spectrometry (MALDI-IMS). Positive ion mode was used to detect the macropinocytosis inhibitor, EIPA (EIPA diffused approximately 400-500µM), and choline, a metabolite not expected to be affected by macropinocytosis inhibition. The range of ion detection corresponding to the heat maps shown for each metabolite is included for each image; scale bar, 2mm. (images are representative of n = 2 KP mice with triplicate reservoirs). (B) Serial sections from the same tumors described in a. were examined by MALDI-IMS in negative ion mode to assess levels of the amino acids glutamine and histidine. The position of the device (red circle with black arrow showing direction of EIPA delivery) was used to orient the serial sections analyzed in negative ion mode relative to those analyzed in positive ion mode. The location corresponding to EIPA single (see a) is designated by black or white dashed line. The range of ion detection corresponding to the heat maps shown for each metabolite is included for each image; scale bar, 2mm (images are representative of n = 2 KP mice with triplicate reservoirs). (C) Pancreatic cancer cells derived from KP tumors were cultured for 6 hours in media without or with branch chain amino acids (BCAAs), in the presence or absence of 3% albumin, and in the presence of vehicle alone (DMSO) or 20µM EIPA as indicated. Relative levels of leucine and valine under each condition as determined by GC-MS are shown. (D) Pancreatic cancer cells derived from KP tumors were cultured for 6 hours in media containing uniformly labeled ^{15}N and 13C-labeled amino acids in the presence of vehicle alone (DMSO) or 20µM EIPA as indicated. Total intracellular amino acid levels for each condition as determined by GC-MS are shown (n = 3 technical replicates, repeated twice). (E) Pancreatic cancer cells derived from KP tumors were cultured for 6 hours in media containing uniformly labeled ^{15}N and 13C-labeled amino acids in the presence of vehicle alone (DMSO) or 20µM EIPA as indicated. Total intracellular levels of ^{15}N-labeled amino acids for each condition as determined by GC-MS are shown (n = 3 technical replicates, repeated twice). (F) Pancreatic cancer cells derived from KP tumors were cultured for 6 hours in media containing uniformly labeled ^{15}N and 13C-labeled amino acids in the presence of vehicle alone (DMSO) or 20µM EIPA as indicated. Total intracellular levels of 13C-labeled amino acids for each condition as determined by GC-MS are shown (n = 3 technical replicates, repeated twice). For all panels, * denotes $p<0.05$. Ala = alanine; Asp = aspartate; Cys = cysteine; Gln = glutamine; Glu = glutamate; Gly = glycine; Ile = isoleucine; Leu = leucine; Lys = lysine; Met = methionine; Phe = phenylalanine; Ser = serine; Thr = threonine; Val = valine.

Figure B4